An Experimental Study of Radial Temperature Profile Effects on Turbine Tip Shroud Heat Transfer

by

Charles Waldo Haldeman[IV]

B.S. Mechanical Engineering University of Rochester
Rochester, NY 1985

Submitted to the Department of Aeronautics and Astronautics in Partial Fulfillment of the Requirements for the Degree of

Master of Science in Aeronautics and Astronautics

at the

Massachusetts Institute of Technology
August 1989

Signature of Author_

Department of Aeronautics and Astronautics
June 30, 1989

Certified by

Professor Alan H. Epstein
Associate Professor of Aeronautics and Astronautics
Thesis Supervisor

Approved by

Professor Harold Y. Wachman
Chairman, Department Graduate Committee

An Experimental Study of Radial Temperature Profile Effects on Turbine Tip Shroud Heat Transfer

by

Charles Waldo Haldeman[IV]

Submitted to the Department of Aeronautics and Astronautics on June 30, 1989 in Partial Fulfillment of the Requirements for the Degree Of Masters of Science in Aeronautics and Astronautics

Abstract

It has been hypothesized that radial temperature profiles generated by combustors in aircraft gas turbines could fundamentally change the flow field in the turbine stage and thus the heat loading on the turbine tip shroud. This project created a radial parabolic temperature profile to explore the effects of inlet temperature non-uniformity on turbine tip shroud heat transfer. This experiment was done on the MIT short-duration blowdown turbine test facility using a stored matrix heat exchanger to create the radial temperature profiles, while maintaining a circumferentially uniform temperature and constant total pressure.

This project measured the effects of radial temperature profiles, absolute driving temperature (T_{gas}-T_{wall}) to wall temperature ratios, and tip gap on rotor tip shroud heat loading. Measurements were made of the heat flux and static pressure at seven axial locations along the tip shroud; spanning from -.085 to 1.1 % of axial rotor blade chord, and six different circumferential locations which spanned a nozzle guide vane passage.

Measurements were made for three different radial temperature profiles: 16%, 8% and uniform flow at an average driving to wall temperature ratio of .51 , and 11%, 6% and uniform flow for a driving temperature to wall ratio of .32, for three different tip gaps, 1.7%, 2.1% and 2.5% of blade span. Preliminary analysis indicates no variation of heat loading due to the different blade gaps, but a strong dependance on circumferential position. Measurements of heat flux decayed by a factor of five to one axially and varied circumferential by up to 50%.

Using a Nusselt number based on the inlet streamline temperature entering the nozzle guide vanes near the outer wall, the different heat flux patterns for the tests collapsed to one curve for each circumferential location, which has a ratio of leading edge Nusselt number to trailing edge Nusselt number of about four to one. Indicating that the only effect of radial profiles is to change the temperature of the gas at the end-wall upstream of the rotor. Once the different effects of driving temperature have been accounted for, there is little change in heat flux due to radial profiles, showing that the flow field is not been fundamentally altered.

Thesis Supervisor: Professor Alan H. Epstein

Title: '   Associate Professor Of Aeronautics and Astronautics

Acknowledgements

There are many people whom deserves special credit and thanks for their contributions, and suggestions which made possible the completion of this project.

First I would like to thank Prof. Epstein and Dr. Guenette for their continued support and patience. They allowed me the luxury of letting me find the error of my ways in both the experiment and the thesis writing. This experience has given me a greater understanding of the "atmosphere" in which research is conducted and my own strengths and weaknesses as an engineer than I probably would have been exposed to otherwise. In addition, both of these people deserve special thanks for the support they have given me through their attempts to integrate my school work and the experiment, through which I have come closer to finding the proper balance between doing in depth, full-blown analysis and "back of the envelope" calculations, both of which are needed to be a practicing engineer.

In addition to the help I had from these people, the graduate students past and present deserve special thanks for showing me the "light at the end of the tunnel." Special thanks go to the other members of the turbine project, Reza Abhari and Lou Cattafesta for their countless conversations and consultations. In addition Dr. Petros Kotidis, Prof. Mark Lewis, Prof. Tom Bamford, Dr. David Fink, Dr. Phil Lavrich, and Mr. Dan May all helped me with the experiment and the theory, and provided moral support in general.

I am especially indebted to four undergraduates for their support and help. Ike Chuang did most of the computer work for running the profile generator at a time when I did not even know how to access the VAX. Andy Thurling provided the electronics wizardry which was responsible for the optical lever operating, the A-D operating, and the amplifiers working. Mike Fox provided an almost unbounded enthusiasm, even after his facility disintegrated, during the summer months which helped to keep my problems in perspective. And of course I would like to thank my brother for both his continued harassment to finish the thesis and his insights into the experimental problems that I encountered.

I would also like to thank the people at Rolls-Royce, Dr. Rob Norton and company, for their help in constructing the profile generator. Their participation allowed me insights into industrial research and development which greatly added to my experiences at MIT. And of course I am indebted to Rolls-Royce for its financial support of this project.

Of course I need to thank my other teachers, Mr. Jim Nash, Mr. Viktor Dubrowski, and Mr. Roy Andrews for teaching me the ways of fabrication and machining during my summer months here as an undergraduate. That experience kept me from devoting an unreasonable amount of time during my graduate career to finding the proper nuts and bolts to use on the turbine facility.

No one is isolated from the outside world (no matter what MIT thinks) and I owe a great deal of thanks to many people. To my friends both on Team Phred and elsewhere and my roommates for their continued support and friendship (and forgiveness when I ignored them to work in the lab); and to my family whose support and love was desperately needed by both myself and the K-car, to keep us both moving through to the end of this project.

Finally I would like to thank Margaret for her devotion, relative calmness and support that she has provided over the years. Her contribution to this project, and my sanity, go well beyond the fifteen hours she spent xeroxing the graphs down to library standards.

Table of Contents

Note on Organization of the Paper

When organizing this paper I attempted to keep the figures and tables in the main text as much as possible. This was done with the smaller drawings and tables but unfortunately there were some which were just too large for the main body of the thesis and these are put at the back of the chapters with the tables first and then the figures. The numbering of the drawings and tables is based upon where they are referenced in the text and not necessarily in the order of which they are seen. All of these items should be relatively easy to locate for if they are not immediately in the text then they will be at the end of the chapter. A numerical listing of the figures and tables is provided at the beginning of the paper to aid in their location.

Previous work has been referenced as footnotes on the individual pages in which they occur. A cumulative alphabetical listing of all the references cited is provided in the bibliography.

List of Figures

List of Tables

Chapter 1. Introduction

The tip gap region in the turbine section of a gas turbine engine is a particularly attractive area of engineering study since approximately 25-30 % of the turbine efficiency loss occurs in this area[1]. Thus the practical rewards which come from a clearer understanding of this region are substantial. Experimental investigations of heat transfer in the tip casing region have in the past yielded different results from industrial experience. Turbine shrouds show signs of greatest decay and structural damage at the trailing edge. This is counter-intuitive since the highest energy flow would be at the leading edge of the shroud, towards the combustor. It could be hypothesized that differences between experimental measurements and the perceived reality (the burn-out of tip casings at the trailing edge) might result from key flow parameters not being accurately modeled in the experiments. For example if this problem was believed to be primarily an unsteady three dimensional flow, than linear cascade measurements would not yield accurate results. Work by Guenette[2] at the MIT turbine facility[3] showed decay in tip casing heat transfer from the leading to the trailing edge of a shroud (see figs. 1-1 and 1-2).

Figure 1-1
Time Averaged Heat Flux
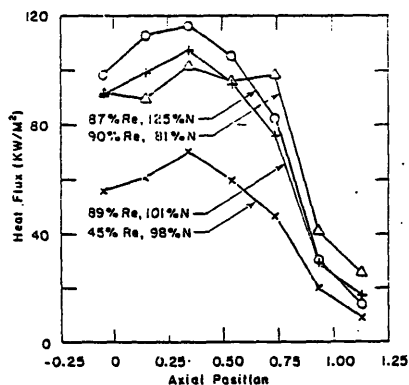
Figure 1-2
Time Averaged Nusselt No.
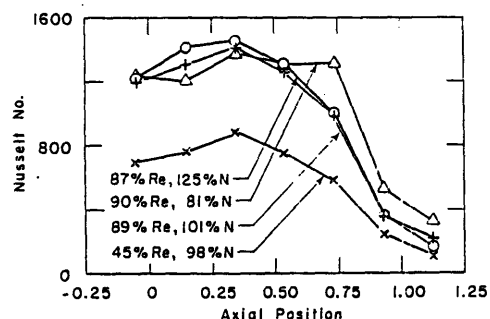
These graphs represent the influence of different turbine loading conditions on the turbine shroud heat transfer rate (N- corrected speed, Re-Reynolds number, Axial position normalized by blade chord)[4]. These measurements were made in a fully scaled rotating facility.

---

[1] Booth, T.C. "Tip Clearance Effects in Axial Turbomachines: Importance of Tip Clearances Flows in Turbine Design" Presented at "The Von Karmin Institute for Fluid Dynamics Lecture Series: 1985-05" on April 15-19, 1985.

[2] Guenette, Gerald "A fully scaled Short Duration Turbine Experiment" ,MIT Ph.D Thesis, Aeronautical and Astronautical Engineering Department, Aug 26, 1985

[3] Epstein, Alan, Gerald Guenette and Rob Norton "The Design of the MIT Blowdown Turbine Facility"; GTL report 183, April 1985.

[4] Guenette, Gerald "A fully scaled Short Duration Turbine Experiment" Aug 26, 1985 MIT Ph.D, p. 145,147.

If disagreement between the experimental and industrial observations are not due to three dimensional or unsteady effects, then perhaps they are due to either temperature and pressure profiles or turbulence created by the combustor. Combustors by their nature have both strong radial and circumferential temperature and pressure profiles[5,6]. Theoretical work done on the effects of an inlet temperature distortion on turbine performance and flow patterns, summarized by Butler[7], have been confirmed by experiments done by Butler[8] and Stabe[9] which show the creation of strong secondary vortices and the migration of hot gases to the pressure side of a rotor and the cold gases to the suction side. However, both of these experiments dealt with the main rotor flow and not with tip casing heat transfer. And since experiments have shown that inlet temperature profiles affect the underlying flow field in the turbine region, it is reasonable to assume that there may be an effect on tip shroud heat transfer.

The object of this project was to attempt to explain the non-agreement between experimental results and industrial experience by more accurately modeling the inlet flow to the turbine to determine which flow parameters influence tip shroud heat transfer. At the MIT facility, the turbine inlet flow is uniform. Of the three areas in which the inlet flow could be modified to appear more like a combustor: the pressure profile, the temperature profile, and the turbulence generation, this project only modeled the temperature profile.

This was primarily due to experimental reasons. The effect of all these variable might complicate the flow regime to the point where useful information might not be extrapolated. Secondly, the equipment involved in the creation of the pressure profiles and turbulence generation could represent a significant increase in manufacturing effort. In addition, this project was even more focused since circumferential temperature profiles were not investigated. These were eliminated from the field of investigation since the expected information gathered from such an experiment would not be worth the extra effort, at this point, needed to make the facility acceptable to circumferential measurements.

As a result, this project measured the effect on tip shroud heat transfer of radial temperature profile, average gas temperature and tip gap clearance (these last two parameters are based primarily on theory and previous experiments which show their effect on the tip

[5] Dils, R.R. "Use of Thermocouples for Gas Temperature Measurements in Gas Turbine Combustors" National Bureau of Standards no. 561: Proceedings of the 10th Materials Research Symposium on Characterization of High Temperature Vapors and Gases . October 1979, p.1056

[6] Cox, G.B; Tiller, A.R., and J. LeTourneau "Pattern Factor Improvement in the F-100 Primary Combustion System" Journal of Engineering for Power, Transactions of the ASME 81-GT-25, March, 1980

[7] Butler, T. L. and O. P. Sharma "Redistribution of an Inlet Temperature Distortion in an Axial Flow Turbine Stage" AAIA-86-1468

[8] T.L. Butler, ibid.

[9] Sabe, R.G., W. Whitney, and T Mofitt "Performance of a High-Work Low Aspect Ratio Turbine Tested with a Realistic Inlet Radial Temperature Profile" AAIA-84-1161

flow). Chapter two outlines the experimental hardware used. It gives a brief description of the blowdown facility and discuses the design, construction and test result of the profile generator. Instrumentation, including the tip shroud, tip clearance measuring device and total pressure and temperature rakes are described in chapter three. The experimental procedure and the calibration procedure are discussed in chapter four. The data analysis techniques, steady state results and time resolved measurements are presented in chapter five. The final chapter analyses the data and discusses possible future work. In addition there are three appendices: the first has the drawings and some construction notes on the profile generator. The second has drawings for the tip casing. The final appendix has four tables outlining the performance of the generator over the entire test matrix.

Chapter 2: The Experimental Apparatus

2.1 The MIT Blowdown Turbine Facility

As mentioned at the beginning of the paper, the backbone of this project was the MIT Blowdown Turbine Facility. All the equipment manufactured for this project was designed to fit this facility. The turbine facility is a fully scaled, rotating facility with the ability to cool the nozzle guide vanes and the rotor either separately or together. The scaling parameters for the facility are given in table 2-1.

Table 2-1
MIT Blowdown Turbine Scaling[1]

	Full Scale	MIT Facility
Fluid	Air	Ar-R12
Ratio of Specific Heats	1.27	1.27
Mean Metal Temperature (T_m)	1118 °K (1550 °F)	295 °K (72 °F)
Metal to Gas Temp. Ratio (T_m/T_g)	.63	.63
Inlet Total Temperature (T_g)	1780 °K (2750 °F)	478 °K (400 °F)
Cooling Air Temp	790 °K (960 °F)	212 °K (-77 °F)
Airfoil cooling Mass Flow as a		
Ratio of Total Air Flow	12.5%	12.5%True NGV Chord
Reynolds Number based on NGV		
Chord and isentropic exit conditions	$2.7*10^6$	$2.7*10^6$
Inlet Total Pressure Atm (Psia)	19.6 (289)	4.3 (64)
Outlet Total Pressure	4.5 (66)	1.0 (14.7)
Outlet Total Temperature	1280 °K (1844 °F)	343 °K (160 °F)
Prandtl Number	.752	.755
Rotor Speed, RPM	12,734	6,190
Mass Flow, Kg/sec	49.00	16.55
Power (Kw)	24,880	1,078
Test time	Continuous	.2 Sec

Figures 2-1 and 2-2 show the flow path for the facility. The facility is operated by heating the supply tank to the appropriate level (roughly 500 °K) using an oil heating system. When the

---

[1] Epstein, Alan; Guenette, Gerald; and Rob Norton The Design of the MIT Blowdown Turbine Facility: MIT GTL Report no 183, April 1985. p. 15.

supply tank is at uniform temperature, the test gas is mixed at constant temperature and added to the supply tank until the desired testing pressure is reached (approx. 80 psia). The supply tank is separated from the test section and the dump tank by the fast acting valve which allows the test section and dump tank to be evacuated. When the test gas achieves thermal equilibrium in the supply tank, the rotor is spun above the test speed which primes the A-D system and as it slows down it triggers the valve to open, starts the eddy brake and starts the data acquisition process. The eddy brake is used to provide the necessary amount of power absorption to insure that the corrected speed of the turbine stays constant.

Once the valve opens, the nozzle guide vanes become choked, pressure transients in the tunnel have dissipated by 250 ms after the initial valve opening. At this point the facility has come to a steady state operating point which will last until the nozzle guide vanes become unchoked, at around 500 ms. The total test time (250 ms to 500 ms) corresponds roughly to 1000 blade passings. In addition, the boundary layers are bled off right before the contraction into the nozzle guide vanes which contributes to an almost completely uniform flow entering the turbine. This flow gets directed to the dump tank without going through the rotor assembly and accounts for about 30% of the total mass flow leaving the valve.

The A-D system has four different internal clock settings which can sample up to 200 KHz each. The A-D is divided into a high speed side (usually reserved for rotor and/or test instrumentation) and a low speed side (facility instrumentation: pressure transducers in the supply tank, Pressure rakes, etc.) which multiplexes sixteen channels into one high speed channel. Thus the sampling of the low speed instrumentation is always one sixteenth of the high speed (if all the channels on the multiplexer are full). During an actual test one normally samples at 20 KHz from start to 250 ms, where the clock changes and sampling occurs at 200 KHz from 200 to 550 ms. Then it goes to 5 KHz to 1200 ms where the clock goes to 50 Hz until the end of the test five minutes after starting (when the tunnel comes to equilibrium again). Using these clock settings, 419,430 data points per channel were taken for these tests.

2.2 The Radial Temperature Profile Generator

2.2.1 Design Goals

The specific goal of the profile generator was to model the radial temperature profile generated by an actual combustor. Variations in the total pressure profile, while present in the combustor exit flow, were to be eliminated in this design to aid in isolating the effects of temperature profiles on heat transfer to the shroud. While both generation of circumferential temperature profiles and high level of turbulence would be beneficial, it was more important to

be able to hold these variables to constant values. Thus the creation of turbulence or circumferential variation were secondary design criteria.

To model the combustor profile, it was important to establish a non-dimensionalized measurement of the profiles so they could be scaled to the MIT facility. A typical combustor profile is shown in fig 2-3.

Figure 2-3
Typical Combustor Profile
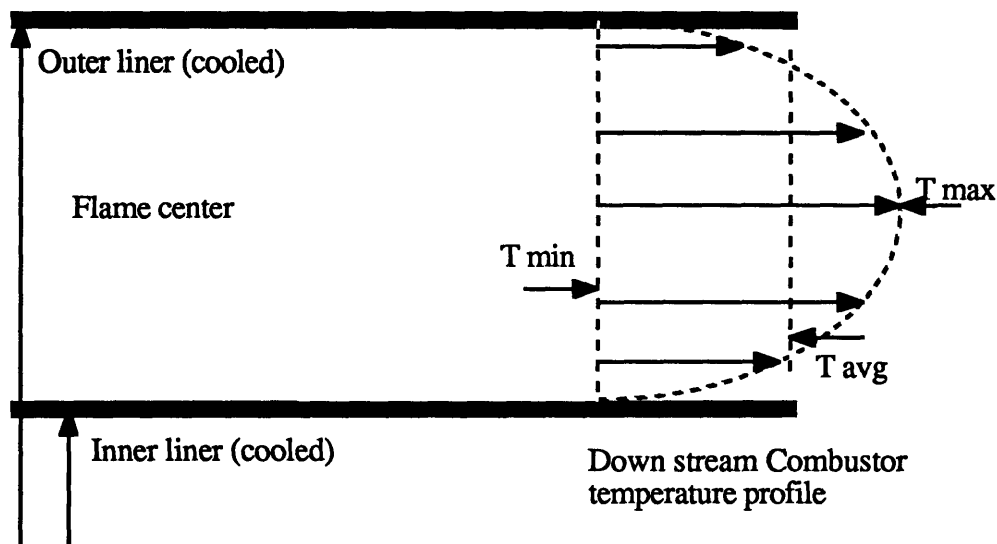
The maximum temperature occurs near the center of the passage while the minimum temperature occurs on the walls which are generally cooled. A non-dimensional description of this profile is the Radial Temperature Distribution Factor (RTDF) which is defined as:

$$RTDF = \frac{T_{Max}-T_{Mean}}{T_{Ref}}$$

(1)

T_{max} is the maximum temperature of the fluid leaving the combustor, T_{mean} is some average of all the fluid leaving the combustor, and T_{ref} is a reference temperature used for normalization. Generally T_{mean} is a mass-averaged mean temperature and T_{ref} the combustor rise temperature. A good assumption is that the profile is parabolic in shape, given the geometry and the boundary conditions inside an engine; and the relation between the maximum, minimum and mean temperatures becomes:

$$T_{Max}-T_{Mean} = \frac{1}{3}*(T_{Max}-T_{Min})$$

(2)

Since profiles vary among different types of combustors, the nominal profile modeled was an RTDF of 8%. For this turbine the combustor rise temperature is approximately 1010 K which is scaled down for this facility and yields the appropriate maximum, minimum and average temperatures for any profile under consideration. Typically for an 8% RTDF at 475 °K average temperature, the peak and minimum temperatures are 493 and 425 °K.

2.2.2 Possible Generator Configurations

Initially two fundamentally different types of generators were considered: an injection system and a storage matrix set-up. The main idea of the injector was to add either hot or cold, gas or liquid at the center of the annulus (or at different radial locations) to create the temperature gradient. The gas would be supplied from an outside source, probably another blowdown set-up in order to match the blowdown characteristics of the supply tank. This has many advantages. First by actually injecting another fluid into the main environment turbulence levels would increase. Another advantage would be that since the injected fluid would also be controlled by a blowdown process, one could match the blowdown time constants, making it easier to match the conditions throughout the test time. The difficulties in this approach occur in implementation. The supply tank needed would have to be large and there was little space for it. The cost, construction and running of another blowdown set-up were beyond the resources available. Also there was no way to guarantee uniform total pressure downstream of the injectors, which was important if the effects of the temperature profiles were to be isolated. From an analytical standpoint, altering the fundamental flow as little as possible was important and adding another fluid with a different temperature and thermal properties could only complicate the flow. Eventually the practical limitations of the injection scheme led to the idea of a storage heat exchanger.

A storage heat exchanger involves heating a metal matrix to a desired temperature profile before the test. During a test it transfers its energy to the fluid (see figure 2-4).

Figure 2-4
Possible Storage Heat Exchanger Configuration

Metal Storage Matrix

R outer

R inner

R outer and R inner to match MIT Facility

A

A

T min

Matrix Temperature Profile at location A-A

T max
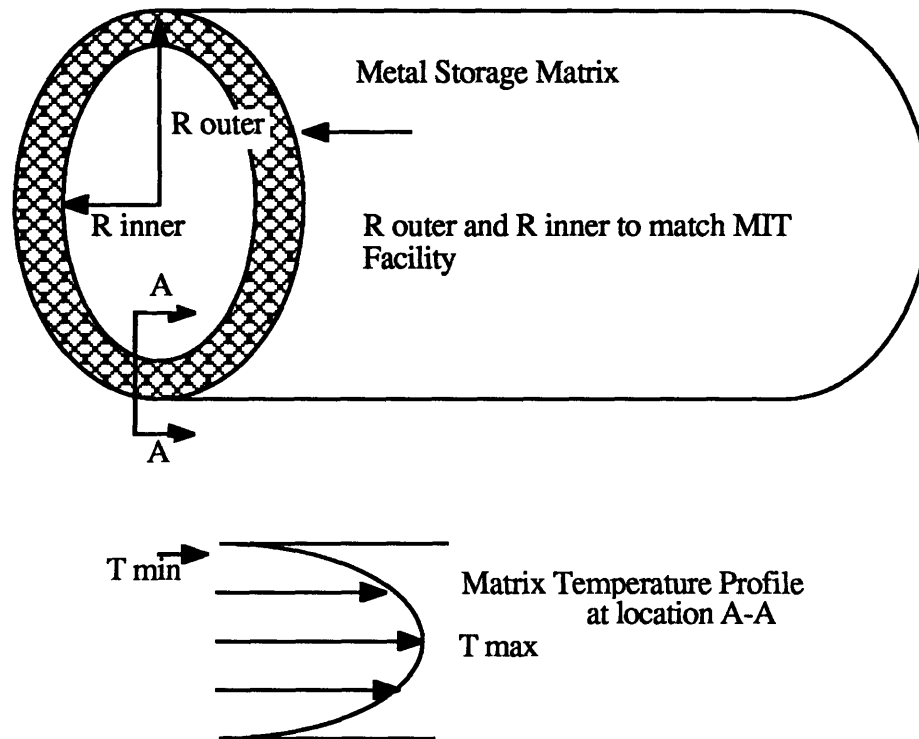
This device would fit between the fast acting valve and the test section, upstream of the boundary layer bleeds.

This generator would operate by heating the center with some type of heater (power in) and cooling the walls (power out). In this manner one can set the maximum temperature (at the heater) and the minimum temperature (at the walls) and obtain a profile. The trick in designing this system is not only to create enough energy storage so as to heat the fluid to the appropriate level for the entire test time, but also to ensure that it transfers its energy efficiently.

In this set-up the only thing added (or subtracted) to the flow is energy, therefore the facility can longer be described as isentropic, complicating the blowdown equations[2]. Storage heat exchangers also had the promising property of being able to split the design into two parts. The first problem was to ensure that the matrix could efficiently transfer its energy, and the second was to create the proper temperature profile in the matrix. But like the injector set-up, there were some disadvantages. Turbulence would have to be generated with another, separate device. Operation of the facility would be slightly harder since the flow entering the turbine would no longer have an isentropic temperature decay. This would cause problems in setting the eddy brake on the turbine, which keeps the corrected speed of the turbine constant. Despite

---

[2] See appendix A of "The Design of the MIT Blowdown Turbine Facility" MIT GTL report 183

the drawbacks, the storage type heat exchanger offered the best chance of success and was chosen as the profile generation system to be further studied.

Of course by choosing this system, one more design goal was created; the ability to operate in a steady state condition. This was purely a practical consideration to aid in running the facility. If the generator could hold a profile for only a few minutes, it would become quite difficult to coordinate all the equipment before a test. The desire was to be able to set the profile, and then leave the generator alone in the final half an hour before the test, when the instrument calibrations are done, without worrying about a changing profile.

2.2.3 Temperature and Heat Transfer Limitations

The testing envelope, created by the MIT facility imposed the bounds on the total heat transfer which would be needed by the generator and the materials which could be used. Since the total heat transfer rate needed in this experiment is given by

$$q=mC_p\Delta T_{avg} \tag{3}$$

where q is the heat transfer rate, m is the mass flow rate C_p is the specific heat of the gas and ΔT_{avg} is the temperature change in the gas.

Estimating the maximum ΔT needed yields the required power. The accurate representation is given by the integral from the inner to outer radius of the passage of the ΔT multiple by the mass flow rate (given as $2\pi r[\partial r]\rho$) as shown in equation 4. This reduces to (3) if ΔT is replaced by the mass averaged ΔT_{avg}.

$$q=C_p\rho 2\pi \int_{R_i}^{R_0} \Delta T_r \ r \ dr \tag{4}$$

A worst case analysis would be if the gas had to be raised from room temperature to the peak operating temperature of the facility 533 °K. Then ΔT would be 233 °K and q=2.9 Mw. The nominal profile for the combustor associated with the ACE rotor of 8% implies for this facility a ΔT =67 °K or q=.86 Mw

In addition to the ultimate power levels needed, the high operating temperature of the facility indicated that aluminum could not be used for structural reasons (a large fraction of its strength is lost at these elevated temperatures). Since temperature variations of the order of a 100 °K would have to be maintained over a 2" gap, a low thermally conductive metal was needed; eliminating copper and other similar metals. The metal which was most commercially available that fit the required needs of strength and thermal conductivity was stainless steel.

Using stainless steel as the matrix material imposed a maximum metal thickness on the matrix. The thermal diffusivity of stainless steel is approximately 3.5×10^{-6} (M^2/sec) which coupled with a .5 sec test time implies a thermal wave propagation length of .053". Thus the matrix could not be any thicker than twice this length, or .106" since any part of the matrix which is more than .053" from the gas path would not contribute to the heating of the gas during the test time and only add to the flow blockage.

2.2.4 Analytic Modeling of the Profile Generator

Modeling the heat exchanger basically involved four distinct problems: 1) The problem of transferring the heat from the metal to the fluid. 2) Predicting the pressure drop which would occur across the exchanger. 3) Estimating the thermal conductivity of the matrix. 4) Designing the cooling jackets to pull the heat out of the matrix, to ensure a steady state environment.

2.2.4.1 Heat Transfer Modeling

Creating an analytical model for a storage heat exchanger to use in evaluating the performance of the many different construction possibilities was the first step. The energy transfer between the metal storage system and the gas can be modeled as a system in which energy flows into a control volume from the surrounding metal. A diagram is given in figure 2-5.

Figure 2-5
Passive Heat Exchanger Model
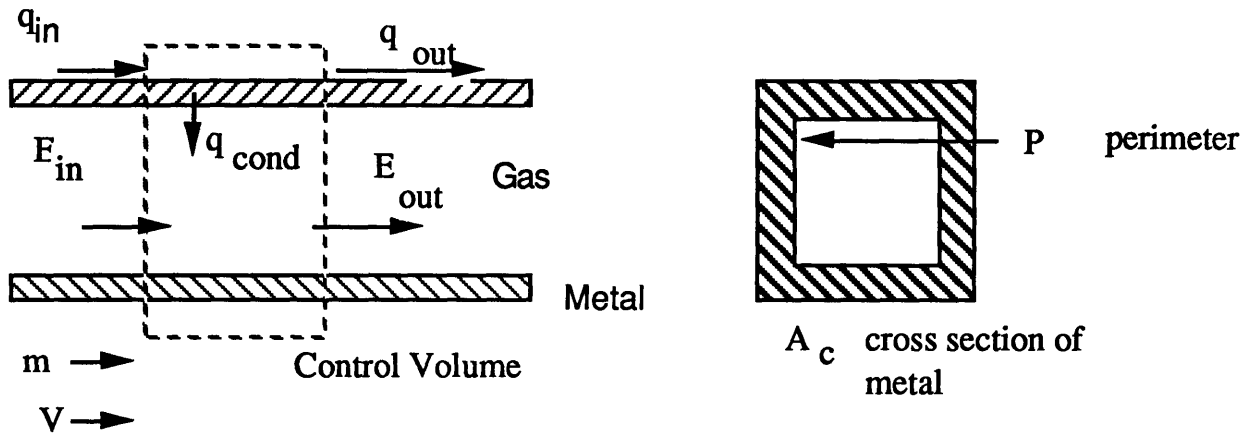
By setting up a time rate of change for the energy balance for both the metal and the gas reduces to eqn 5 (metal) and eqn 6 (gas).

$$\partial T_m/\partial t = -h\,P\,(\,T_m\text{-}T_f)/(\rho_m\,A_c Cp_m) - K_m/\,(\rho_m\,Cp_m)\,\partial^2 T_m/\partial x^2 \tag{5}$$

$$\partial T_f/\partial x = h\,P\,(\,T_m\text{-}T_f)/(m\,Cp_f) - (1/\,V)\,\partial T_f/\partial t \tag{6}$$

where:

$T_m(t)$ is the metal temperature	$T_f(t)$ is the fluid temperature
P is the perimeter of the tube	m is the mass flow rate
h is the heat transfer coefficient	A_c is the metal cross section
ρ_m is the metal density	Cp_m is the heat capacity of the metal
Cp_f is the heat capacity of the fluid	V is the velocity of the fluid
t is the time	x is the distance along the tube

Besides the fluid and metal temperatures which vary with time, the mass flow rate decreases with time (since the temperature of the supply gas drops). However in this analysis only the initial mass flow rate is important since it provides an upper limit on the heat transfer needed.

Characteristic length scales (λ) and time scales (τ) for these equations can be derived from the underlying heat transfer which is occurring. If λ and τ are given as follows:

$$\lambda = m\,Cp_f/h\,P \qquad\qquad \tau = \rho_m\,A_c\,Cp_m/h\,P$$

then λ represents the ratio of the energy needed to heat the flow (m Cp_f) over the heat transferred per length of tubing (hP). And τ is the ratio of the energy stored in the metal (ρ_m A_c Cp_m) to the speed at which energy is transferred (hP, just another way of looking at this combination of variables). Non-dimensional gas and metal temperatures can be defined as:

$$\theta = (T_f - T_{f0})/(T_{m0} - T_{f0}) \quad \text{(gas)} \qquad\qquad \emptyset = (T_m - T_{f0})/(T_{m0} - T_{f0}) \quad \text{(metal)}$$

In this case these variables represent ratios of the actual temperature at any time, minus an initial temperature to the initial difference between metal and gas temperatures. This allows $\emptyset$ to go from 1 (at the start) down towards zero and θ to go from zero towards one. Using these variables along with non-dimensional versions of time and length:

$$t^* = t/\tau \qquad\qquad x^* = x/\lambda$$

one arrives at non-dimensional versions of eqns. 5 and 6.

$$\partial\emptyset/\partial t^* = -K_m \tau/(\lambda^2 \rho_m C_{pm}) \partial^2\emptyset/\partial x^{*2} - (\emptyset - \theta) \qquad \text{Metal} \qquad (7)$$

$$\partial\theta/\partial x^* = -\lambda/(v \tau) \partial\theta/\partial t^* + (\emptyset - \theta) \qquad \text{Fluid} \qquad (8)$$

For equation 7, using typical values for stainless steel $K_m = 15$ W/(M-K) $\rho_m = 8000$ Kg/M^3 and $C_{pm} = 460$ J/(Kg-K) one finds that as long as τ/λ^2 is less than about 10^4 (sec/M^2) the $\partial^2\emptyset/\partial x^{*2}$ can be ignored. Similarly if $\lambda/(v \tau)$ remains below 10^{-2} then the $\partial\theta/\partial t^*$ term in eqn. 8 can be ignored. Dropping these terms for now[3] the final representation of eqns 5 and 6 are:

$$\partial\emptyset/\partial t^* = -(\emptyset - \theta) \qquad \text{Metal} \qquad (9)$$

$$\partial\theta/\partial x^* = (\emptyset - \theta) \qquad \text{Fluid} \qquad (10)$$

These equations imply that the time rate of change of the metal temperature is equal to the negative of the axial rate of change for the fluid temperature (taking the proper dimensionalizations into account). By using these variables, knowledge of the particular profile being studied is immaterial since initial gas-metal temperature differences are normalized away. The solutions to equations 9 and 10, in terms of $\emptyset$ and θ, can be written as functions of t* and x* and are shown in figures 2-6 and 2-7. Figure 2-6 shows the non-dimensionalized gas temperature θ as a function of non-dimensional length x* at different non-dimensional times t*. Similarly, figure 2-7 shows the decay in gas temperature at any given length over time. Thus by calculating the characteristic length and time one can set overall parameters such as total length or percentage of initial temperature at end of run to find the performance of any particular design. This completely separates the design problems involving how heat is transferred to the matrix from those involving how to create the proper profile in the matrix.

---

[3] These conditions are checked after the characteristic lengths and times are calculated for each design.

2.2.4.2 Pressure Loss Modeling

In the storage matrix heat exchanger, there are three main mechanisms by which pressure is lost. Loss of the dynamic head (or fraction of it) when entering and exiting the flow, friction losses in the tubes and losses due to heating. These three losses are compared on an order of magnitude basis.

Using figure 2-8 as an example of the flow through the matrix, the dynamic head, $\rho_0 V^2$, depends on the initial pressure and γ (ratio of specific heats) of the gas in the supply tank , since the Mach number upstream of the the generator is fixed by the area ratios. For the MIT facility the upstream area is 238.76 in^2 and the choked area is 30.192 in ^{2} (this takes into account both the choked nozzle guide vane area; 22.03 in^2, and the choked area of the boundary layer bleeds; 8.162 in^2, which is important since a third of the mass flow through the exchanger will end up in the boundary layer bleeds). This implies a Mach number upstream of .074. Since V^2 can be written as:

$$V^2 = M^2 C^2 \text{ (Mach number and speed of sound)} \tag{11}$$

using the ideal gas law the pressure P:

$$P = \rho R T \tag{12}$$

one can rewrite the dynamic head as:

$$\rho_0 V^2 = \frac{P}{RT} \gamma R T M^2 = P \gamma M^2 \tag{13}$$

Where γ is the ratio of specific heats, R the gas constant and T , the temperature

Using typical test pressures of 70 psia and γ of 1.286 the typical dynamic head is .493 psi.

Figure 2-8
Geometry of Exchanger Used for Pressure Loss Modeling

$A_2 = (1- \text{Blockage})* A_1$

A *

NOT DRAWN TO
SCALE

A_1

Station 1

Station 2

Cross section of tube

L

M
V
T

M
V
T

Blow up of Tube
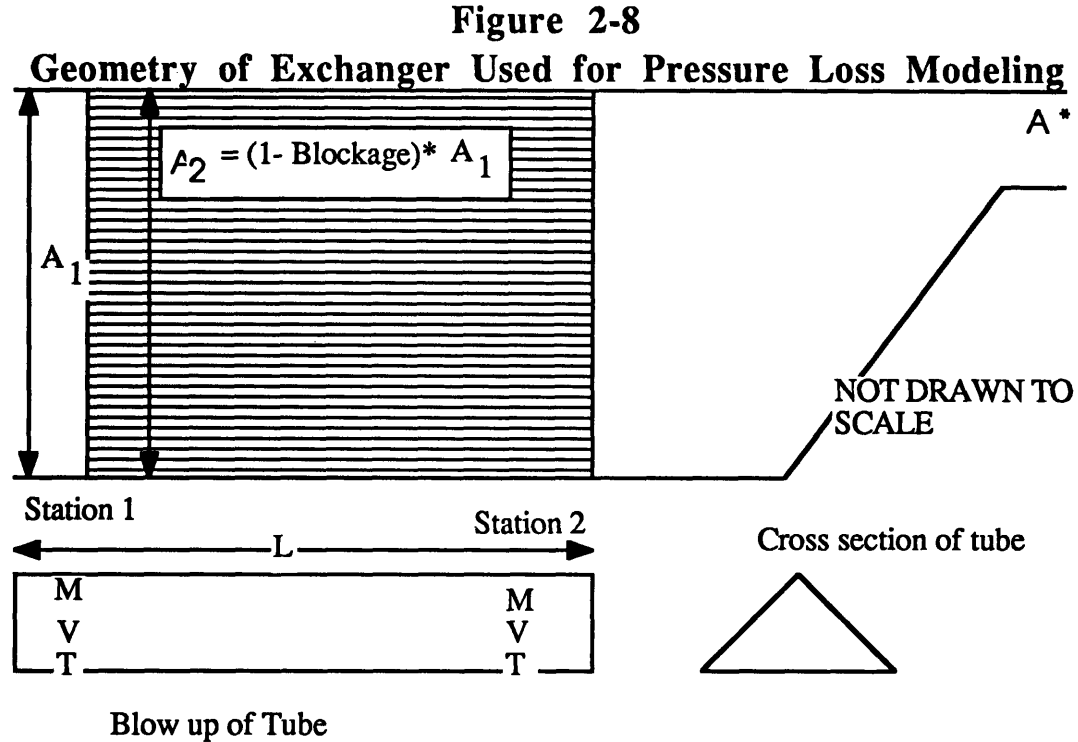
Estimating the friction loss in the pipes is harder since friction factors are based on tube Reynolds number (based on hydraulic diameter, D^4) and the ratio of roughness to hydraulic diameter (e/D), both of which could vary between different designs. The pressure loss in a pipe due to friction is given by:

$$\Delta P = \rho f \frac{L}{D} \frac{V^2}{2} \tag{14}$$

Using the continuity equation and assuming that the densities do not change, the velocity in the tube can be related to the upstream velocity by:

Continuity: $(AV)_1 = (AV)_2$ thus $V_2 = V_1 \frac{A_1}{A_2}$ (15)

If the total area in the matrix is given as a percentage of the initial area then:

$$A_2 = (1-P)A_1 \tag{16}$$

where P is the fraction blocked off by the metal matrix

Rewriting eqn 14 in terms of the upstream velocity and the blockage the pressure drop becomes:

$$\Delta P = \rho f \frac{L}{D} \frac{V_1^2}{2} \frac{1}{(1-P)^2} \tag{17}$$

Equation 17 represents the dynamic head loss multiplied by a constant.

---

4 The hydraulic diameter (or D=4* A/P   where A is the cross sectional flow area of the tube and P is the perimeter) was used to compare different shaped tubes

The last mechanism through which pressure can be lost is through heat addition to the flow. Examining a control area which encompasses only the tubes so that station one is at the beginning and station two at the end, the linear momentum equation gives the pressure loss from station 1 to 2 as:

$$\Delta P = (\rho V^2)_2 - (\rho V^2)_1 \tag{18}$$

From continuity:

$$(\rho VA)_1 = (\rho VA)_2 \tag{19}$$

Since the areas are the same, the Mach numbers will be the same, but the speed of sound

$$C = \sqrt{\gamma RT} \tag{20}$$

will be different. Writing ρ_2 as a function of the upstream conditions and V_2 as a function of the Mach number and the speed of sound, the pressure drop can be found to be

$$\Delta P = (\rho V^2)_1 \, (\sqrt{(T_2/T_1)} - 1) \tag{21}$$

For peak values of T_2 of 550 °K and low values of T_1 at 300 °K this term is approximately a third of a dynamic head.

The total pressure loss in the generator depends on parameters which can vary greatly during manufacturing; the roughness of the tubes and the inlet and exit flow coefficients. Since the friction factor could vary by a factor of three from a smooth tube to a rough one, the constant in equation 17 is probably in the range of five to thirty (depending on the specific L/D) dynamic head losses. Since the dynamic head is approximately .5 psi (equation 13), pressure losses of up to 15 psi could be encountered. Since the dynamic head is small, there is latitude for variation in construction.

2.2.4.3 Modeling the Thermal Conductivity

In order to calculate the steady state power needs to create a profile in the matrix, the thermal conductivity of the matrix had to be calculated. Figure 2-9 shows the model used for calculating the effective thermal conductivity of one type of matrix, the triangular tube system. The methodology would be the same for any other type of matrix configuration (round, square, etc.) only the geometry would change.

Figure 2-9
Effective Thermal Conductivity Model
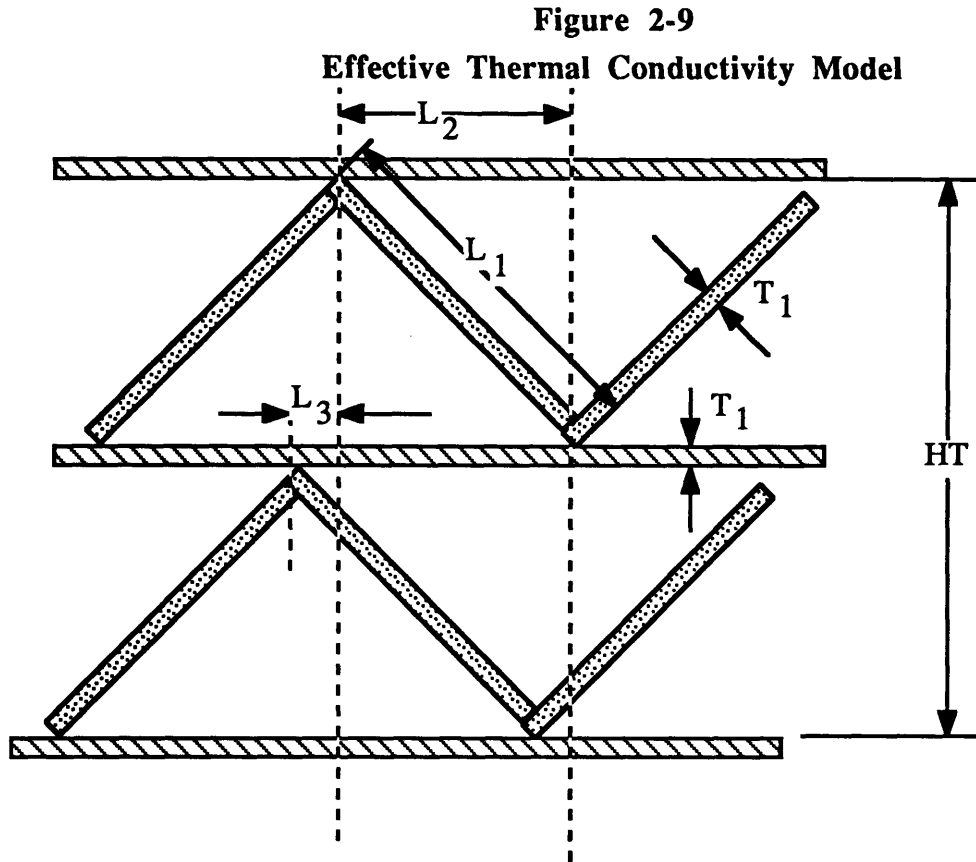
The basic idea is to calculate the resistance path that heat travels through the matrix and equated with a slab of imaginary metal of similar size, but different thermal conductivity.

$$R_t = \frac{L_1 N}{k_s A} + F(\frac{N T_1}{k_s A} , \frac{L_3}{k_s A})$$ Thermal resistance path   (22)

where: N= number of layers k_s= Thermal Conductivity of Stainless (14.9 W/[m-K])
A= Cross sectional area of metal

Equation four translates into the resistance path = resistance in the matrix + a function of the resistance across separators and the length in the separators due to mis-alignment. By assuming no misalignment (i.e. L_3 goes to zero) $k_{effective}$ is maximized therefore This maximizing q, giving a worst case scenario. In this case R_t becomes:

$$R_t = \frac{L_1 N}{k_s A} + \frac{N T_1}{k_s A}$$ (23)

Where it is assumed that the cross sectional area of the spacers is the same as matrix layers To find the effective thermal conductivity R_t is equated to equation (24)

$$R_{te} = \frac{HT}{k L_2 L_t}$$ (24)

Where L_2 is the equivalent length over which R_t was analyzed and L_t= length of heat exchanger, thus $A=L_tT_1$

For this case L_t=20" or .508 m, L_1= .125", T_1=.01", and $L_2= \frac{L_1}{\sqrt{2}}$, $\frac{HT}{N}=T_1 + \frac{L_1}{\sqrt{2}}$ and it reduces to:

$$k_{effective}= \frac{[\frac{L_1}{T_1} + \sqrt{2}]k}{[\frac{L_1}{T_1} + 1]\frac{L_1}{T_1}} = 1.22 \text{ W/[m-m-K]} \tag{25}$$

2.2.4.4 Modeling the Cooling Jackets

To dissipate the energy in the matrix, cooling jackets had to be designed for both the inner and outer walls. To make the jackets as simple and as versatile as possible they were designed to use either city water which flows at about 10 Gal/min (.63 Kg/sec) or as a backup, oil from the oil heating system used to heat the supply tank[5]. In order to create a system which would stand up to any condition, a worst case scenario was created where the flow in the cooling jackets would be considered laminar, fully developed with constant wall temperatures, and the maximum temperature drop from center to annulus would be 250 °C. For these conditions the Nusselt number would take on the low value of 3.66 and the convective heat transfer rate would be given by:

$$h = \frac{Nu \ k_f}{D_h} \qquad k_f=.631 \text{ W/[m-K]} \qquad D_h=.00635 \text{ m} \tag{26}$$

Yielding: h=363 w/[m-m-K]

D_h is the hydraulic diameter for the jackets and k_f is the thermal conductivity of water.

To find the worst case heat loads on the cooling jackets the steady-state conduction equation has to be solved for both the inner and outer annulus as shown in figure 2-10.

---

[5] "The Design of the MIT Blowdown Turbine Facility" MIT GTL report 183

Figure 2-10
Worst Case Scenario for Cooling Jackets
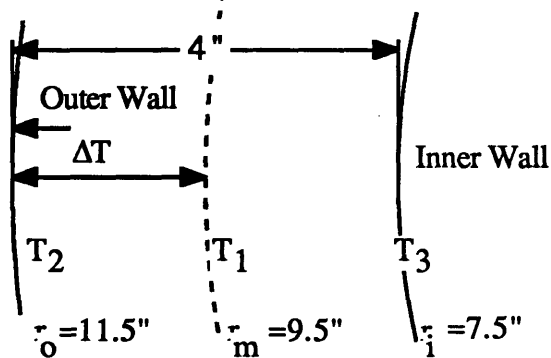
Steady-state conduction equation from midpoint to wall location is given by:

$$\frac{1}{r}\frac{\partial}{\partial r}(kr\frac{\partial T}{\partial r})=0 \qquad (27)$$

which has as its solution:

$$T(r)=C_1 \ln(r) + C_2 \qquad (28)$$

Solving for the flow heat flow to the outside and inside walls:

$$q(r)=\frac{2\pi Lk(T_1-T_2)}{\ln(\frac{r_o}{r_m})} \quad \text{For Outer section} \qquad q(r)=\frac{2\pi Lk(T_1-T_3)}{\ln(\frac{r_i}{r_m})} \quad \text{for Inner section} \qquad (29)$$

For the triangular matrix, $k_{effective}$ can be used to find q_{total}, q_{in}, and q_{out} for the worst case :

$$q_{in} = 4.125 \text{ Kw} \qquad q_{out} = 5.096 \text{ Kw} \qquad q_{total} = 9.2 \text{ Kw}$$

Given that A_o = .932 m² and A_i =.608 m² then q''_{out} = 5.46 Kw/m² and q''_{in} = 6.8 Kw/m² .

If the walls are at 550 °C (823 °K) and the water comes into the jacket at 300 °K then the maximum heat transfer that the water would have to absorb (does not account for temperature drop across wall of matrix) is:

$$q_{water}=m_{water} \; C_p \; \Delta T \qquad (30)$$

where m_{water} = mass flow of water (.6308 Kg/sec), C_p = specific heat of water (4.18 KJ/Kg-K). This implies that the temperature increase in the water is:

$$\Delta T=5096/.6308 \; 4180 \Leftrightarrow \Delta T= 2 \text{ °K} \qquad (31)$$

And at the lowest limit of h (363 w/[m²k]) the q''_{in} is achieved if ΔT from wall to water is bigger than 20 °K. This implies that the cooling jackets, given reasonable thermal connections to the matrix, should be able to extract the power used during the experiment. In order to obtain more turbulent flow, pins (basically obstructions placed between the outer wall of the

matrix and the cooling jacket) were inserted for the dual purpose of breaking up the flow and supporting the outer cooling jacket from being crushed (see appendix I, The Radial Temperature Profile Generator Drawings).

2.2.5 Possible Storage Heat Exchanger Configurations

Using the analytical models, different possible configurations were explored, sent to manufactures for comments, and compared. What developed were mechanical and practical limitations on what could be manufactured which had to be addressed, as well as the analytical constraints. The most restrictive was the availability of stamped stainless steel since manufacturing operations do not allow thickness to length ratios to be larger than 1/10.

The original ideal was to place thin film heaters in between arbitrarily shaped matrix elements (see figure 2-11).

Figure 2-11
Original Idea for Heater Matrix, Thin Film Heating Elements

Thin Film heater
with Mica insulation
on both sides to avoid
electrical shorts

Heating matrix with
$t/L < .1$
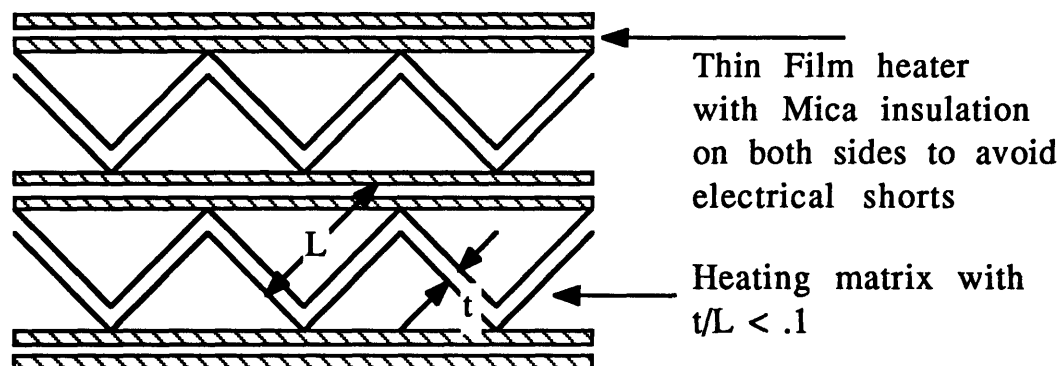
This would allow for accurate control of the temperature, both radially and circumferential, but the frontal blockage to heat transfer surface was high, leading to long heat exchangers and hefty pressure losses. In addition, there was the practical problem of creating the matrix so that it could be disassembled to replace the heaters and insure good thermal contact during heat-up (in a vacuum).

Two other configurations: brazed tubes and a wrapped matrix, both of which would be powered by a heater wire in the center, were more promising. The brazed tube configuration was just that, a whole series of tubes furnace brazed together to provide the heating matrix. This had a large advantage in that the thickness to length (or in the tubes case, diameter) was not fixed at being less than .1. However it used many fewer tubes, resulting in a longer overall

matrix. The wrapped matrix was a sandwich of a shaped piece of stainless between two flat pieces. Wrapped from the inner wall to the outer wall in a spiral configuration and then furnace brazed together.

Both of these systems had a variety of different sizes which could be constructed. Table 2-2 gives a comparison of the two best designs (in terms of manufacturability and meeting design criteria) from each system.

Table 2-2[6]
Design Comparison of Wrapped Matrix and Brazed Tubes

	Wrapped Matrix	Brazed Tubes
Characteristic Length λ	4.32"	16.25"
Characteristic Time τ	.675 Sec	4.16 Sec
Effective Thermal k_{eff} conductivity	1.22 w/[m^{2}K]	1.54 w/[m^{2}K]
Length of Matrix	20"	36"
Number of Tubes	28,308	4,304
Tube Wall Thickness	.01"	.028"
Hydraulic Diameter	.067"	.194"

There was an overall maximum length associated with the profile generator due to physical limitations in the facility of around 3 feet. Given the nature of the problem, the shorter characteristic length of the wrapped matrix allowed a greater margin of error in fabrication since the largest value of x^* (see figure 2-6) could be around 2 for the brazed tube configuration, but for the wrapped matrix, x^* of 4.5 could be achieved in just twenty inches, reducing the overall cost of the project considerably. The final decision was to use the wrapped matrix shown in figure 2-12. The temperature versus time trace at the end of the matrix (20 ") is shown in figure 2-13 with the final efficiency at a little over 95%

2.2.6 The Input Power

With the final matrix configured and the cooling jackets designed, the last part of the generator had to be specified: the heater wire. The matrix was broken into three circumferential sectors, each powered by one phase of a three phase 208 VAC, 30 Amp line. This allowed the

---

[6] One can check these values of the characteristic time and length against the conditions set-up in the analytical section and see that the assumptions allowing the dismissal of the second order terms exist.

matrix to be heated to three different patterns, if desired, which provided some degree of circumferential variation. It also reduced the amount of rewiring which would be necessary if the heater wire failed. The main limit in selecting the heater wire was the expected sheath temperature which translates directly to the power density (Watts supplied/surface area). When the wire is in good thermal contact with the surrounding metal, the power density can be significantly higher than when the wire is in a vacuum since the energy which would raise the temperature of the sheath above its melting point is conducted away. The wire would be woven through the matrix the appropriate number of times to give the proper total resistance and maximum allowable power density. Since parts of the wire are exposed to the vacuum (where the wire is looped back into the matrix), the length of the wire had to be such that the total surface area of the wire was large enough to lower the power density to below the melting point of the wire in vacuum.The heater wire decided on was an ARi manufactured wire shown in figure 2-14.

Figure 2-14
Cross-section of ARi Heater Wire

Inconel Sheath

Two heater wires

MgO_2 insulation
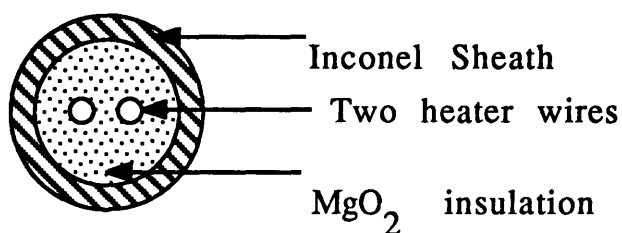
Properties of Heater Wire (joined in Parallel)

Resistance: .102 Ohms/ft   Diameter: .114" (originally it had been .125" and .045
Ohms/ft)
Perimeter: .358"

To obtain the proper peak power levels without increasing the power density levels beyond the limitations of the wires, the wire was quite long, ultimately being fed through every other tube. The final power connections are shown in table 2-3.

Table 2-3
Power wiring (per sector at peak conditions)

Resistance of wire: .102 Ohms/ft   Total Resistance: 14.7 Ohms

Total length of wire in matrix: 21.75"   Length of wire in bends (avg): 2.5"

Voltage: 208 VAC

Sector	A	B	C
#tubes Available	102	98	99
Measured Resistance[7]	10.3 (ohms)	9.3 (ohms)	9.6 (ohms)
Peak Amps	20.2 A	22.4 A	21.6 A
Peak Power	4.2 Kw	4.6 Kw	4.5 Kw

(Note: In practice Voltages above 100 V were seldom used so power densities were in the range of 2.25 w/in^2 which would put the matrix temperature in the 500-600 °F range)

2.2.7 Final Design and Implementation

The final piece of hardware used in this experiment differed from the designed piece in that instead of being one continuous matrix 20 inches long, there were four separate matrices each five inches long and separated by a 3/4" gap. This was due to the inability of the manufacturer to make one continuous piece. The extra spacing between the matrices raised serious questions about the generators overall performance. The possibility existed for there to be a much greater loss of dynamic head since the flow entered and exited four matrices instead of just one. In addition, it was not known to what extent the flow would diffuse or mix in the spaces between the matrix.

There were also mechanical problems with the construction of the generator which had profound consequences on the experiment. There were significant gaps between the matrix and the walls which varied both circumferential and axially. This caused non-uniform conduction radially and produced circumferential wall temperature variations. In addition the thermal expansion coefficient of the brazing oxide and the metal are different. Every time the generator was heated up small particles of oxide would break-off and come down into the turbine and basically sand-blast the instrumentation. This phenomenon decreases every time the generator is run, but even after twenty tests, there was enough of an effect to destroy 57% of the top gauges on the tip casing. Unfortunately, due to time constraints the experiment had

---

[7] Measured at the power connector on the outside of the generator (average room temperature figures, resistance varies with matrix temperature)

to be run with the equipment as it arrived. The ability to either steam clean it or "pickle it' with acid was not available.

There are some limitations to the the operating temperatures of the RTDFG in the present set-up. The basic problem is that the bounds on the absolute driving temperature (the bulk temperature) are set at the high end by the highest operating temperature of the oil (around 500°F), and at the low end by the wall temperature of the highest RTDF run on a low bulk temperature run. This corresponds to a range of about 70 °K and is shown below in table 2-4.

Table 2-4
Temperature Limitations on RTDF

	RTDF		
	High 16%	Low 8%	None
Avg. Temp. 470	Peak=515 Min=381	Peak=493 Min=425	Peak=470 Min=470
[All Temps in K]			
Avg. Temp. 400	Peak=445 Min=310	Peak=423 Min=357	Peak=400 Min=400

The minimum temperature is the lower limit here. The wall temperature cannot be below room or city water temperature.

Here the average temp. is the limit since the oil cannot be heated much past this point (pipe insulation burns)

2.2.8 Actual Performance of the Temperature Profile Generator

The performance of the generator is relatively easy to characterize. The properties which are of interest are the total pressure drop across the device, the ability to create a desired temperature profile, and the ability to hold the profile over the test time. And despite the manufacturing problems with the generator, the device performed quite well. Tables 1-4 in appendix III show the response of the generator over the entire test matrix. To examine the performance of the generator in comparison to theory only two types of runs need to be examined, the no profile run and a high profile run[8]

---

[8] The two runs used as an example are Test120 and Test121

Thermally, as shown in figure 2-13, at 400 ms the design efficiency (i.e the the value of θ, the non-dimensional gas temperature) of the matrix was .954. The uniform profile run displays an efficiency which was a little lower, between .94 and .95. For the high profile run the efficiency was 1.01 on average and had some radial locations at 1.04 efficient. This seems highly unlikely and the problem probably resides in the instrumentation. The initial matrix temperature is suspect since the spatial resolution did not exist to resolve local hot spots in the matrix. In addition there are also limitations on the measurement accuracy due to the four separate matrices, which are not thermally linked together, except by the heating wire. Thus the no profile runs (Test 121, Test 124, and Test 130) probably provide the best estimate on thermal performances.

Overall the performance of the generator was quite close to prediction. The total pressure profiles after the generator as well as the pressure drop across it remains relatively stable over the entire test time. The average pressure fluctuates by only 6.9% of the test average for the high profile run. In the radial direction, the standard deviation for the total pressure rake was 1% of absolute measurements and the pressure drop across the generator corresponded to about 10.9 dynamic head losses. Table 2-5 shows the performance of the generator for the 375-400 ms time interval; more detailed tables are given in appendix III.

Table 2-5
Generator Performance During Test Sequence
Averaged from 375-400 ms

	Test 120	Test 121	Test 122	Test 124	Test 125	Test 126	Test 127	Test 130	Test 131
TT2	462.36	459.38	396.18	398.86	391.53	451.41	459.09	462.5	459.87
RTDF	17.2	.1	12.6	.0	6.7	8.5	7.4	.5	17.1
PT2	3.7103	3.5292	3.7024	3.5618	3.6388	3.6035	3.5985	3.4916	3.7344
--(R Var)	.027	.023	.027	.024	.024	.022	.024	.041	.020
--(T Var)	6.9	3.4	6.9	9.5	8.1	9.0	8.9	10.4	6.6
Press Drp	.330	.317	.323	.326	.317	.320	.324	.345	.315

Definitions:

TT2 Avg= Area average of the upstream temperature rake

RTDF= Based on area average T mean and the measured profile

PT2 = Area average of the pressure rake behind the generator (Turbine inlet total pressure) in Atm

--(R var) = Radial variation of total pressure averaged over 375-400 ms. Standard deviation of all rake sensor measurements (Atm)

--(T var) = Variation of average pressure over entire test time [200 -475 ms] (percent)

Press Drp = Pressure drop across generator (Atm)
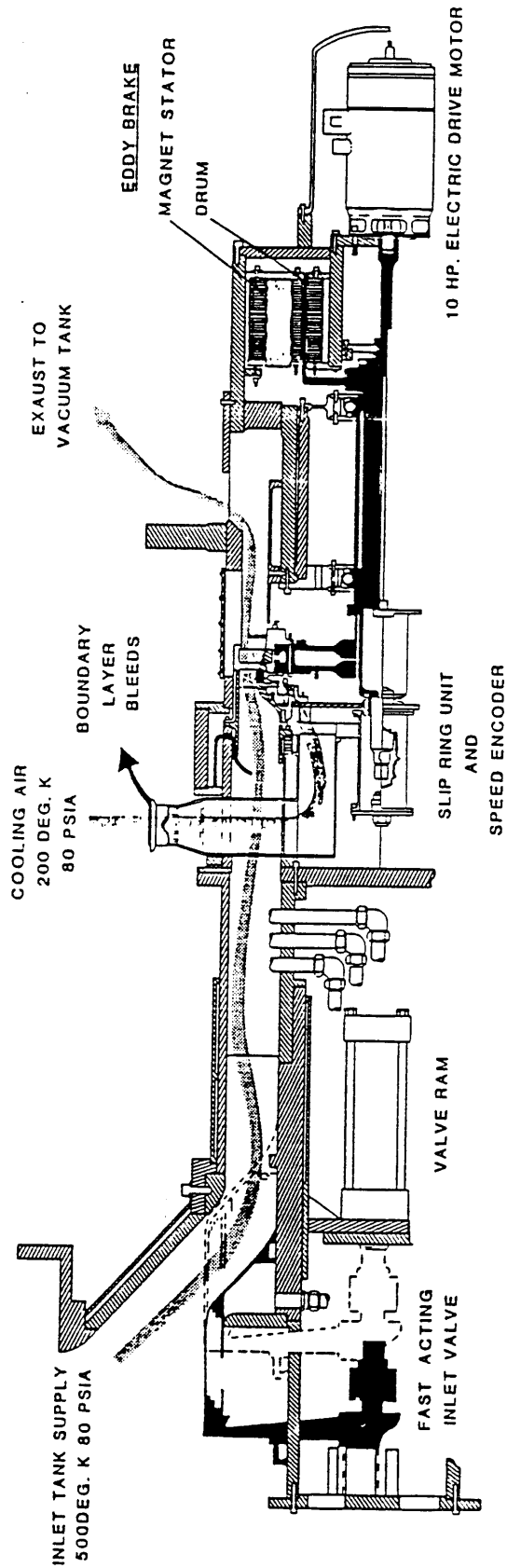
FIGURE 2-1: TURBINE FACILITY FLOW PATH

Guenette, Gerald " A Fully Scaled Short Duration Experiment", MIT PhD Thesis
August, 1985: p. 55

INLET TANK SUPPLY
500DEG. K 80 PSIA

COOLING AIR
200 DEG. K
80 PSIA

BOUNDARY
LAYER
BLEEDS

EXAUST TO
VACUUM TANK

EDDY BRAKE

MAGNET STATOR

DRUM

10 HP. ELECTRIC DRIVE MOTOR

SLIP RING UNIT
AND
SPEED ENCODER

VALVE RAM

FAST ACTING
INLET VALVE
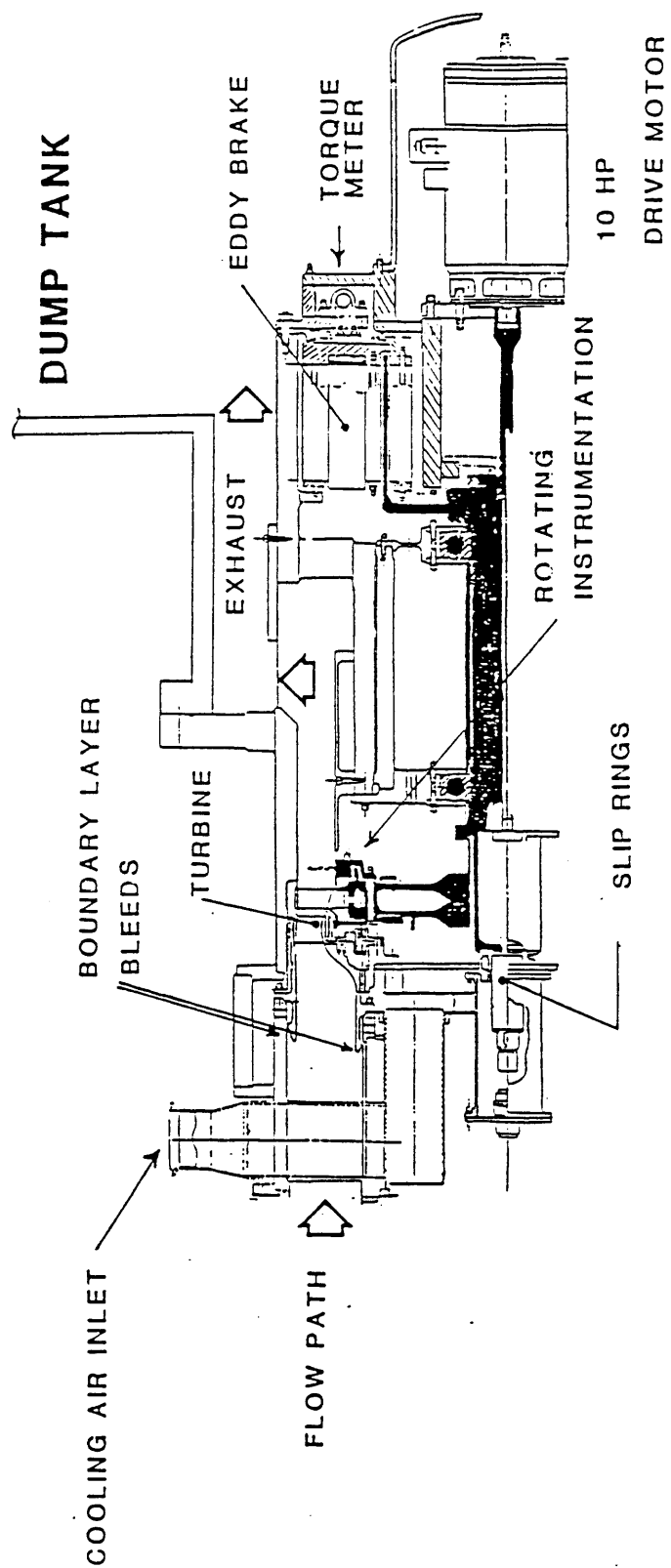
FIGURE 2-2: TEST SECTION DETAIL

Guenette, " A Fully Scaled Short Duration Experiment", p. 56

FIGURE 2-6: GAS TEMP VS AXIAL LENGTH (NONDIMENSIONALIZED)

NONDIMENSIONAL GAS TEMPERATURE Θ

NONDIMENSIONAL LENGTH X*

INCREASING T* FROM 0 TO 6, .5 INCR

41
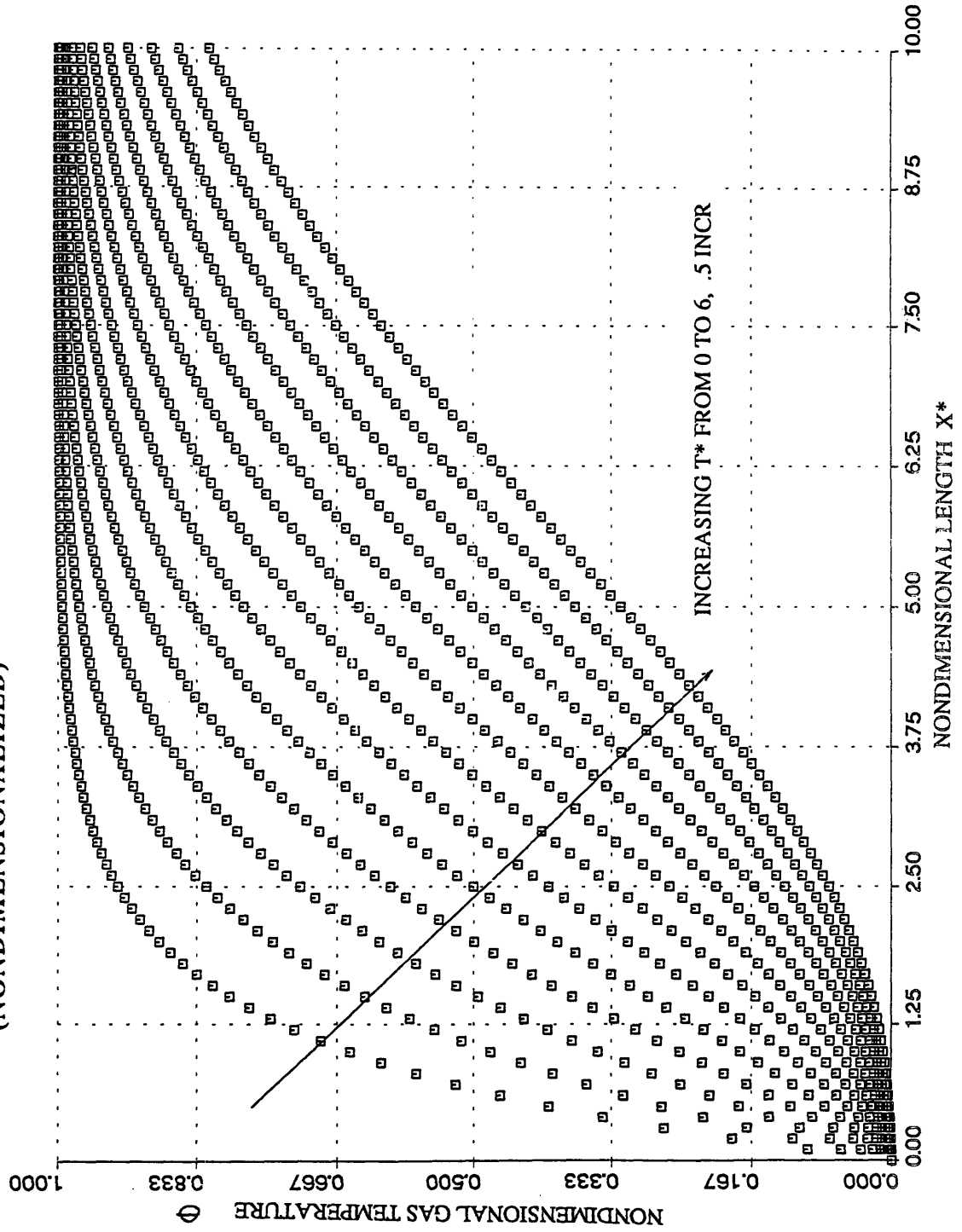
FIGURE 2-7: GAS TEMP VS TIME (NONDIMENSIONALIZED)

NONDIMENSIONAL TIME t *

NONDIMENSIONAL GAS TEMP θ

INCREASING X* FROM 2 TO 10, 2 INCR

42
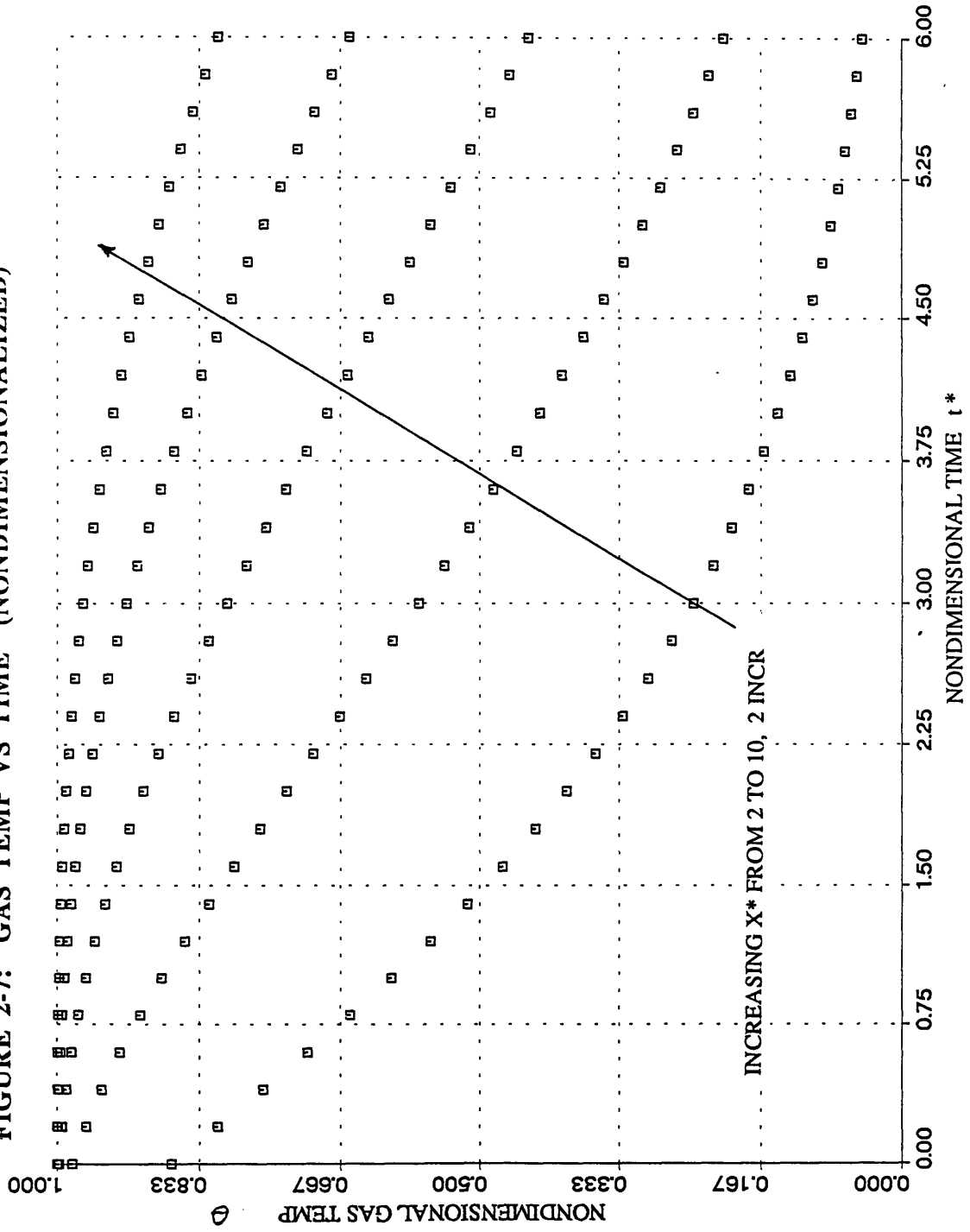
Figure 2-12 Final Heater Matrix Configuration (All dimensions in inches, Material: Stainless Steel)

scale .10 to 1

Approx. 43 layers total in matrix. Manufactured by wrapping alternate layers bent and straight pieces and brazing all at once

Center Matrix for Heater Wire (This one layer is continous along the length of the heat exchanger)

.01

.01

.125

.01

.250

43
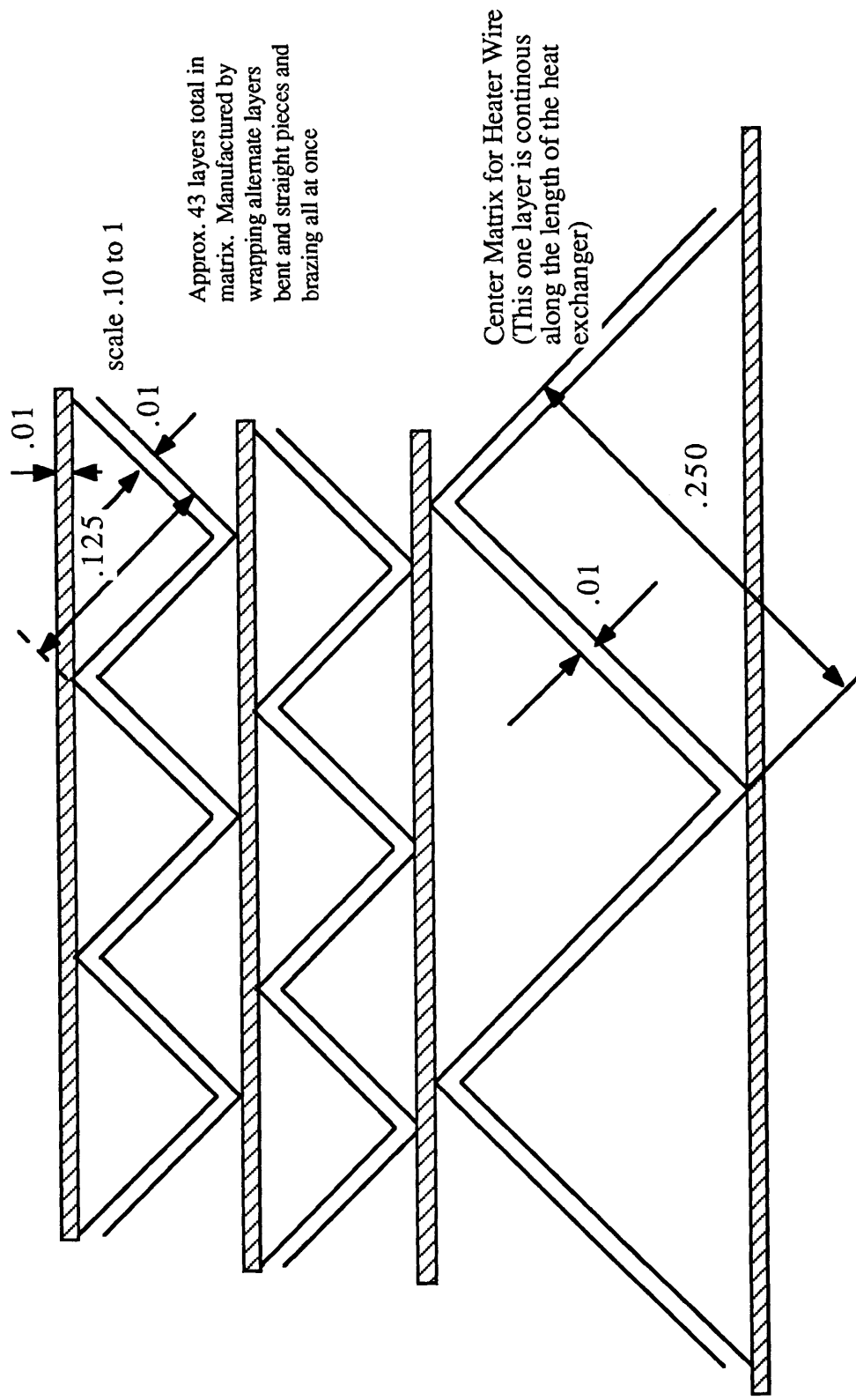
FIGURE 2-13: NONDIMENSIONAL GAS TEMPERATURE VS
TIME AT X*=4.6296 (20 INCH LONG MATRIX)

44
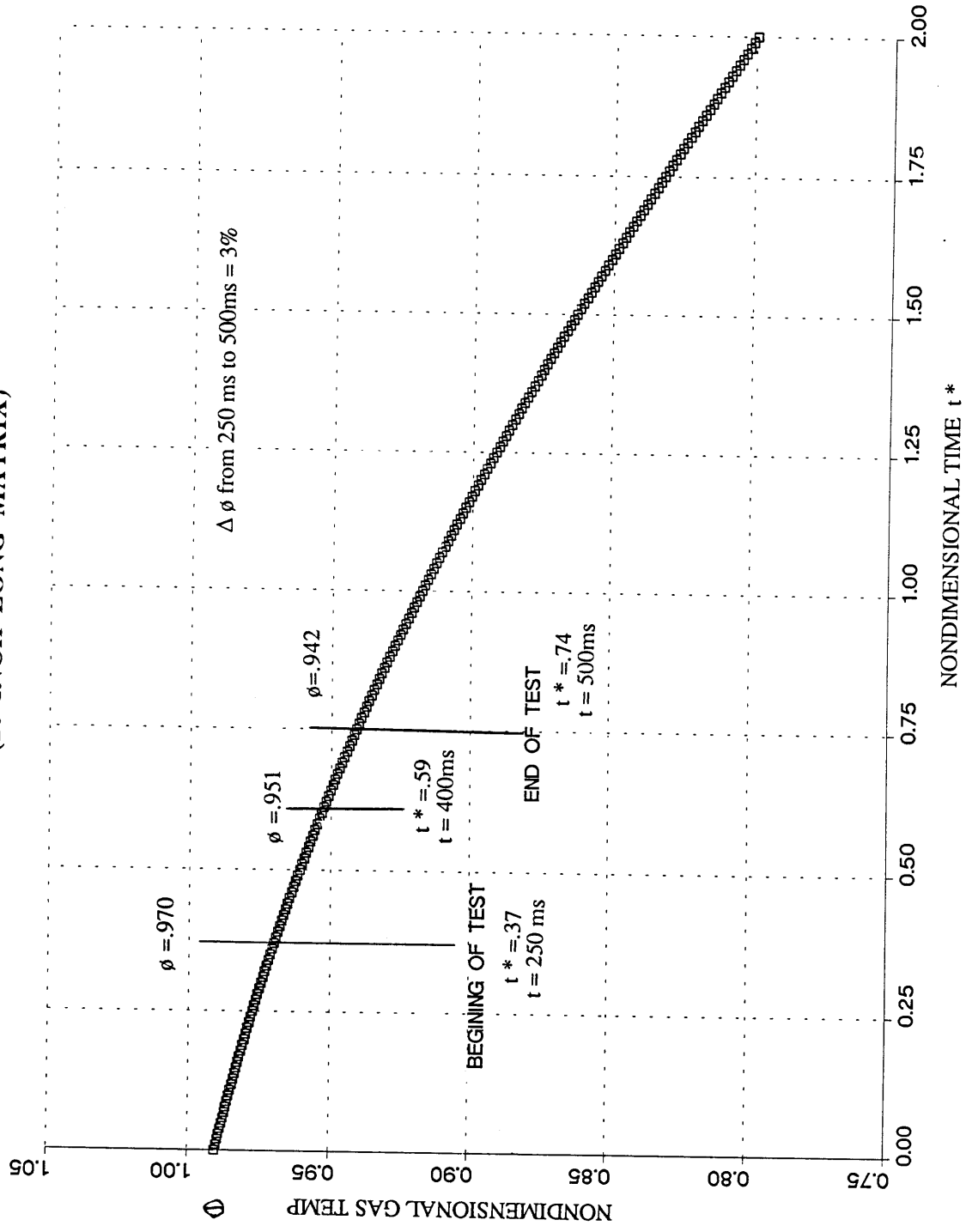
Chapter 3 Instrumentation

As mentioned earlier, this experiment is designed to explore the effects of a radial inlet temperature profile on tip shroud heat transfer. The three variables under investigation, total average temperature, temperature profile, and tip clearance all need to be measured during the tests. To accomplish this three groups of instrumentation were required: the facility aero-instrumentation, the instrumented tip shroud, and finally, the tip clearance device.

3.1 Facility Instrumentation

The MIT facility has instrumentation to measure pressure and temperature in the supply tank, the rotor speed, and downstream pressure measurements at various locations[1]. In addition to the facility instrumentation which was used to define the conditions of the flow entering the generator; the total temperature and pressure rakes, designed and modeled previously at the Gas Turbine Lab[2], were used to characterize the flow entering the nozzle guide vanes. Figures 3-1 to 3-4 show, respectively, the upstream and downstream location for the measurements, and the geometry of the respective probes.

The upstream total pressure rake was used to measure the variation in total pressure aft of the generator, the total temperature rake measured the actual profile produced, and the downstream pressure rake was used to measure the overall pressure drop across the turbine stage. The upstream pressure rake, with six transducers was designed to specifically measure the inlet profile while the downstream rake with five sensors was designed to be insensitive to variations in flow angle. The total temperature probe has five sensor positions each measuring 20% of the total flow area. In this way, T_{mean} for the profile can be calculated as an area-averaged number which reduces to the numerical average of all the sensors on the rake. In addition the total temperature rake was designed to be heated to the expected average temperature to increase responsiveness of the probe. However, during these tests, this feature was not used so as not to create random errors caused by bad heating adjustments. Without using this feature, a systematic error of an increasing temperature of a few degrees over the test time was inserted. But since the rake measurements were used only to characterize the

---

[1] Epstein, Alan; Gerald Guenette and Rob Norton "The Design of the MIT Blowdown Turbine Facility" ; GTL report no. 183, April 1985

[2] Cattafesta, Lou. "An Experimental Investigation of the Effects of Inlet Radial Temperature Profiles on the Aerodynamic Performance of a Transonic Turbine Stage"; Master's thesis Aeronautical and Astronautical Department, MIT August 1988.

profile of several hundred degrees Kelvin ,the error which arose from this process was small compared to the error introduced through setting the run conditions.

3.2 Instrumented Tip Shroud

3.2.1 Background

The flow area under investigation is the gap between the turbine blades and the outer engine lining; the tip shroud. The position of the tip casing is shown in figure 3-5. The gap between the tip of the blade and the casing allows air to pass from the pressure side over the tip of the blade to the suction side, creating a loss in efficiency (fig 3-6). This gap is generally quite small; usually less than 1% of the blade span. For the ACE turbine stage studied the nominal gap was .8% of span (1.5" at leading edge) resulting in a nominal gap of .012".

Figure 3-5
Tip Casing Location
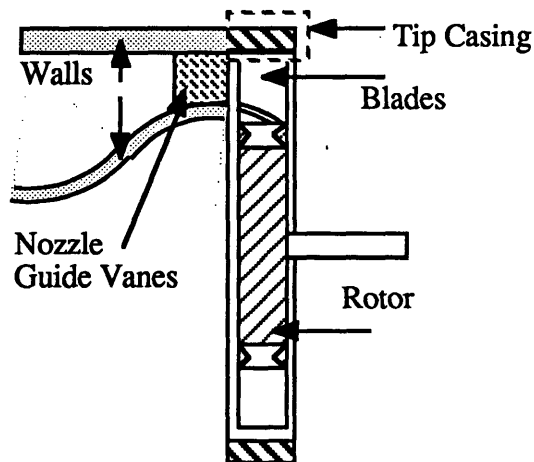
Figure 3-6
Tip Gap Flow Area

Walls
Tip Casing
Blades
Nozzle Guide Vanes
Rotor

Tip Casing

Flow direction (pressure side to suction side of blade)

Blade
Span at Leading Edge
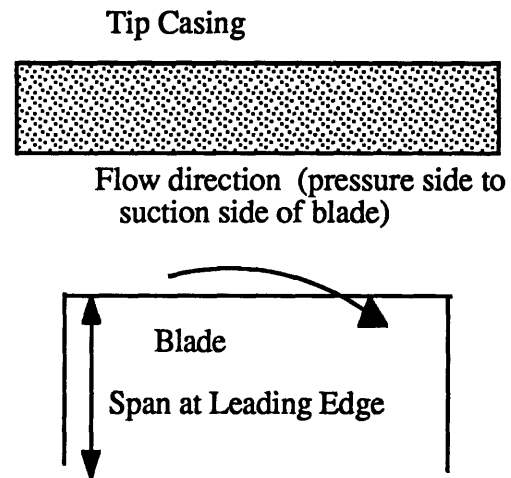
The MIT facility has two removable tip shrouds, 120 ° apart which can be instrumented. Figure 3-7 shows the basic dimensions of the shroud which spans four blades. There are two basic types of measurements which can be made on the shroud, static temperature and static pressure. To increase spatial coverage without increasing the amount of instrumentation required, the tip casing was to be rotated around center pins. Since the fluid dynamics in the region of the tip casing may be coupled to the locations of the nozzle guide vane wakes, the instrumentation needed to be positioned to give full resolution of the nozzle guide vane flow field. The tip casing had to provide three sets of measurements: the static gas temperature at

the wall, the metal temperature, and the static pressure. The instrumentation used to accomplish this were heat flux gauges, reference temperature devices (RTD's), and absolute pressure transducers and the next four sections discuss these instruments more fully.

3.2.2 Instrumentation Used on Tip Shroud

The heat flux gauges used on the casing are the same as the ones developed previously at MIT[3] which are essential two resistance thermometers separated by a layer of Kapton (figure 3.8 shows the layout of one resistance thermometer, fig 3.9 shows the combination of a top with a bottom to form a heat flux gauge). These gauges, which change resistance in response to temperature changes, are used as one side of a Whetstone bridge which outputs a voltage signal which can be fed into the A-D system. The gauges are manufactured in sheets of fourteen and are easily glued to any part of the turbine under experimental investigation. Heat flux measurements are obtained from gauges using a variety of techniques. For steady levels (≤ 20 Hz) the heat flux is just the difference in the upper and lower temperatures multiplied by the thermal conductivity and divided by the thickness:

$$q = \frac{k}{D}(T_u - T_l) \tag{1}$$

For frequencies ≥ 1500 Hz a semi-infinite model of the heat flux can be used in conjunction with just the upper temperature. For the range in between, a numerical technique is employed, developed by Oldfield[4] and used by Guenette[5].

The reference temperature devices (Omega model F3105 thin film RTD's) were used to measure the temperature of the tip shroud at the beginning of the test. These compliment the lower heat flux sensor measurements which sometimes drift from test to test and are subject to erosion. The RTD's provide reference measurements which the heat flux sensors usually use as a zero at the beginning of the run. The RTD's also provide a separate means (besides the heat flux gauges) to verify that temperature gradients are not present in the tip shroud at the end of a run; that in fact, the casing has come to equilibrium. The pressure transducers used were Kulite model XCQ-062-25A type absolute pressure measuring devices. They had absolute pressure ratings of 75 psia, were temperature compensated from 60 °F to 160 °F, drift coefficients of around 2% full scale/100 °F and sensitivities of around 2 mV/psia. They were

[3] Guenette, Gerald: " A fully Scaled Short Duration Turbine Experiment" , MIT Ph. D. Thesis, August 1985.

[4] Oldfield, M.L.G., Burd, H.J. and Doe, N.G., "Design of Wide-Bandwidth analogue Circuits for Heat Transfer Instrumentation in Transient Tunnels," Heat and Mass Transfer in Rotating Machinery, papers from the 16th Symposium on the International Center for Heat and Mass Transfer, Dubrovnik, September 1982, Hemisphere Publ. Corp. N.Y.

[5] Guenette, Gerald: " A fully Scaled Short Duration Turbine Experiment" , MIT Ph. D. Thesis, August 1985.

epoxied into tubes which would fit into the holes of the tip casing and were held in place by the clamping mechanism used on Lemo connectors. The ends were covered with a light coating of RTV 511 (Emerson and Cummings) to protect from debris and to smooth off the surface of the tip casing. During assembly two of the seven transducers (number six and seven) were broken and were mounted downstream for most of the runs.

3.2.3 Instrumentation Placement

Instrumentation placement was designed to meet the necessary design conditions stated previously. There were two methods which could be used. The instrumentation could be placed along a blade chord line or in a straight axial line (see figure 3-10) a previous tip casing[6] used a combination of both; chord locations for the pressure transducers and axial measurements for the heat flux gauges. If the number of measurements were to be expanded by rotating the tip casing, then instrumentation placement along the cord would be useless, since after the system was rotated, the gauges would be completely out of alignment. The heat flux gauges, because they are manufactured in a sheet, would have to be cut and glued down separately to obtain the proper stager associated with cord placement. Given these problems with cord placement the instrumentation was positioned along axial lines as shown in figure 3-11.

One set of heat flux gauges was positioned at one half nozzle guide vane spacing (NGV) from the location pins (.945"), and the other set was one quarter NGV (.4725") on the other side (total distance between the two rows of gauges is 3/4 NGV). Four pressure transducers were 1/4 NGV away and three 1/8 NGV away (seven could not be put side-by-side). Thus when the tip casing was rotated one would in theory have temperature and pressure measurements at four locations. Three platinum RTD's are positioned in the tip casing in line with the gauges to give measurements of the metal temperature along the same axial location. Figure 3-12 shows the position where the measurements occur with respect to the nozzle guide vane trailing edge for both positions of the tip shroud. As shown, the temperature measurements span an entire nozzle guide vane passage and the pressure transducers span half a nozzle guide vane passage.

---

[6] Guenette, Gerald: " A fully Scaled Short Duration Turbine Experiment" , MIT Ph. D. Thesis, August 1985.

3.2.4 Tip Shroud Construction

The tip casing was stripped and clear anodized at Durelectra in Natick, MA. The anodization keeps the gauges from shorting to the shroud. Feed-throughs for connecting the gauges to the other side of the tip casing were manufactured by placing Vector boards (84P44) with Vector pins (T46) in them in the main holes and potting them with Eco-Bond104 (Emerson and Cummings epoxy) cured at 250-300 °F. These feed-through where fastened directly to Bendix 20-41 male connectors which were mounted to a plate having a limited range of motion independent of the tip casing for alignment purposes. These are then screwed down to the outer window with nuts. The temperature compensation modules for the pressure transducers are held in Vector boards mounted to the top side of the tip casing, below the Bendix connector plate. The wires run directly from the compensation modules through the Bendix connectors, to the amplifiers. Two of them RTD's 1 and 2 were hooked up in a four wire configuration staring at the sensor. RTD 3, due to lack of feed-through connections had only two wires leading to the male Bendix connector. The female connector became a four wire set-up.

There are two Bendix connectors, each carrying about half the instrumentation . There are two sets of cables, about 20 feet long, with Female Bendix 20-41 wire connectors at one end and lemo connectors on the other end which make the connection from the tip shroud to the turbine facility A-D system. The only things slightly unusual in the wiring is that to reduce the number of feed-through pins in the tip-casing and to reduce the size of the Bendix connectors, the ground wires for two gauge would be run together to one pin, and then split apart again in the female Bendix connector to run to separate amplifiers. Thus instead of needing eight wires for two gauges, four top and four bottom, only five were used.

3.2.5 Tip Shroud Instrumentation Calibration Procedures

Two calibrations of the heat flux gauges are needed to convert the data to engineering units. First the gauges and the RTD's have to be calibrated against a known thermometer to obtain the proper temperature coefficient of resistance (the scales and zeros for conversion of voltages to temperatures). This is usually done before the test matrix and after the test matrix in an immersion bath using Flo-inert as the bath liquid. This calibration is done with the tip-casing hooked up through the A-D system just as it will be when it takes data. Therefore anything which is specific to a particular channel or amplifier is accounted for in the calibrations.

The second calibration verifies properties of the Kapton substrate which allow for conversion from temperatures to heat flux in both steady and unsteady situations. As outlined in ref [5], the two gauge properties which have to be measured are the k/D (the thermal conduction of the Kapton divided by the thickness) and the $\sqrt{\rho Ck}$ (the square root of the density * Specific Heat * Thermal conduction) both of which are functions only of the Kapton substrate. The process uses a constant heat flux from a laser, finding the temperature difference between a upper and lower gauge in a steady state environment and calculating the implied k/D. Ideally this could be done both before and after the testing, but to obtain absorption of the laser light, the gauges have to be darkened with a pen (Staedtler Lumograph model 316 non-permanent marking pen). Usually this can be done without increasing the resistance greatly, but since the gauges are only a few thousand angstroms thick, the potential to ruin a gauge is always present so it is generally done only after the tests.

The pressure transducers are calibrated after individual tests using the facility pressure gauges as a reference. Usually two or three measurements are taken as the facility is being evacuated after a test to obtain data points to derive a scale and zero. Ideally the scales and zeros should not change over the test matrix, but as demonstrated during the test, these transducers are quite sensitive to temperature.

3.3 Tip Clearance Measurements

Actually measuring the gap during a turbine run was important to characterize the growth of the blades as well as to obtain an accurate measurement of the gap. The device used to accomplish this was an optical lever. The optical lever shines a light on the blade and measures the reflection to determine the distance and is discussed by Cook and Hamm[7]. The optical lever has the important advantage of being quite simple to construct and operate. It's main disadvantage is that it is extremely sensitive to environmental factors which could change the reflectivity of the blades and thus it is hard to get an absolute measurement.

To create the different blade heights, some blades would be slightly altered to decrease their span. The rotor contains sixty-one blades, after measuring the average height of all the blades, five blades (blades 46-50) were selected to represent the average height: the reference set. These were lightly machined to provide a reflective surface for the optical instrument. Since the tip clearance of the ACE engine translates into a clearance of about .8 % span (12 mils or .012 ") on the blowdown turbine, two more sets of five blades were machined. The first (blades 26-30) to .006" (1.2 % span) and the second (blades 5-9) to .012" (1.6 % span)

[7] Cook, R. O. and C. W. Hamm "Fiber optic Lever Displacement Transducer"; Applied Optics, Vol. 18, No. 19, 1 October 1979; pp. 3230- 3240

below the reference set (corresponding to a fifty percent and 100 percent increase in gap, respectively).

Placement of the transducer is aided by the fact that the actual device is quite small. The transducer is mounted at the end of a long tube which is in turn mounted with O-ring seals in the optical lever holder which screws into the tip shroud. Due to the complexity and congestion of the instrumented tip casing, the optical lever was mounted on another tip shroud (window A) and the tip-casing was mounted in window B (these are roughly 120° apart). Figure 3-13 shows both a schematic of the optical lever itself as well as the holder and its position on the tip shroud. Placement of the optical lever in this window created the need for two accurate measurements in addition to the calibrations: the distance from the optical lever in window A to the actual gauges on the tip casing in window B and the relative difference in gap between window A and B (due to nonuniformities in the tip shroud).

To calibrate the optical lever two different sets of experiments were run. A static calibration used a machined blade as a stationary target mounted on a x-y table to accurately control the distance between the lever and the blade which resulted in a scale factor of 1 Volt=5.56 mils (thousandth of an inch). Another calibration was to measure the output of the lever during three different runs in a vacuum at low speed, high speed, and then low speed again. If changes are due only to growth in the blades, then the first and third runs should be at the same absolute level and the blade traces should be the same shape for all runs. The data from these tests support three general conclusions.

1) For all three sets of blades, the shape and amplitude of both low speed runs are the same. This implies that any difference between these measurements and those of the high speed runs are do to either elastic growth or a systematic error in the optical lever.

2) Data which is averaged over ten revolutions is the same as any given revolution which demonstrates that the optical lever signal for any blade is constant over a test (i.e there are no debilitating random errors in the signal during a test).

3) In general, blade shapes remain relatively constant from low to high speed runs. There are some blades which do change shape but are no different from the other blades in that group in terms of amplitude; indicating that something to do with the effective reflectivity of the blade changed, perhaps the angle?

Figure 3-14 and 3-15 compare the optical lever signal from the high speed run to an actual turbine run. The large change in absolute voltage (3 to -3.4 V) as well as changes in the blade patterns indicate that the flow field affects the optical lever to the point where comparisons between the calibration runs and the turbine runs are useless.

However, using the vacuum runs, a scale and zero can be calculated by comparing relative gap differences in a low speed run between two different blade groups and using that

data to find the growth of the blades from low to high speed. Unfortunately, while the patterns remain similar for all runs, they jump around considerably implying that this system is particularly sensitive to angle of mounting, surface finish and dirt. When an amplifier was pinned, wiping a clean finger across what was seemingly a clean blade reduced the signal considerably. The variation in signal intensity over any blade is over half the difference between blade groups. Thus determining the average voltage for a blade is difficult. A straight numerical average of all the the voltages over five blades in the low speed calibration run yields a scale factor of 12.7 mils to the volt if one measures from the small clearance blades to the reference set. This is over twice the value measured on the bench. In addition, static measurements of the turbine tip clearance indicate that the base clearance was not .012" but rather .026". As a result the actual gaps of the three groups of blades became: 1.7% of span for the reference set, 2.1% for the small clearance group, and 2.5% for the large gap group.

The optical lever is too susceptible to reflective differences to be of much use in the operating turbine environment now, but from the calibration a rough approximation of the growth of six mils (23% of reference blade gap) is obtained. The optical lever, while unable to give absolute measurements of the blade gap during the run was able to characterize the behavior of the blade growth as purely elastic and give an upper bound on the actual growth.
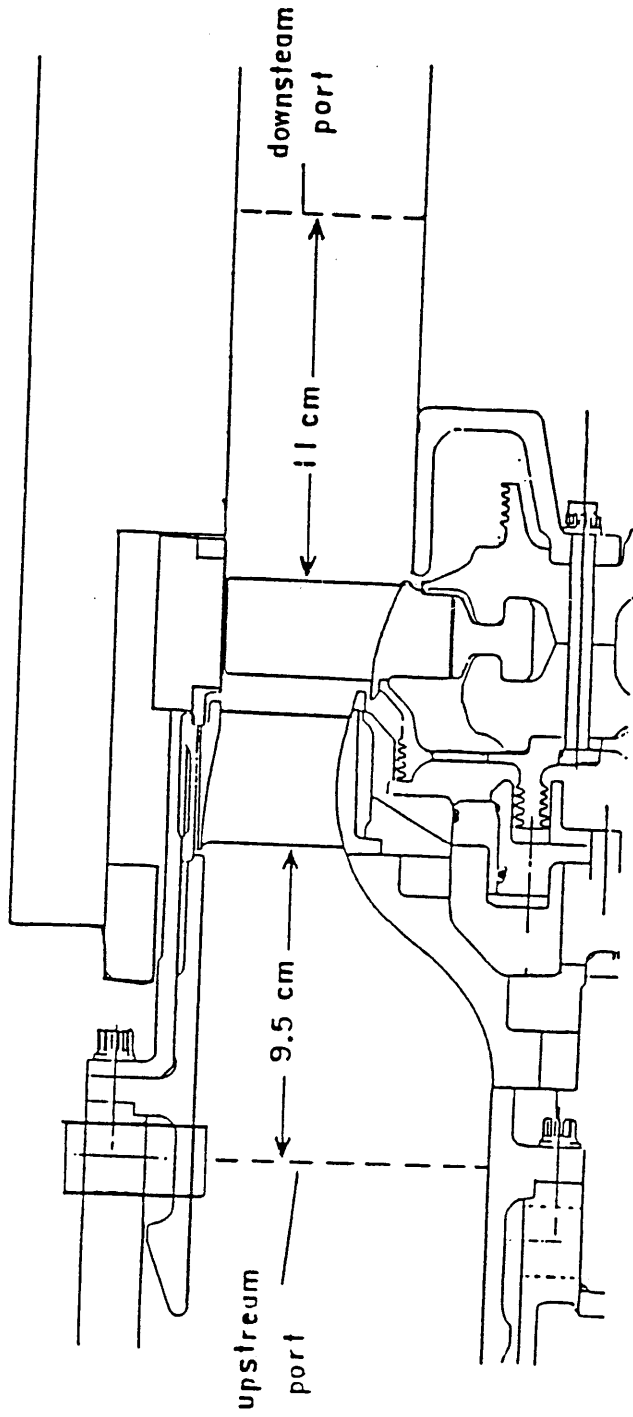
FIGURE 3-1: UPSTREAM AND DOWNSTREAM MEASURING STATIONS FOR TOTAL TEMPERATURE AND PRESSURE RAKES
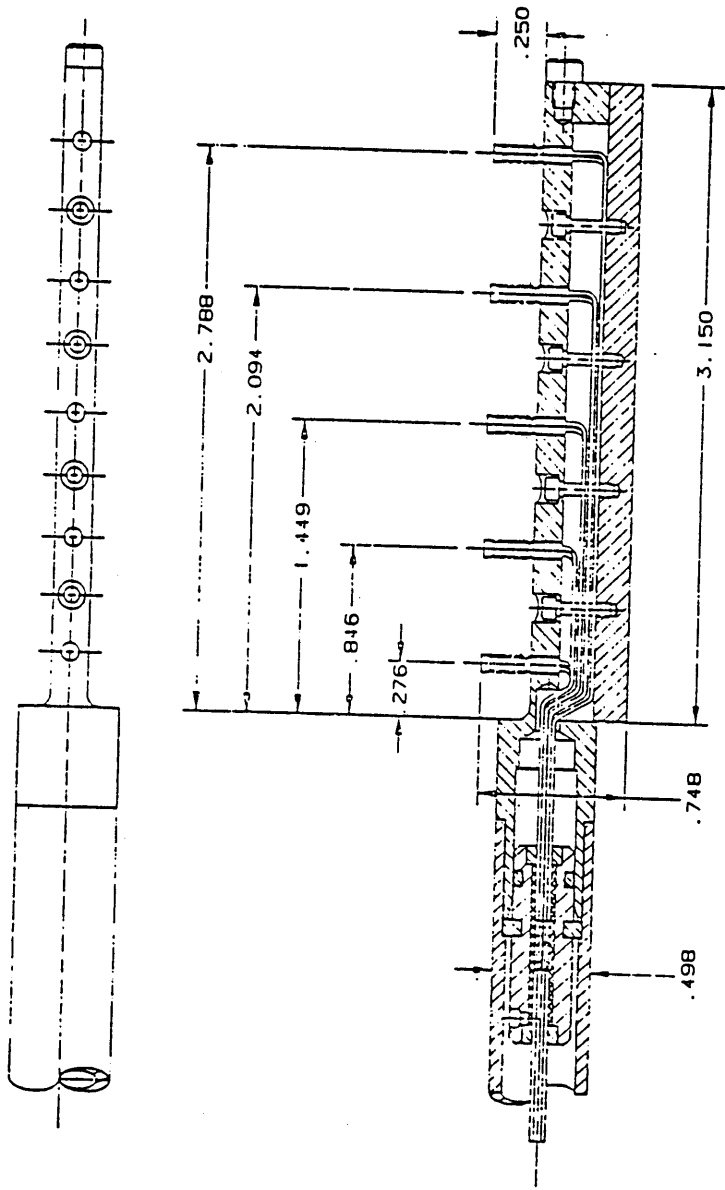
FIGURE 3-2: UPSTREAM TOTAL TEMPERATURE PROBE DIMENSIONS

Cattafesta, p. 121

0.5"

0.125" O.D.
0.090" I.D.

0.25"

1.25"

TIP

1   2   3   4   5   6

HUB

0.875"

0.225"

0.29 0.59 0.55 0.51 0.485 0.465 0.25"
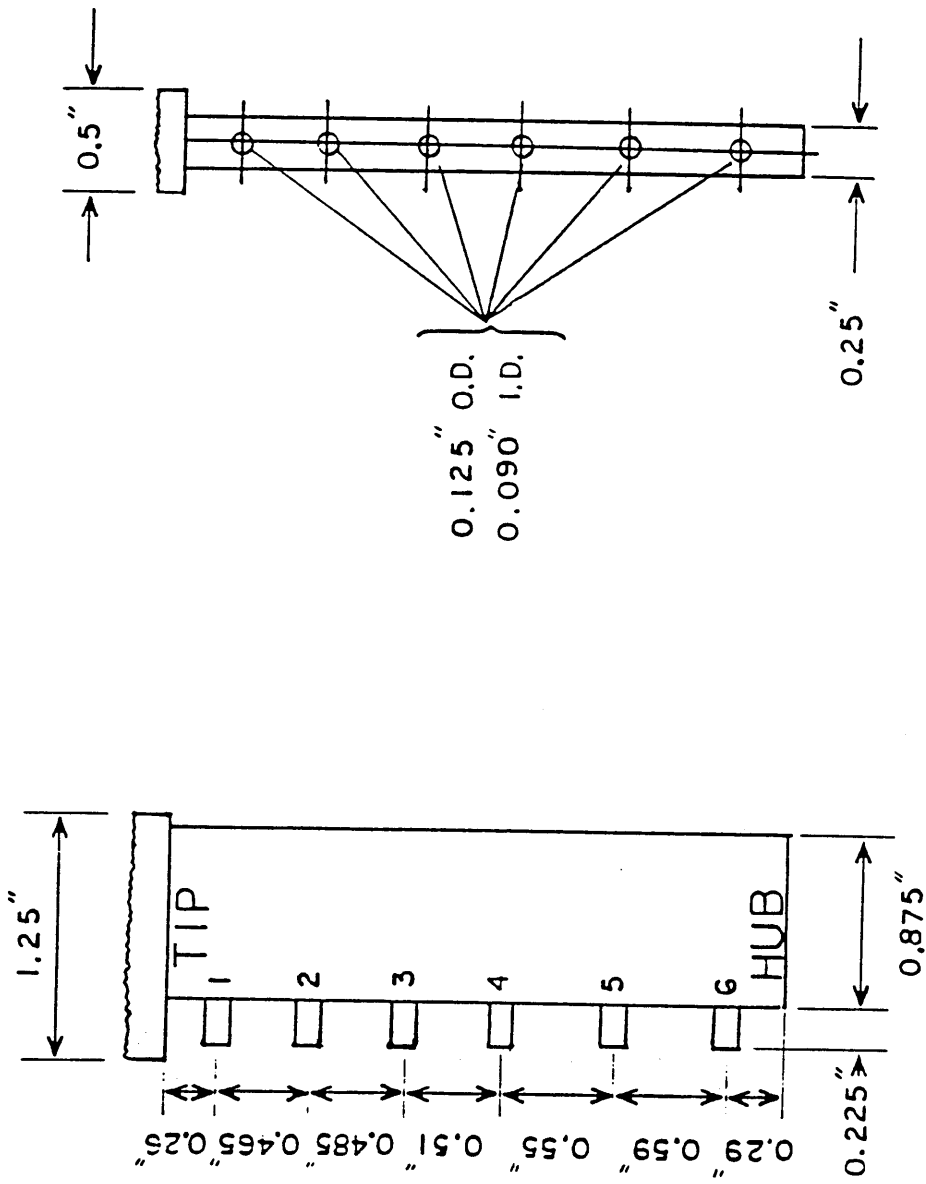
FIGURE 3-3: DIMENSIONS OF THE UPSTREAM TOTAL PRESSURE PROBE

Cattafesta, p. 94
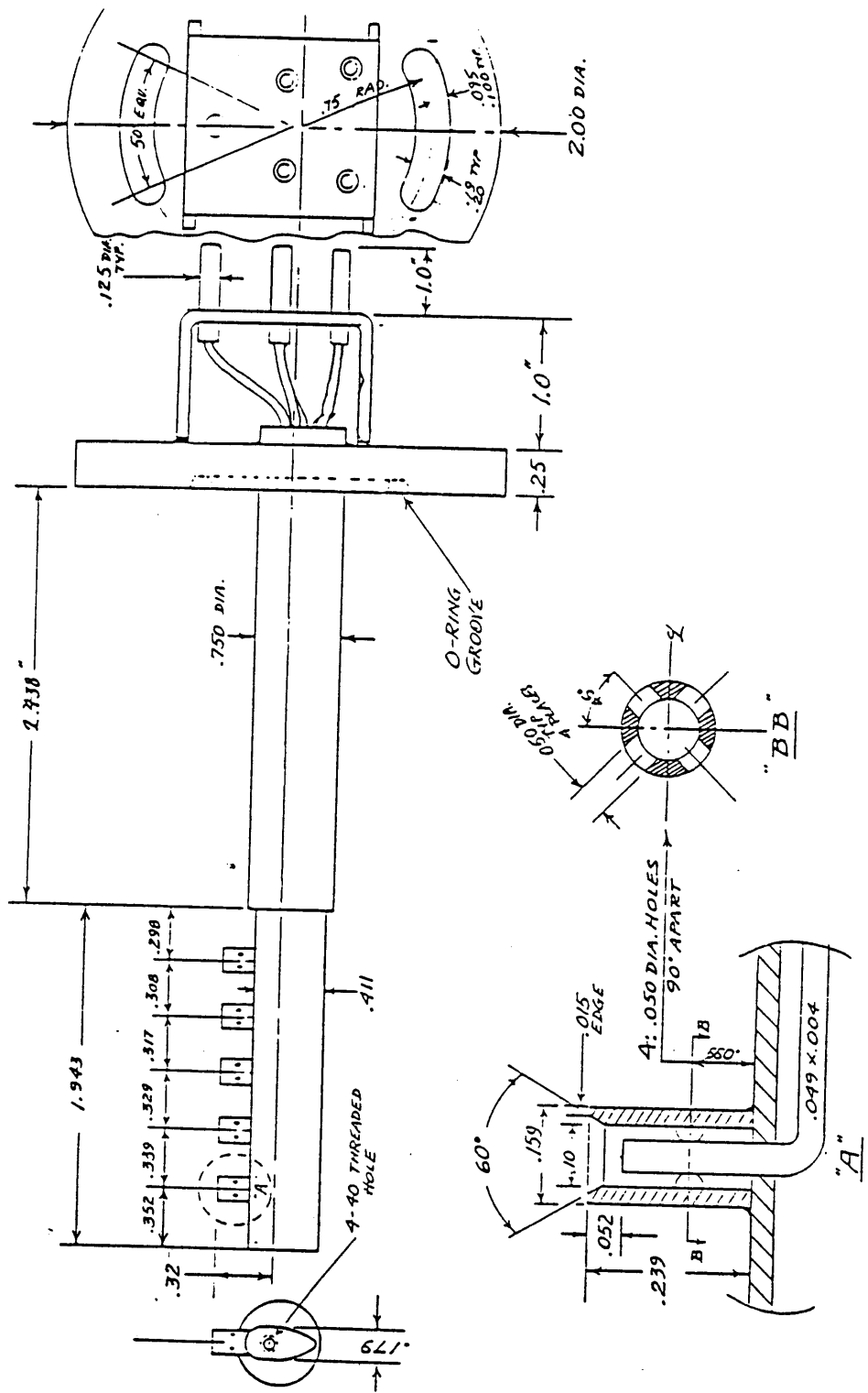
FIGURE 3-4: DIMENSIONS OF THE DOWNSTREAM TOTAL PRESSURE PROBE

Cattafesta, p. 95

Figure 3-7
Instrumented Tip Shroud Overall Dimensions
Scale 1.5 to 1:   Dimensions in inches

Holes for mounting covers

Feed-thru holes for Instrumentation

4.960

4.325

A

Cover

View A-A

Center Line

21.7 D

.1

.2

.7

.265

.1

.1

21.7 OD

.25 R

.05

.461

.2

.5

.2

.1

.15

.25

.35

.4

.05

.05

.365

C) SENSOR DETAIL

B) SENSOR & LEADS

A) SHEET

Leading Edge
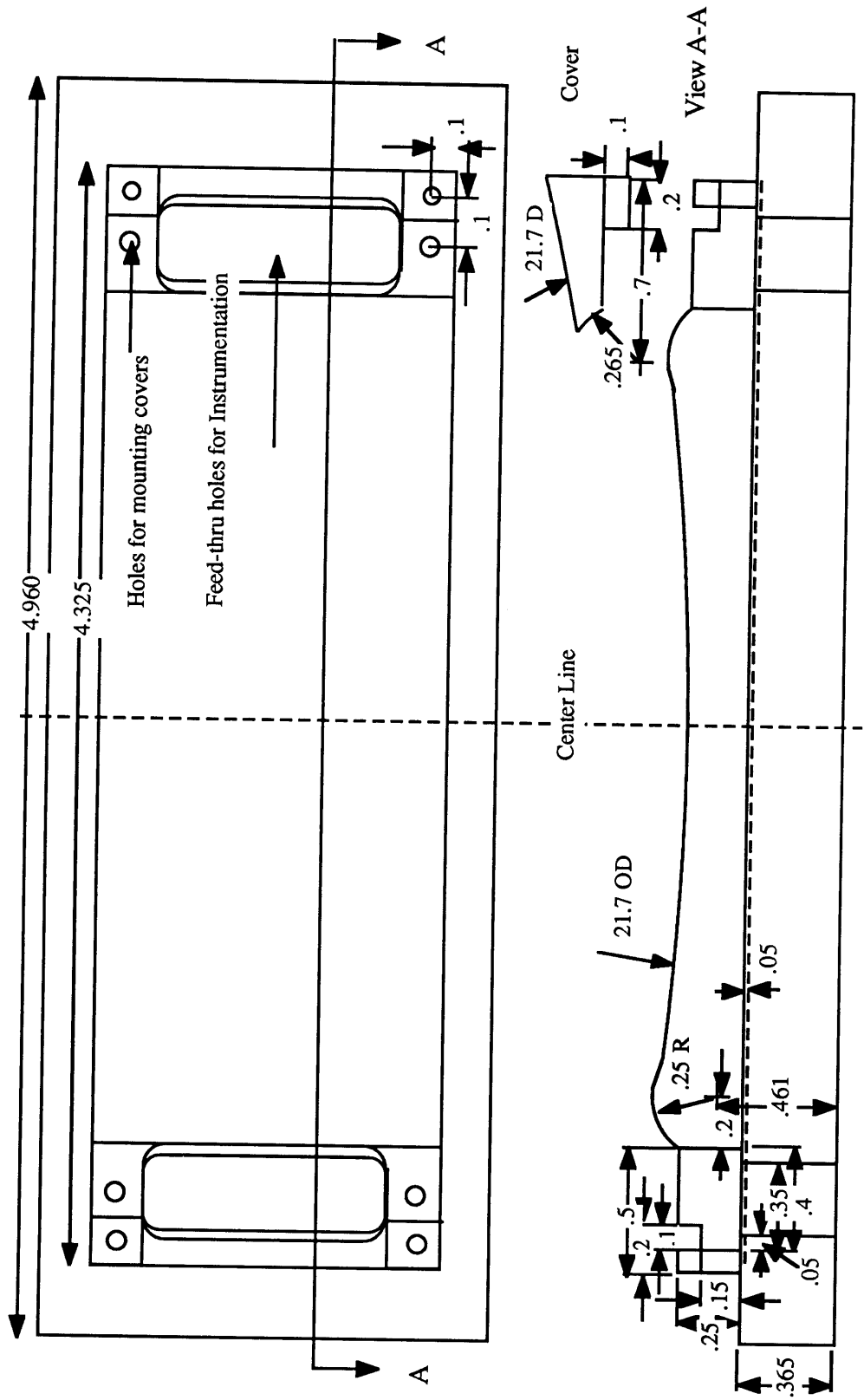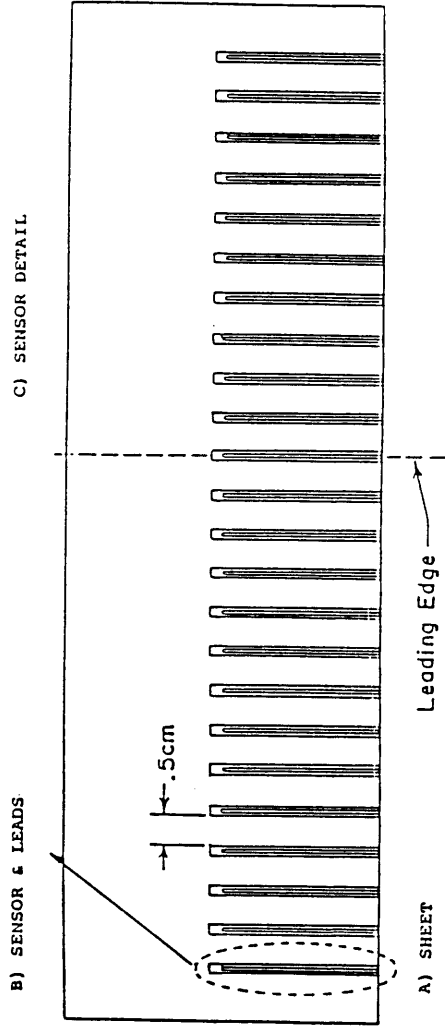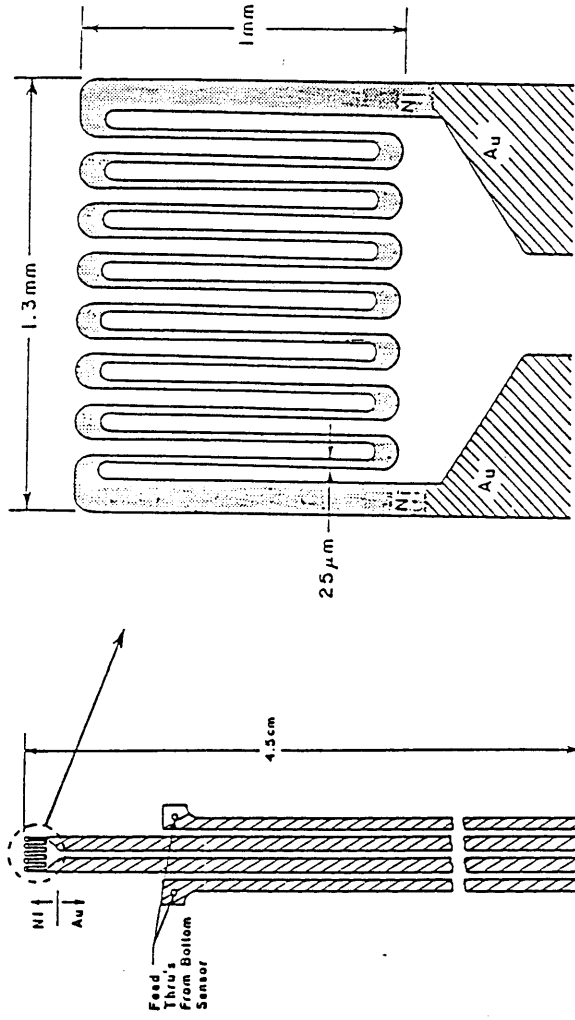
FIGURE 3-8: GAUGE GEOMETRY SHOWING SENSOR
DETAIL, SENSOR AND LEADS, AND GAUGES ON
MANUFACTURING SHEET

Guenette, "A Fully Scaled Short Duration Experiment", p. 113
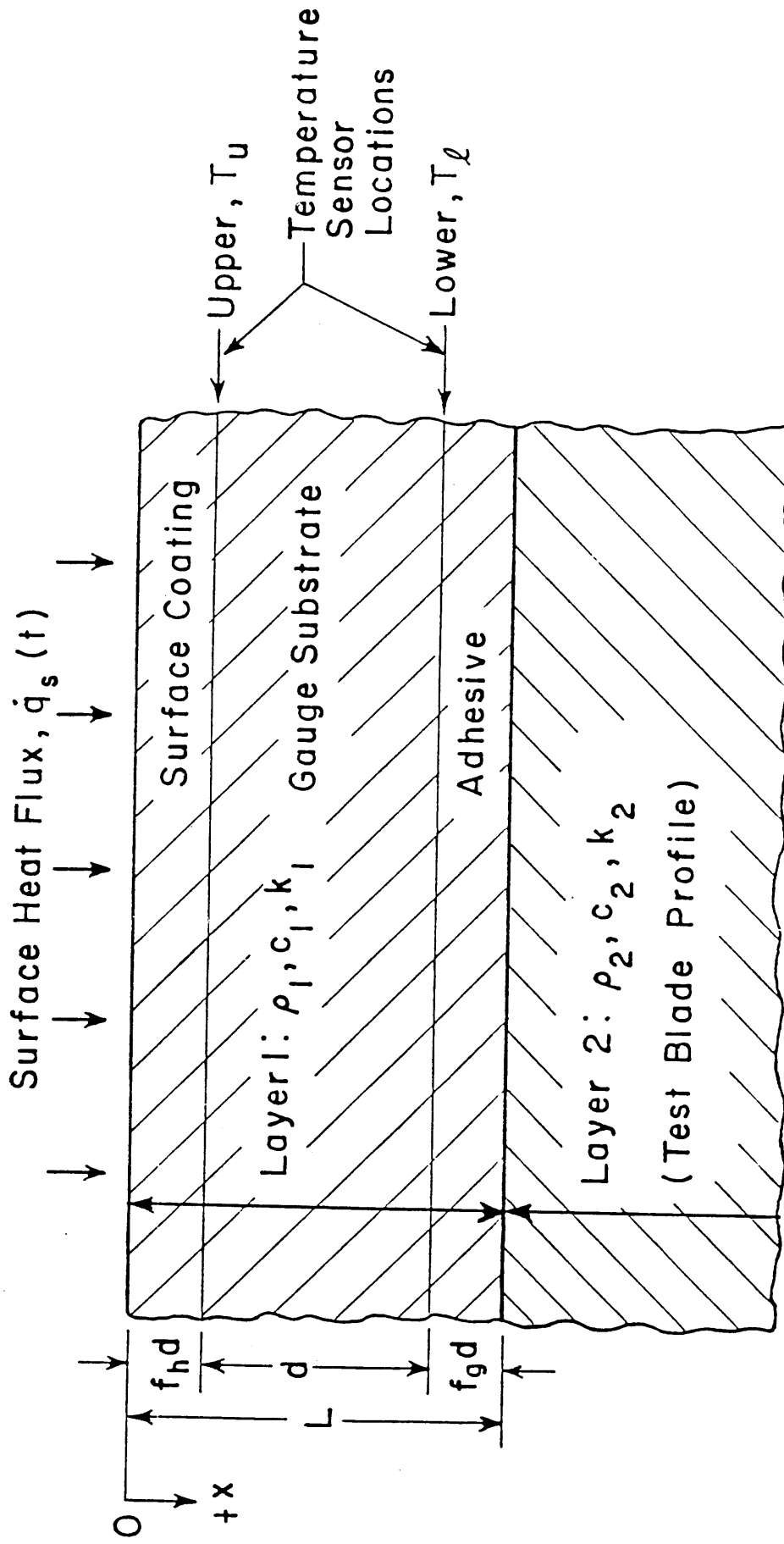
FIGURE 3-9: GEOMETRY OF GAUGE IN ANALYTICAL MODEL

Guenette, " A Fully Scaled Short Duration Experiment", p. 109

FIGURE 3-10: POSSIBLE INSTRUMENT PLACEMENT CONFIGURATION
(casing viewed from rotor)

NGV Trailing Edge Plane

○ Blade Chord Configuration   □ Axial Configuration
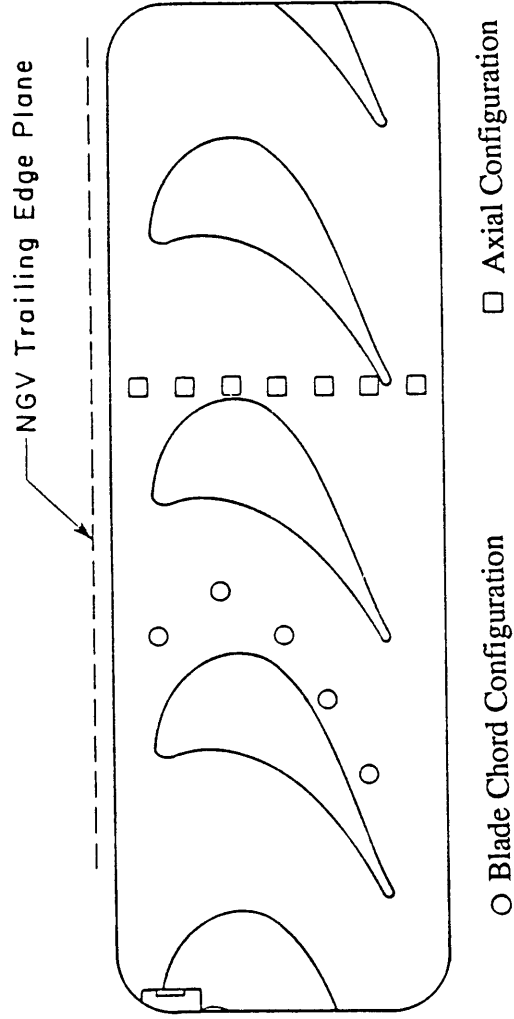
Figure 3-11
Placement of Instrumentation
and Key Dimensions (Scale 2:1)
(Bottom View)
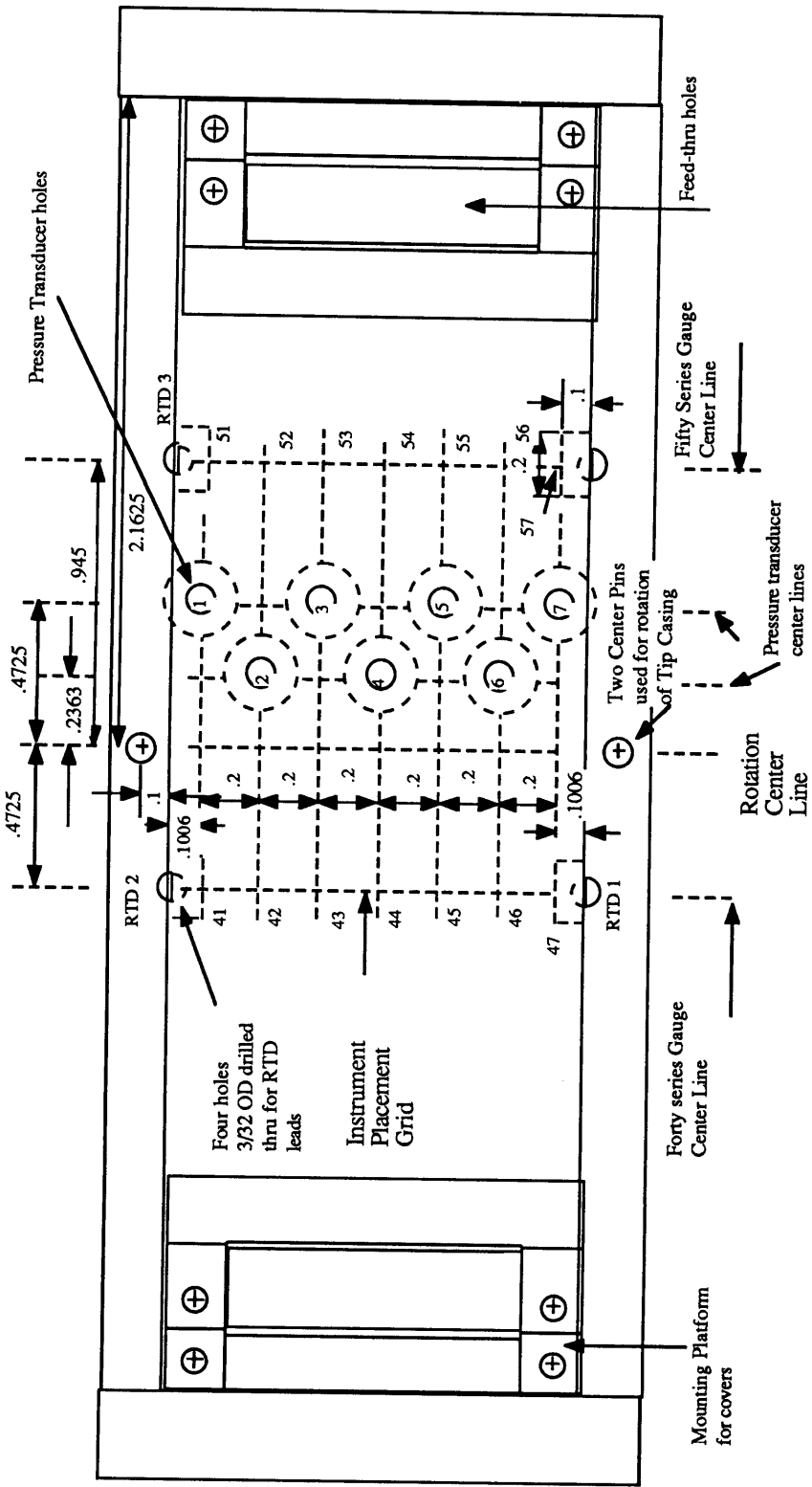
Figure 3-12
Instrumentation Locations with respect to Nozzle Guide Vanes

ROTOR ROTATION DIRECTION

CENTER OF TIP SHROUD ROTATION

Outline of Blade

Circumferential Position

1.89"

.1"

NOZZLE GUIDE VANE TRAILING EDGES

Center Nozzle Guide Vane

	Circumferential Pos.	Distance From Center NGV
		NGV Spacing
	1	.447
	2	.197
	3	.072
	4	-.178
	5	-.303
	6	-.554

□ Heat Flux Gauge Location

○ Pressure Transducer Location

▭ Location of instrumentation for first seven runs (Gauges 41, 51 upstream)

▨ Location of instrumentaion for last three runs (Gauges 57, 47 upstream)

62

Figure 3-13   Optical Lever Schematic, Holder and Tip Shroud
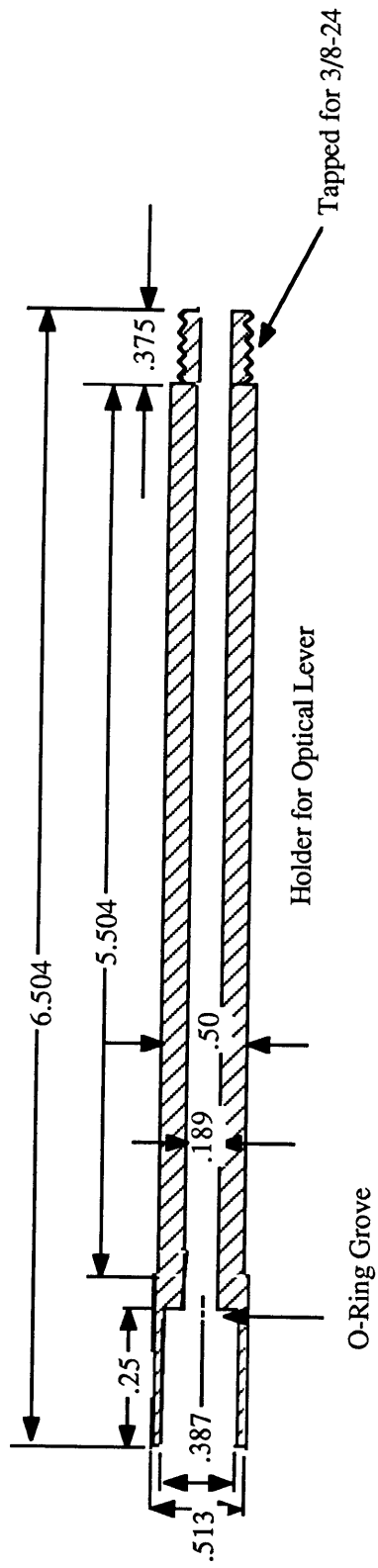
Tapped for 3/8-24

Holder for Optical Lever

O-Ring Grove

6.504

5.504

.375

.189

.50

.25

.387

.513

Schematic of Optical Lever Operation

Illuminating

Output

Receiving

Bundle
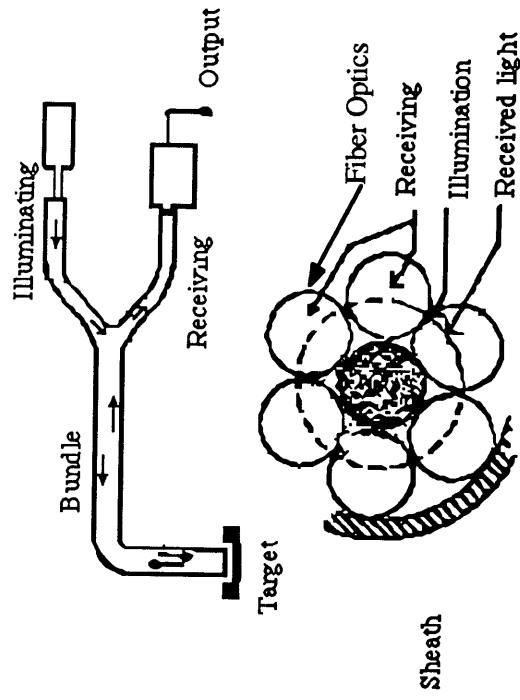
Target

Fiber Optics

Receiving

Illumination

Received light

Sheath

Optical Lever Tip Shroud
(Half Scale)

Mounting Hole for Optical
Lever Holder

Leading Edge

.750

2.48

FIGURE 3-14
OPTICAL LEVER SIGNAL
HIGH SPEED RUN (100 RPS)

64
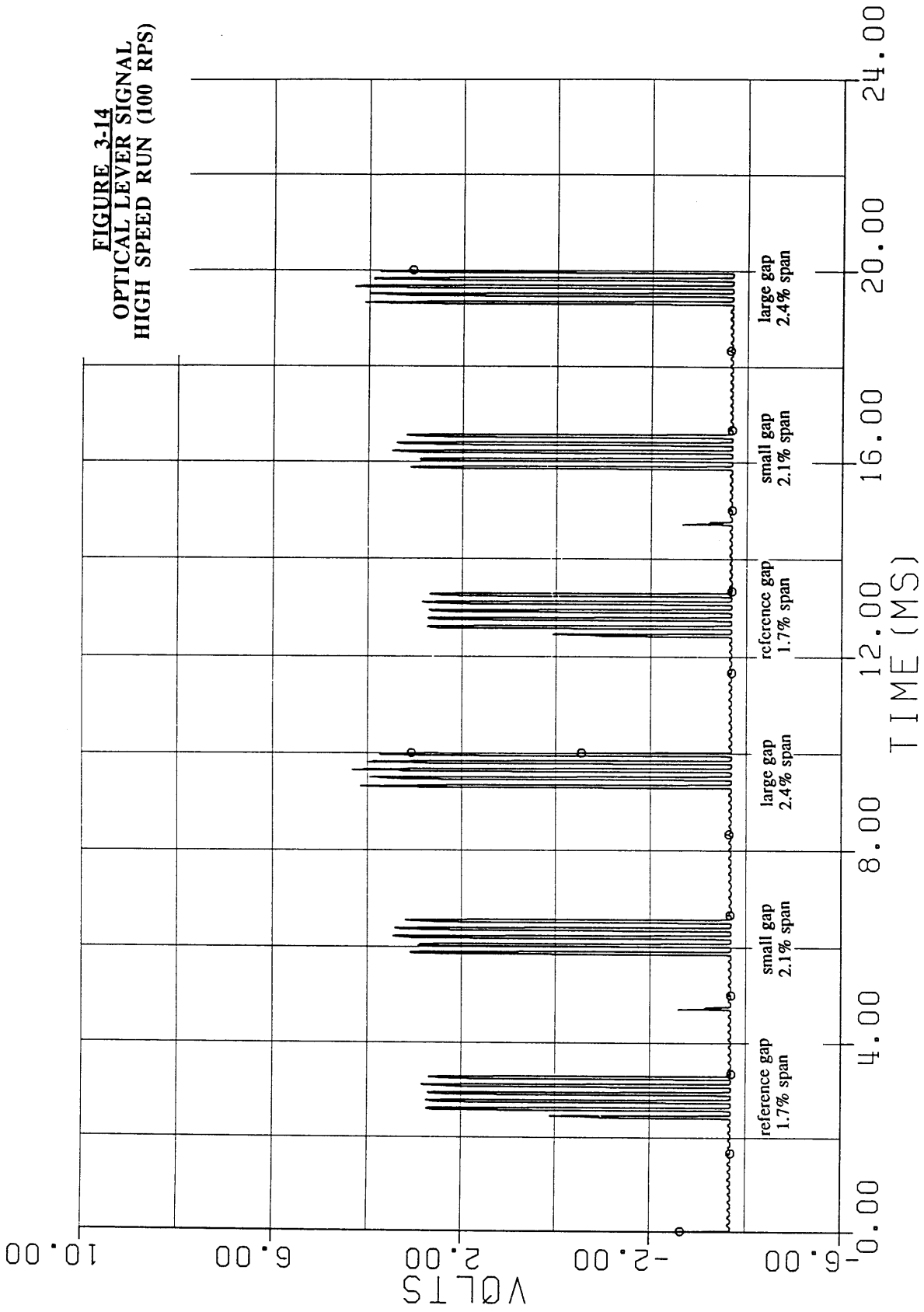
FIGURE 3-15
OPTICAL LEVER SIGNAL
Turb 130
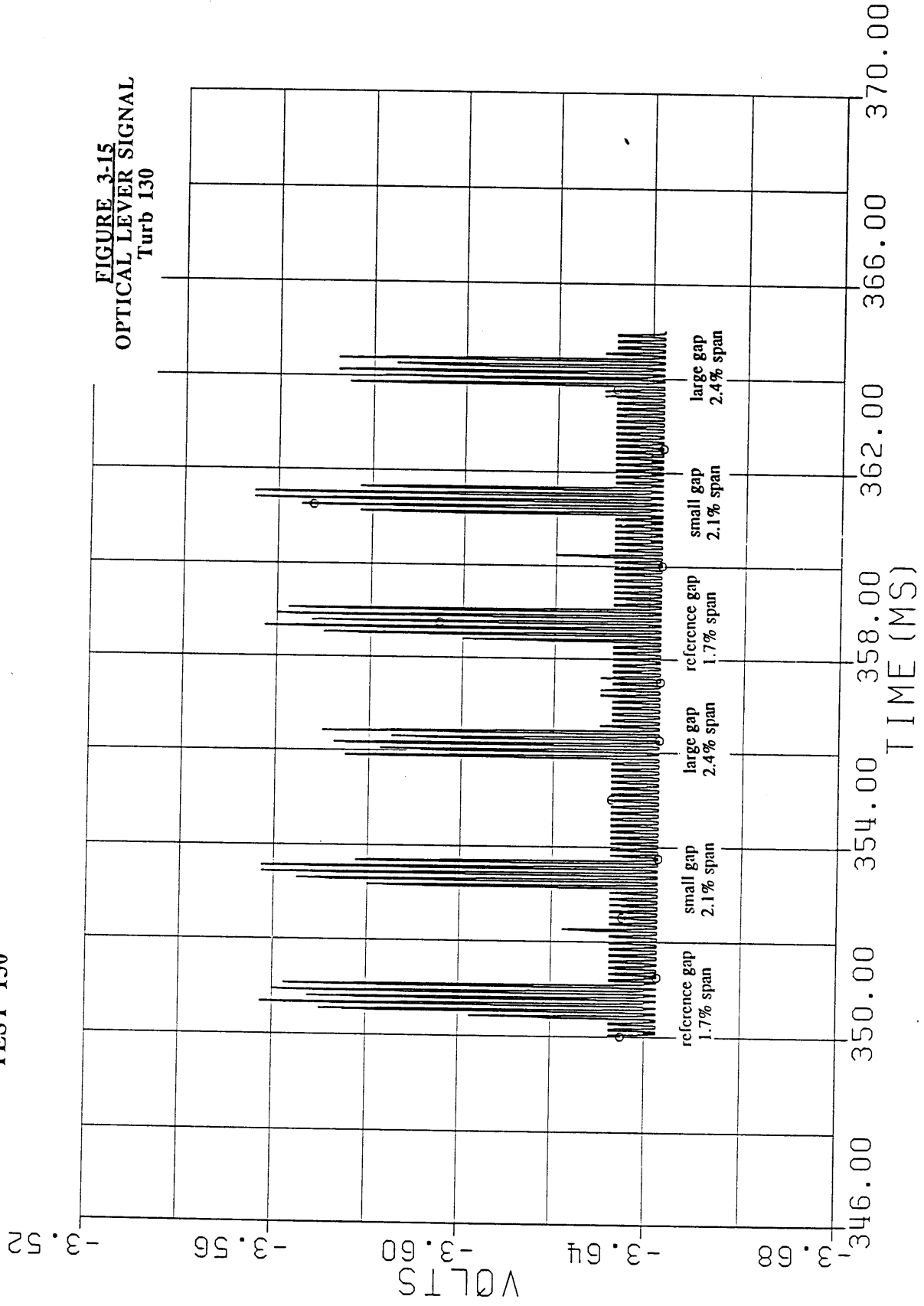
Chapter 4: Experimental Procedure and Calibrations

This chapter deals specifically with the experimental procedure, the experimental problems, and the data reduction process. During the testing, the unforeseen problem of having the heat flux gauges eroded away by small particles of brazing oxide from the profile generator, caused a reexamination of the calibration procedure and the data reduction methodology.

4.1 Tests Performed

With the equipment assembled, it was necessary to determine the investigation range of the three independent variables: temperature profile, average temperature and tip gap. Ideally for this investigation one would wish to test over the greatest range of profiles and average temperatures. However, the present set-up of the facility imposes a trade-off between the absolute temperature and profile (discused in section 2.2.6). The compromise settings which give the greatest range of profiles and average temperatures are to run three profiles: no profile (uniform flow), low profile (8%) and high profile (16%), at the two mass average temperatures of 400 °K and 475 °K. To measure circumferential non-uniformities in the test facility and to give better resolution of the nozzle guide vane flow area the tip shroud was inverted. The final test matrix configuration is shown in table 4-1.

Table 4-1
Test Matrix

Average Temperature	Profile Settings		
	High	Low	None
High 475 °K	Test 120	Test 126	Test 121
Low 400 °K	Test 122	Test 125	Test 123 &Test 124
High (Tip shroud reversed) 475 °K	Test 127	Test 131	Test 130

The convoluted method in which the tests were done represented the order of importance which was placed on the individual tests. This method attempted to extract the most information from the tests done in case of catastrophic failure during the testing sequence.

The placement of the tip casing is shown in figures 4-1 and 4-2. For tests 1-7 the tip casing was positioned so that gauges 41 and 51 are upstream (fig. 4-1). When the tip casing was inverted for test 8-10, gauges 57 and 47 were upstream (fig 4-2). Figure 3-12 shows the

casing instrument locations for all tests with respect to the nozzle guide vanes. Figure 4-3 shows the gauge locations with respect to rotor coordinates.

Figure 4-1
Tests 120-126 Tip Casing Orientation
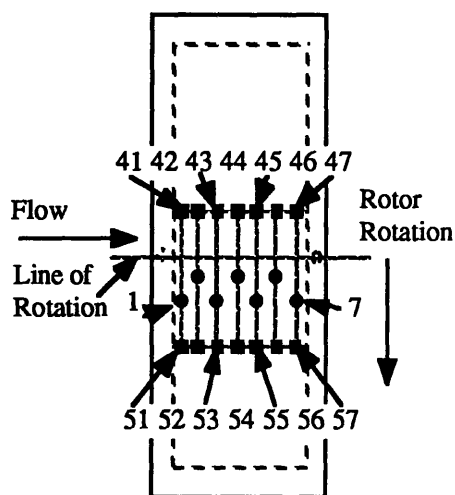
Figure 4-2
Tests127-131 Tip Casing Orientation
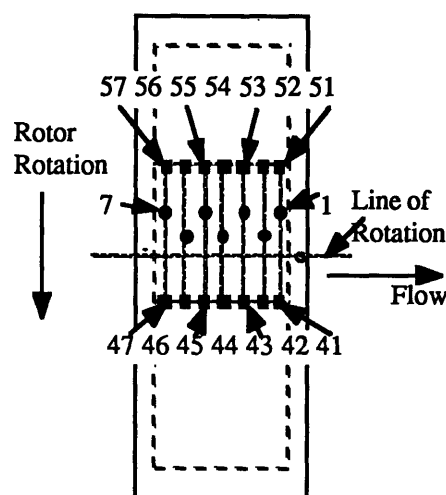
- ● Pressure Transducers
- ■ Heat Flux Guages

4.1.1 Test Procedure

The test procedure had two distinct levels. There were the calibrations which needed to be done before and after the test matrix and there were the calibrations which needed to be done during each test. Before it was installed in the facility, the tip shroud had to be calibrated in a temperature bath to obtain the proper conversion factors to transform the voltages measured by the gauges and the RTDs into temperatures (Cal 1). During each run the facility differential pressure transducers were calibrated twice. Once before the test gas was added to the supply tank and once afterwards, just before the test. After the test is completed and the data has been stored on the computer (five to ten minutes after firing), the absolute pressure transducers on the tip shroud are calibrated at different times and pressures as the gas is evacuated from the facility. After the test matrix was finished, two more temperature bath calibrations were done (Cal 2 and Cal 3) to obtain final temperature-voltage conversions for comparison against Cal 1. The final calibration performed involved verifying the Kapton properties needed to convert

temperature measurements to heat flux measurements using the laser set-up described by Guenette[1].

4.1.2 Test Results

Ten tests were performed over the space of fifteen days. Test 123 was performed under conditions not used in the test matrix because of a mistake in the absolute temperature settings and was redone under the name of Test 124. A summary table of the test characteristics is given in table 4-2 (a more complete table with variations over the test time is given in appendix II).

Table 4-2
Run Conditions and Test Variances
Averaged from 375 to 400 ms

	Test 120	Test 121	Test 122	Test 124	Test 125	Test 126	Test 127	Test 130	Test 131
TT2 Avg	462.36	459.38	396.18	398.86	391.53	451.41	459.09	462.50	459.87
RTDF	17.2	.1	12.6	.0	6.7	8.5	7.4	.5	17.1
Corr. Spd	1.48	1.47	1.46	1.47	1.49	1.52	1.51	1.52	1.51
Speed	122.47	121.66	111.83	113.58	113.67	124.60	125.14	125.83	124.79
Fract. Spd	1.20	1.19	1.18	1.19	1.21	1.23	1.23	1.223	1.22
PT2	3.71	3.53	3.70	3.56	3.64	3.60	3.60	3.49	3.73
PT5	.89	.82	.88	.85	.89	.88	.85	.82	.89
Press. Ratio	4.19	4.28	4.20	4.17	4.07	4.10	4.22	4.23	4.21

Definitions:

TT2 Avg= Area average of the upstream total temperature rake

RTDF= Based on area average T mean and the measured profile (eqn 1, chapter 2)

Corr. Spd = Corrected Speed=$\dfrac{N}{\sqrt{T/T_{ref}}}$

Speed = Tip speed in revolutions per second

Fract. Spd = Speed/Design Speed

PT2 = Area average of the pressure rake behind the generator (Turbine inlet total pressure)

PT5 = Area average of the total pressure downstream of the rotor

Press. Ratio = PT2/PT5

Neither the profiles nor the temperatures were the exactly the ones which were aimed for. The reason for this was that once the first test of either the high average temperature series or the low average temperature series was run, the desire was to replicate the average temperature obtained on that run. Thus when Test 120 obtained an average temperature of 462 °K that was the average temperature aimed for in tests 121, 126, 127, 130, and 131. The profiles obtained in both of the high average temperature runs was close to what was planned. For the low

---

[1] Guenette, Ph.D thesis

average temperature run the peak profile was limited to 12 % by the outside wall temperature. Thus to compare to the other temperature range it was decided to measure at half of this profile (i.e. at 6 %) instead of the planned 8 % and in this manner the effect of the profiles could be normalized between the two temperatures for better comparison.

The tests ran according to plan except for the unexpected sand-blasting of the instrumentation by the brazing oxide from the profile generator. This was a serious problem: 57% of the top gauges were destroyed by the end of the testing sequence. Many gauges, while not completely destroyed, did not yield useful information during a run for a variety of reasons. The erosion of the gauges caused changes in the scale factors and zeros (the conversion factors which convert the voltages measured to temperature). This caused problems for previous calibration schemes and required a new run-time calibration scheme described in the data reduction section.

4.2 Instrumentation calibration

4.2.1 Voltage-Temperature Calibrations

As outlined in the MIT facility report[2] The heat flux gauges are set up as one side of a Whetstone bridge. Changes in resistance are converted to voltage changes which are amplified and can be set to vary from -5 to 5 volts, corresponding to the maximum and minimum temperatures expected to be encountered during a test. The nature of a whetstone bridge is to be stable when the resistance being measured is close to a balance resistor in the bridge. The amplifiers are constructed to put a resistor of nominally the same value as the gauge on the other arm of the bridge and to fine tune the resistance to exactly match the gauge at some reference temperature with a variable resistor. If however, the resistance of the gauge changes greatly, the amplifier becomes more unstable, sometimes pinning or oscillating requiring the rebalancing of the amplifier, or replacement of the balance resistor with a new one.

This has serious repercussions for the calibration procedures outline in the previous chapter. The bath calibrations, which are done with the shroud connected to the amplifiers used during the test, use straight line fits to calculate the temperature from the measured voltage. However the scales (°C/V) and the zero (X volts =Y ° C) measure are a combination of the scales and zeros of the gauges and the biases and zeros of the amplifiers. Thus changes in amplifier settings during the run can cause great changes in the measured scale and zero for the gauge, even if the actual scale and zero changes only a little.

---

2 MIT Report no 183

Three separate temperature bath calibrations were performed on the tip shroud. Cal 1 was before tunnel testing, Cal 2 was after tunnel testing, and Cal 3 was immediately after Cal 2 with a new balance resistor for TCB47T and rebalancing for the gauges marked to observe the effect that changing the amplifier had on the gauge scales and zeros (Table 4-3). One can see that changes in the scales and zeros is less than 1% for the gauges which were not rebalanced, but for those gauges which were altered variations existed between .2% and 3%, indicating the variety of reactions between the different amplifiers. As a comparison, some of the bottom gauges (the reference set, 41B, 42B, 43B, and 47B) vary in scales by less than 1% over the entire test matrix (table 4-4).

The comparison between Cal 2 and Cal 3 shows the strong influence of the amplifiers on the measured scales and zeros for the gauges. Unfortunately the sand blasting caused significant changes in the resistance of the gauges (table 4-5) necessitating amplifier changers during the test matrix (table 4-6).

The sensitivity of the calibration factors to the calibration range also needs to be investigated. Two different calibration ranges, using two different error reducing techniques, were used in both Cal 1 and Cal 2 ranging from a 30 to 50 °C range to a 30-85 °C range. For the reference bottom gauges (those gauges which were uneroded over the test sequence) table 4-4 shows the changes in calibration for scales and zeros for both cals and then over the entire test sequence. The variation within any one calibration is less than .64 % and the total variation in scales over the test sequence is independent of the range to within .9%.

4.2.2 The Heat Flux Calibration

As mentioned in the previous chapter, the laser calibrations are used to obtain the properties of the kapton which are used to calibrate the heat flux. The laser calibrations require that the power levels be constant over the testing times, and that the steady-state heat flux measurements be one dimensional in nature. In both cases, these can be hard to insure during testing. The laser beam in its unaltered form has a beam diameter of approximately 1.3 mm (beam diameter is defined by the diameter in which 1/e of the energy of the beam is contained). This is roughly the same size as the gauges (1.3 mm x 1 mm) leading to two dimensional effects on the edges of the gauges. Expanding the beam eliminates these effects but also drives the power density down. Calibrations need to be done in the power density range measured in the actual experiment, so a 4 Watt Argon laser was used. The step response in the laser beam was created by an electo-optical modulation system (rise time of 25 ns) which ideally can obtain extinction ratios of 250:1. However, the modulator can only work on one wavelength, so the output of the beam was split and a maximum power of .8 W (a 30% loss through the

modulator) was obtained after the modulator at maximum laser power. While the $\sqrt{\rho Ck}$ measurements require constant power, the K/D measurements require proper scales and zeros to provide the upper and lower temperatures. The power levels can fluctuate during a test for three reasons: power jumps in the laser, modulator drift, and focusing effects due to the fluid used for the calibration. To observe power fluctuations based on the first two problems, an optical power meter was positioned behind a reflective ND2 filter after the modulator . Thus 1% of the power was transmitted to the meter and 99% was reflected onto the gauge. The trace of the power meter could be stored on an oscilloscope and compared with others to see if the power levels fluctuated. Data for the calibrations were taken on a digital oscilloscope and transferred to a floppy disk for storage. Using this method, power fluctuations could be observed to an accuracy of about 5%.

Unfortunately, the last source of power fluctuations, due to focusing effects of the fluid on the laser beam is not easily quantifiable during the test conditions since the amount of curvature present in the fluid at the time of the test is not readily quantifiable. The fluid used for the calibrations, Dibutyl phthalate was chosen because it did not dissolve the ink used to darken the gauges, and because it presented a relatively flat surface to the laser beam. However the overall accuracy of this calibration depends a great deal upon the technique used. To insure a proper calibration technique a calibration block with a gauge with known properties was used with different amounts of DBT (Dibutyl phthalate) and different amounts of inking. For a test with the edge of the DBT placed close to the gauge a $\sqrt{\rho Ck}$ measurement was 493.3 $(\dfrac{W}{m^2 \sqrt{Sec} \, ^\circ K})$ while placing an amount of DBT of about 1.5 cm in diameter produced a $\sqrt{\rho Ck}$ of 584 (accepted value is 586.$\dfrac{W}{m^2 \sqrt{Sec} \, ^\circ K}$ The amount of inking is also important since it tends to change the time delay before one can see a straight correlation between $\sqrt{time}$ and temperature (as measured by extrapolating the slope of the fit between time and temperature until it crosses the time axis). This is an indication of how well the gauge performes is corresponding to the model and can be used as an indication of calibration problems. Usually time delays of less then 10 ms are observed, but different inking levels can obtain time delays of up to 40 ms. Using techniques which worked best on the calibration block, the $\sqrt{\rho Ck}$ of the gauge was found to be 593 $(\dfrac{W}{m^2 \sqrt{Sec} \, ^\circ K})$.

The accuracy of the k/D tests is directly proportional to the accuracy of the scales and zeros as well as the overall calibration procedure. Using the above value for $\sqrt{\rho Ck}$ six measurements of k/d were made at 8067, 8079, 8434, 8203, 8379, and 8365 $\dfrac{w}{m^2}$ for the gauges which survived the test sequence. The differences may be due to inaccuracies in the

scales and zeros calculated for the different gauges. A sensitivity analysis of the measurement of k/D based on fluctuations in the power and changes in the upper scale sensor is shown below. The basic relationship between k/D, $\sqrt{\rho Ck}$, and temperature is given as:

$$k/D = \frac{\sqrt{\rho Ck}\ \sqrt{\pi}\ m}{(T_u - T_l)2} \tag{1}$$

where m is the slope of the response of the temperature to $\sqrt{time}$. If Δm is the change in slope due to changes in power and ΔS is the change in the upper sensor scale factor, then the change in calculated k/D can be written as the old k/D plus $\Delta k/D$ as shown in eqn 2.

$$k/D + \Delta k/D = C_1 * \frac{(m + \Delta m)(1+\Delta S/S)}{(T_u (1+\Delta S/S) - T_l)} \tag{2}$$

where C_1 represents $\frac{\sqrt{\rho Ck}\ \sqrt{\pi}}{2}$ and S is the old scale factor for the top sensor. This reduces

to $\quad \frac{\Delta k/D}{k/D} = \frac{1+\Delta S/S + \Delta m/m}{1 + \dfrac{T_u\ \Delta S/S}{T_u - T_l}} - 1 \tag{3}$

for the calibrations which we used $(T_u - T_l)/T_u$ ranged from about .7 to .8. Using .75 as an approximate value yields a .3% decrease in k/D for a 1% increase in gauge scale factor and one to one correspondence to increases in k/D to increases in power. A 5% change in power and a 5 % change in scale factor will result in a 3% change in k/D measured. Nominal k/D's for Kapton have been measured at 8086 (W/m^2) which yield a range of 8328 to 7843 (W/m^2).

The variations in k/D measured are most likely due to the variations in scale and zeros caused by the darkening process and variations in the laser power. Resistance changes in the gauge which gave high values offers credence to this explanation since the gauge that gave the closest values to 8086 was the only one whose resistance did not change after the darkening process. Another check on the suitability of gauge to the calibration process is by checking the implied power levels from gauge to gauge, provided that the power remains relatively constant. For example during these calibration runs two different power levels were recorded; 38 and 49 Kw/m^2, at nominally the same power level. This represents a 29% increase in the power levels which indicating a change in the scaling factors.

The final result, is that most of these gauge had been so badly damaged during the testing that they were too sensitive to the inking process to keep constant scale factors. After every test the gauges would have to be recalibrated using a bath calibration. The resources were not available to pursue the problems mentioned here in depth, mostly because the laser was giving out (it would have to be rebuilt) and the gauges were breaking after repeated applications of the pen ink. To obtain an estimate of how k/D value could vary from gauge to gauge, results from

previous work with these gauges which were extensively analyzed were employed which showed that the k/D value changed by 1.5% of the mean value. Thus, given the limitations in calibrating the individual gauges on this shroud, the average value calculated from the gauge which did not change resistance was used with this variation as an estimate of the k/D values or the other gauges. Using this gauge, a value of $\sqrt{\rho Ck} = 593$ $(\frac{W}{m^2 \sqrt{Sec} \cdot K})$ and a k/D = 8073 W/m^2 were used as the average values which relate well to established values based on good gauge of 580 $(\frac{W}{m^2 \sqrt{Sec} \cdot K})$ and 8086 W/m^2.

4.2.3 The Pressure Transducer Calibrations

Calibration of the pressure transducers was done after the test as the facility was being evacuated. During the evacuation process readings would be made by turning off the pumps temporarily and taking temperature and pressure measurements. There were some intrinsic problems with this procedure that were unavoidable. For instance, temperature changes, due to the facility cooling, caused the transducers to drift. A time trace of this procedure is shown in figure 4.4 for Test 131. One can see the spikes where the A-D was disconnected for the measurements. It is apparent that transducer number five has some considerable time lag associated with it. In addition, by using an average scale and zero calculated over all the runs (a good approximation since the total variance of these properties is small over the test sequence), a measurement of how much drift occurs due to temperature can be found by looking at the response of the pressure transducers during the bath calibrations. Figure 4.5 shows the variation of the pressure measurements around the one atmosphere condition as the temperature decreases in the bath. Over the entire test matrix, the scales and zeros of the pressure transducers are good to with a 5% error (see table 4-7 for exact figures) and the accuracy of the RTD's (2 and 3) are good to within 2% (table 4-4).

4.3 Methodology Used for Data Recovery

As mentioned earlier, the standard calibration procedures developed for this facility do not work well when the instrumentation goes through a continuous process of erosion due to sand blasting. The main engineering question imposed by this process is "Can scales and zeros be accurately reconstructed at the end of a test, which represent, on average, what actually occurred during the run?"

The erosion process probably reveals itself in two ways: through constant low level erosion which results in gradual changes in the scales and zeros of the gauges over the test time, and in the visual jumps in the data which probably occur when significantly sized pieces of debris hit the gauge and damage it (fig. 4-6). The problem is exsasperated because in the past, jumps in the data are due to electrical problems which do not reflect a change in gauge resistance. Even if a methodology for reproducing the actual scales and zeros after each jump existed, the jump would still have to be located. This problem is not important during the actual test time, where sampling speeds can sort out random fluctuations from jumps, but at the beginning of the test the temperature gradients are of the same order as the sampling speed and thus it becomes quite hard to tell where a jump is. The final problem imposed by the jumps is that once they are located they have to be evaluated to compensate for them. This is usually not easy since it creates an error which generally can not be evaluated in any method other than a worst case scenario (i.e. within the peak to peak variation of the cycle before it). Working with the limitations imposed by the erosion, a method for evaluating the scales and zeros for each gauge and every test was developed.

The problem becomes one of finding the appropriate reference thermometer. As shown in table 4-4, the "reference gauges" had scales which varied by less than 1 % over the entire test matrix, and while the zeros changed any where from 7 to 3 % the RTD's (2 and 3) have scales and zeros good to about 3% .

The calibration scheme developed was to use an average of RTDs 2 and 3 (the most stable ones) to give a reference temperature at the beginning of the run. This temperature was used to provide the appropriate zero for the reference gauge set. Now that the reference gauge set had scales (from the bath calibrations) and a zero specific to the test, the temperature at the end of the run can be found from the reference gauges (in fact one could also get it from the RTDs and a comparison between the reference gauge temperatures and the RTDs is shown in table 4-8). Using the final temperature, gauges which had all the jumps removed could be calibrated against its bottom gauge (if it was part of the reference set) or against an average of the reference set gauges to get appropriate scales and zeros for that test. In order to do this, the gauges had to be clear of jumps from the end of the testing time until the end of the run dramatically increasing the number of jumps which had to be removed, and thus the error imparted to the data.

Table 4-9 shows the number of corrections made to gauges before the end of the test time at 500 ms (the number in "()" is the number of jumps removed during the entire test).

Table 4-9
Jumps in Data Before 500 ms, () after 500 ms

Gauge	Run								
	120	121	122	124	125	126	127	130	131
TCB41T	D	D	D	D	D	D	D	D	D
TCB42T	2 (3)	6 (0)	2 (P)	1 (2)	D	D	D	D	D
TCB43T	2 (4)	3 (5)	1 (2)	2 (3)	0 (3)	1 (1)	1 (2)	NU	2 (3)
TCB44T	NU/DD	NU/DD	NU/DD	0 (3)	0 (2)	NU	1 (2)	1 (3)	0 (2)
TCB45T	0 (0)	2 (0)	0 (0)	P/NU	1 (2)	5 (5)	1 (1)	D	D
TCB46T	0 (2)	0 (0)	0 (0)	2 (2)	0 (1)	0 (0)	NU	D	D
TCB47T	0 (0)	0 (0)	0 (2)	0 (0)	0 (0)	0 (0)	0 (0)	1 (BA)	1 (P)
TCB51T	0 (TM)	2 (3)	1 (TM)	D	D	D	D	D	D
TCB52T	NU	D	D	D	D	D	D	D	D
TCB53T	3 (P)	D	D	D	D	D	D	D	D
TCB54T	1 (P)	2 (0)	NU	1 (2)	1 (3)	0 (1)	1 (1)	0 (0)	2 (5)
TCB55T	2 (0)	NU	1 (2)	3 (4)	1 (1)	0 (0)	0 (P)	D	D
TCB56T	0 (0)	NU	0 (1)	1 (1)	0 (0)	0 (0)	1 (2)	3 (3)	2 (9)
TCB57T	0 (0)	0 (0)	NU	0 (0)	NU	0 (1)	0 (TM)	NU	1 (2)

where NU represents a gauge which was not used due to either to many jumps in this time period or due to a problem with an A-D channel yielding bad data (DD). D indicates a dead gauge, P a pinned amplifier. TM state that there are too many small jumps to sort out. BA represents a bad amplifier after the testing time.

Once the jumps were eliminated, the gauges could be rescaled. However, there were some gauges which either pinned after the test time, or contained so many jumps they could not be rescaled; another, separate method for checking the scales and zeros was needed.

Many methods were tried, but the one which met with the most success was to plot the tail end of the data, from when the turbine stopped to when the test was over (from about 160 - 300 secs). Based on how well the top gauge tracked with the bottom gauge during this time differentiated the different gauge classifications. Gauges which were within .4 ° C of the bottom gauge when the rotor stopped were considered class A gauges. Class B gauges were those which tracked within .4 to .8 ° centigrade, and C+ gauges were those over .8 ° C. Some gauges could not be rescaled either because they pinned after 500 ms or contained too many jumps and were classified as group C. B+ gauges were those gauges which exhibited higher drift, but looked as though, given the spread of the other gauges, this was do to the casing not being at equilibrium.

A temperature difference of .4 °C between the upper and lower sensor of a gauge, at the point were the rotor stops, corresponds approximately to a heat flux of 3229 W/ m². If one

divides by an average temperature difference of 100 °C as the difference between the gas temperature and the metal temperature at this point, then the heat transfer coefficient is approximately 32 [W/(M²-K)], a reasonable value for free convection. Table 4-10 shows the final grouping of the gauges.

Table 4-10
Final Grouping of Gauges

Gauge	Run								
	120	121	122	124	125	126	127	130	131
TCB41T	D	D	D	D	D	D	D	D	D
TCB42T	A	A	C	NU	D	D	D	D	D
TCB43T	A	B	A	A	B	B+	A	NU	A
TCB44T	NU	NU	NU	A	A-	NU	A	A	B
TCB45T	A	B	A	NU	A-	B	A	D	D
TCB46T	A	A	A-	A	A-	B+	NU	D	D
TCB47T	A	A	A	A	A-	B+	B-	NU	C
TCB51T	C	NU	C	D	D	D	D	D	D
TCB52T	NU	D	D	D	D	D	D	D	D
TCB53T	C	D	D	D	D	D	D	D	D
TCB54T	B	B	NU	A	B+	B+	A	A	B-
TCB55T	B	NU	C+	A	A	B+	D	D	D
TCB56T	A	NU	A	A	A	B+	A	NU	C
TCB57T	A	A	NU	A	NU	B+	C+	NU	C

where NU represents a gauge which was not used due to either to many jumps in this time period or due to a problem with an A-D channel yielding bad data (DD). D indicates a dead gauge, P a pinned amplifier.

4.4 Approximate Uncertainty Analysis

4.4.1 Error in Heat Flux Gauge Calibrations

Moffat[3] describes a system of categorizing test variables into three different groups each of which has its own error term associated with it; zeroth order, first order and nth order, roughly correlating to errors associated with time invariant phenomenon (reading a

[3] Moffat, R.J. "Contributions to the Theory of Single Sample Uncertainty Analysis" in Journals of Fluids Engineering; June 1982, vol. 104, p. 250-259.

measurement wrong), only time variant phenomenon (drift in calibrations over time), and everything else (misalignment in transducers, etc.). In an ideal situation, one can not get better than the zero[th] order errors and by running the experiment several times before the actual data is taken (i.e mock runs), approximate values for these errors can be derived and thus a conclusion reached about whether the experiment is refined enough to continue on and take data, or whether any data obtained would be so racked with error as to render it useless.

Past experiments using this facility have treated individual heat flux gauges as one instrument which undergoes drift during the testing sequence, recorded by comparing the pre-test and post test bath calibrations. The difference in the scale factors and zeros measured in these two calibrations becomes the uncertainty associated with the gauges over the entire testing sequence. The experimental problems exhibited during this project suggests that perhaps a more accurate representation of the sensors would be to consider them completely seperate instruments for each test, since the amplifiers are reset in almost every test. If this assumption is accepted the problem becomes one of estimating the uncertainty involved in calculating the scales and zeros for each test.

To find the effect of uncertainty of the scales and zeros on the calculated heat flux the Steady-state Heat Flux equation (1) can be reduced to the components that are measured through eqn (2) to get (3) which allows partial derivatives to be taken and used in eqn. (4) which describes the uncertainty in heat flux as a function of measured parameters. The steady-state heat flux is:

$$Q = (k/D)*(T_u - T_l) \tag{1}$$

Where Q is the heat flux, k/D is the thermal conductivity of the Kapton/Kapton Thickness, T_u is the upper temperature and T_l is the lower temperature.

In terms of what is actually measured:

$$T = (V - Z)S \tag{2}$$

Where T is the calculated temperature, V the measured voltage, Z and S are the calculated (or calibrated, depending on how one looks at it) zero and scale for a particular gauge. Thus Q in terms of measured quantities is:

$$Q = (k/D)*[(V_u - Z_u)S_u - (V_l - Z_l)S_l] \tag{3}$$

Thus if one uses the standard form for constant odds error, then the error in Q, ΔQ becomes:

$$\Delta Q = [(\frac{\partial Q}{\partial X_i})^2 \, \Delta X_i^2]^{.5} \tag{4}$$

where X_i represents the ith variable and ΔX_i the error (what ever that definition of error may be) associated with that variable. In Moffat's analysis ΔX_i would be the culmination of all zeroth, first, and n^{th} order terms for that particular variable, which he states will be dominated, in general, by the nth order terms. Equation 4 can be rewritten as a percent error equation after taking the appropriate derivatives and substituting the steady state level of heat flux.

$$\frac{\Delta Q}{Q} = \left((\frac{\Delta(k/D)}{k/D})^2 + \frac{1}{(T_u - T_l)}^2 * ERR \right)^{.5} \tag{5}$$

Where ERR is:

$$ERR = \left(\Delta V_u^2 * (S_u^2 + S_l^2) + (V_u - Z_u)^2 S_u^2 ((\frac{\Delta S_u}{S_u})^2) \right) +$$

$$\left((V_l - Z_l)^2 S_l^2 (\frac{\Delta S_l^2}{S_l}) + (Z_u S_u)^2 \frac{\Delta Z_u^2}{Z_u} + (Z_l S_l)^2 \frac{\Delta Z_l^2}{Z_l} \right)$$

The problem is estimating the different uncertainties in eqn. 5. ΔV is just the cut on the A to D or $2.44 * 10^{-4}$ V ($\Delta V_l = \Delta V_u$). Estimates of $\frac{\Delta k/D}{k/D}$ could be obtained from the laser calibrations, but due to the lack of usable data from this experiment, an estimate for this term of 1.5% was used which came from extensive testing on gauges in previous experiments.

Using this model there are many ways to obtain the variations in scales and zeros. One could use the variation between bath cals over the entire test matrix; or one could calculate the change of scales and zeros from one run to the next as the uncertainty. Both of these methods include, in the error terms, variations which are necessary to get better signals. Another way to estimate the uncertainty in the calculated scales and zeros for each run is to try to match the sensors at points other than just the beginning and the end of the run, yielding an independent calculation of the scales and zeros which can be compared to the previous one to obtain an uncertainty. If one assumes that there is no error in the lower gauge (this implies that the lower gauge acts as a reference thermometer) then the upper gauge can be matched to the lower gauge at the end of the run and when the rotor stops turning (for the reasons mentioned in the previous section, see figure 4.7)

Figure 4-7
Schematic for Recalculating Scales and Zeros
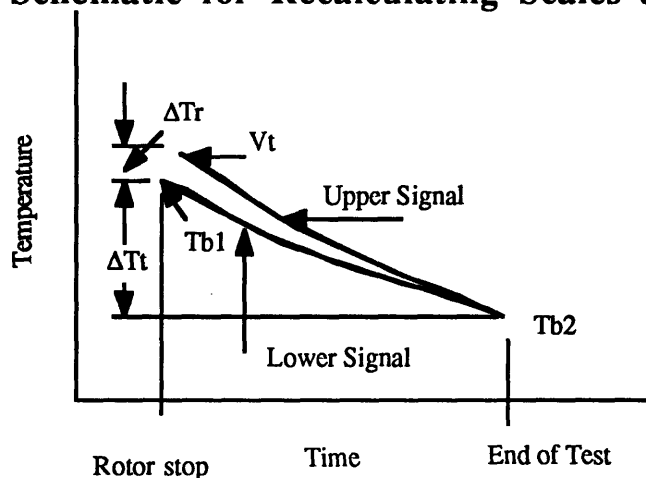
Unfortunately recalculating the zeros and scales in this manner is susceptible to error since ΔT_r is on the order of .2 to .4 ° C and the absolute temperature difference, ΔT_t is about 2 °C and the noise in the signal is .06 °C.

Another method which could be used would be to calculate the uncertainties directly due to temperature and k/D and not reduce it to the actual measured quantities. For example, assuming that there is no error in the lower gauge (as done earlier), taking the partial derivitives of Q as a function of k/D and T_u in eqn 1 yields:

$$\Delta Q = (T_u - T_1) \frac{\Delta k}{D} + \frac{\Delta K}{D} \Delta T_u \qquad (6)$$

Dividing by Q and squaring the error terms yields:

$$\frac{\Delta Q}{Q} = \left[\left[\frac{\Delta k}{D} / \frac{k}{D} \right]^2 + \frac{\Delta T_{u2}}{T_u} \right]^{1/2} \qquad (7)$$

This form has the advantage of being directly measurable from the calibrated data. Using this method, the uncertainty in the DC heat flux is shown in table 4-11. This method overestimates the error as well since one would expect some residual heat transfer to occur to the surrounding metal (since the gas is still much hotter than room temperature) after the rotor stops

4.4.2 Error in Pressure Transducer Calibrations

The pressure measurements, while not subject to the same type of problems as the temperature measurements have their own problems with time, temperature and pressure drift. Our uncertainty is contained in our ability to correctly estimate both the scale and the zero of the transducer over any particular test. By writing the equation for the percent error of pressure as a function of the percent error in scales and zeros we get

$$(\Delta P/P)^2 = \sqrt{(\Delta S/S)^2 + (\Delta Z/Z)^2 * Z^2/(V-Z)^2} \qquad (10)$$

If we use the average total variation of the transducers over the entire matrix of roughly 4% for both scales and zeros (which is what is actually measured) the total error of the pressure becomes about 9%. This of course is another worst case analysis, but given the temperature drift of some of the sensors the pressure drift of others, an average over the entire test matrix is probably not a bad estimate, although it could be improved upon for individual transducers. As will be shown in chapter five, the different pressure transducers have different response patterns and in all probability only two or three of the transducers are actually working well. This information coupled with the poor temperature independence of some of the transducers indicates that the actual error on the operating transducers is probably less than the 9% listed here and will be improved upon at a later date.

Table 4-3
Effects of Amplifier Changes on Calibrations

Gauge Name	Cal 2	Cal 3			% DEL	% DEL	REBALANCED
	Scale	Zero	Scale	Zero	SCALE	ZERO	
TCB43T	-11.286	6.958	-11.339	6.89	-.47	.98	
TCB44T	-11.095	7.021	-11.194	6.959	-.89	.89	
TCB47T	-8.518	8.162	-8.23	7.598	-3.38	7.42	Y
TCB54T	-11.405	6.892	-11.454	6.809	-.43	1.23	
TCB56T	-8.885	7.696	-8.934	7.731	-.55	.46	
TCB57T	-7.57	8.203	-7.602	8.154	-.43	.6	
TCB41B *	-7.045	8.567	-7.062	8.279	-.24	3.49	Y
TCB42B *	-8.653	7.601	-8.689	7.531	-.41	.93	
TCB43B *	-8.905	7.538	-8.951	7.485	-.51	.7	
TCB44B	-10.533	7.234	-10.529	7.204	-.04	.42	
TCB45B	-7.213	8.508	-7.245	8.146	-.45	4.45	
TCB46B	-7.75	7.893	-7.774	7.824	-.31	.87	
TCB47B	-9.292	7.418	-9.323	7.367	-.33	.69	
TCB51B	-8.307	8.044	-8.346	7.637	-.47	5.33	Y
TCB52B	-8.23	8.507	-8.339	7.737	-1.31	9.95	Y
TCB53B	-11.631	8.214	-11.934	6.54	-2.53	25.61	Y
TCB54B	-11.948	6.124	-12.062	6.456	-.95	5.42	Y
TCB55B	-11.541	6.905	-11.631	6.61	-.77	4.47	
TCB56B	-8.684	7.56	-8.736	7.522	-.59	.51	
TCB57B *	-7.046	8.268	-7.076	8.226	-.43	.52	
RTD 3	24.692	-3.957	24.828	-3.954	.55	-.09	
RTD 2	24.752	-3.96	24.823	-3.959	.29	-.02	
RTD 1	24.554	-4.003	24.718	-4.004	.67	-.02	

Gauges left at end of test matrix

% Del = (Max-Min) *100/Minimum value
Scale = Scale Factor of Gauge
Zero = Zero of Gauge
* gauges are part of reference set

Table 4-4
Dependance of Calibrations on Temperature Range

Guage Name	Cal 1	Cal 2		OVERALL	
	% DEL SCALE	% DEL ZERO	% DEL SCALE	% DEL ZERO	% DEL SCALE	% DEL ZERO
TCB41B *	-.09	.04	-.22	.14	-.24	3.2
TCB42B *	-.27	.16	-.14	.08	-.5	8.71
TCB43B *	-.32	.21	-.43	.26	-.9	6.07
TCB47B *	-.28	.14	-.63	7.24	-.82	7.33
RTD 3	2.57	-1.22	2.01	-.86	2.57	-1.34
RTD 2	2.32	-1.08	2.14	-.9	2.42	-1.22
RTD 1	1.97	-.87	3.22	-1.4	3.85	-1.4

Table 4-5

Resistance Changes in Gauges over Test Matrix

Temp (°C)	7/18/88 After Glueing 33.5	8/24/88 After Test 120 26.9	8/26/88 After Test 121 32.6	8/31/88 After Test 122 28.4	9/1/88 After Test 124 27.1	9/1/88 After Test 125 31.8	9/3/88 After Test 126 29.2	9/6/88 After Test 127 27.1	9/6/88 After Test 130 32.7	9/7/88 After Test 131 29.9	9/9/88 After Cal 2 26.	9/23/88 After Cal 3 25.9	% change over Tests
TCB51T	3540.	3749.	3825.	D									
TCB52T	3217.	D											
TCB53T	3558.	D	D										
TCB54T	2781.	2786.	2820.	2834.	2845.	2876.	2877.	2885.	2900.	2990.	2984.	2985.	7.52%
TCB55T	2222.	2230.	2340.	2344.	2365.	2391.	2389.	D					
TCB56T	2279.	2269.	2339.	2345.	2373.	2386.	2380.	2441.	2530.	2666.	2657.	2652.	16.98%
TCB57T	2264.	2255.	2258.	2269.	2268.	2286.	2281.	2309.	2339.	2429.	2422.	2421.	7.29%
TCB41T	2662.	3613.	D										
TCB42T	1687.	1707.	3706.	3592.	4166*	D							
TCB43T	2594.	2659.	2717.	2728.	2761.	2813.	2860.	2910.	2951.	2969.	2962.	2962.	14.46%
TCB44T	2946.	2961.	3114.	3125.	3131.	3152.	3208.	3237.	D	3427.	3421.	3421.	16.33%
TCB45T	2750.	2742.	2767.	2775.	3612.	3447.	3492.	3483.	D				
TCB46T	2935.	2957.	2972.	2983.	2991.	3009.	3007.	3168.	D				
TCB47T	2442.	2433.	2449.	2451.	2450.	2461.	2456.	2482.	2604.	2757.	2749.	2741.	12.90%
TCB51B	2922.	2909.	2911.	2913.	2911.	2922.	2916.	2910.	2923.	2916.	2909.	2909.	-0.21%
TCB52B	2354.	2452.	2460.	2462.	2459.	2469.	2462.	2468.	2486.	2479.	2472.	2458.	5.31%
TCB53B	2561.	2551.	3917*	2974.	2947.	2883.	2852.	2857.	2878.	2870.	2860.	2828.	12.07%
TCB54B	2293.	2284.	2416.	2416.	2413.	2422.	2417.	2412.	2422.	2427.	2421.	2427.	5.84%
TCB55B	2195.	2198.	2279.	2280.	2277.	2285.	2286.	2292.	2315.	2312.	2414.	2416.	5.33%
TCB56B	2203.	2190.	2193.	2194.	2191.	2202.	2196.	2190.	2203.	2196.	2189.	2189.	-0.32%
TCB57B	2199.	2185.	2188.	2189.	2186.	2197.	2191.	2186.	2199.	2192.	2184.	2184.	-0.32%
TCB41B	1986.	1976.	1979.	1980.	1978.	1989.	1986.	1981.	1993.	1987.	1981.	1984.	0.05%
TCB42B	3062.	2976.	2980.	2982.	2978.	2933.	2984.	2978.	2994.	2985.	2976.	2977.	-2.51%
TCB43B	2031.	2018.	2020.	2022.	2019.	2031.	2024.	2018.	2032.	2024.	2017.	2017.	-0.34%
TCB44B	2432.	2418.	2421.	2423.	2419.	2431.	2425.	2421.	2434.	2437.	2443.	2419.	0.21%
TCB45B	2825.	2817.	2820.	2822.	2818.	2832.	2827.	2820.	2837.	2828.	2819.	2820.	0.11%
TCB46B	2330.	2319.	2321.	2323.	2320.	2331.	2324.	2319.	2332.	2325.	2318.	2319.	-0.21%
TCB47B	2740.	2726.	2729.	2730.	2727.	2739.	2732.	2726.	2741.	2733.	2725.	2725.	-0.26%

Table 4-6
Amplifier Modifications

After:	Test 120	Test 121	Test 122	Test 123	Test 124	Test 125	Test 126	Test 127	Test 130	Test 131
TCB41T	Rebal	Rebal	Dead	N. R	Unstable	Dead	Rebal			
TCB42T		Rebal	N. R		Rebal	Rebal	Rebal	Rebal	Rebal	
TCB43T		Rebal	Rebal		Rebal		Rebal	Rebal	Rebal	
TCB44T		Rebal					Rebal			Dead
TCB45T		Rebal								Dead
TCB46T		Rebal								
TCB47T		Rebal	Rebal				Rebal	Rebal	Rebal	
TCB41B		Rebal	Rebal				Rebal	Rebal		
TCB42B		Rebal					Rebal		Rebal	
TCB43B		Rebal						N.R.		
TCB44B		Rebal								
TCB45B		Rebal					Rebal			
TCB46B		Rebal							Rebal	
TCB47B		Rebal								
TCB51T		Rebal	Rebal	Dead						
TCB52T		Dead								
TCB53T		Dead								
TCB54T		Rebal	Rebal	Rebal	Rebal	Rebal	Rebal	Rebal		
TCB55T		Rebal	Rebal		Rebal	Rebal	Rebal			
TCB56T		Rebal	Rebal	Rebal	Rebal		Rebal	N.R.	Rebal	
TCB57T		Rebal	Rebal	Rebal		Rebal			Rebal	
TCB51B		Rebal								
TCB52B	Rebal	Rebal	Rebal	N.R	Rebal	Rebal	Rebal	Rebal	Rebal	
TCB53B		Rebal	Unstable					Rebal	Rebal	
TCB54B		Rebal	Rebal							
TCB55B		Rebal	Rebal				Rebal	Rebal	Rebal	
TCB56B		Rebal							Rebal	
TCB57B	Rebal	Rebal	Rebal				Rebal		Rebal	

Key:
Rebal= Amplifiers Rebalanced   Unstable = Amplifer went unstable
Dead= Dead Gauge
N.R. = New Balance Resistor installed

Table 4-7
Average Scales and Zeros for Pressure Transducers

	Press. Trans 1		Press. Trans 2		Press. Trans 3		Press. Trans 4		Press. Trans 5		TAVG
	Scale	Zero	Scale	Zero	Scale	Zero	Scale	Zero	Scale	Zero	
Test 120	3.700	-4.623	5.151	-4.575	7.277	-4.633	3.090	-4.612	NA	NA	33.97
Test 121	3.753	-4.781	5.104	-4.547	7.308	-4.753	3.132	-4.729	2.602	-4.375	46.06
Test 122	3.656	-4.668	5.099	-4.612	7.097	-4.688	3.068	-4.662	2.352	-4.470	32.37
Test 124	3.676	-4.721	5.048	-4.615	7.069	-4.721	3.082	-4.713	2.693	-4.462	38.56
Test 125	3.677	-4.670	5.088	-4.613	7.199	-4.674	3.072	-4.675	2.228	-4.502	33.78
Test 126	3.736	-4.752	5.095	-4.613	7.272	-4.734	3.115	-4.748	2.459	-4.459	41.07
Test 127	3.817	-4.701	5.198	-4.579	7.460	-4.706	3.174	-4.694	2.588	-4.049	42.38
Test 130	3.784	-4.798	5.051	-4.605	7.120	-4.809	3.156	-4.751	2.621	-4.360	47.23
Test 131	3.744	-4.585	5.158	-4.561	7.390	-4.618	3.115	-4.590	2.188	-4.430	34.08
Average	3.727	-4.700	5.110	-4.591	7.244	-4.704	3.112	-4.686	2.466	-4.388	38.83
Max %	4.41	-4.43	2.97	-1.47	5.53	-3.97	3.46	-3.39	23.11	-10.06	45.92

Variables:

Max % = (Max value-Min Value)100/Min Value

Tavg = Average temperature Deg. C

TABLE 4-8

Comparision of Final Temperatures

RTD's 2 & 3 and Reference Guages (TCB41B, 42B, 43B, and 47B)
Values averaged from 290-300 sec

	Test 120	Test 121	Test 122	Test 124	Test 125	Test 126	Test 127	Test 130	Test 131
RTD 3	49.88	58.06	43.51	48.42	44.52	54.37	57.64	61.93	53.17
RTD 2	51.01	59.00	43.94	48.97	45.00	55.29	58.10	62.36	55.51
Average	50.45	58.53	43.73	48.69	44.76	54.83	57.87	62.15	54.34
TCB41B	50.96	59.17	43.82	49.09	43.84	56.75	57.91	62.08	53.05
TCB42B	50.84	58.97	43.78	48.98	43.49	55.29	57.98	62.03	53.05
TCB43B	50.68	58.93	43.81	48.92	43.40	55.13	57.82	62.03	53.02
TCB47B	50.72	58.78	43.83	48.86	43.39	54.95	57.91	62.03	53.01
Average	50.80	58.96	43.81	48.96	43.53	55.53	57.90	62.04	53.03
STD. DEV	0.12	0.16	0.02	0.10	0.21	0.83	0.06	0.03	0.02
ABS(MEAN RTD-MEAN REF)/STD. DEV									
	2.84	2.66	4.36	2.65	5.86	0.85	0.61	4.01	59.68

Table 4-11
Fational Error of Heat Flux

Gauge	Gauge Type	Test 120	Gauge Type	Test 121	Gauge Type	Test 122	Gauge Type	Test 124	Gauge Type	Test 125	Gauge Type	Test 126	Gauge Type	Test 127	Gauge Type	Test 130	Gauge Type	Test 131
57	A	0.03	A	0.02	A		A	0.05			B+	0.02	C+	0.10			C	2.85
56	A	0.02			A	0.04	A	0.02	A	0.13	B+	0.02	A	0.04			C	1.26
55	B	0.06			C+	1.13	A	0.02	A	0.03	B+	0.05						
54	B	0.05	B	0.02	A		A	0.02	B+	0.08	B+	0.04	A	0.02	A	0.02	B-	0.08
53	C	6.46																
52																		
51	C	6.74	C		C	11.40												
47	A	0.02	A	0.02	A	0.02	A	0.03	A-	0.02	B+	0.02	B-	0.09			C	5.32
46	A	0.14	A-	0.04	A-	0.25	A	0.09	A-	0.27	B+	0.08						
45	B	0.02	A	0.03	A	0.06	A		A-	0.06	B	0.13	A	0.02				
44							A	0.02	A-	0.03			A	0.02				
43	A	0.03	A	0.02	A	0.04	A	0.02	B	0.13	B+	0.02	A	0.02	A	0.02	B	0.03
42	A	0.03	C	0.02	C	11.80	B	0.02			A	0.02	A	0.02	A		A	0.02
41																		

Figure 4-3

Axial Gauge Location and Coordinates with Respect to the Rotor Blade
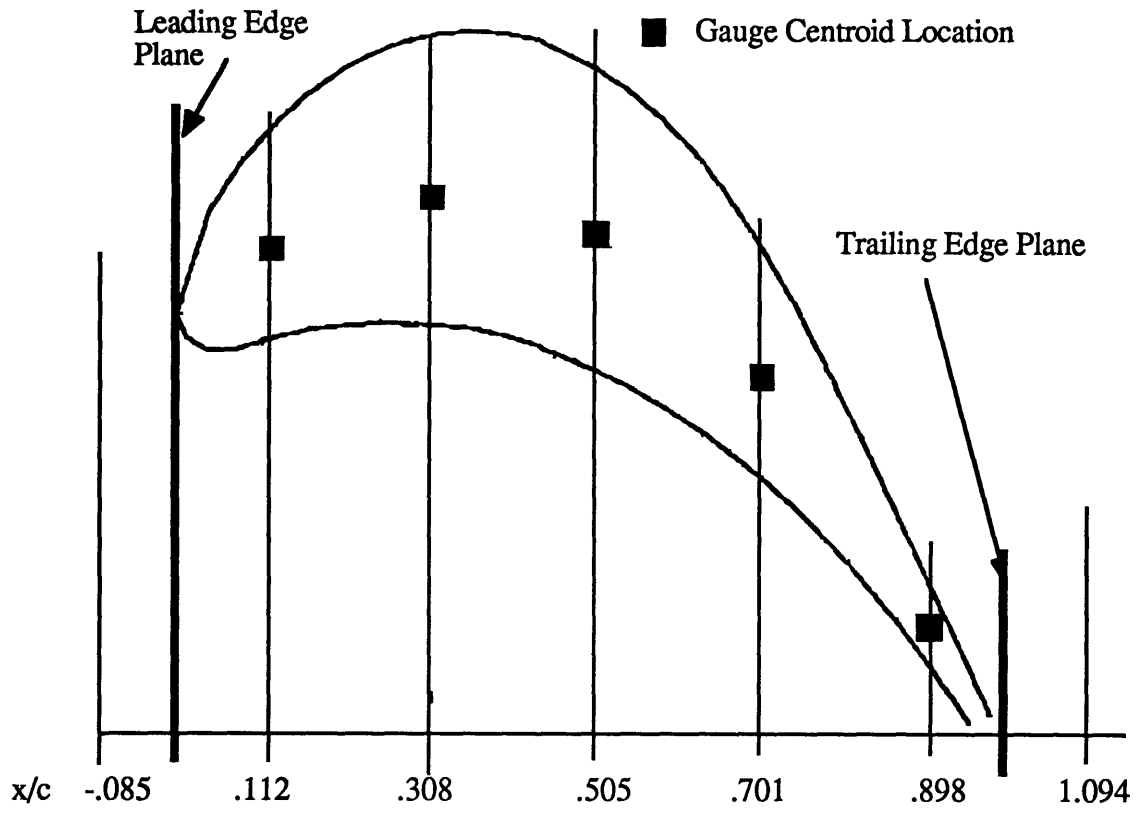
| x/c | -.085 | .112 | .308 | .505 | .701 | .898 | 1.094 |
| mm | -2.184 | 2.885 | 7.965 | 13.045 | 18.125 | 23.205 | 28.285 |

Gauge Location

| 1 | 2 | 3 | 4 | 5 | 6 | 7 |

Gauge Position

(Units)	1	2	3	4	5	6	7
Distance from leading edge of tip shroud (inches)	.1006	.3006	.5006	.7006	.9006	1.1006	1.3006
Distance from leading edge of blade (inches)	-.086	.1136	.3136	.5136	.7136	.9136	1.1136
Axial Distance C	-.085	.112	.308	.505	.701	.898	1.094
Position of center of blade relative to center of blade at gauge 2 (+ is opposite rotation direction) (inches)	N.A.	REF	-1.835	-.291	5.271	14.69	NA
Blade thickness Span	N.A	.284	.391	.410	.324	.132	N.A

Span= 28.517 mm distance between blades

N.A.= Not Applicable
REF= Reference

FIGURE 4-4: RESPONSE OF TIP CASING PRESSURE
TRANSDUCERS DURING CALIBRATION PROCEDURE FOR
TEST 131
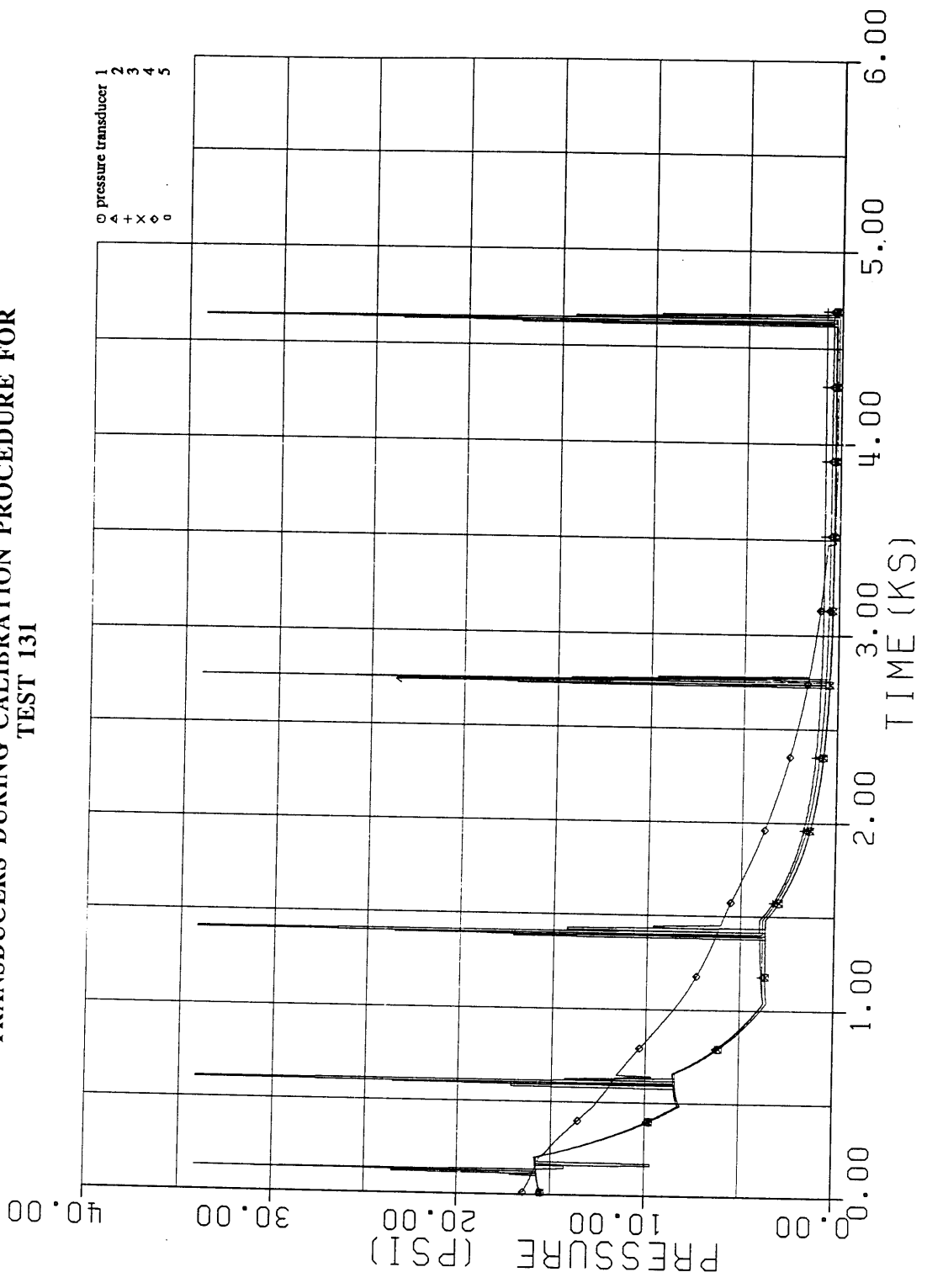
FIGURE 4-5: TIP CASING PRESSURE TRANSDUCER
DEPENDENCE ON TEMPERATURE
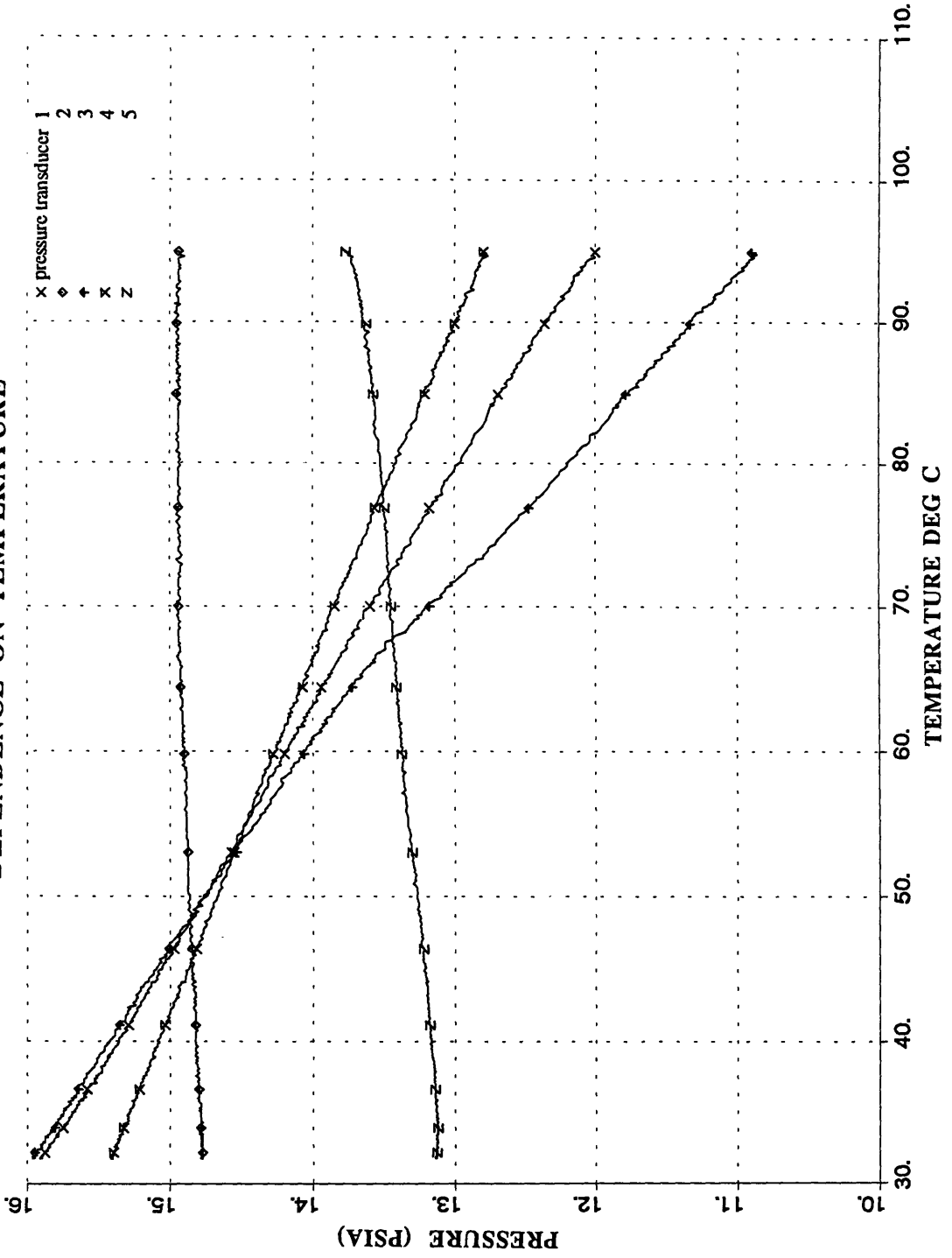
FIGURE 4-6: TYPICAL JUMP IN DATA
(Gauge 46T, Test 124)

90
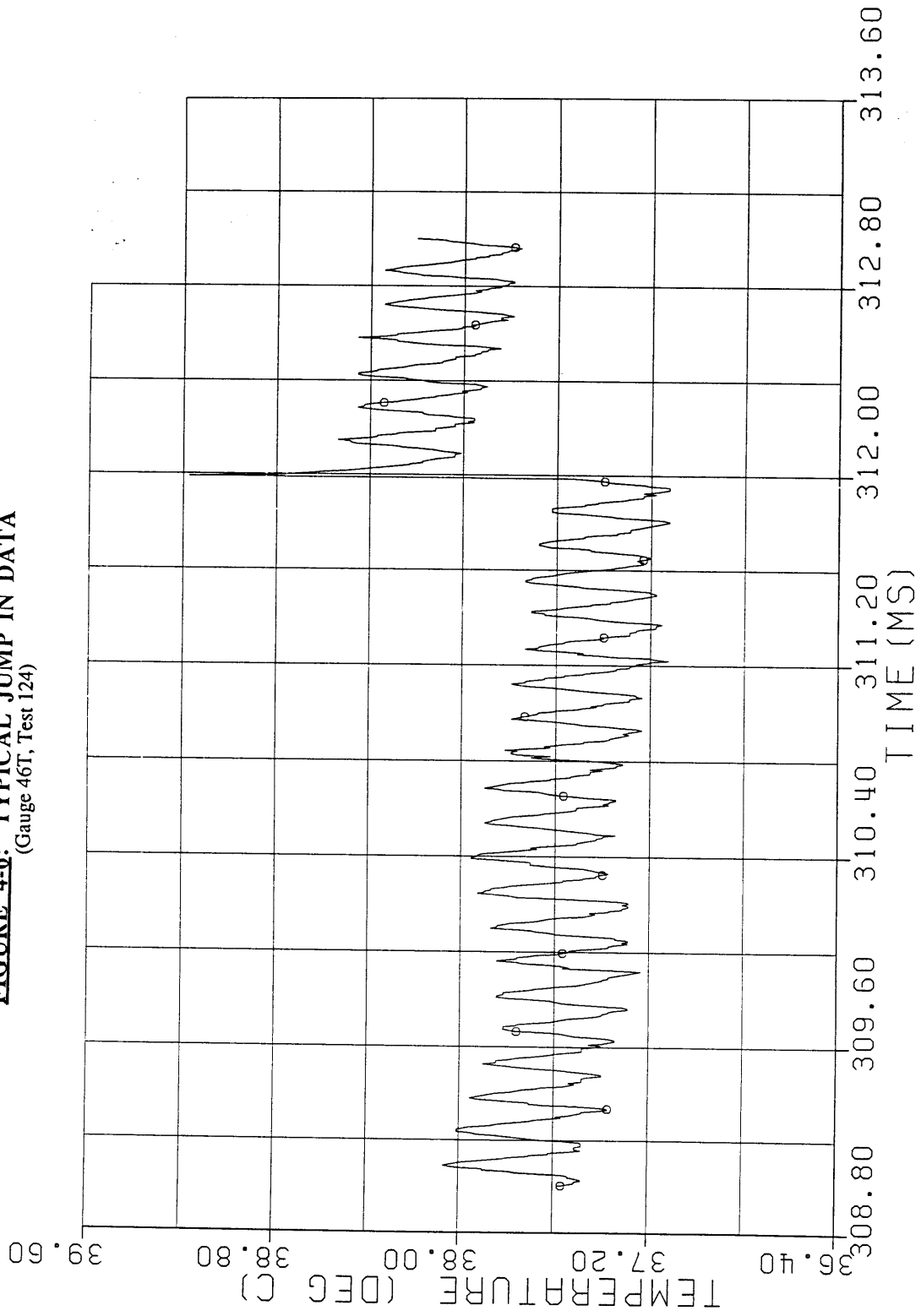
Chapter 5: Data Presentation

The previous four chapters dealt with the set-up and running of this project; this chapter shall present the data and attempt to quantify the effects of tip gap, temperature profile, and average gas temperature on the tip shroud heat flux. The first section of this chapter outlines the different components of heat flux which are studied, the physical significance of the non-dimensional parameters used for comparing the different tests, and some of data reduction techniques used. The second section of the chapter confronts the main engineering questions which were the purpose of this investigation: what are the effects of profile, gap and absolute temperature on heat flux to the tip shroud. The final section discusses briefly the results of the total uncertainty associated with the heat flux measurements and the pressure data. Analysis and conclusions are stated in the final chapter along with recommendations for future work.

5.1 Data Reduction

The fundamental goal of this experiment was to accurately measure the affect of the independent variables on the heat flux to the tip shroud. The heat flux is primarily an unsteady process and can be divided into two components: a time averaged part and an instantaneous part. Thus the total heat flux at any point can be described as a combination of these two variables (eqn 1).

$$q = \overline{q} [X_i] + q'[Y_i] \tag{1}$$

where $\overline{q}$ $[X_i]$ is the time averaged heat flux influenced primarily by the geometric and flow parameters $[X_i]$ and $q'[Y_i]$ is the time dependent heat flux which may depend on geometric and flow variables as well as time. In splitting the heat flux into these two parts it is important to ensure that the averaging period selected does not influence the results of the time averaged quantity. The experimental question is what do the independent variables $[X_i]$ and $[Y_i]$ physically represent. Are they related mostly to geometric properties such as the nozzle guide vane geometry or the tip clearance; are they flow variables such as total temperature, total pressure, or the profile, or are they a combination of the two.

Thus one has to be careful in how the data analysis is done to ensure that possible variations among these variables for different tests are not eliminated as noise. One way to do this would be to run several different tests at one condition; yielding an appropriate value of the randomness associated with any one set of geometry and flow variables. Another method which would allow separation of some geometric variables would be to take measurements at the same axial location, but different circumferential locations. There, is of course, all independent of a separate question; how accurately do the measurements taken at any point

reflect the flow that occurred.

These goals of multiple tests at the same conditions and different circumferential measurements were not completely fulfilled due to the erosion of the gauges. There were no multiple runs since there were virtually no gauges left at the end of the first test matrix and there were not enough operating gauges at any one point to yield many circumferential comparisons. The sand-blasting also had an effect on the calibration procedures and the data reduction process limiting the extent of the uncertainty analysis. These problems imply that some limits exist on the conclusions that can be drawn from this experiment. Answering the ultimate question of what the data really represents (i.e what causes the flow to behave the way it does, which is beyond the scope of this project), may require additional work. Much of the investigation of the data done in this paper will look at the questions of how well does one know the flow field and what are the significant effects present in the data, in the hope that this data can better guide future experiments.

5.1.1 Interpretation of Non-Dimensional Quantities

The questions which can be answered revolve around the influence of the various investigation variables on the tip shroud heat transfer in both a time-averaged environment and the time resolved regime. However the question remains as to what is the best way to compare different tests to bring out the points of interest - what is the best way to non-dimensionalize the data for the different possible causes (the variables $[X_i]$ and $[Y_i]$ in eqn. 1). Two traditional non-dimensional parameters which could be used, the Nusselt number and the Stanton number have problems in their implementation. The Nusselt number, which is a comparison of the convective heat transfer to the conduction through a slice of fluid L units thick (eqn 2):

$$Nu_L = hL/k_f \tag{2}$$

where h is the convective heat transfer coefficient given by $h = q/(T_{ref} - T_{wall})$, L is the length scale and k_f is the thermal conductivity of the fluid.

requires a free stream total temperature (T_{ref}) for the calculation of h, which is not available. The Stanton number:

$$St_l = \frac{h}{\rho C_p U_\infty} = \frac{Nu_L}{Re_L Pr} \tag{3}$$

Where Re_L is the Reynolds number based on the same length scale as the Nusselt number and Pr is the Prandtl number.

has the same problem since it to relies upon a calculation of h. Thus the only physical interpretation left for these numbers in this case, is a global interpretation which would be

based on the inlet total temperature and on some global length scale (perhaps blade chord or rotor diameter). The total temperature could be either the mass-average temperature entering the turbine stage, or the temperature at the tip of the upstream temperature rake.

Thus the question of how to best resolve the different geometric and flow influences remains largely unresolved. Differences can be observed and compared, but the analytical framework is not developed to the point where their underlying causes can be evaluated. Nusselt numbers will be used to compare test of different conditions but because of limits on what is known, (the Nusselt and Stanton numbers represent global information; information which may be of use in designing a stage, but which is of little use in understanding the dependence of heat flux on the flow variables) most comparisons, where appropriate, will be done between heat flux measurements.

Another problem is defining the inlet conditions in non-dimensional terms so that they can be properly compared. For these tests, generally, global variables are used. For the description of the temperature profile, the RTDF parameter is used, as described in chapter two, eqn. 1, using the measured peak, mean and minimum temperatures at the upstream temperature rake. The blade gaps were normalized by the blade span at the leading edge of the rotor blade. And the inlet temperature was normalized by calculating a driving temperature ratio:

$$\text{Driving Temperature Ratio} = \frac{T_g - T_w}{T_w} \tag{4}$$

where T_w is the metal temperature at the beginning of the test and T_g can be either the average temperature at the Nozzle guide vane inlet, or the temperature at the tip of the nozzle guide vane.

5.1.2 Analysis of the Time-Averaged and Instantaneous Heat Flux.

The decomposition of the total heat flux into the two groups, time-averaged and instantaneous requires different observational methods in isolating the various effects. When looking at the time-averaged data alone one has to be certain the fluctuations in the results due to different averaging periods are small compared to the other errors present in the data. One would expect that as the averaging period is increased, the percentage of change in the results decreases. Thus , when the appropriate level is reached this part of the data becomes "steady" (even though the process is primarily unsteady). Comparison between "steady" data is relatively straight forward, however the possibility exists that although the "steady" (or DC as it will be referred to from here on) may be the same for different tests, the heat load could be occurring in different ways which could lead to the problems exhibited in jet engine tip shroud

burn out. It has been noted that the AC (time resolved) fluctuations are large, sometimes 30% of the peak heat flux loads indicating that the problem is not generally one of small perturbations and thus examining the changes which occur in the AC loading are important.

How one does this is not clear. Since interconnections between AC fluctuations in the heat flux and the mechanical degradation of aircraft engine parts has not been fully established analyzing the AC data becomes almost purely qualitative. Magnitudes, shapes and variations based on axial and circumferential positions can be observed, but more sophisticated models of the flow are needed for technical conclusions. When answering the engineering questions poised at the beginning of this chapter, both the DC and the total heat flux (AC+DC) data will be presented.

5.1.3 Data Processing

There were many different programs used to help decipher the data, some of which were used to organize the data and others which were used to fundamentally change it. Three of these programs actually change the data and should be mentioned: the filtering program, the averaging program, and the unsteady heat flux calculating program.

Filtering the Data-

To reduce the random noise which occurs during the experiment, a low-pass filter program was used to cut the signals off at above 40 KHZ. This is approximately five times the blade passing frequency. The filter used is a "Nearly Equal Ripple" type (based on papers by Kaiser and co.[1]) which is specified by the cut-off frequency, the band width of the transition zone, and the relative error allowed in the ripple after the transition period. Unless otherwise noted the filter program used during these tests was a 40 Khz cut-off with a 3 Khz transition and a 40 Db error. As a comparison, some data was re-run with a 3 Db error and no difference was detected. This is probably due to a high signal to noise ratio and the fact that by 40 Khz the harmonics are as small as the noise which is an order of magnitude less than the main harmonics.

Averaging-

There were many different types of averages which are of interest during the tests. There are averages of blade "A" with blade "A" one revolution later and so on over the specified number of revolutions (Blade averaging). Rotor averages consist of every blade being averaged together (all 61 blades) for the required number of revolutions. And there are group

---

[1] Kaiser, J.F. and W. A. Red, Review of Scientific Instruments, 48,1447 (1977); 49,1103 (1978)

averages, which average the different blade values over one group. The results of these procedures would be, if one was averaging over 10 revolutions: for a blade average, 61 separate signals per revolution, where each signal represents one blade passing which is the average of that exact blade over ten revolutions. The rotor average would have one pattern, repeated 61 times (per revolution) and would be the result of an average of 610 blades. The group average would be the average of the five blade averaged signals in one group (reference, small, or large) and would represent an average over 50 blades. Unless otherwise noted, all DC data presented will be rotor averages from 350 ms over 10 revolutions and will be revered to as the standard average.

To do the averaging, a position encoder is located on the rotor system that provides the angular position of the rotor at any point in time. This provides a once per revolution signal which occurs in the same physical location for every test (it changes only when the rotor is removed), but can occur at different times depending on where the rotor was at the beginning of the test. This information is important because since the data really starts being averaged when the first "once/rev" signal occurs after the initial starting time. In this manner the data can be averaged exactly over the proper number of revolutions. The 1/rev signal is also used to convert the time axis to blade passing. Data for different tests have been time shifted to account for the differences in the speed and the once/rev signal, but variations in the signal between axial positions for any given test have been preserved.

The Heat Flux Program-

Steady state heat flux is obtained relatively easily by measuring the upper and lower sensor temperatures at any given time and multiplying by the k/D of the gauge. For the time resolved measurements, a model of the Kapton as a filter was used to calculate the heat flux. The theory behind this program comes from a paper done at Oxford by Oldfield[2] and verified at the MIT Gas Turbine Lab[3]. This allows the complete reduction of the heat flux over the entire frequency range. For these tests the Frequency range of the model was from 200 Hz to 40 KHZ using a nine stage model

[2] Oldfield, M.L.G. and H.J. Burd, N.G. Doe "Design of Wide Bandwidth Analogue Circuits for Heat Transfer in Transient Tunnels" Oxford University Engineering Laboratory Report 1382/81

[3] Epstein, A., G. Guenette, R. Norton, and C. Yuzhang "High Frequency Response Heat Flux Gauge." in Review of Scientific Instruments, Vol. 57, No. 4, April 1986, pp. 639-649.

5.2 Data Presentation

5.2.1 Instrument Locations

When presenting the data, it is important to remember the parameters which are changing and how they relate to the instrumentation position. This information is culled from the preceding chapters and reproduced in the following tables. Table 5-1 shows the different circumferential positions in which measurements are taken (see fig. 3-12 for more information). Table 5-2 shows the different axial locations of the instruments, and table 5-3 shows the different blade gaps studied.

Table 5-1
Circumferential Position of Instruments

Test	40 series gauges	50 series gauges	Odd # Pressure Transducers	Even #
120	Circ. Pos. 2=.197	CP 6=-.554	CP 5=-.303	CP 4=-.178
121	CP 2	CP 6	CP5	CP 4
122	CP 2	CP 6	CP 5	CP 4
124	CP 2	CP 6	CP 5	CP 4
125	CP 2	CP 6	CP 5	CP 4
126	CP 2	CP 6	CP 5	CP 4
127	CP 5 = -.303	CP 1 = .447	CP 2= .197	CP 3 =.072
130	CP 5	CP 1	CP 2	CP 3
131	CP 5	CP 1	CP 2	CP 3

Where positions 1-6 are defined in figure 3-12.

Table 5-2
Axial Location of Instrumentation

Gauge 40's	50's	Tests 120-126 Axial Location number.	Tests 127-131 (see fig 4-3)	Location #	Position (x/C)
TCB41	TCB51	1	7	1	-.085
" 42	" 52	2	6	2	.112
" 43	" 53	3	5	3	.308
" 44	" 54	4	4	4	.505
" 55	" 55	5	3	5	.701
" 56	" 56	6	2	6	.898
" 57	" 57	7	1	7	1.094
Pressure Trans. 1		1	5		
" 2		2	4		
" 3		3	3		
" 4		4	2		
" 5		5	1		

Table 5-3
Blade Gaps

Blade Group	Nominal Static Gap	Amount Removed	Gap/Span
Reference	.026"	0.000	1.7%
Small		.006"	2.1%
large		.012"	2.5%

5.2.2 Preliminary Analysis and Analysis Techniques

Before the heat flux dependance on temperature and profile can be studied three questions must be asked. The first question involves developing a proper analytical procedure for evaluating the data. Questions such as "What defines the average value?", "Should one average the temperature data and then calculate the heat flux, or calculate the heat flux and then average it ?" or "Does it matter how one does it ?" must be answered. The last two questions involve the dependence of the data on the tip gap and the circumferential locations of the instruments. One might expect some variation due to either of these geometric variables, but they may not be visible in this experiment and thus their elimination could reduce the amount of separation needed in the data. Answering these last two questions can eliminate some of the options in the first question and establish a consistent way of presenting the data developed.

For the DC data the problem becomes one of averaging times. Should a blade average, group average or a rotor average be used to express the mean values of the data. If one uses group or blade averages then only a small amount of total time is being averaged and the final results may be susceptible to the averaging period. One way around this problem is to ask if there is indeed any visible variation between different tip gaps, for if there is no variation, this problem can be eliminated.

5.2.3 Differences Due to Tip Gaps

Table 5-4 (a) lists the heat flux measurements for all the tests for the 1.7% gap and the 2.5% gap blades (for types "A" and "B" gauges, see chapter four). The data presented is a filtered group average of the 1.7% gap blades and the 2.5% gap blades. Heat flux measurements can be used in this case (versus non-dimensional measurements) since comparisons are being made only for one gauge at any one run condition. There is not even a comparison between different gauges at the same axial location for the same run, thus all the variables are the same except blade gap and non-dimensionalization is not needed. Table 5-4

(b) shows the differences between these two different gaps (1.7%-2.5%), normalized by the 1.7% gap. Two key points lead to the conclusion that variations in tip gap do not play an important role in the DC data. First, no clear pattern establishing which gap maintained a larger heat flux was present; half the time it changed from one group to the next. The second point is that while a few gauges demonstrated large fluctuations between groups, the majority had low levels of variations. The only exception occurs on the low temperature tests where the absolute level of heat flux becomes quite low (even negative on one run) making the percentage change large. This suggests that variations between blade groups are too small to be acceptably quantified in this experiment. A majority of the differences are of the same order of magnitude as the error introduced through the calibration process (see table 4-11). However, a supplemental question needs to be addressed before a conclusion is reached. How accurately do these averages represent the "true average " of the data.

Unfortunately multiple runs at the same conditions were not done so the only process available to estimate the variation in the data averages is to establish its dependence on the averaging times. The averaging times can influence the data through the selection of the starting time and the length of averaging period. To check the influence of the averaging technique on the results, different blade averages were calculated as well as a rotor average (the rotor average has the effect of dramatically increasing the averaging times). Comparing these results there was no significant difference beyond the levels seen separating the two different blade gaps. Figures 5-1 (a-c) show the different heat flux patterns for the blade averaged values of 5, 7, and 11 revolutions for test 120 gauge 46. While there is some difference it is small compared to the overall circumferential variation seen throughout the rotor. Fig 5-1 (d) compares these plots directly on an expanded time scale. From this information it is apparent that the data does not depend on the averaging technique to any greater extent than the data depends on the average gap variations. The final question which must be answered before the tip gaps are eliminated as a variable is, "Is there any variation due to the clearance present in the AC data?".

Figure 5-2 (a-f) show the "turbine signatures" (blade averaged data) for three different runs (high temperature high profile, high temperature no profile, and low temperature no profile). The blade passing frequency is approx. 7.2 Khz and two gauges are plotted for each run. Gauge 47 at the trailing edge where there is little direct blade interaction and gauge 43 where the blade thickness represents approximately 40 % of the blade spacing. If there is any effect due to tip gaps, one of these two extremes should show indications of it. From these graphs it is apparent that variations exist in the rotor but they do not seem directly linked to the blade height. There are only three groups of blades, and the reference gap (1.7% span) represents 84 % of the blades and any variation which is due to blade gap should appear

concentrated around the small and large gaps, which it does not. To get more detail, group averages of the 1.7% gap blades and the 2.5% gap blades were compared for different tests. Test 120 provides a good example of the differences.

Figure 5-3 (a-j) compares the blade averaged AC heat flux of the 1.7% group with the 2.5% gap group. Test 120 shows evidence of circumferential variations between different gauges at the same axial location which can be large. Typically, the 1.7% gap has higher AC values of heat flux than the 2.5% gap; however on many gauges, such as gauge 56, the variations between gaps is smaller than the blade to blade variation within a gap. In addition the greatest variance seems to be between gauges at the same axial position, but different circumferential positions. This behavior suggests that the variation due to gap clearance, if they exist, are drowned out by the circumferential and blade to blade variation.

Thus it appears as if the influence of tip gap on this experiment is of a much smaller scale than the other investigation variables. This may be due to an increase in the static gap of the MIT facility which is essentially twice the design condition or it could be due to the resolution of the instruments. But based on these results: no steady-state effect or transient effect, the task of analyzing the rest of the data will be simplified. Instead of using blade or group averages, the unsteady data can be averaged over many more blades using a rotor average which should help to provide more consistent measurements.

5.2.4 Procedure for Evaluating the Time-Resolved Data

A remaining problem is analyzing the data involving the unsteady measurements. The program which calculates the unsteady heat flux is a non-linear system; meaning that if one filters some data and then uses this program, the result may not be the same as if one applies the heat flux program directly to the data and then filter it. For data which is averaged over many cycles either before or after this program is run the data results should converge. Using many different procedures, data from a variety of tests was evaluated. For the main procedure in question, should one first rotor average the data and then perform the heat flux calculations , or do the heat flux calculations and then average the result; no difference was found in the final results when a rotor average of the data was used.

The conclusion at this point is that there is no variation due to tip gap. This implies that the best averaging technique to use is a rotor average, since it averages enough blades to guarantee no cut-off due to the filtering aspects of the Kapton in the steady state calculations. For the unsteady investigations there is no difference in results due to the order of operation, and thus for all unsteady data, the data will be calculated using a standard filter and the standard rotor average (350 ms over 10 revolutions). The last question is, "Are the variations due to

circumferential location important in all the runs?"

5.2.5 Circumferential Variation in the Results Due to Instrument Location

Table 5-5 shows the DC values of the heat flux measurements for each run using the standard data. Since only gauges are compared which are in the same run, using the heat flux measurements as a indication of the variation is legitimate. The only variations are due to the different circumferential measurement locations which are not accounted for in the non-dimensional parameters studied so far. All the gauges which produced some kind of data are presented and the ones which are in group B or below (see chapter four) are highlighted. The chief suspect for circumferential variation would be the presence of the nozzle guide vane wakes. To quantify the circumferential position of the gauges, the nozzle guide vane closest to the center of the tip casing (see fig. 3-12) was used as a reference (see table 5-1). The measurement used in table 5-5 is the distance of the gauges from this nozzle guide vane divided by the nozzle guide vane spacing with the positive axis being counter rotational. The variations were calculated by taking the difference in circumferential values and normalizing by the free stream value of heat flux (the value obtained in the center of the nozzle guide vane passage). It should be noted that using this system is only good for comparison purposes since during any different set of run conditions the gas exiting the nozzle guide vanes may have vastly different angles associated with it implying that the wakes due to the nozzle guide vanes could be offset by quite a large amount. But since we are examining comparisons between gauges for one run condition it is only important to know the relative distances between the two measurement locations, not where they occur in the nozzle guide vane wake, to show a difference.

The results indicate variation which seems to be both a function of profile and absolute temperature. As an example, notice that the amount of variation seems to decrease as the profile decreases for the high temperature runs. And for the low temperature runs, the relationship seems to invert, with the highest values of heat flux being closest to the nozzle guide vanes. Figure 5-4 (a-u) represents a comparison of the total unsteady heat flux for all runs which have two gauges at the same axial location (basically the AC+DC plots of the points discussed in table 5-4 b). The time axis has been normalized in these plots to represent blade passing. This data has many interesting points. Most of the blade shapes are similar between axial location, except for positions six and seven where a distinct difference between the circumferential positions develops. As an example, looking at figures 5-4 (a-d, test 120) it is apparent the maximum heat flux variations (the AC component) are of a similar order of magnitude, but in the troughs a secondary peak appears in fig 5-4 (c, location 6, test 120) which develops into a bigger peak at the next axial location 7 (fig 5-4 d). One may notice the

strange time shift for gauges 47 and 57 in tests 127 and 131 (fig. 5-4, r and u). This is probably the influence of the nozzle guide vane wakes since in these runs, gauges 57 and 47 are at the leading edge. Another interesting point is that in most cases, positions with large differences in steady-state results have differences in AC results, although the relationship between the magnitudes of the two measurements is not clear. An example of this is shown in fig 5-4 (k, test 125, location four), where the DC difference is 25 % and the variability in the magnitudes of the AC data is relatively small (since the two signals are slightly shifted vertically due to their shapes) and fig 5-4 (q, test 127, location 4) where the DC difference is 10 % and the differences in AC values are quite large. There is also a tendency for the AC component of the heat flux to decay slightly as one approaches the trailing edge.

In conclusion there does appear to be variation with circumferential position, although its causes are not clear. DC variations of up to 50 % have been observed, however the median variation is about 20%. The amount of variation also appears to be loosely coupled with both the axial position and the profile, with the amount of variation increasing with axial position and decreasing with profile, although not consistently. It also appears as if the sensors are detecting some flow phenomenon such as the wakes behind the nozzle guide vanes and the development of the second spike (perhaps a shock or wake) at the trailing edge of the casing. The conclusion that can be reached at this point is that directly comparing gauges from different circumferential positions is not valid and when examining the effects of profile and temperature on heat flux to the shroud, measurements taken at different circumferential positions have to be separated.

5.2.6 Turbine flow With and Without the Profile Generator Installed.

Perhaps one of the most fundamental questions, from the standpoint of comparing data from this test to past experiments is does the physical addition of the flow generator alter the flow. To answer that question the operating conditions of this test sequence where chosen to match a run done several years earlier, test 21. The two tests involved in this experiment were test 121 and test 130, the high temperature, uniform flow runs (test 130 had the tip casing inverted). A nominal comparison of the run conditions is given below in table 5-6.

Table 5-6
Run Conditions of High Temperature, Uniform Flow Runs

	Test 21	Test 121	Test 130
Total Temp (°K)	468.72	467.71	471.15
Total Pressure (atm)	3.504	3.547	3.511
Speed (rps)	121.74	121.71	125.68
Gamma	1.279	1.284	1.281
Mean Tip Gap	.8 (est)	1.7	1.7
(% of Span)			

As one can see the run conditions are close. Comparison of these tests should be done with Nusselt numbers even though the test conditions are marginally the same. Before this can be done the uncertainty of the heat flux measurements are needed.

Presently there are two sources of error in the heat flux measurements; those from the calibration procedure and those due to the averaging technique. These errors have been estimated; the calibration error was shown in table 4-11 and the error due to averaging was estimated earlier by comparing the different results between the group averages (more on this in the final section). These errors can be combined using the root mean square of the terms because they are independent. The Nusselt number in terms of what is measured is given by eqn. 4:

$$Nu_L = \frac{Q_{measured} L}{k_f (T_{ref} - T_{wall})} \tag{4}$$

By taking the partial derivatives of this equation one finds the error in Nusselt number as a function of the percentage changes of the unknown variables Q, T_{ref}, and T_{wall} is shown in eqn 5.

$$\frac{\Delta Nu_L}{Nu_L} = \sqrt{[\frac{\Delta Q}{Q}]^2 + [\frac{\Delta T_{ref}}{(T_{ref} - T_{wall})}]^2 + [\frac{\Delta T_{wall}}{(T_{ref} - T_{wall})}]^2} \tag{5}$$

The last two terms can be neglected since the gas temperature is , at its smallest level is 70 °K above the wall temperature. Typical values for $\Delta T_{ref}/T_{ref}$ are on the order of .16 %[4]. Calibration errors associated with the upper sensor on the heat flux gauge, while unknown, can be estimated in the same fashion as the calibration error was in chapter four and therefore ΔT_{wall} is on the order of .2 to .4 °C. Therefore the errors in these last two terms will be much smaller than the error estimated for Q and as a result the error in Q becomes the error in Nusselt number.

Table 5-7 shows the heat flux, errors, and variations between test 21 and tests 121 and

---

[4] Cattafesta, Lou "An Experimental Investigation of Inlet Radial Temperature Profiles on the Aerodynamic Performance of a Transonic Turbine Stage", Master's Thesis, August 1988, p.65

130. Table 5-8 shows similar results for the Nusselt number. The length scale used for the Nusselt number calculations is the rotor blade chord, and the Nusselt number was calculated using both the area-averaged inlet total temperature (which is the same as the mass averaged inlet temperature in this facility) and the total temperature at the tip of the temperature rake. The data used is a filtered and rotor averaged from 350 to 400 ms (these results are plotted in figures 5-5 , heat flux and 5-6, a and b, Nusselt numbers based on average and tip temperatures respectively).

Table 5-7
Heat Flux Measurements and Variation
for Tests 121, 130, and 21
(KW/M²)

	Test 121							Test 130	
	57	54	47	46	45	43	42	54	44
Circumferential Pos.	-----6-----		----------------2---------------					1	5
Heat Flux (avg)	32.1	113	29.2	31.1	69.0	103	111	99.2	92.5
Calibration error (table 4-11, %)	2	2	2	4	3	2	2	2	2
Averaging error	1.83	0	1.68	0	.43	0	0	.20	.65
Total Error (%)	2.7	2	2.61	4.	3.03	2	2	2.01	2.1
Heat Flux Test 21	13.5	105	13.5	30	82.5	116	112	105	105
Circumferential Pos	------------------- 5 ----------------							------5-------	
% Variation	81.6	7.3	73.5	3.6	17.8	11.9	.9	5.6	13.6
Group Types for Test 121,130	A	B	A	A	B	A	A	A	A

Errors are in percentage change of variables
Variation from Test 121 and 130 to test 21 is (Maximum-Minimum)/Average

Table 5-8
Nusselt Numbers
for Tests 121, 130, and 21

	Test 121							Test 130	
	57	54	47	46	45	43	42	54	44
Circumferential Pos.	-----6-----			-----------------2--------------------				1	5
Nusselt No.	390	1450	353	376	860	1310	1430	1220	1130
Based on total temperature at tip									
Nusselt No.	379	1400	343	365	834	1270	1380	1190	1110
Based on total average temperature									
Total Error (%)	2.7	2	2.61	4.	3.03	2	2	2.01	2.1
Nusselt No Test 21	164	1309	164	363	991	1454	1418	1309	1309
Circumferential Pos	------------------------- 5 -------------------------							------5-------	
% Variation									
T_{tip}-Test 21	81.6	10.2	73.1	3.5	14.2	10.4	.8	7.0	14.7
T_{avg}-Test 21	79.2	6.7	70.6	.55	17.2	13.5	2.7	9.5	16.5
Group Types	A	B	A	A	B	A	A	A	A
for Test 121,130									

Errors are in percentage change of variables
Variation from Test 121 and 130 to test 21 is (Maximum-Minimum)/Average

First, it should be noted that the circumferential location of test 21's measurements coincide with circumferential location 5, the same location as the 40 series on the high temperature tip casing reversed tests of which there is only one measurement. But a comparison will still be made in the hope that some useful information will be obtained. Two key points shown in table 5-7. First is the significant increase in heat transfer at the trailing edge of the tip casing for both circumferential positions. The second is the circumferential variation which occurs between gauges at the same axial location (not surprisingly). The steady-state data definitely suggests that something unexpected is happening at the trailing edge of the tip casing, examination of the time resolved measurements may provide more evidence as to what is happening in this region.

Figures 5-7 (a-f) compares the total unsteady Nusselt number based on average temperature at the nozzle guide vane inlet for the gauges in tests 121, 130 and 21. One can see that tests 121 and 21 have nominally equal Nusselt numbers at the trailing edge. At the 70% blade chord (axial position 5) the AC component of the Nusselt number for test 21 has begun to shrink compared to test 121 which continues to the leading edge. In addition to changes in levels of heat flux, the blade patterns change for test 21 (it starts out with two distinct peaks per blade passing and then becomes one peak as the flow progresses down stream). In comparison tests 121 and 130 have blade shapes and relative fluctuations which stay approximately constant for all the axial locations. Figure 5-7 (e) also shows the variations

which seem to exist for three different circumferential measurements.

These two items: the difference in heat flux at the trailing edge and the changes in blade shape at the leading edge, suggest that the flow field which presently exists is not exactly the same as when the data was taken for test 21, but is quite similar. This could be due to the different circumferential measurement locations or it is possible that due to mechanical reasons involving the MIT facility, the blade gap may have grown from the design gap, due to modifications of the facility and tip shroud erosion. This leaves unresolved the exact influence of the profile generator on the flow of the facility. The variations which are seen are generally small compared to the blade to blade variation, except at the trailing edge, were the DC differences between test 21 and 121 and 130 are large, possibly due to the different circumferential locations involved. To fully solve this problem more measurements will be needed.

5.2.7 Variation Due to Temperature Effects

There are two questions here which need to be separated for analysis; what is the effect due to driving temperature and what is the effect due to the profile. One way to separate these questions would be to estimate the true driving temperature for the Nusselt number calculation (T_{ref} in eqn 2) and in this way the effects due to temperature can be isolated from the profile effects. However, as mentioned earlier, that option is not available and the best which can be done is to use the temperature at the tip of the rake, at the nozzle guide vane inlet, as the normalizing temperature. While this is a better approximation that the average bulk temperature, the implicit assumption or hope is that the flow patterns through the nozzle guide vanes do not change greatly over the different test conditions. To answer these questions, runs with different test conditions have to be compared which means that the best form of comparison will be the Nusselt number (despite its limitations) and the average heat flux measurements, are given only as a reference.

5.2.7.1 Variation Due to Driving Temperature

To separate the effect of absolute gas temperature from profile effects, the three uniform flows runs (test 121, 124, and 130) were compared. The run conditions were set so that the turbine would be operating on the same efficiency curve for the same corrected speed, thus the only variation between these runs should be due to the change in inlet temperature. Figures 5-8, 5-9, and 5-10 show the difference in heat flux, Nusselt number based on the average temperature and Nusselt Number based on the tip temperature for the three runs. Since there are apparent differences in the circumferential measurements the 50 series and 40 series gauges

are plotted separately. It should also be noted that the circumferential positions of the gauges in the tip casing reversed runs (127-131) are not the same as the other runs and some variation may be due to that.

Figure 5-8 shows a decrease in heat flux, which is expected, due to the lower gas temperature for the low temperature run. Figures 5-9 and 5-10, the different representations of the Nusselt number, are almost identical since the variation between the average gas temperature and the tip temperature is quite small. Focusing on fig. 5-10 (since the tip temperature probably has a closer relationship to the temperature at the tip of the rotor than the average temperature) one sees that the gauges group more closely around a central curve. Unfortunately there are not really enough points at the same axial location to make a good comparison. At the trailing edge differences due to circumferential position can be observed.

The total time resolved values of the Nusselt number (based on the tip temperature) are shown in figure 5-11 (a-f) for the uniform flow runs. These graphs show that while the blade shapes and the relative magnitude of the AC fluctuations remain relatively constant for the different runs for different axial positions, circumferential variations are present. And normalizing with respect to the inlet temperature did not collapse these curves to one shape since the Nusselt number variation is greater (although only marginally so) at all axial locations for the low temperature test (124).

5.2.7.2 Variation in Heat Flux Due to Radial Profiles

There are three separate cases which can be studied to observe the effects of radial profile; the high temperature runs (tests 120, 121, and 126), the low temperature runs (tests (122, 124, and 125) and the reversed casing runs (tests 127, 130, and 131). Any effects which are due solely to radial profiles should be observed in all cases, otherwise the phenomenon could be due to the absolute temperature differences between the runs. In addition, the tip casing reversed runs should display similar patterns as the high temperature runs since the only difference between these runs are the circumferential measurement locations. Figures 5-12, 5-13 (a and b), and 5-14 show the heat flux for the averaged data with the different circumferential positions plotted for the three different cases Since the high temperature, tip casing reversed runs (127-131) have different circumferential locations than the other runs and offer so few measurement that it is plotted with the other high temperature runs in fig 5-13 (b). Plots of the DC Nusselt number using the average temperature of the gas as the reference temperature yields figures 5-15, 16(a and b), and 17, while using the tip temperature yields figures 5-18, 19(a and b), and 20. The Nusselt number plots based on average temperature do not show any physical dependance of the heat flux on the average temperature; but when the Nusselt number based on tip temperature is used the curves tend to collapse to a signal curve

for any given circumferential position, indicated a dependence of heat flux on inlet temperature. This behavior is most pronounced in the high temperature runs (figure 5-20) where the difference between circumferential locations is greater than the difference between runs. For the low speed runs the difference in circumferential positioning is not as important.

The AC component of the unsteady Nusselt number is not enlightening either. Similar to fig. 5-11 (shown before), the variation is large, 33% of the peak values and remains relatively constant over the entire length of the tip shroud, indicating that the variations are easily the same order as the time average values at the trailing edge. The relative magnitudes of the fluctuations seem to be dependent on both the profile and the axial position.

5.3 Conclusions

The analysis of what this data actually means and the work which needs to be done is addressed in the next chapter. This section discusses the last two items needed to complete this chapter: the DC uncertainty analysis and the pressure data.

5.3.1 The DC Uncertainty Results

As the data is represented, there are two distinct sources where error can be introduced into the final calculation of the heat flux (and ultimately into the Nusselt number as shown in section 5.2.6). One is through the calibration procedure of the individual gauges and the other is through the error introduced in the averaging process. As shown earlier in this chapter this error is small, generally less than 4%, and it represents the uncertainty associated with the average value chosen for the calculations. For instance instead of using a rotor averaged value we could have used a blade average for either one of the different gap groups. These errors are independent of each other and can be combined using the root-sqaure method. Table 5-9 yields the final approximation of the DC heat flux error for the different gauges using the method the:

$$\% \text{ total error} = \sqrt{(\text{Calibration Error})^2 + (\text{Averaging Error})^2}$$

It should be kept in mind how these numbers were arrived at since there are many approximations involved.

It is conceivable that this uncertainty analysis could be improved with a considerable amount of work. The question which must be asked in this case is whether, given what this data represents is it worth the effort. The experiment was designed to show trends, which it does, but there just may not be enough data to support any more exact conclusions even if an exact error analysis is known.

5.3.2 The Pressure Data

Figure 5-21 (a-e) show the blade averaged traces of the pressure transducers for tests 120. It is apparent that some of the transducers work well and actually picked up the variation due to tip gap (transducers 2 and 4, although they give opposite readings) while transducer # 3 seems not to be able to decipher between the blade groups, and transducer # 5 appears to be damped (which it is given the time lag shown in the calibrations (see fig 4-4). Thus there is probably more information which can be gathered about the flow in the passage from the transducers which are working properly, but that effort will have to come at a later time and is discussed in the next chapter.

As a preliminary analysis, assuming that the techniques developed for reducing the heat flux data can also be used on the pressure data, figure 5-22 shows the different pressure signals for the high temperature runs (tests 120, 121, and 126) as a function of temperature profile. The data used is a filtered blade averaged representation of the 1.7% gap blades. The DC data is shown in figure 5-23. Two things are apparent from these graphs. First, if some of this data is correct, the variations due to profile seem to only occur at the DC level, with the pressure dropping as a function of wall temperature (temperature profile). Secondly, the data is questionable since two of the transducers (two and five) record high levels of fluctuations, while the two between them (three and four) show much lower levels of variation in the blade passage. This may be a real phenomenon or it could be an artifact of any of the transducers and more work will be needed to decide which it actually is.

Table 5-4 (a)

Time Average Heat Flux Measurements (KW/M**2) Based on Gap and Circumferential Location

	High Temperature Runs						Tip Shroud Inverted						Low Temperature Runs					
	Test 120		Test 121		Test 126		Test 127		Test 130		Test 131		Test 122		Test 124		Test 125	
RTDF	17%		0%		8%		6%		0%		16%		11%		0%		6%	
Span	1.7%	2.5%	1.7%	2.5%	1.7%	2.5%	1.7%	2.5%	1.7%	2.5%	1.7%	2.5%	1.7%	2.5%	1.7%	2.5%	1.7%	2.5%
Gauge																		
57	30.0	28.5	32.7	32.1	19.0	20.4									11.0	11.2		
56	34.2	34.0			27.1	29.3	106.0	106.0					2.4	3.0	11.1	12.1	4.7	5.3
55	74.5	72.8			67.7	68.3									37.0	37.3	24.5	24.7
54	89.3	88.8	113.0	113.0	78.5	78.9	88.9	88.4	99.2	99.0					61.5	61.1	32.0	32.0
53																		
47	20.9	21.4	29.7	29.2	18.2	18.8							-6.7	-6.5	6.1	7.3	-5.6	-5.0
46	18.3	19.3	31.1	31.1	25.5	27.3							11.7	12.5	9.7	11.3	7.1	8.3
45	53.1	52.1	69.3	69.0	54.0	54.3	99.5	101.0					27.6	27.1			21.9	21.7
44					80.3	79.9	79.7	80.4	92.7	93.3	87.0	89.4						
43	78.4	75.5	103.0	103.0			58.2	59.7			52.0	53.9	39.3	38.7	61.5	61.5	40.4	39.8
42	71.7	69.2	111.0	111.0											64.9	63.9	27.6	26.7

Table 5-4 (b)

Percent Variation of Heat Flux Relative to 1.7% Gap (Q(1.7%) - Q(2.5%))/Q(1.7%)

	High Temperature Runs				Tip Shroud Inverted		Low Temperature Runs		
	Test 120	Test 121	Test 126	Test 127	Test 130	Test 131	Test 122	Test 124	Test 125
RTDF	17%	0%	8%	6%	0%	16%	11%	0%	6%
Gauge									
57	5.0%	1.8%	-7.4%	.0%			-28.5%	-1.8%	-12.9%
56	.6%		-8.1%					-9.0%	-.8%
55	2.3%		-.9%					-.8%	.0%
54	.6%	.0%	-.5%	.6%	.2%			.7%	
53									
47	-2.4%	1.7%	-3.3%				1.8%	-18.4%	9.9%
46	-5.5%	.0%	-7.1%				-6.8%	-16.1%	-17.2%
45	1.9%	.4%	-.6%	-1.5%	-.6%		1.8%	.0%	.9%
44				-.9%		-2.8%			
43	3.7%	.0%	.5%	-2.6%		-3.7%	1.5%	1.5%	1.5%
42	3.5%	.0%							3.3%

Statistics on Gap Variations

33 Gauges sampled:

12% (4 gauges)	5.5 to 8.1 %
3% (1)	" 4 to 5 %
12% (4)	" 3 to 4 %
12 % (4)	" 2 to 3 %
12% (4)	" 1 to 2 %
48 % (16)	0 to 1 %

For High Temperature Runs

45 % (15) had larger large gap heat fluxes

For Low Temperature Runs

21 gauges sampled: 47.6 % (10 had larger large gap Heat Fluxes

5% (1 gauge) had a variation of 28%

19% (4) have a variation of 13 to 19 %

14 % (3)	" 6 to 10 %
71 % (15)	" 0 to 3.6 %

Table 5-5

Time Average Heat Flux Measurements (KW/M2) Based on Circumferential Location**

	High Temperature Runs			Tip Shroud Inverted			Low Temperature Runs		
	Test 120	Test 121	Test 126	Test 127	Test 130	Test 131	Test 122	Test 124	Test 125
RTDF	17.0%	.0%	8.0%	6.0%	.0%	16.0%	11.0%	.0%	6.0%
Circumferential Position	-0.553	-0.553	-0.553	0.447	0.447	0.447	-0.553	-0.553	-0.553
	Pos [6]	Pos [6]	Pos [6]	Pos [1]	Pos [1]	Pos [1]	Pos [6]	Pos [6]	Pos [6]
Gauge									
57	29.7	32.1	19.2	**41.8**		**102.0**		10.7	
56	34.2		27.6	106.0		**96.3**	2.2	11.0	4.6
55	**74.4**		67.7				**30.0**	37.1	24.6
54	**88.6**	**113.0**	78.5	88.6	99.2	**84.3**		61.4	32.1
53	**87.4**								
Circumferential Position	0.197	0.197	0.197	-0.303	-0.303	-0.303	0.197	0.197	0.197
	Pos [2]	Pos [2]	Pos [2]	Pos [5]	Pos [5]	Pos [5]	Pos [2]	Pos [2]	Pos [2]
47	20.2	29.2	17.9	**46.1**		**79.7**	-7.3	6.2	-5.8
46	17.9	31.1	25.7				11.7	9.8	7.2
45	52.5	**69.0**	**53.4**	99.2			26.9		21.5
44				79.4	92.5	**87.9**		61.6	40.3
43	77.3	103.0	80.6	58.6		53.0	39.3	64.8	**27.6**
42	70.3	111.0					48.2		

Percent Variation in Circumferential Heat Flux Measurements based on 50 series Gauges

Axial loc 7	Test 120	Test 121	Test 126	Test 127	Test 130	Test 131	Test 122	Test 124	Test 125
7	32.0%	9.0%	6.8%	-10.3%		21.9%	-439.2%	42.3%	-56.1%
6	47.7%		6.9%				10.3%	11.3%	12.6%
5	29.4%		21.1%						-25.5%
4				10.4%	6.8%	-4.3%		-.3%	
3	11.6%								

Gauges which are highlighted are in group B or below (see chapter four)

Table 5-9
Fractional Total Error in Heat Flux

Gauge	Test 120 Type	Cal Err	Avg. Err	Total Err	Test 121 Type	Cal Err	Avg. Err	Total Err	Test 122 Type	Cal Err	Avg. Err	Total Err	Test 124 Type	Cal Err	Avg. Err	Total Err
57	A	3.12%	5.00%	5.89%	A	1.99%	1.83%	2.70%					A	5.48%	-1.82%	5.77%
56	A	2.03%	0.58%	2.11%					A	4.00%	-2.85%	4.91%	A	1.85%	-9.01%	9.20%
55	B	5.66%	2.28%	6.10%					C+				A	1.55%	-0.81%	1.75%
54	B	5.19%	0.56%	5.22%	B	2.24%	0.00%	2.24%					A	1.70%	0.65%	1.82%
53	C															
52																
51	C								C							
47	A	1.51%	-2.39%	2.83%	A	1.59%	1.68%	2.31%	A	1.80%	1.80%	2.55%	A	3.39%	-18.43%	18.74%
46	A	13.70%	-5.46%	14.75%	A	3.84%	0.00%	3.84%	A-	24.90%	-6.84%	25.82%	A	8.66%	-16.14%	18.32%
45	A	2.17%	1.88%	2.87%	B	2.93%	0.43%	2.96%	A	6.26%	1.81%	6.52%				
44																
43	A	2.57%	3.70%	4.50%	A	1.56%	0.00%	1.56%	A	4.40%	1.53%	4.66%	A	1.73%	0.00%	1.73%
42	A	2.62%	3.49%	4.36%	A	1.55%	0.00%	1.55%	C				A	1.65%	1.54%	2.26%
41																

Gauge	Test 125 Type	Cal Err	Avg. Err	Total Err	Test 126 Type	Cal Err	Avg. Err	Total Err	Test 127 Type	Cal Err	Avg. Err	Total Err	Test 130 Type	Cal Err	Avg. Err	Total Err	Test 131 Type	Cal Err	Avg. Err	Total Err
57					B+	2.06%	-7.37%	7.65%	C+	9.93%							C	2.85		
56	A	13.10%	-12.88%	18.37%	B+	2.23%	-8.12%	8.42%	A	3.86%	0.00%	3.86%					C	1.26		
55	A	3.46%	-0.82%	3.56%	B+	5.19%	-0.89%	5.27%												
54	B+	7.59%	0.00%	7.59%	B+	3.74%	-0.51%	3.77%	A	1.77%	0.56%	1.86%	A	1.91%	0.20%	1.92%	B-			
53																				
52																				
51																				
47	A-	1.65%	9.91%	10.05%	B+	1.83%	-3.30%	3.77%	B-								C			
46	A-	26.80%	-17.21%	31.85%	B+	8.22%	-7.06%	10.84%												
45	A-	5.68%	0.91%	5.75%	B	13.30%	-0.56%	13.31%	A	1.98%	-1.51%	2.49%								
44	A-	2.66%	1.49%	3.05%					A	1.81%	-0.88%	2.01%								
43	B	13.30%	3.26%	13.69%	B+	2.34%	0.50%	2.39%	A	1.62%	-2.58%	3.05%	A	1.50%	-0.65%	1.63%	B	0.03	-0.0276	0.0443
42																	A	0.02	-0.0365	0.0413

Key:
Cal Err = Calibration error of Gauges
Avg. Err = Averaging error associated in the data reduction process
Total Err = ((Call Err)**2 +(Avg. Err)**2)**.5

FIGURE 5-1(a): TEST 120
GAUGE 46
FIVE REVOLUTION AVERAGE

113
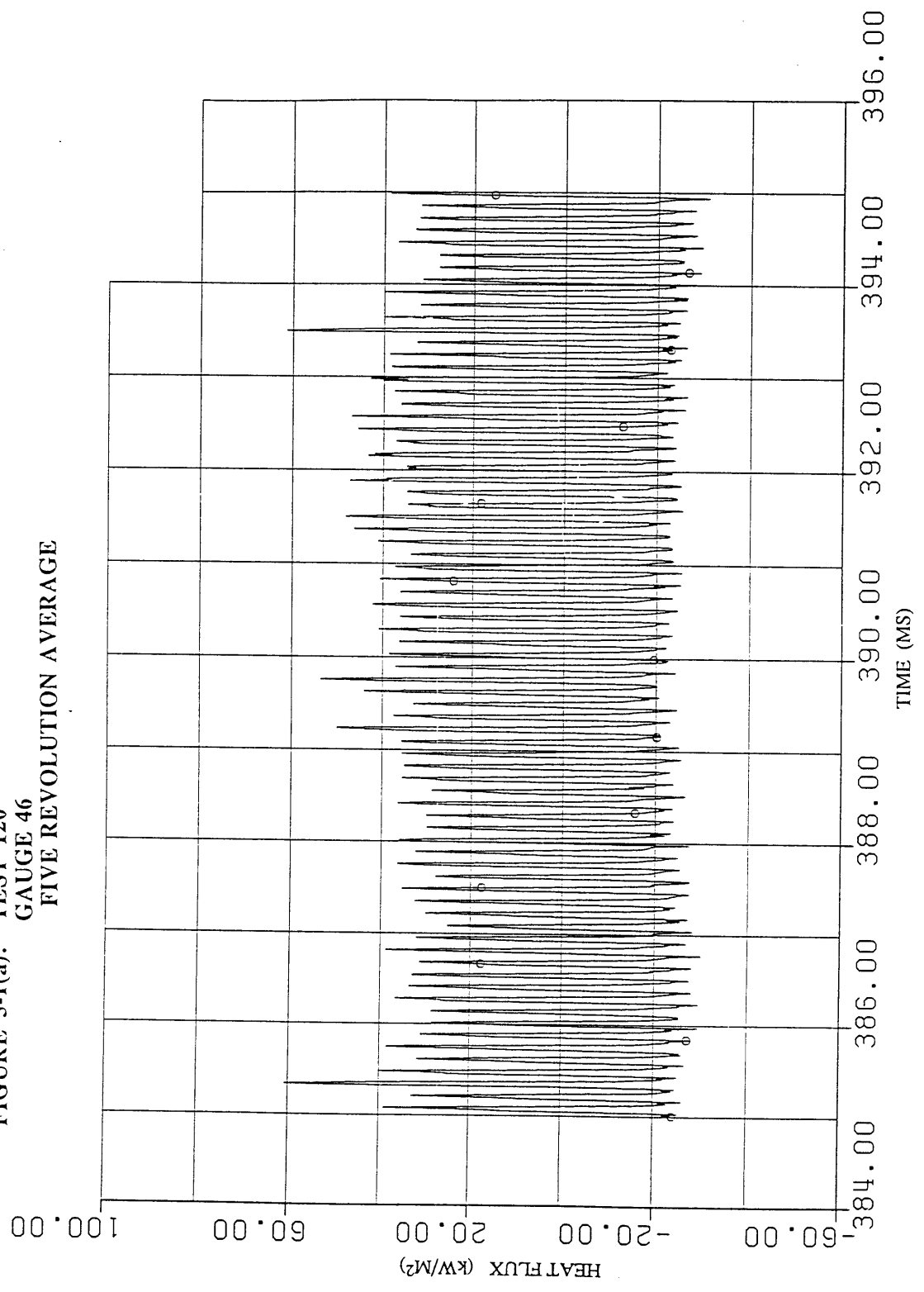
FIGURE 5-1(b): TEST 120
GAUGE 46
SEVEN REVOLUTION AVERAGE
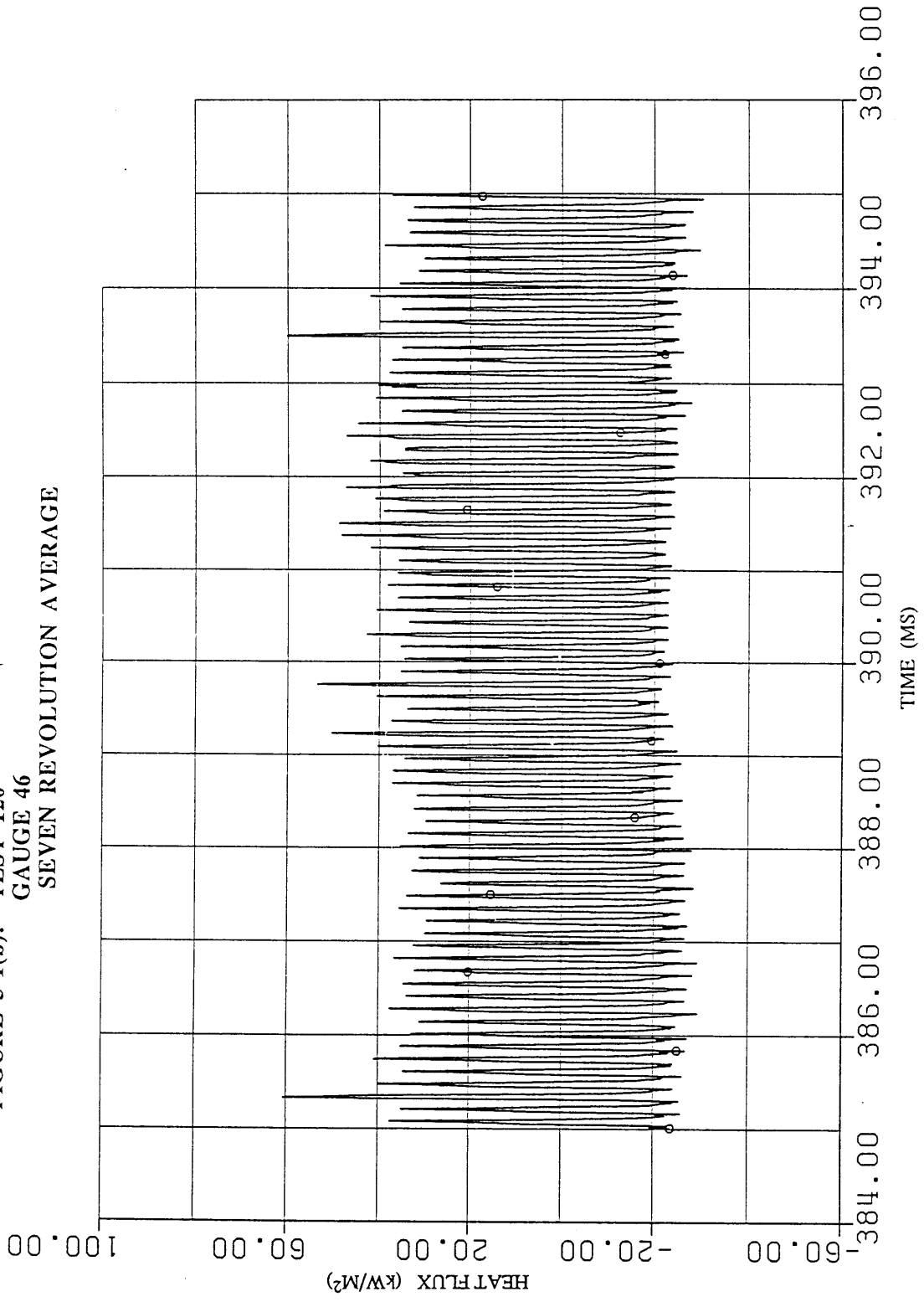
FIGURE 5-1(c): TEST 120
GAUGE 46
ELEVEN REVOLUTION AVERAGE

115
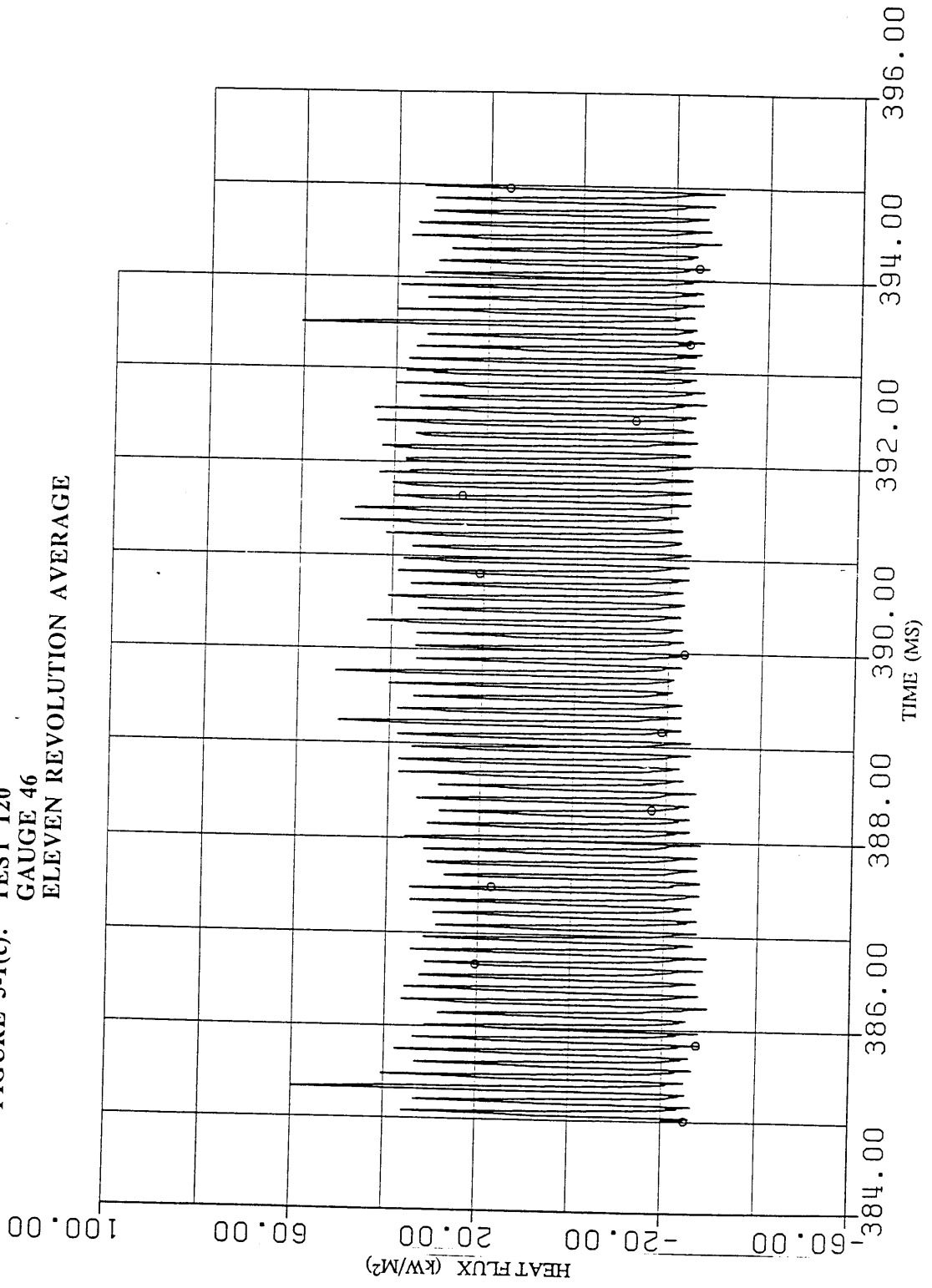
FIGURE 5-1(d): COMPARISON OF DIFFERENT AVERAGES
OVER FIVE BLADES FOR GAUGE 46, TEST 120

116
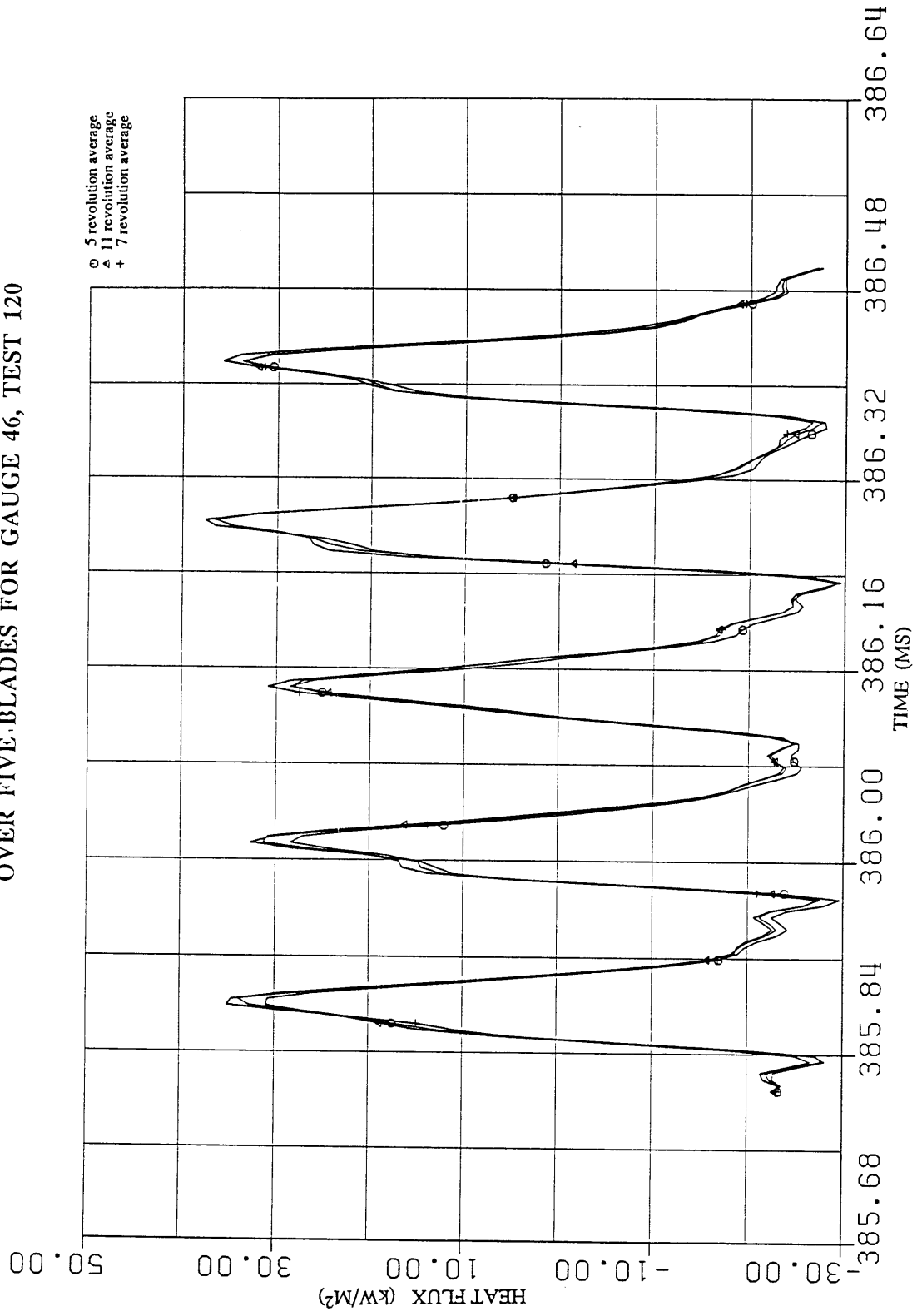
FIGURE 5-2(a): TEST 120, GAUGE 43
(blade average data)

ONE REVOLUTION

large gap
2.4% span

small gap
2.1% span

reference gap
1.7% span

TIME (MS)

HEAT FLUX (kW/M²)

117
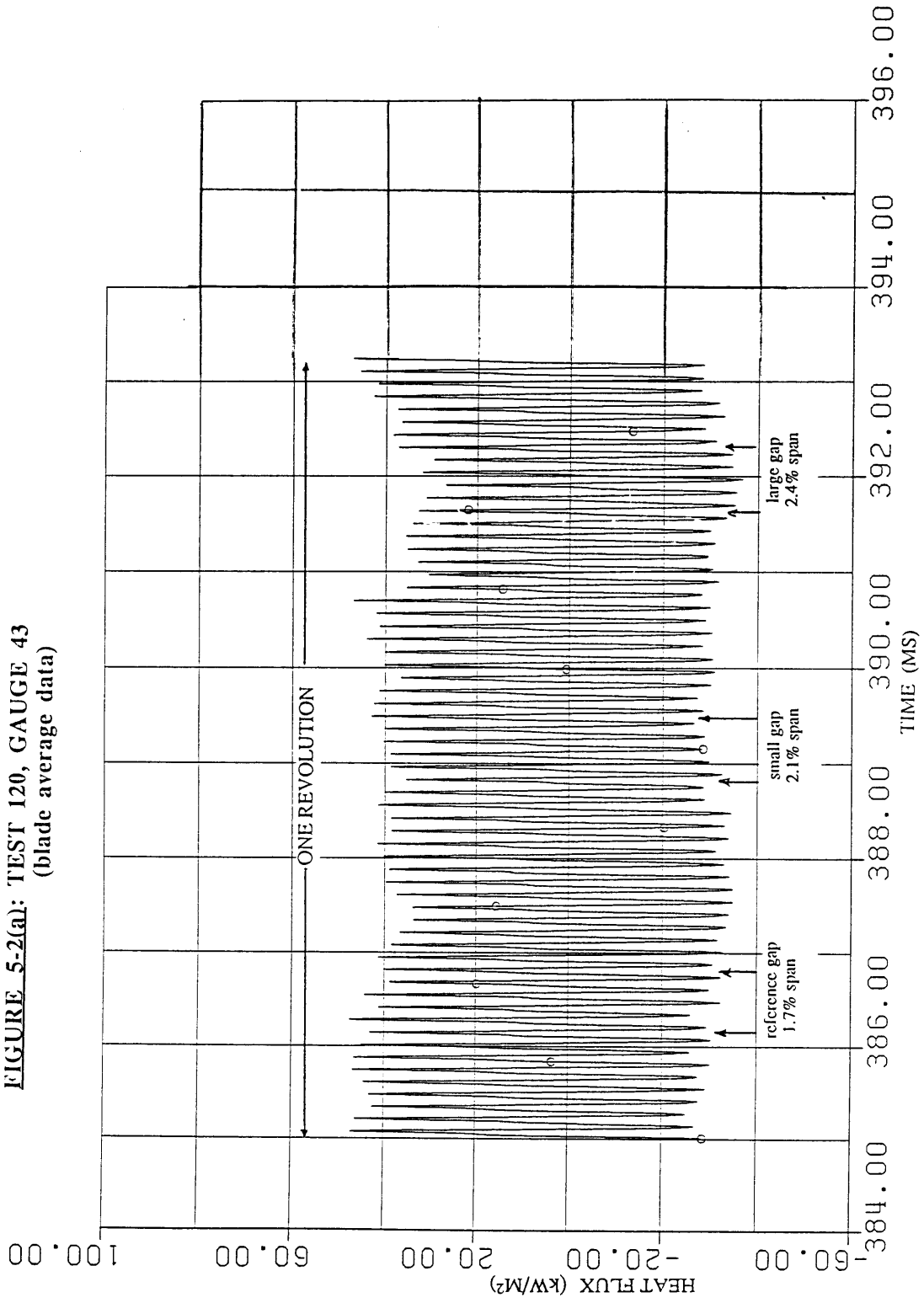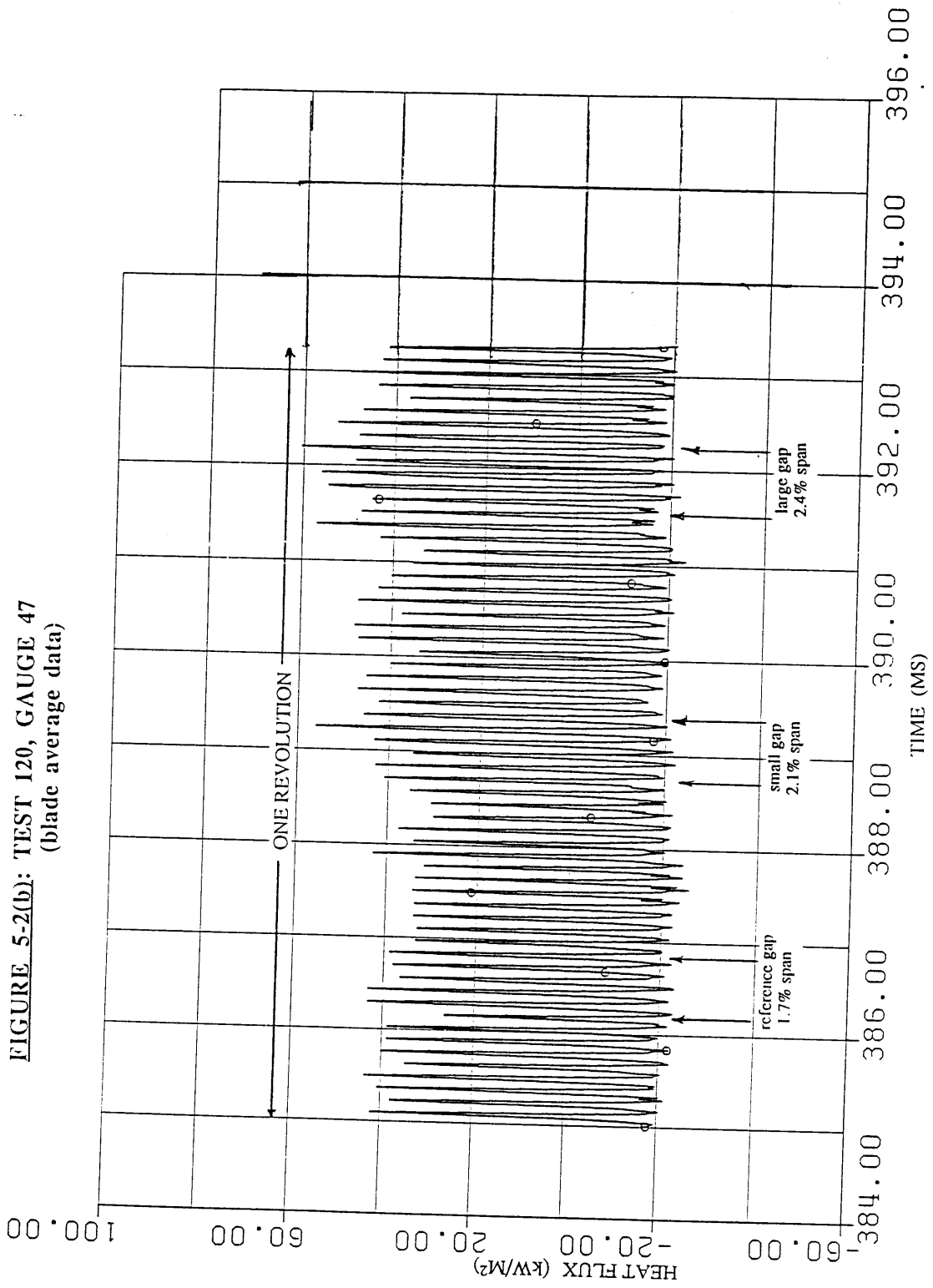
FIGURE 5-2(b): TEST 120, GAUGE 47
(blade average data)

118

FIGURE 5-2(c): TEST 124, GAUGE 43
(blade average data)

119

FIGURE 5-2(d): TEST 124, GAUGE 47
(blade average data)

ONE REVOLUTION

large gap
2.4% span

reference gap
1.7% span

small gap
2.1% span

HEAT FLUX (kW/M²)

TIME (MS)

120
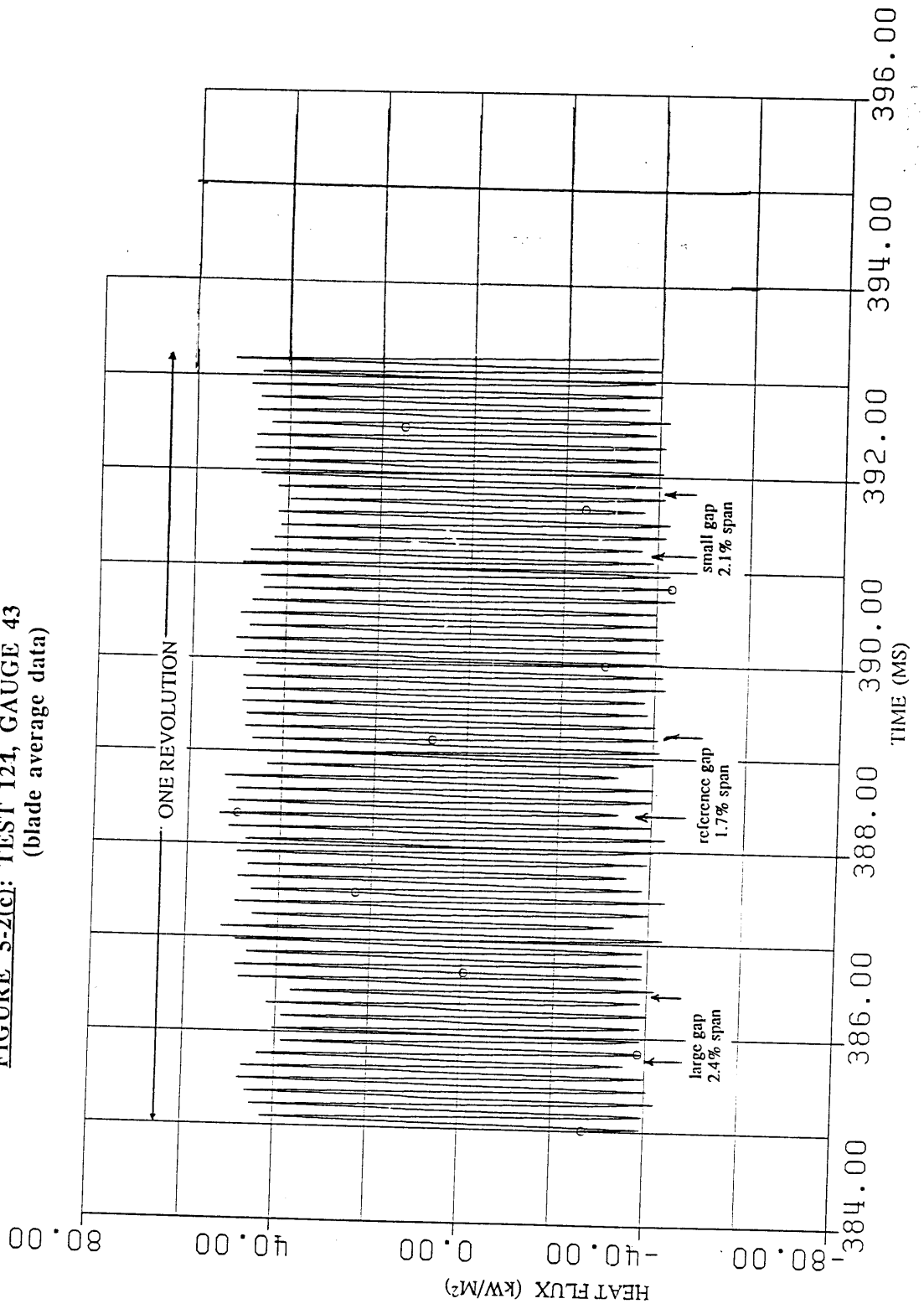
FIGURE 5-2(e): TEST 124, GAUGE 43
(blade average data)
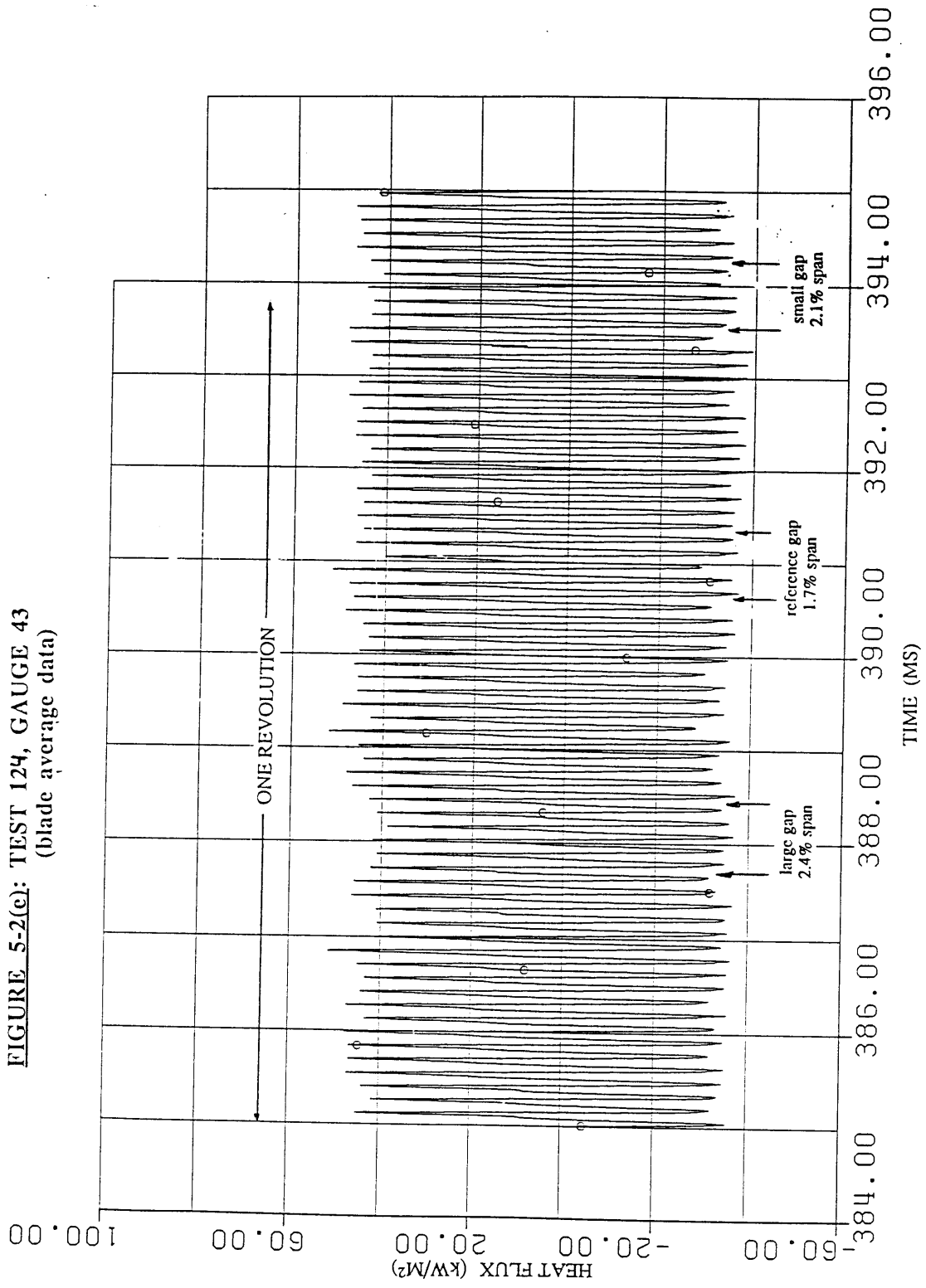
FIGURE 5-2(f): TEST 124, GAUGE 47
(blade average data)

ONE REVOLUTION

large gap
2.4% span

reference gap
1.7% span

small gap
2.1% span

HEAT FLUX (kW/M²)

TIME (MS)

132
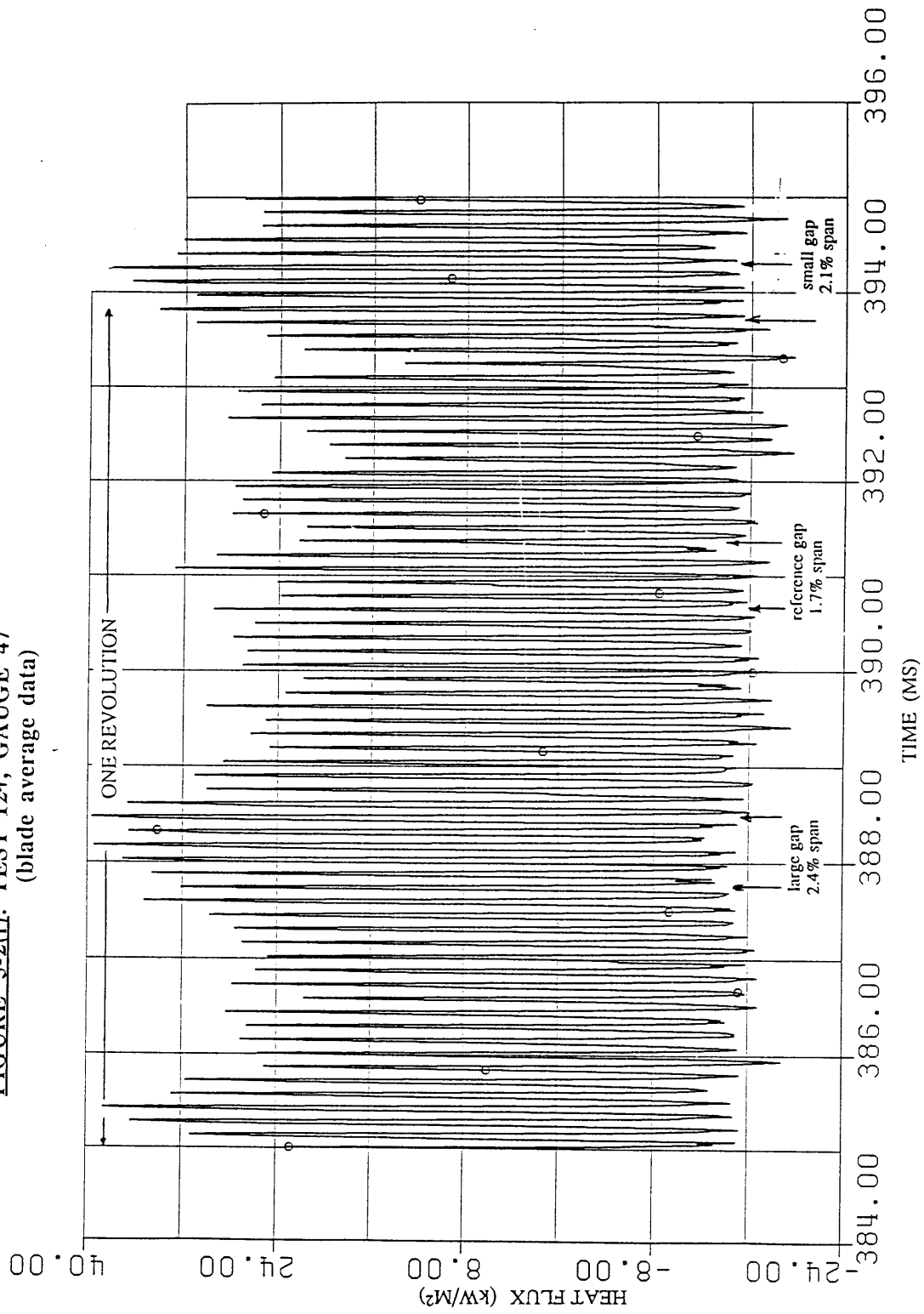
FIGURE 5-3
AC COMPONENT OF HEAT FLUX
FOR 1.7% AND 2.5% GAPS
TEST 120, 17% PROFILE
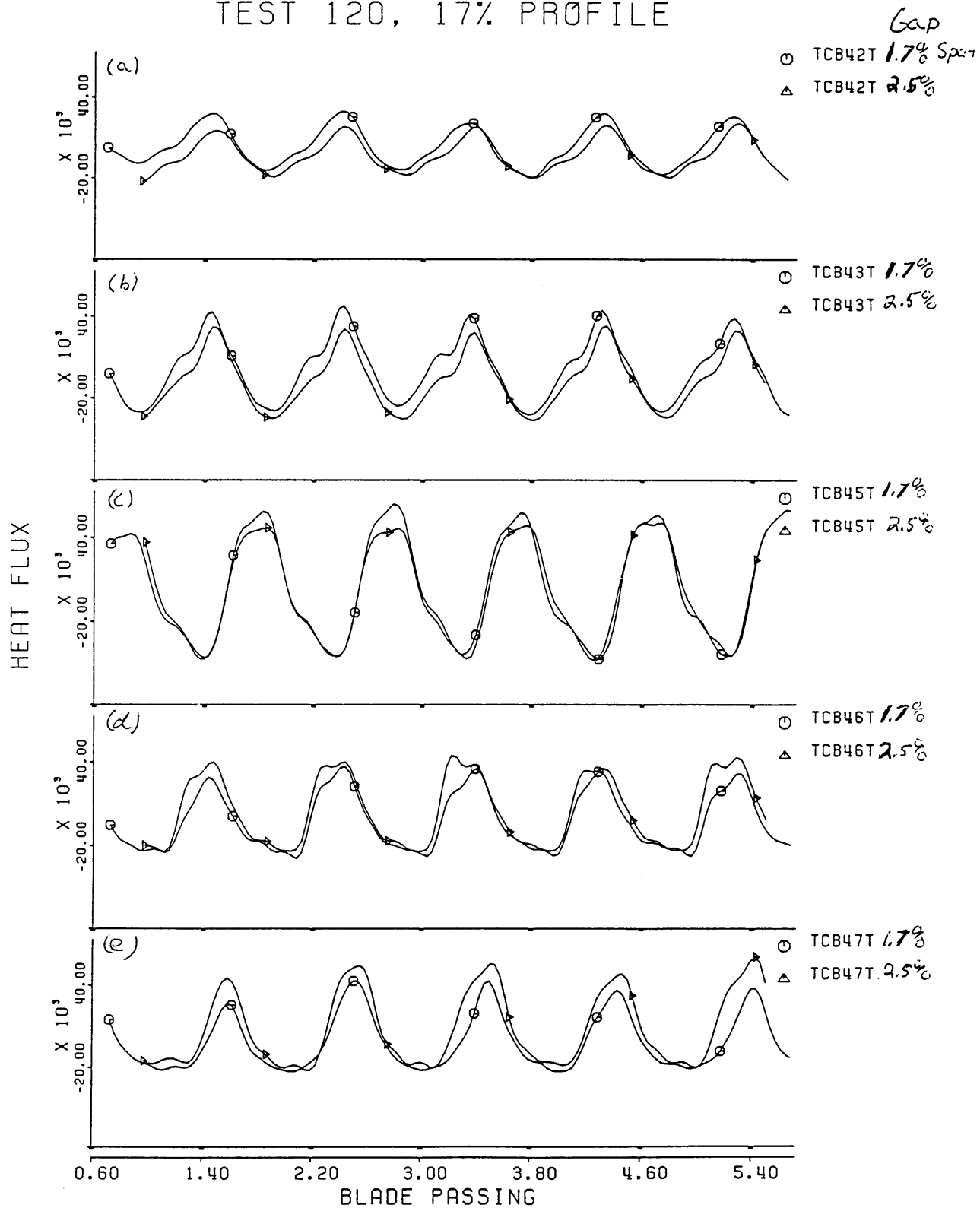
FIGURE 5-3 (Cont.)
AC COMPONENT OF HEAT FLUX
FOR 1.7% AND 2.5% GAPS
TEST 120, 17% PROFILE

Gap

⊙ TCB53T 1.7% Span
△ TCB53T 2.5%

⊙ TCB54T 1.7%
△ TCB54T 2.5%

⊙ TCB55T 1.7%
TCB55T 2.5%

⊙ TCB56T 1.7%
△ TCB56T 2.5%

⊙ TCB57T 1.7%
△ TCB57T 2.5%
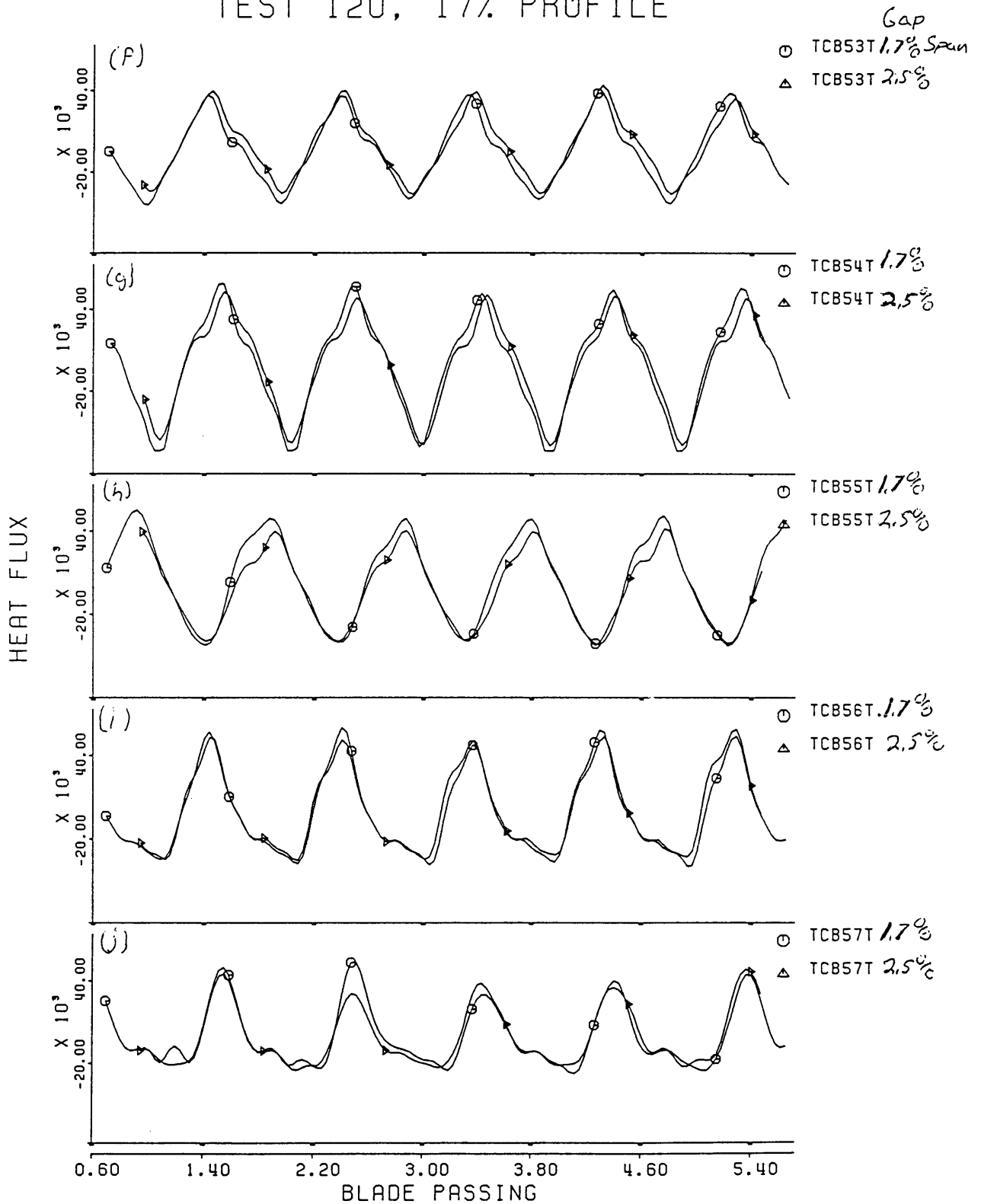
FIGURE 5-4
CIRCUMFERENTIAL VARIATIONS IN TOTAL HEAT FLUX
FOR TEST 120, 17% PROFILE
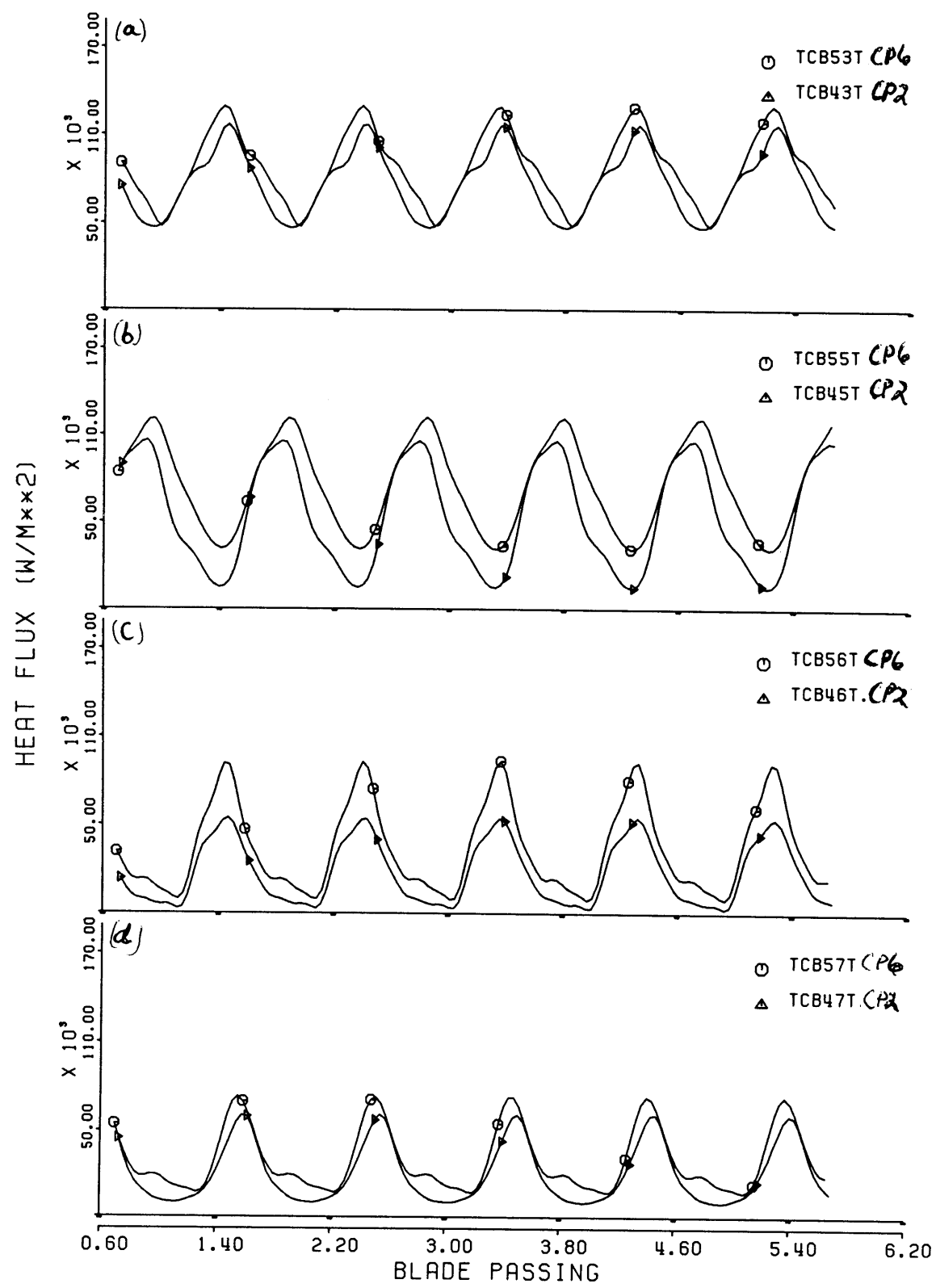
FIGURE 5-4 (cont)
CIRCUMFERENTIAL VARIATION IN TOTAL HEAT FLUX
FOR TEST 121, 0% RTDF

(e)

Legend:
- ⊙ TCB57T CP6
- △ TCB47T CP2

X-axis: BLADE PASSING (0.00 to 5.60)
Y-axis: HEAT FLUX (W/M**2) X 10^3
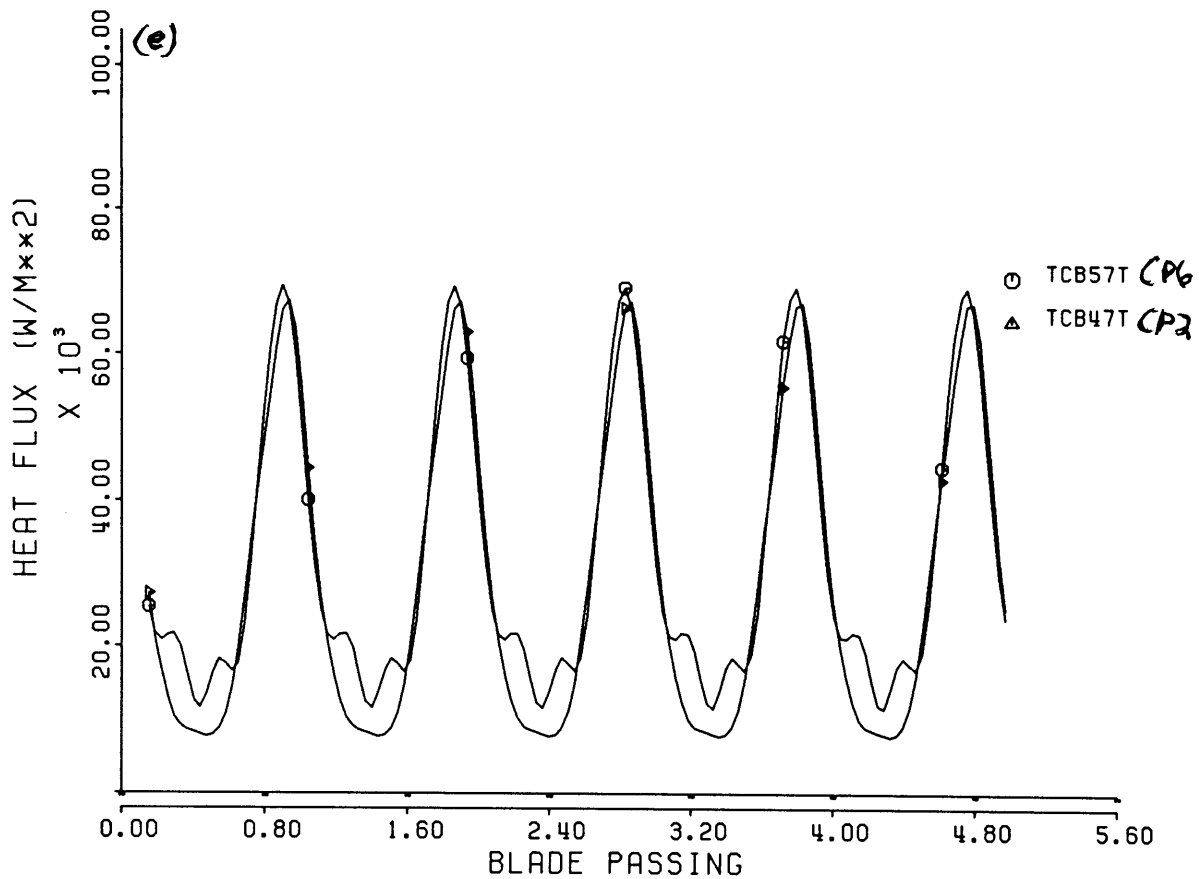
FIGURE 5-4 (Cont)
CIRCUMFERENTIAL VARIATION IN TOTAL HEAT FLUX
FOR TEST 122, 11% RTDF
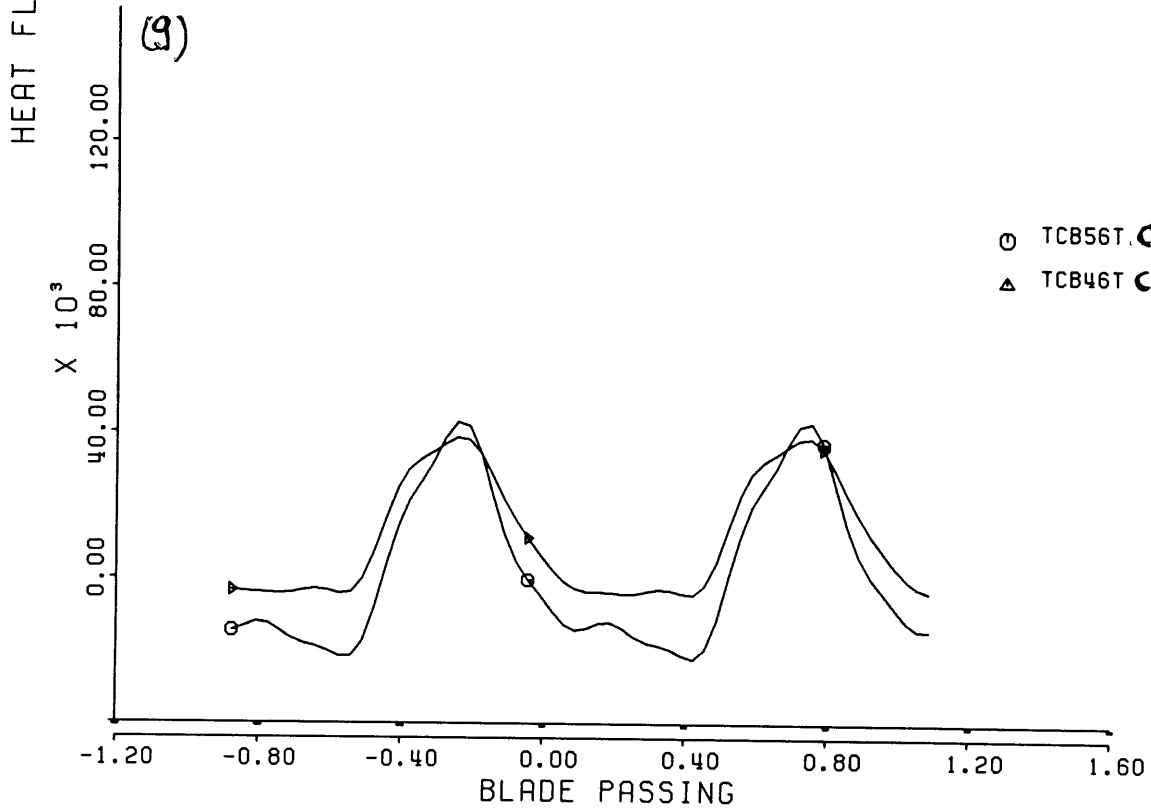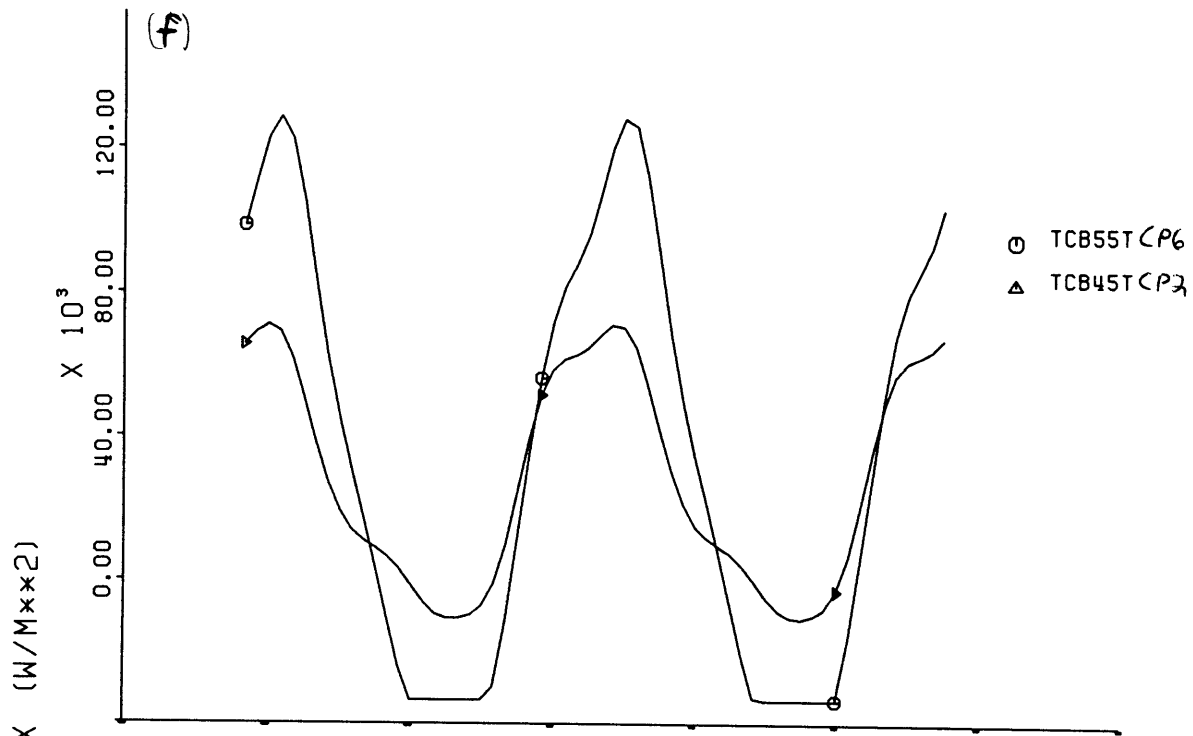
FIGURE 5-4 *(Cont)*
CIRCUMFERENTIAL VARIATION IN TOTAL HEAT FLUX
FOR TEST 124, 0% RTDF

(h)

⊙ TCB54T *CP6*
△ TCB44T *CP2*

(i)

⊙ TCB56T *CP6*
△ TCB46T *CP2*

(j)

⊙ TCB57T. *CP6*
△ TCB47T. *CP2*

HEAT FLUX (W/M**2)

BLADE PASSING
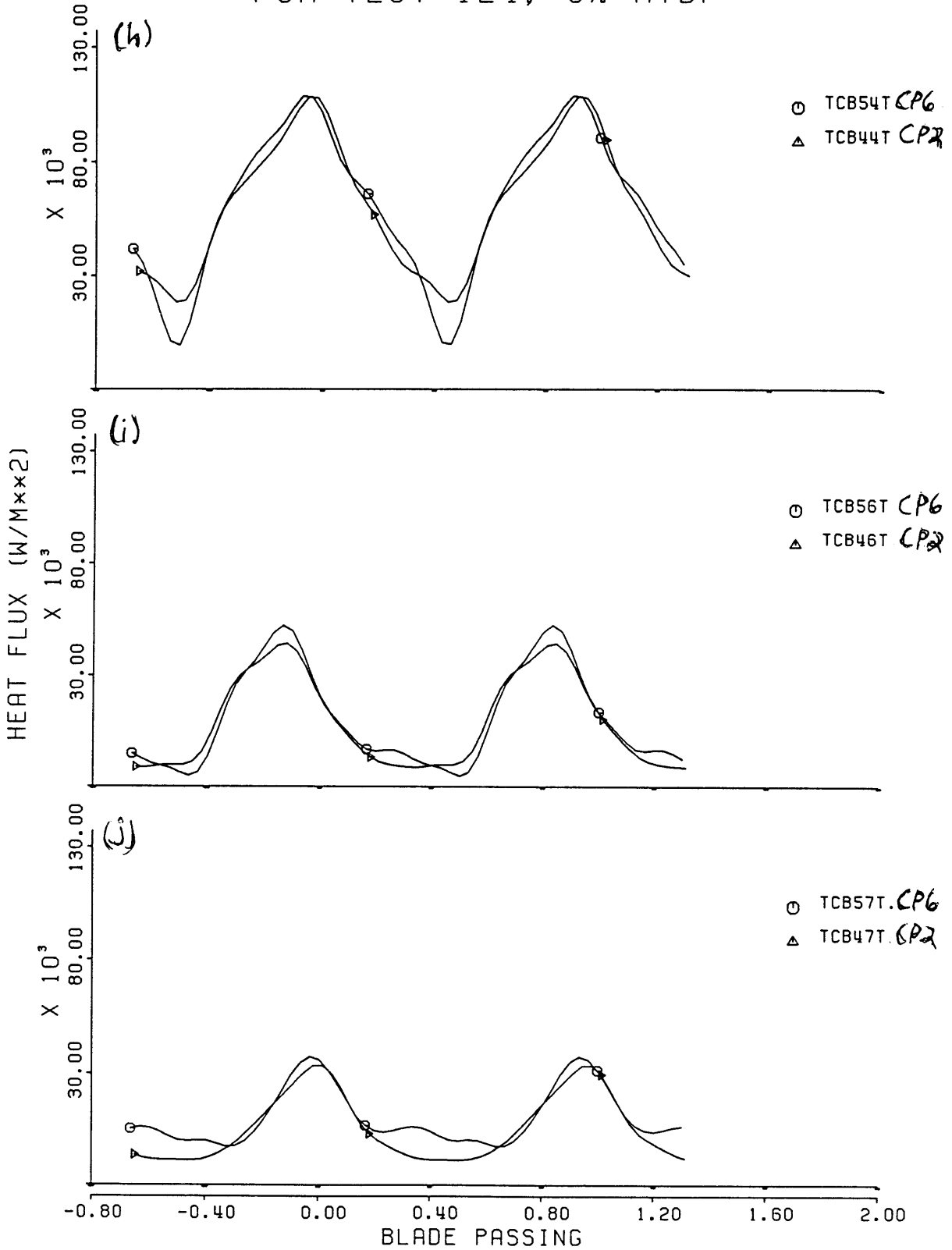
FIGURE 5-4
CIRCUMFERENTIAL VARIATION IN TOTAL HEAT FLUX
FOR TEST 125, 6% RTDF

(k)

⊙ TCB54T *CP6*
△ TCB44T *CP2*

(L)

⊙ TCB55T *CP6*
△ TCB45T *CP2*

(m)

⊙ TCB56T *CP6*
△ TCB46T *CP2*

HEAT FLUX (W/M**2)

X 10³

BLADE PASSING
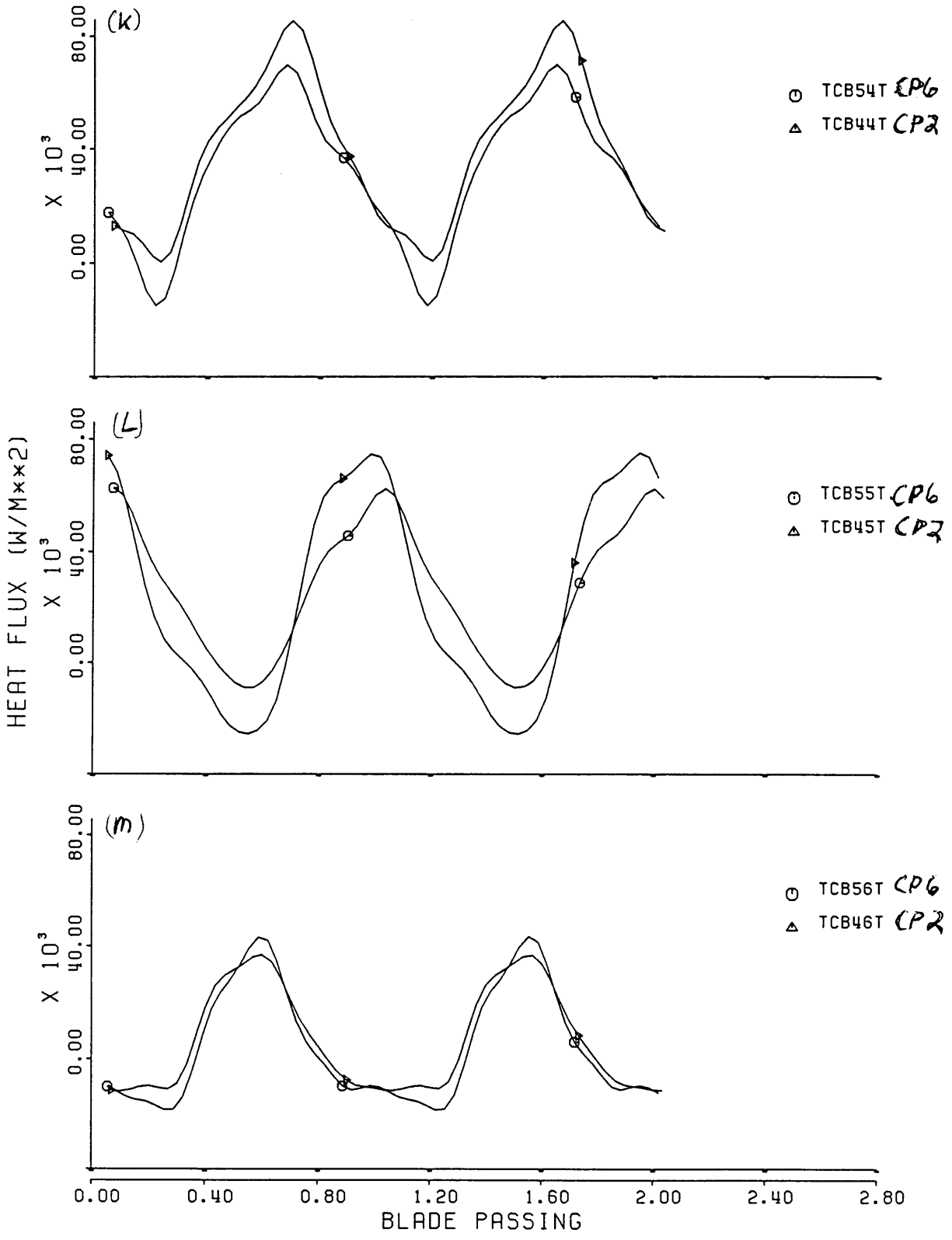
FIGURE 5-4 *(Cont)*
CIRCUMFERENTIAL VARIATION IN TOTAL HEAT FLUX
FOR TEST 126, 8% RTDF

(n)

$X \ 10^3$

⊙ TCB55T *CP6*

△ TCB45T *CP2*

(o)

HEAT FLUX (W/M**2)

$X \ 10^3$

⊙ TCB56T *CP6*

△ TCB46T. *CP2*

(p)

$X \ 10^3$

⊙ TCB57T *CP6*

△ TCB47T *CP2*

BLADE PASSING
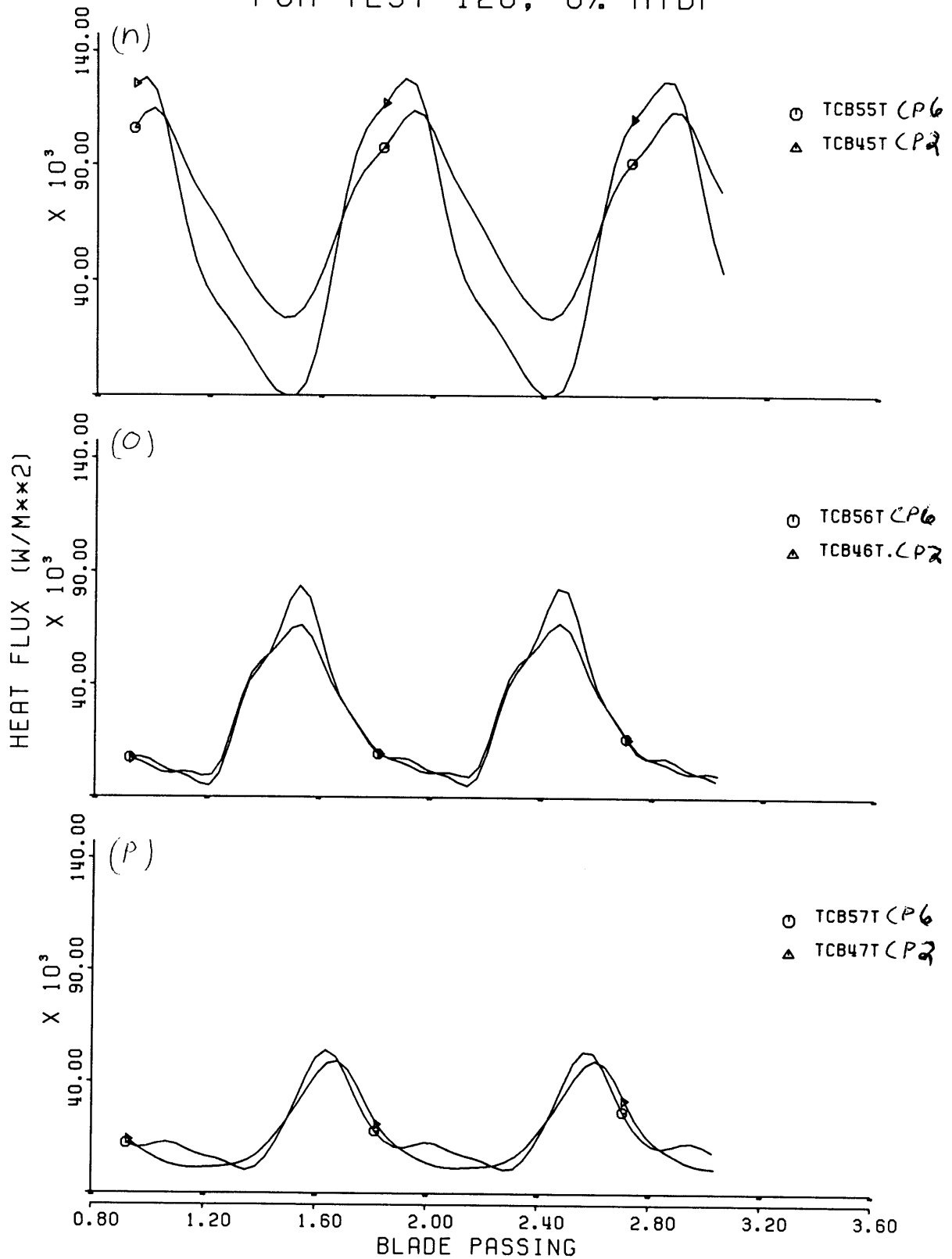
FIGURE 5-4 *(Con't)*
CIRCUMFERENTIAL VARIATION IN TOTAL HEAT FLUX
FOR TEST 127 *6% RTDF*

(q)

HEAT FLUX (W/M**2)

X 10³

160.00
120.00
80.00
40.00

○ TCB54T. *CP1*
△ TCB44T. *CP5*

(r)

160.00
120.00
80.00
40.00

○ TCB57T *CP1*
△ TCB47T *CP5*

-0.80   -0.40   0.00   0.40   0.80   1.20   1.60   2.00
BLADE PASSING
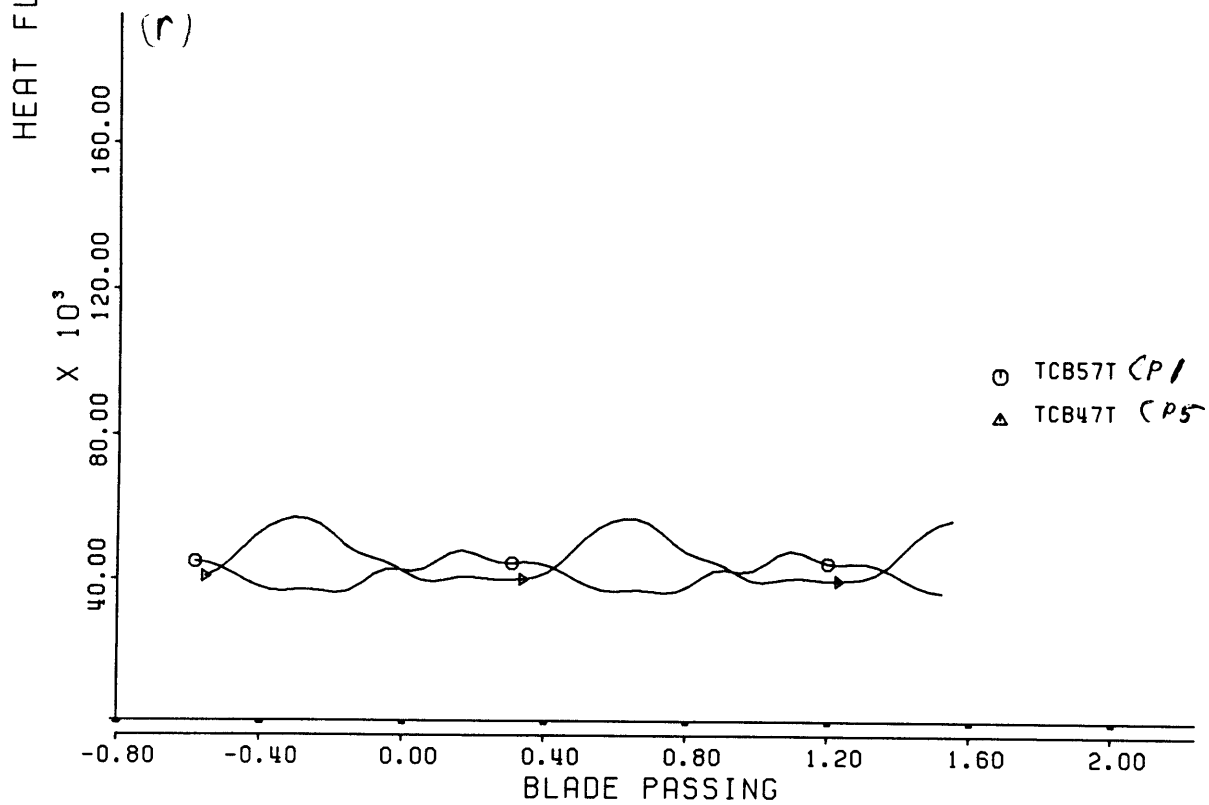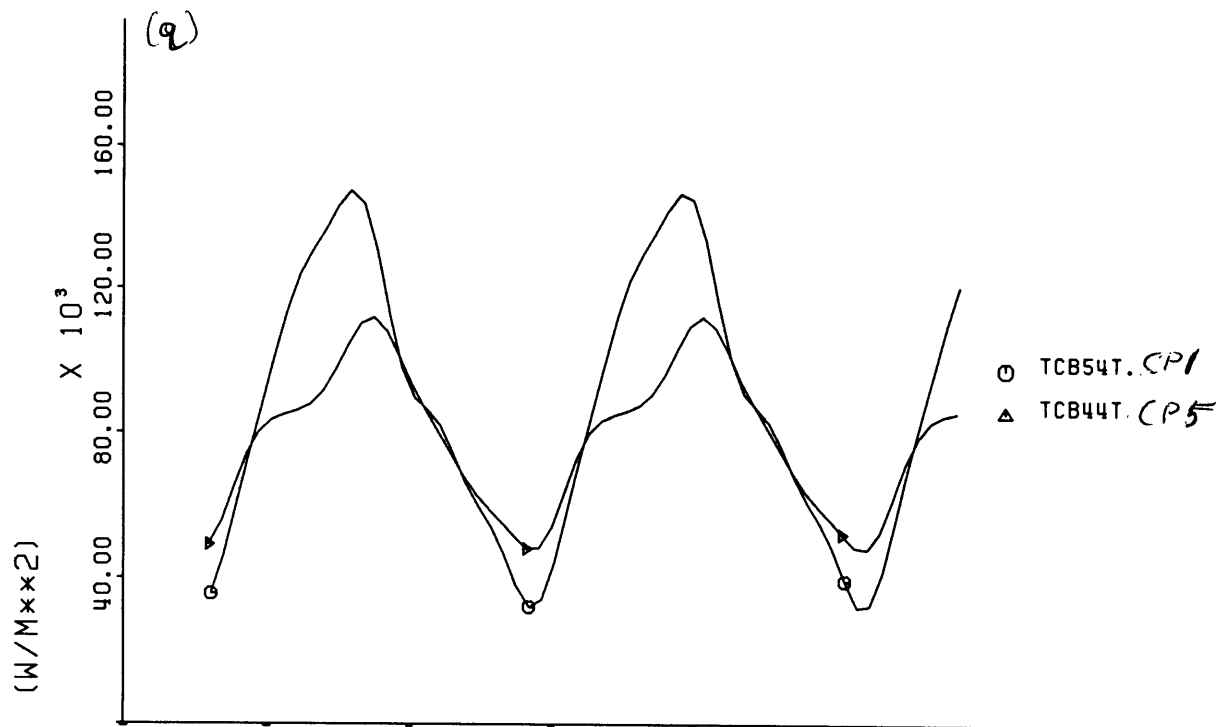
FIGURE 5-4 (cont)
CIRCUMFERENTIAL VARIATIONS IN TOTAL HEAT FLUX
FOR TEST 130, 0% RTDF

(s)

Legend:
⊙ TCB54T *CP1*
△ TCB44T *CP5*

133
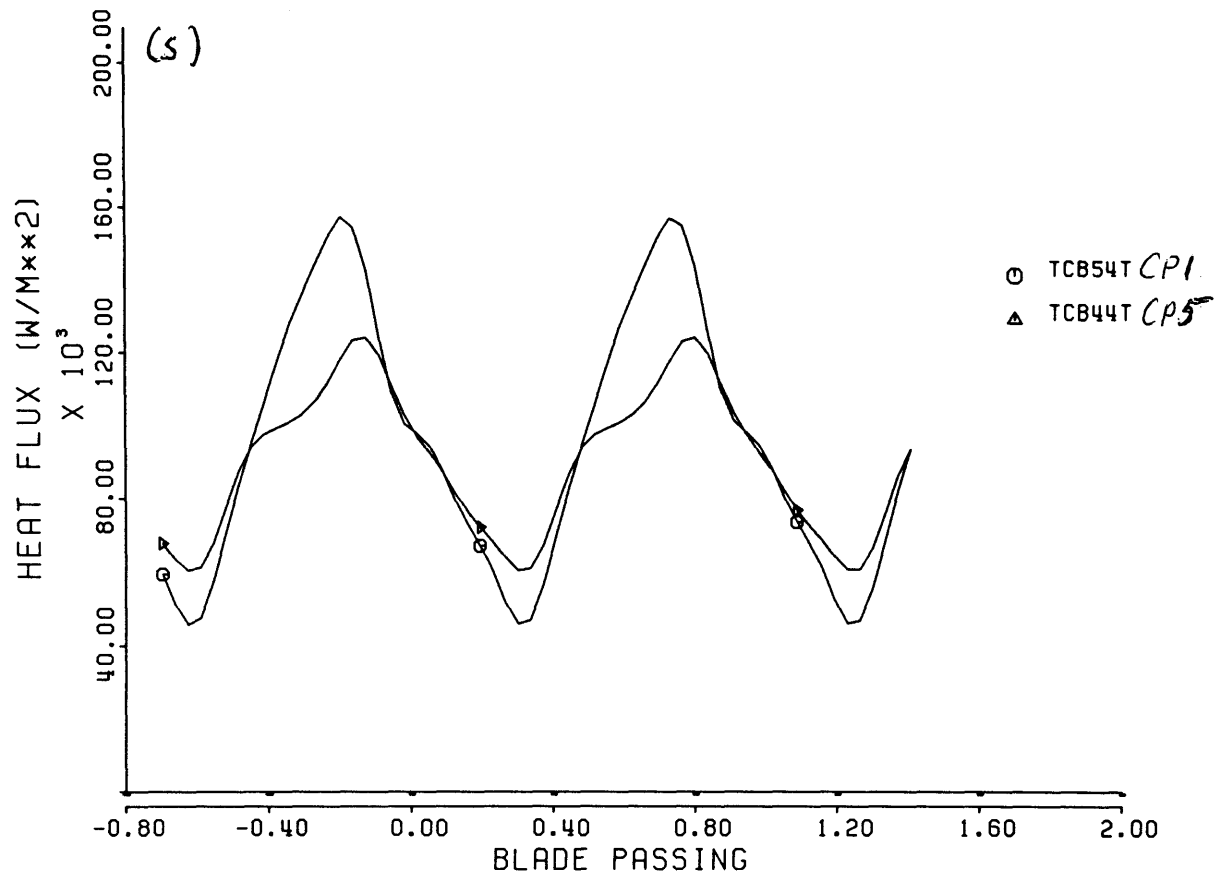
FIGURE 5-4 *(cont)*
CIRCUMFERENTIAL VARIATION IN TOTAL HEAT FLUX
FOR TEST 131, 16% RTDF

(t)

○ TCB54T *CP 1*
△ TCB44T *CP S*

(U)

○ TCB57T *CP 1*
△ TCB47T *CP S*
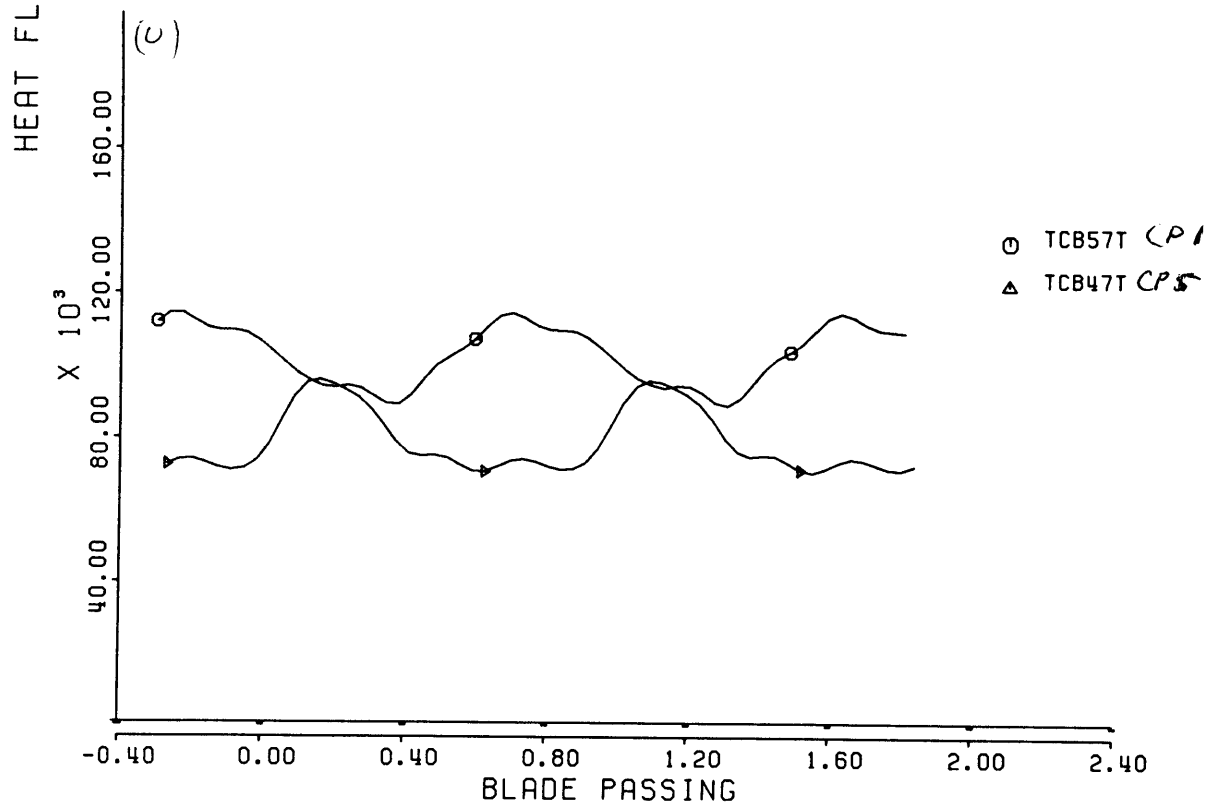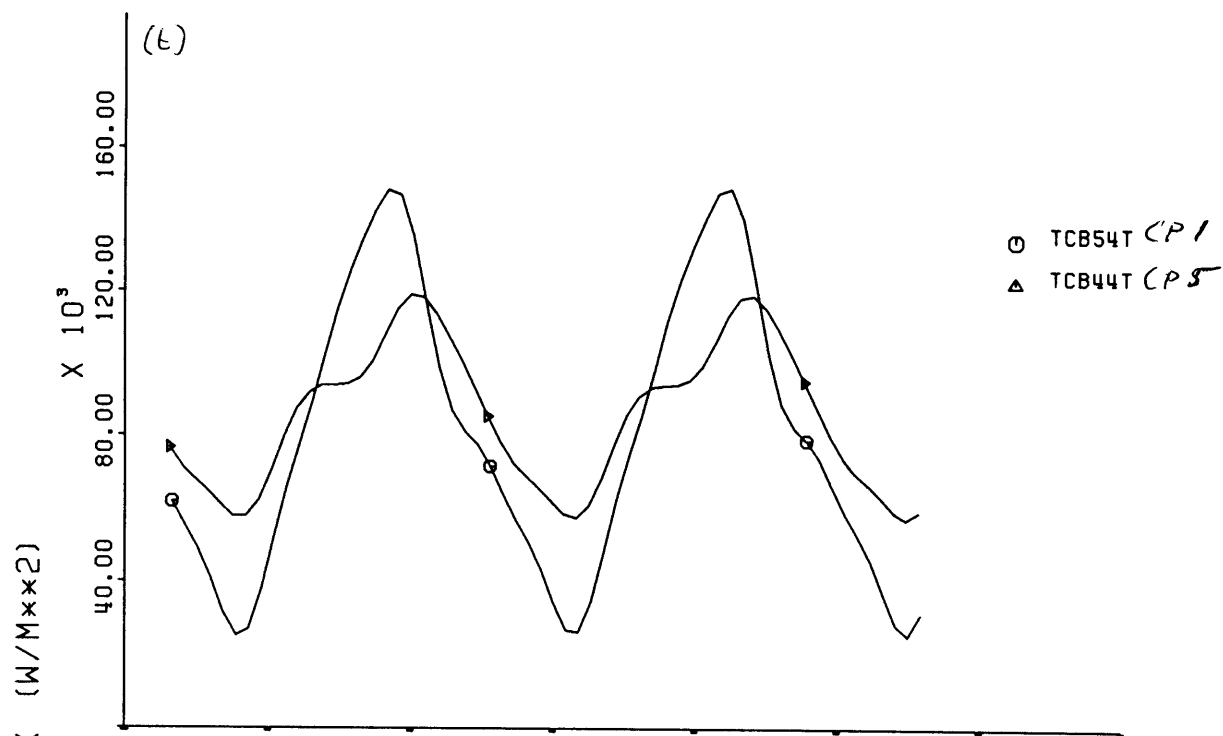
Figure 5-5

Time Averaged Heat Flux for Tests 121, 130, and 21

(Data averaged from 350 to 400 ms)

Test	Cir. Pos.	RTDF	$(t_g - t_w)/t_w$
121	(2)	0%	.51
121	(6)	0%	.51
130	(5)	0%	.53
130	(1)	0%	.53
21	(5)	0%	.54
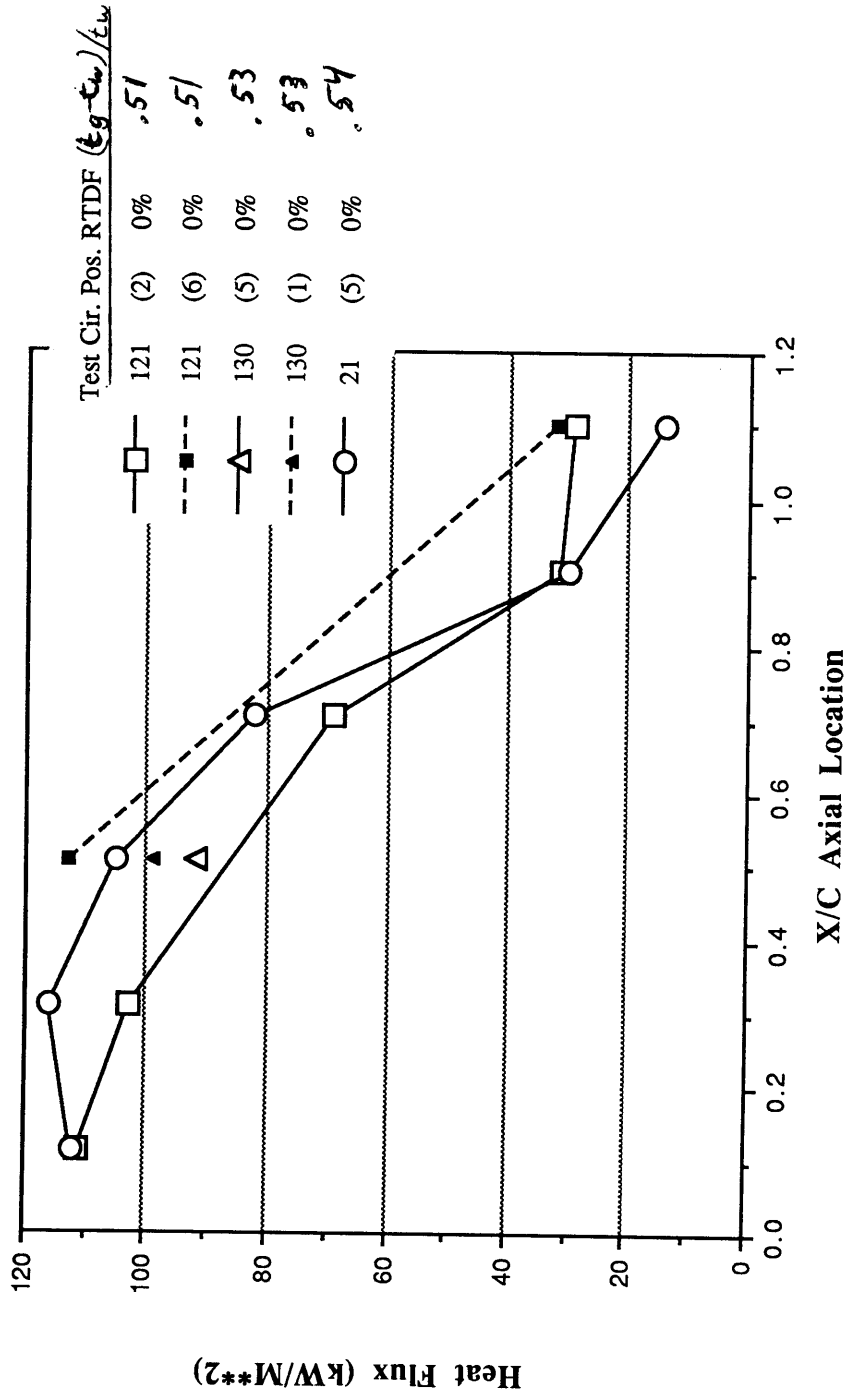
Figure 5-6 (a)

Nusselt Number Based on Bulk Average NGV Inlet
Temperature (=Tg) For Tests 121, 130 and 21

	Test	Cir. Pos.	RTDF	(Tg-Tw)/Tw
□	121	(2)	0%	.51
■	121	(6)	0%	.51
△	130	(5)	0%	.53
◀	130	(1)	0%	.53
○	21	(5)	0%	.54
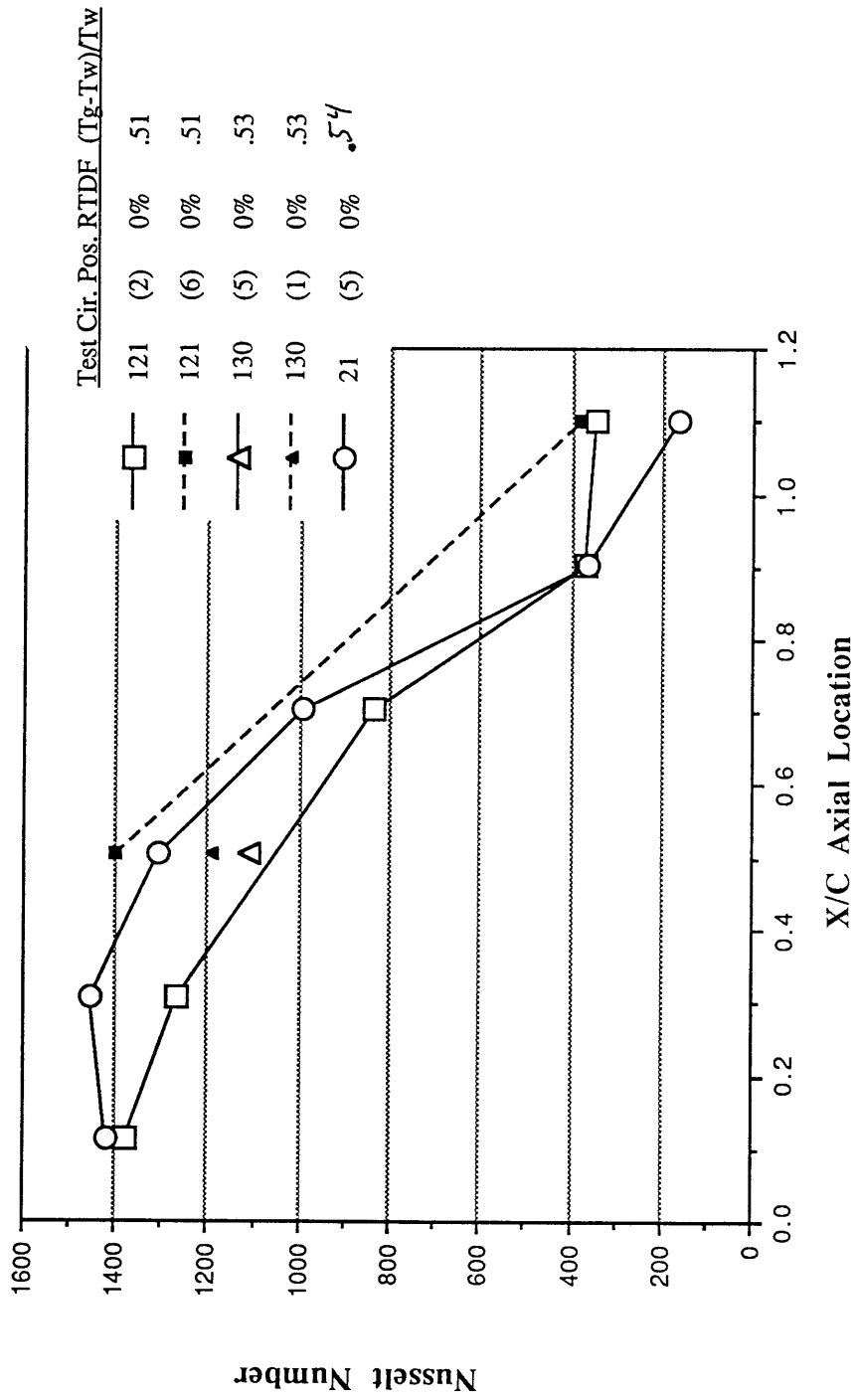
Figure 5-6 (b)

Nusselt Number Based on NGV Tip Streamline

Temperature (=Tg) For Tests 121, 130, and 21

Test	Cir. Pos.	RTDF	(Tg-Tw)/Tw
121	(2)	0%	.49
121	(6)	0%	.49
130	(5)	0%	.51
130	(1)	0%	.51
21	(5)	0%	.51
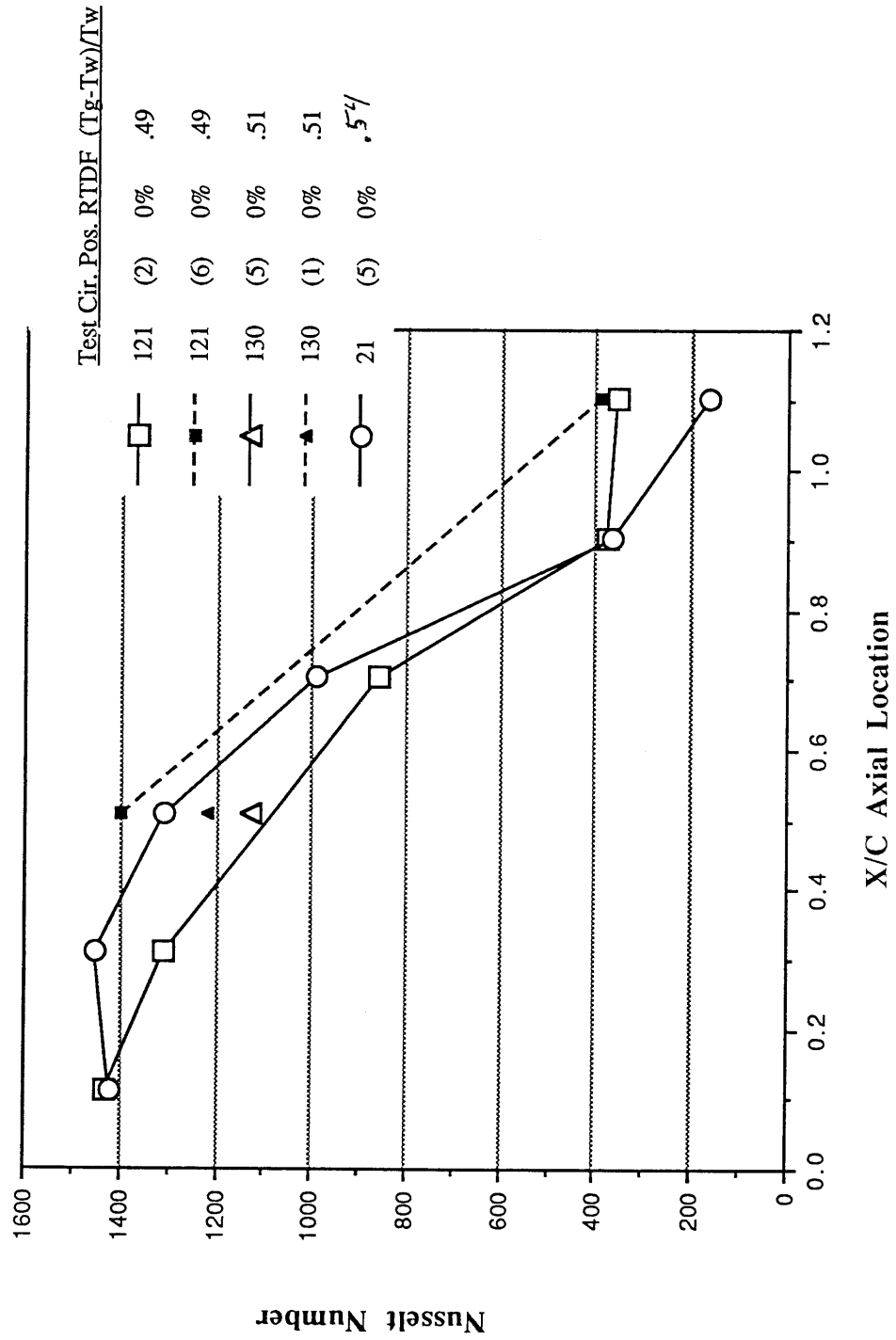
FIGURE 5-7
TOTAL UNSTEADY NUSSELT NUMBER BASED ON
AVERAGE NGV INLET TEMPERATURE
FOR TESTS 21 AND 121 (0% RTDF)
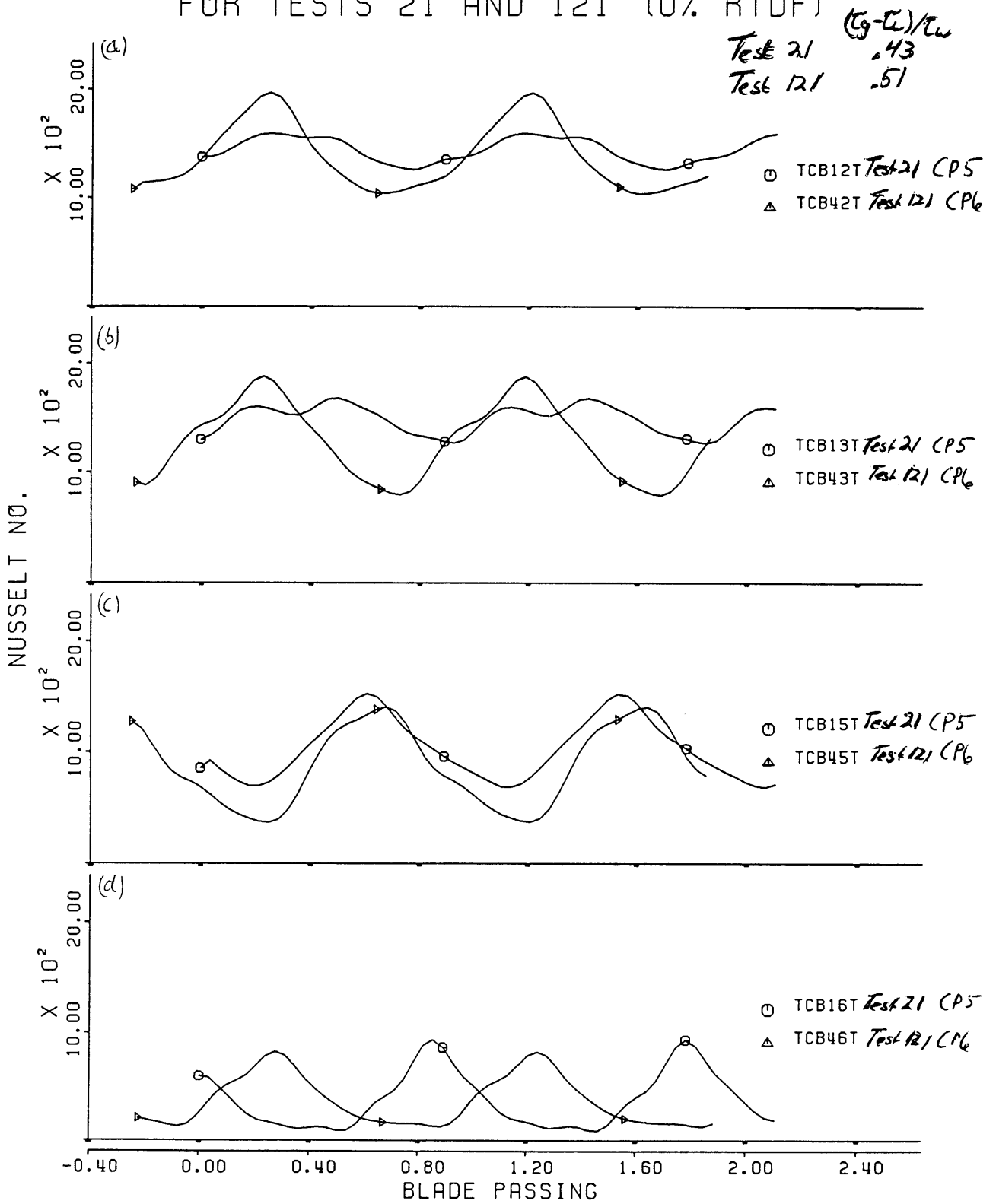
FIGURE 5-7 (cont)
TOTAL UNSTEADY NUSSELT NUMBER BASED ON
NGV AVERAGE INLET TEMPERATURE FOR
TESTS 21, 121, AND 130 (0% RTDF)

$(t_g - t_{w})/t_{w}$

Test 21	.43
Test 121	.51
Test 130	.53

(e)

TCB14T Test 21, CP5
TCB54T Test 121, CP6
TCB44T Test 130 CP5
TCB54T Test 130, CP1

(f)

TCB17T Test 21 CP5
TCB47T Test 121 CP2
TCB57T Test 121 CP6

NUSSELT NO.

X 10^1

BLADE PASSING
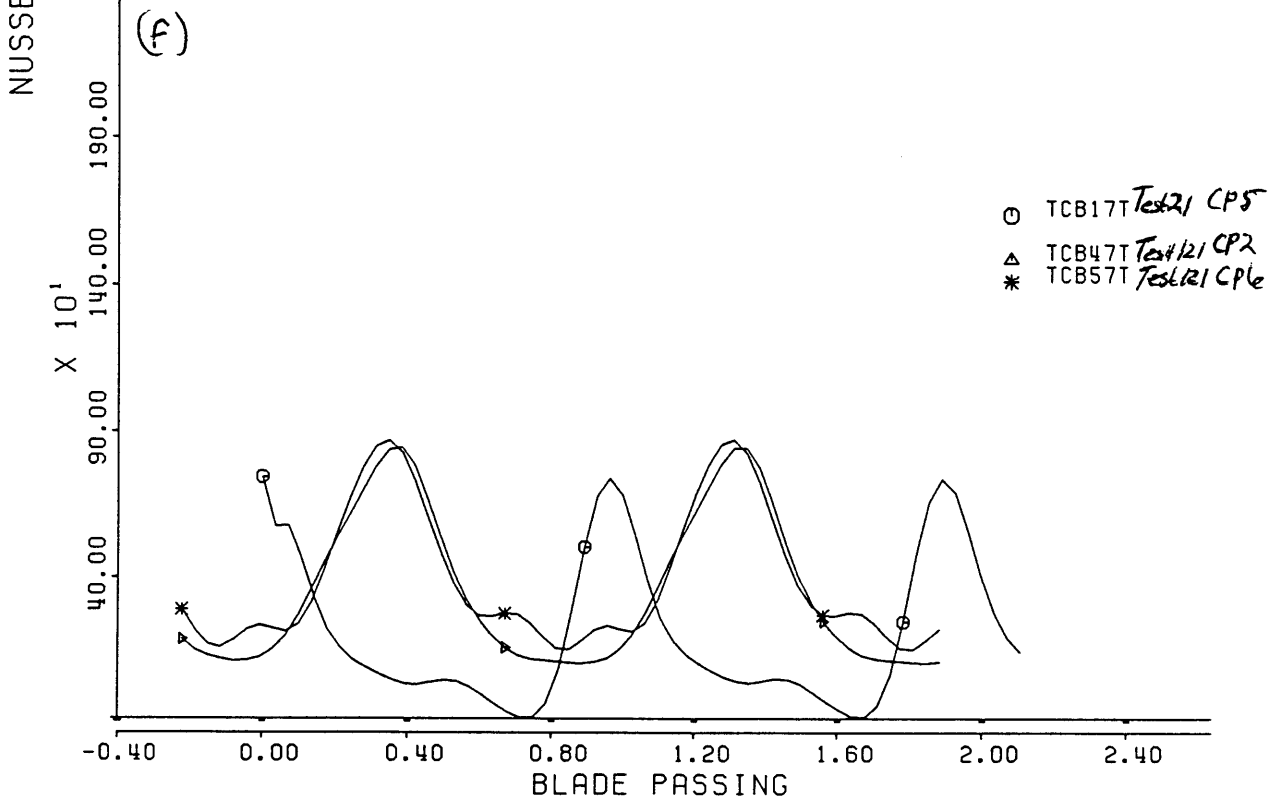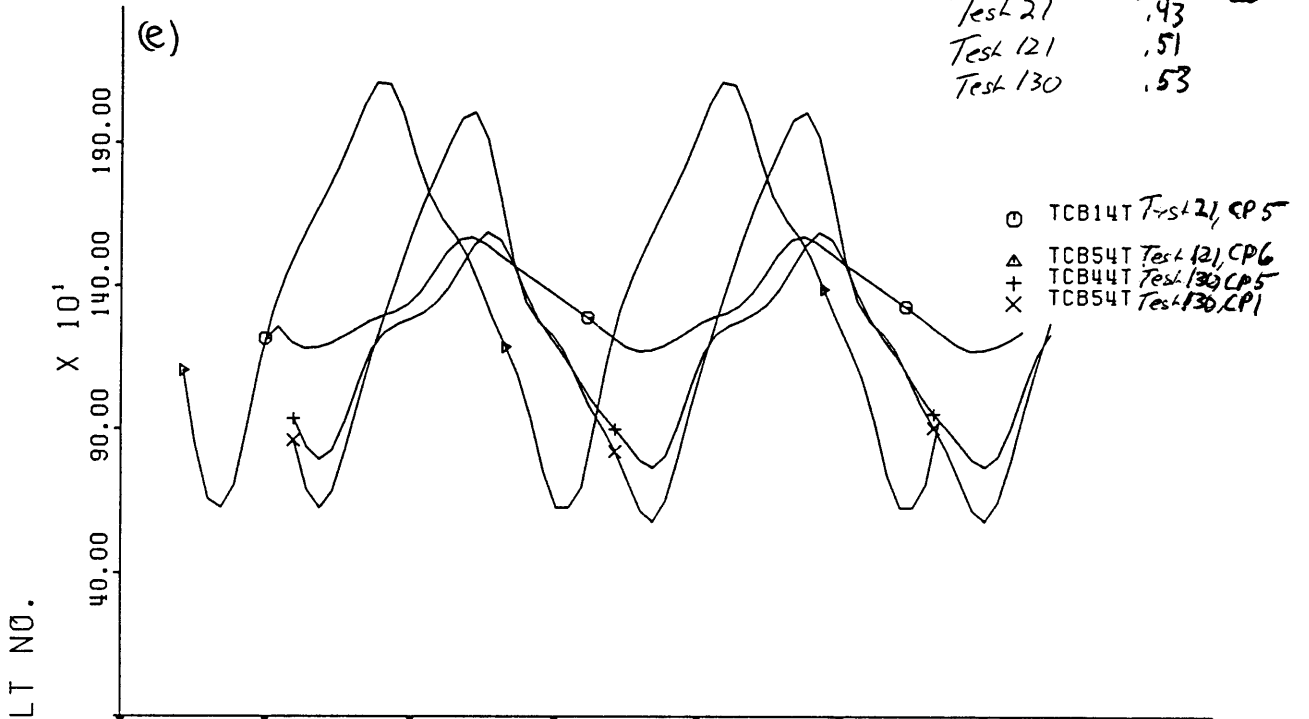
Figure 5-8
Time Averaged Heat Flux
Uniform Flow Tests

	Test	Cir. Pos.	RTDF	$(t_g - t_w)/t_w$
□	121	(2)	0%	.51
■	121	(6)	0%	.51
△	124	(2)	0%	.32
▲	124	(6)	0%	.32
○	130	(5)	0%	.53
●	130	(1)	0%	.53

X/C Axial Location

Heat Flux (kW/M**2)
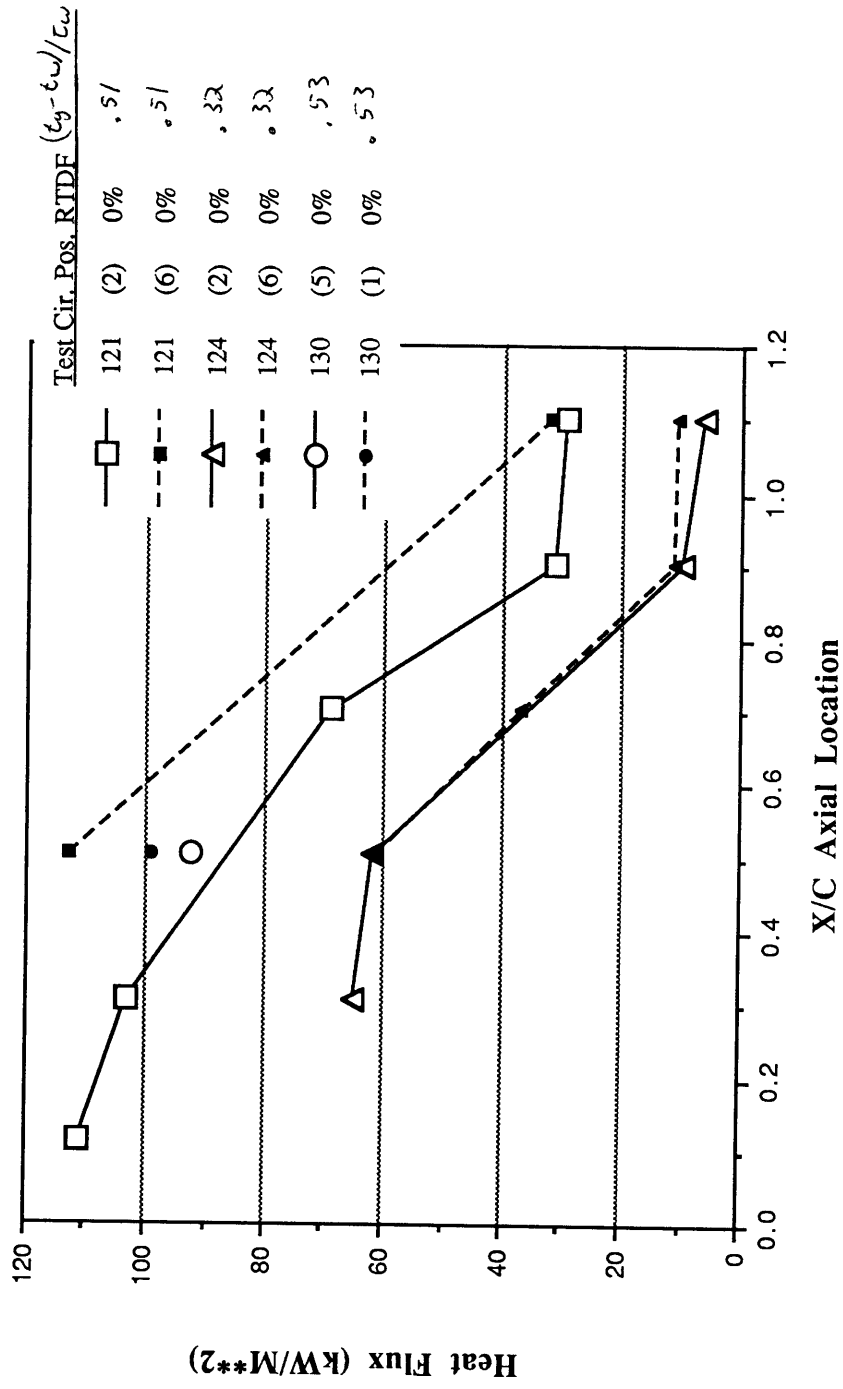
Figure 5-9

Nusselt Number Based on NGV Inlet Average

Bulk Temperature (=Tg) for Uniform Flow Tests
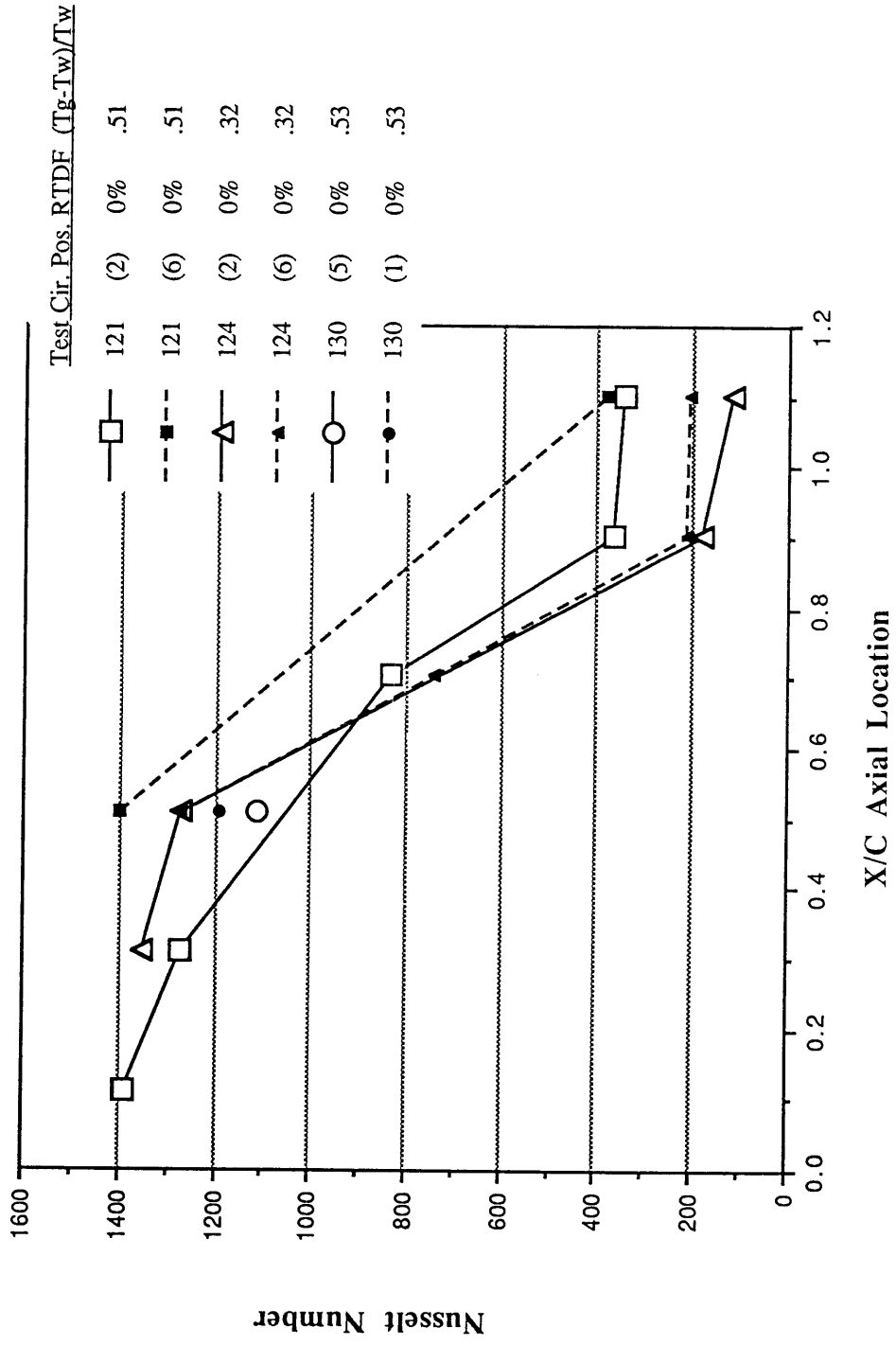
Figure 5-10

Nusselt Number Based on NGV Tip Streamline

Temperature (=Tg) For Uniform Flow Tests

Test	Cir. Pos.	RTDF	(Tg-Tw)/Tw
121	(2)	0%	.49
121	(6)	0%	.49
124	(2)	0%	.32
124	(6)	0%	.32
130	(5)	0%	.51
130	(1)	0%	.51

X/C Axial Location
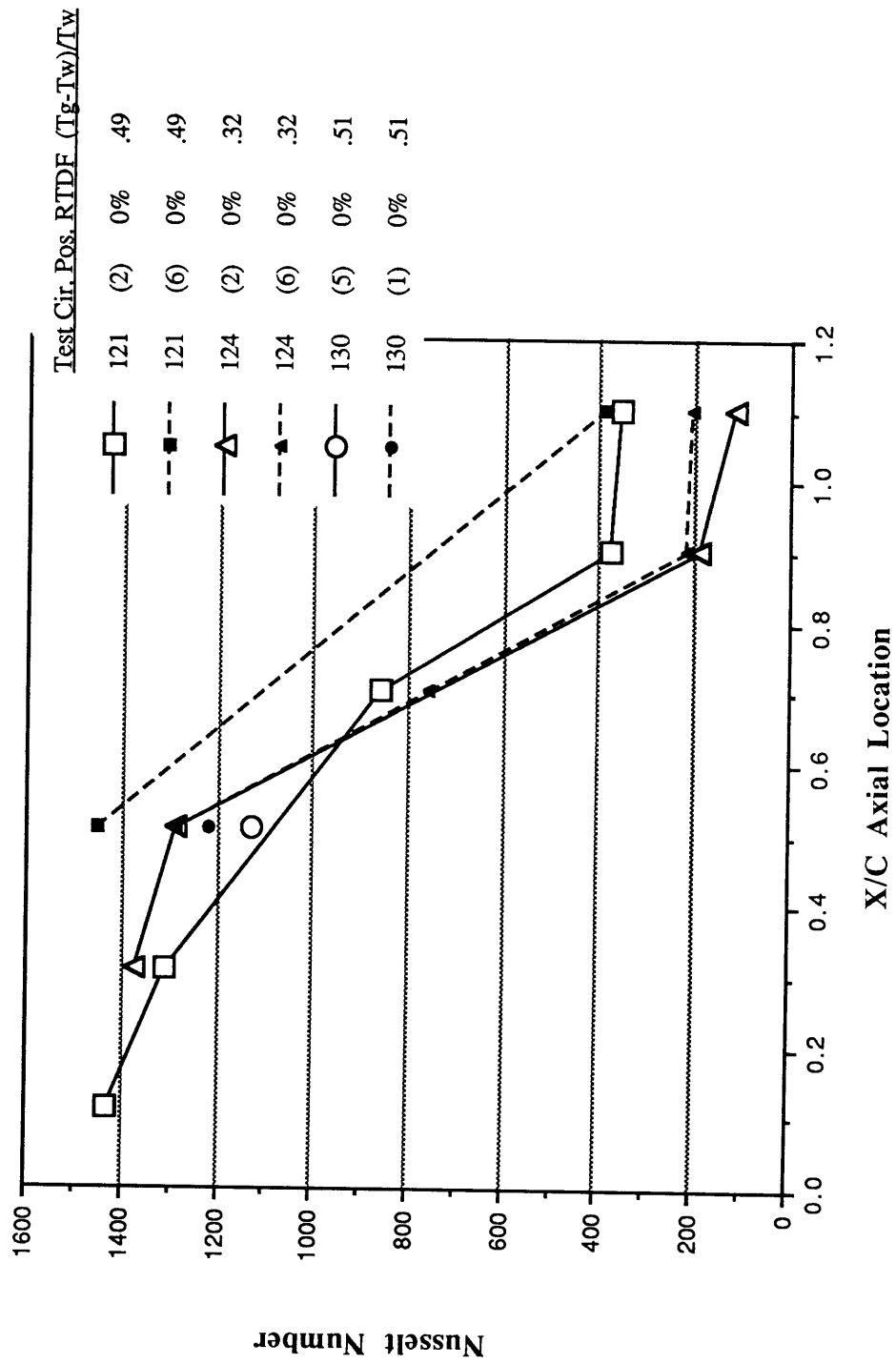
Nusselt Number

FIGURE 5-11
VARIATIONS IN TOTAL NUSSELT NUMBER BASED ON
TIP TEMPERATURE AT NGV INLET
FOR TESTS 121 and 124 (0% RTDF)

$(t_g - t_w)/t_c$
Test 121 .44
Test 124 .32

(a)

TCB43T Test 121, CP2
TCB43T Test 124, CP2

(b)

TCB46T Test 121, CP2
TCB46T Test 124, CP2

(c)

TCB47T Test 121, CP2
TCB47T Test 124, CP2

NUSSELT NO. X 10¹

BLADE PASSING
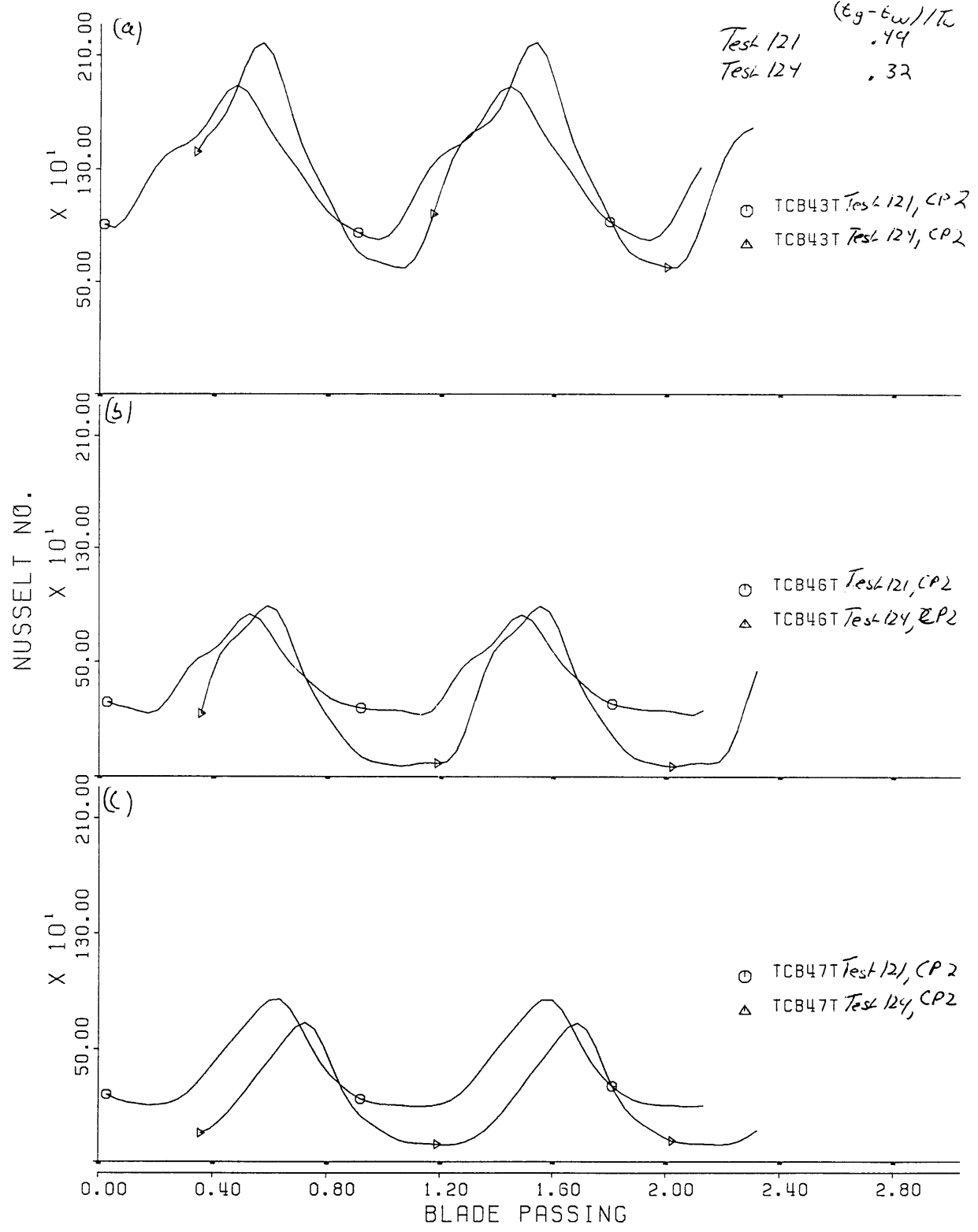
FIGURE 5-11
VARIATIONS IN TOTAL UNSTEADY NUSSELT NUMBER BASED ON TIP TEMPERATURE AT INLET TO NGV FOR TESTS 121, 124, AND 130 (0% RTDF)

$(t_y - t_w)/t_w$

Test 121 .44
124 .32
130 .51

(d)

○ TCB44T Test 124, CP2
♣ TCB44T Test 130, CP5

(e)

○ TCB54T Test 121, CP6
△ TCB54T Test 124, CP6
+ TCB54T Test 130, CP1

(f)

○ TCB57T Test 121, CP6
♣ TCB57T Test 124, CP6

NUSSELT NO.

$\times 10^1$

BLADE PASSING
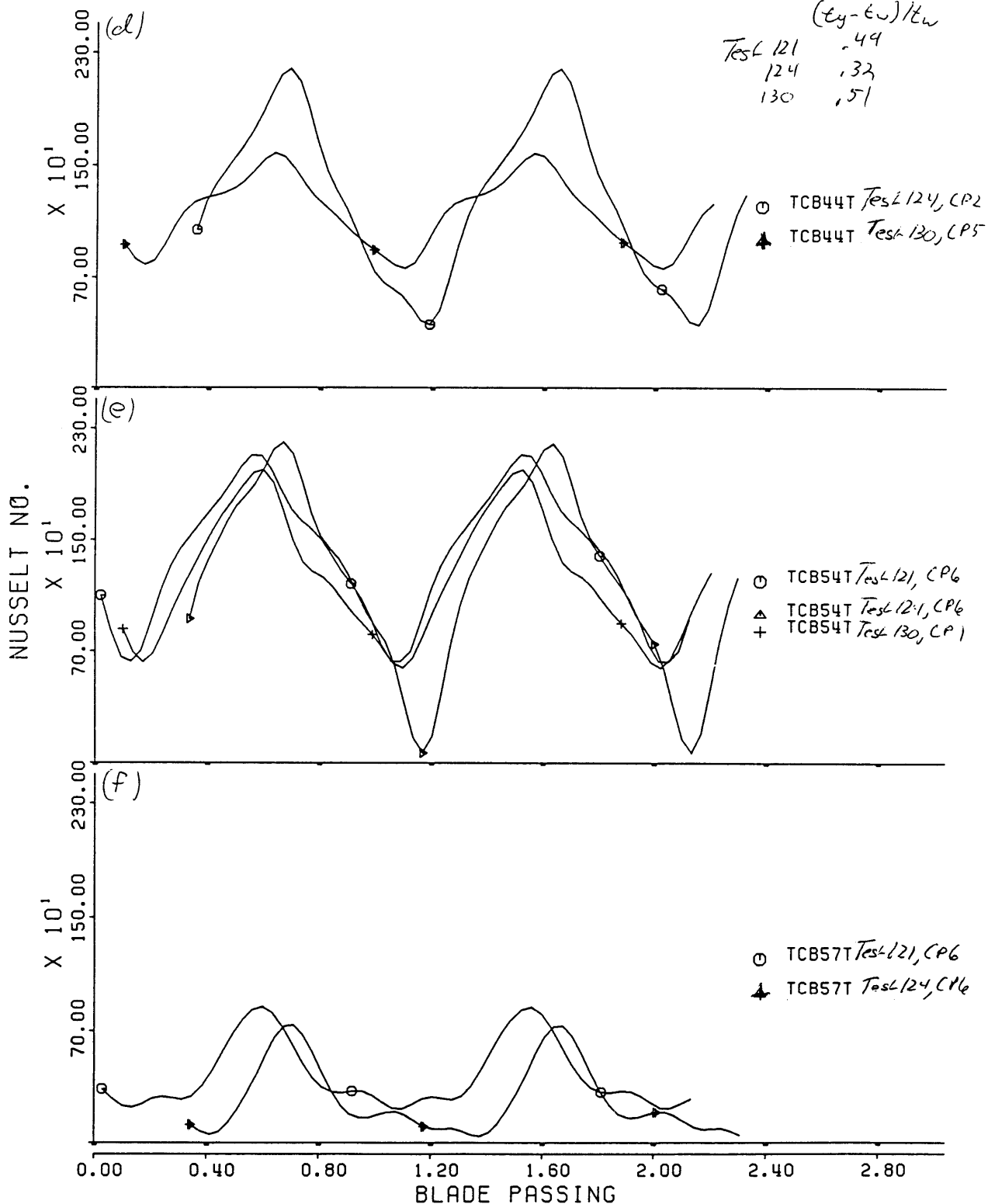
Figure 5-12

Time Averaged Heat Flux

High Temperature Tests
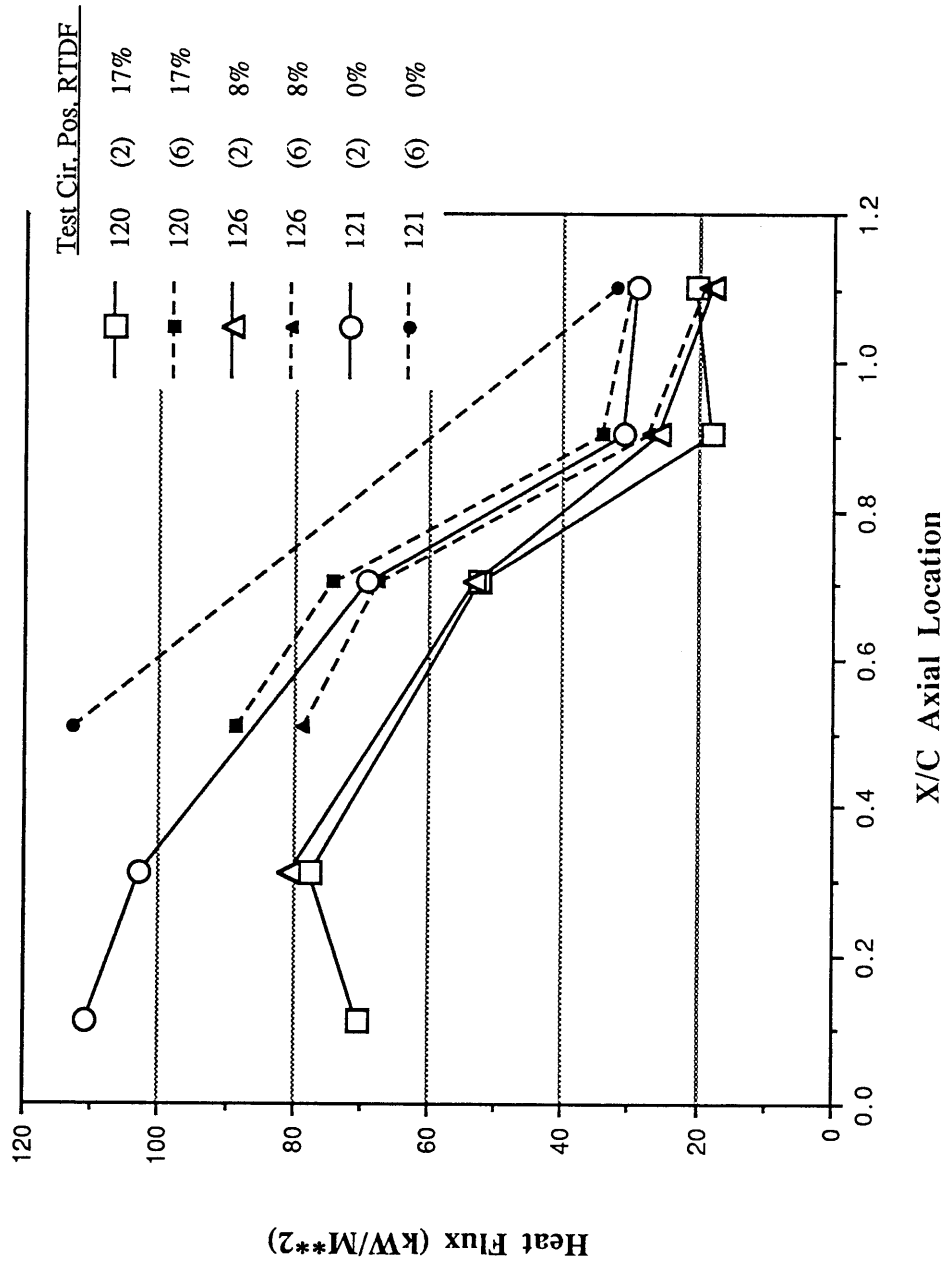
Figure 5-13 (a)

Time Averaged Heat Flux

High Temperature (Casing Reversed) Tests

Test	Cir. Pos.	RTDF
131	(5)	16%
131	(1)	16%
127	(5)	6%
127	(1)	6%
130	(5)	0%
130	(1)	0%

Heat Flux (kW/M**2)

X/C Axial Location

145
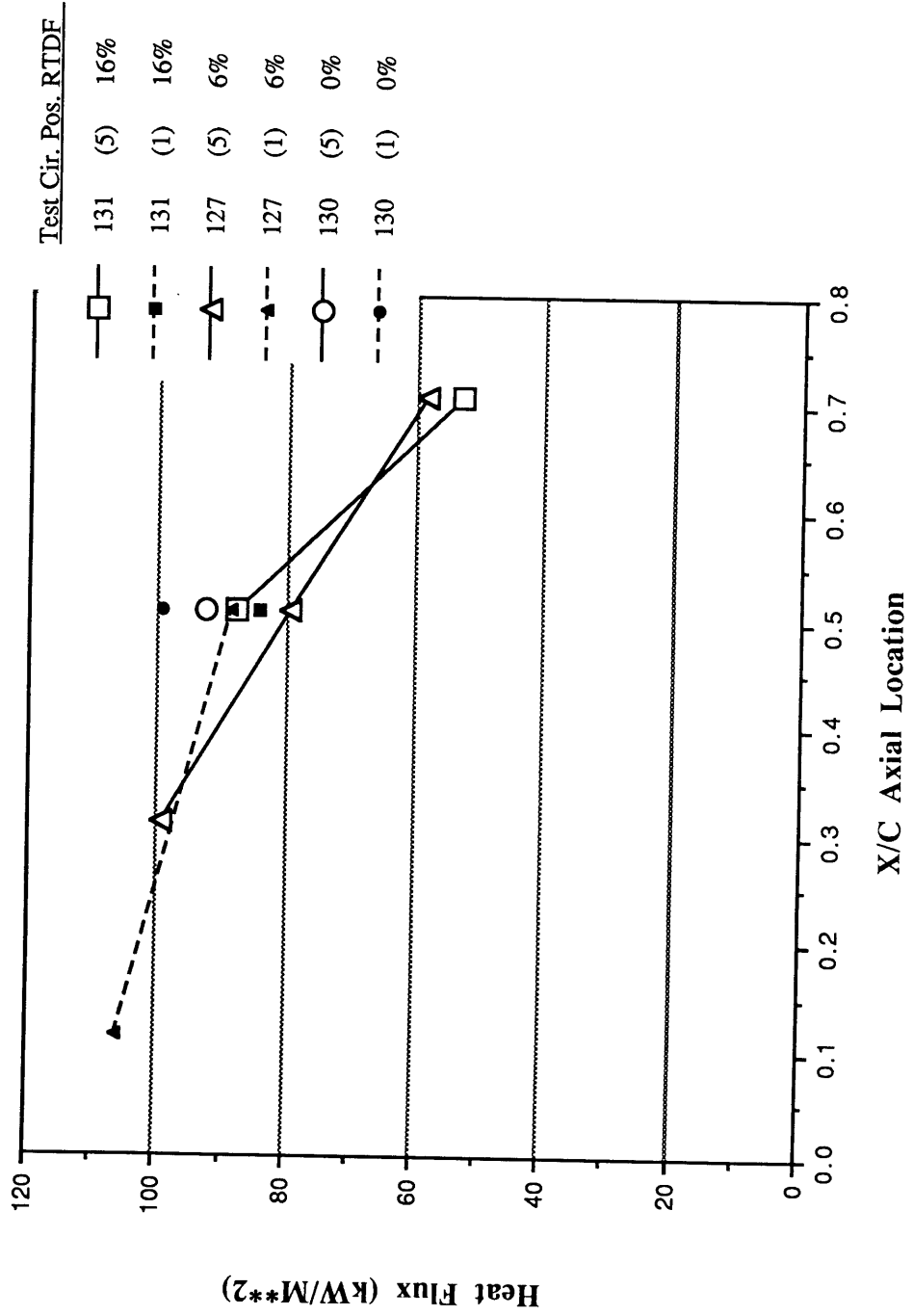
Figure 5-13 (b)

Time Averaged Heat Flux for all

High Temperature Tests

Test	Cir.	Pos.	RTDF
131	(5)	16%	
131	(1)	16%	
127	(5)	6%	
127	(1)	6%	
130	(5)	0%	
130	(1)	0%	
120	(2)	17%	
120	(6)	17%	
126	(2)	8%	
126	(6)	8%	
121	(2)	0%	
121	(6)	0%	

146
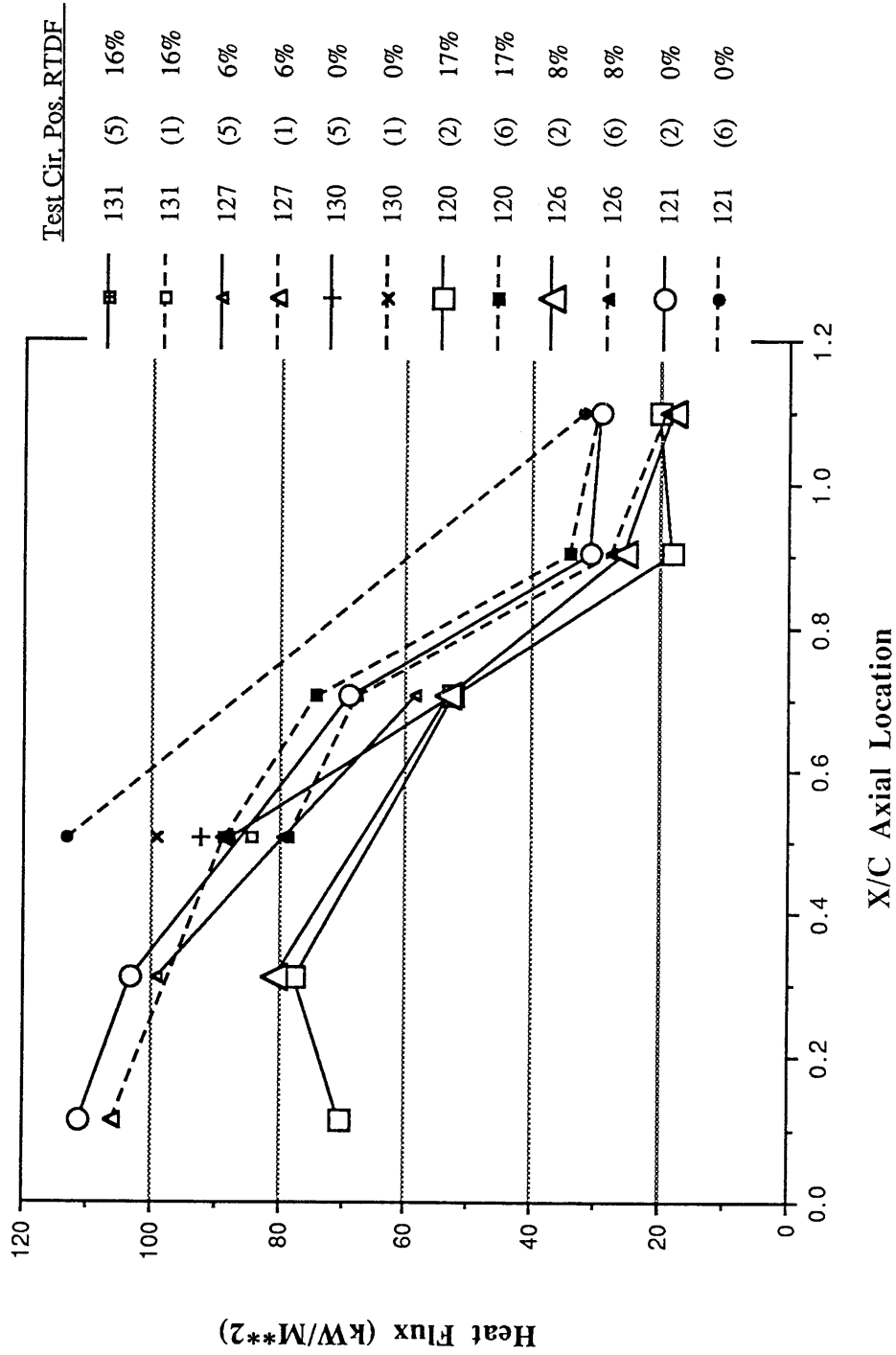
Figure 5-14

Time Averaged Heat Flux

Low Temperature Tests

Test	Cir.	Pos.	RTDF
122	(2)	11%
122	(6)	11%
125	(2)	6%
125	(6)	6%
124	(2)	0%
124	(6)	0%

Heat Flux (kW/M**2)

X/C Axial Location
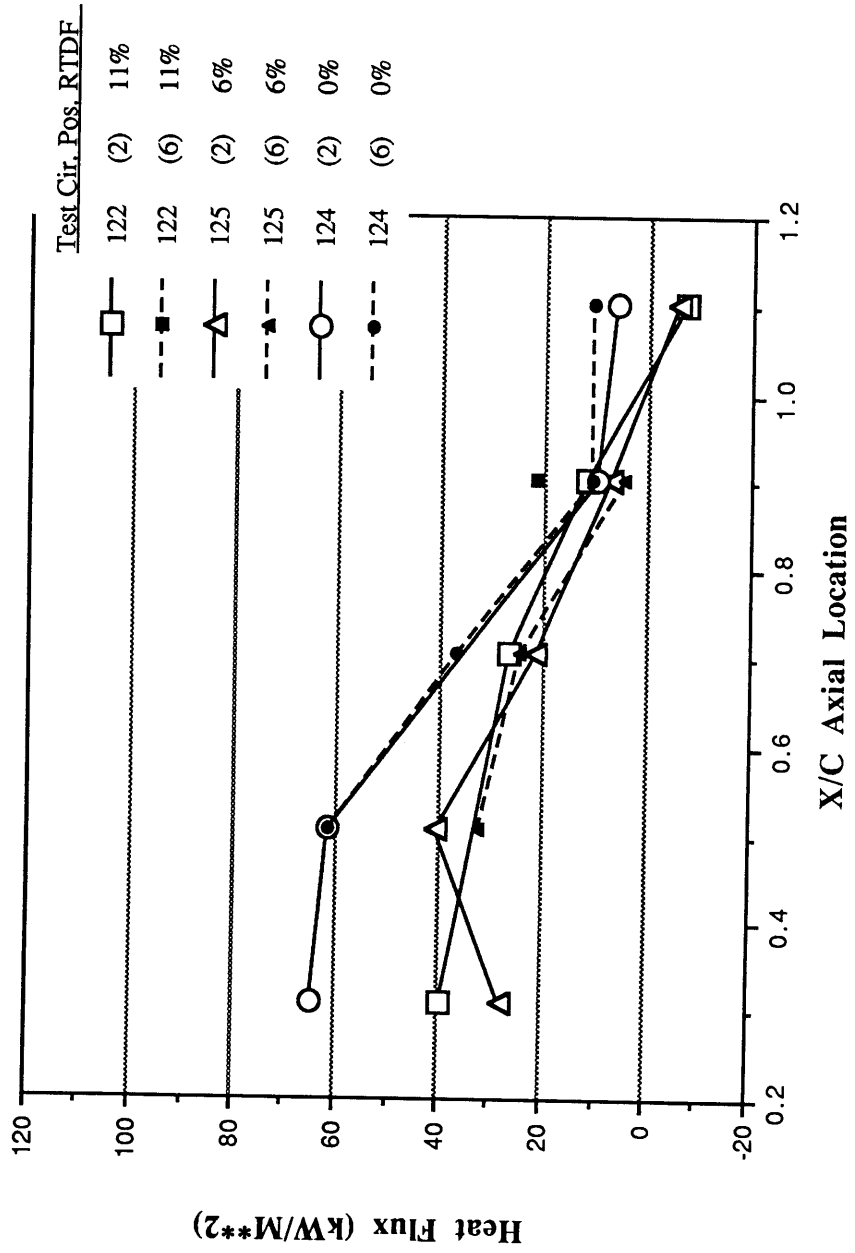
Figure 5-15

Nusselt Number Based on Bulk Average NGV Inlet

Temperature (=Tg), High Temperature Tests
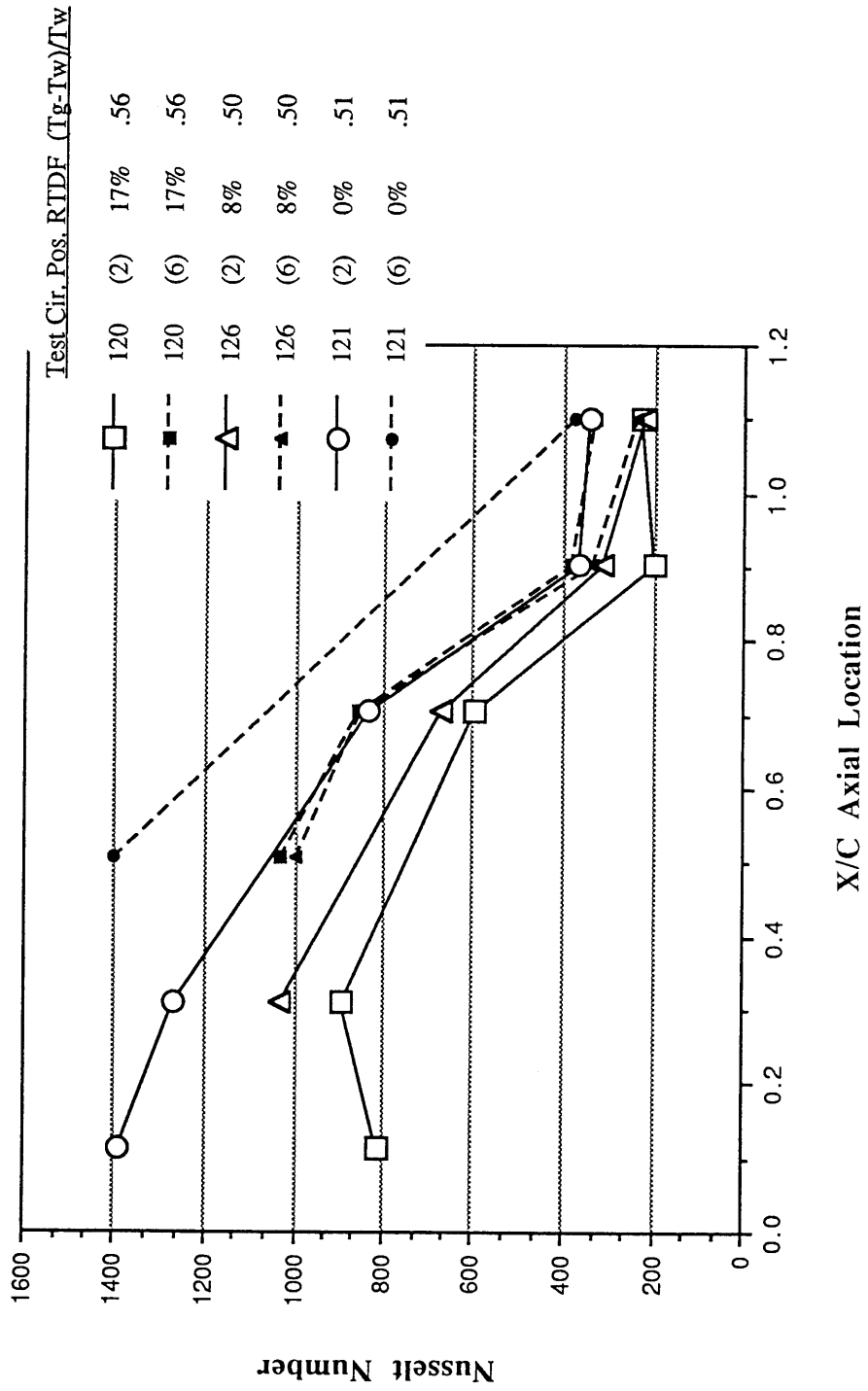
Figure 5-16 (a)

Nusselt Number Based on Bulk Average NGV Inlet

Temperature (=Tg), High Temperature (Casing Reversed) Tests
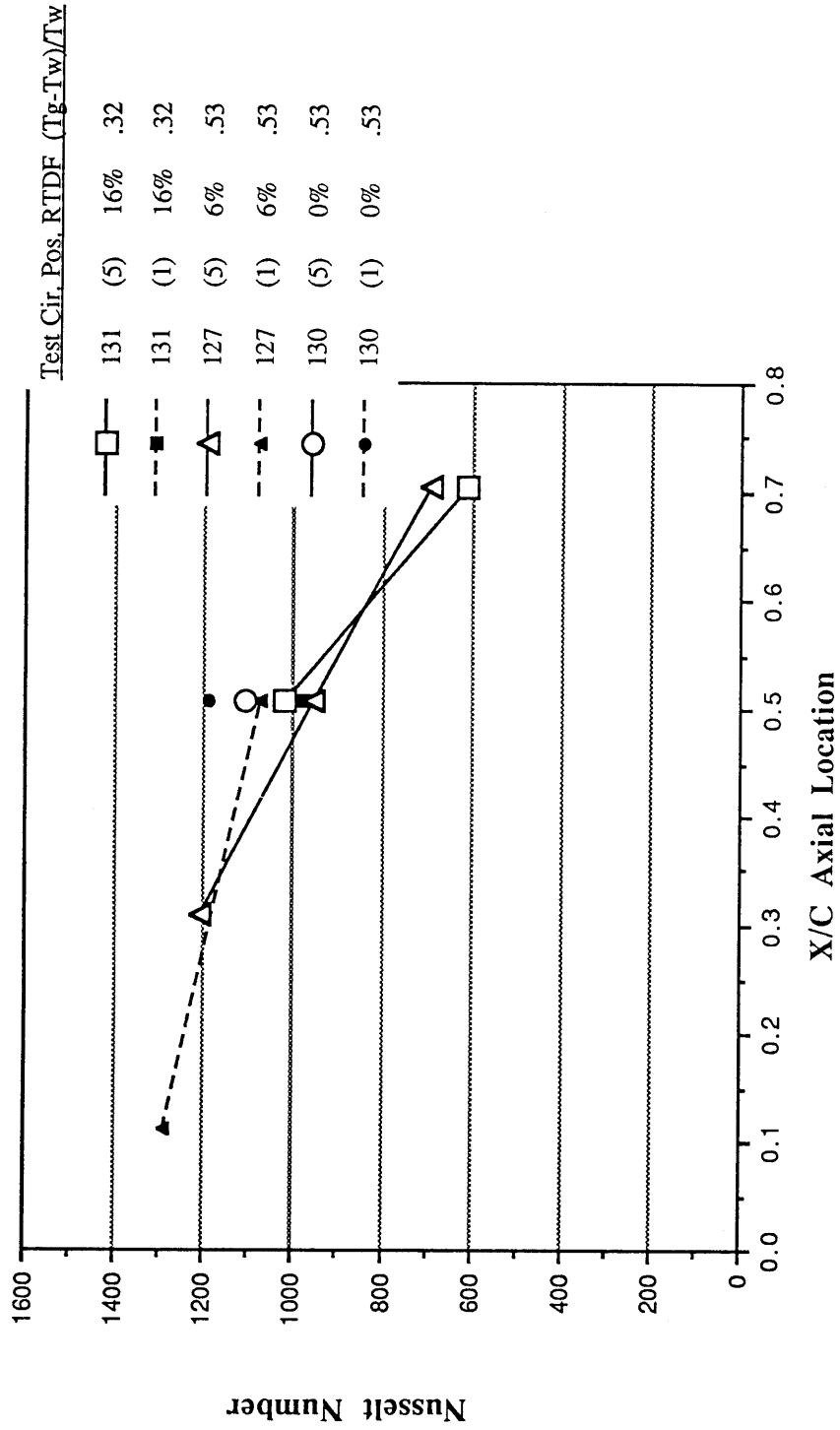
Figure 5-16 (b)

Nusselt Number Based on Bulk Average NGV Inlet Temperature (=Tg), All High Temperature Tests

Nusselt Number
1600
1400
1200
1000
800
600
400
200
0
0.0
0.2
0.4
0.6
0.8
1.0
1.2
X/C Axial Location
Test Cir. Pos. RTDF (Tg-Tw)/Tw
120 (2) 17% .56
120 (6) 17% .56
126 (2) 8% .50
126 (6) 8% .50
121 (2) 0% .51
121 (6) 0% .51
131 (5) 16% .32
131 (1) 16% .32
127 (5) 6% .53
127 (1) 6% .53
130 (5) 0% .53
130 (1) 0% .53
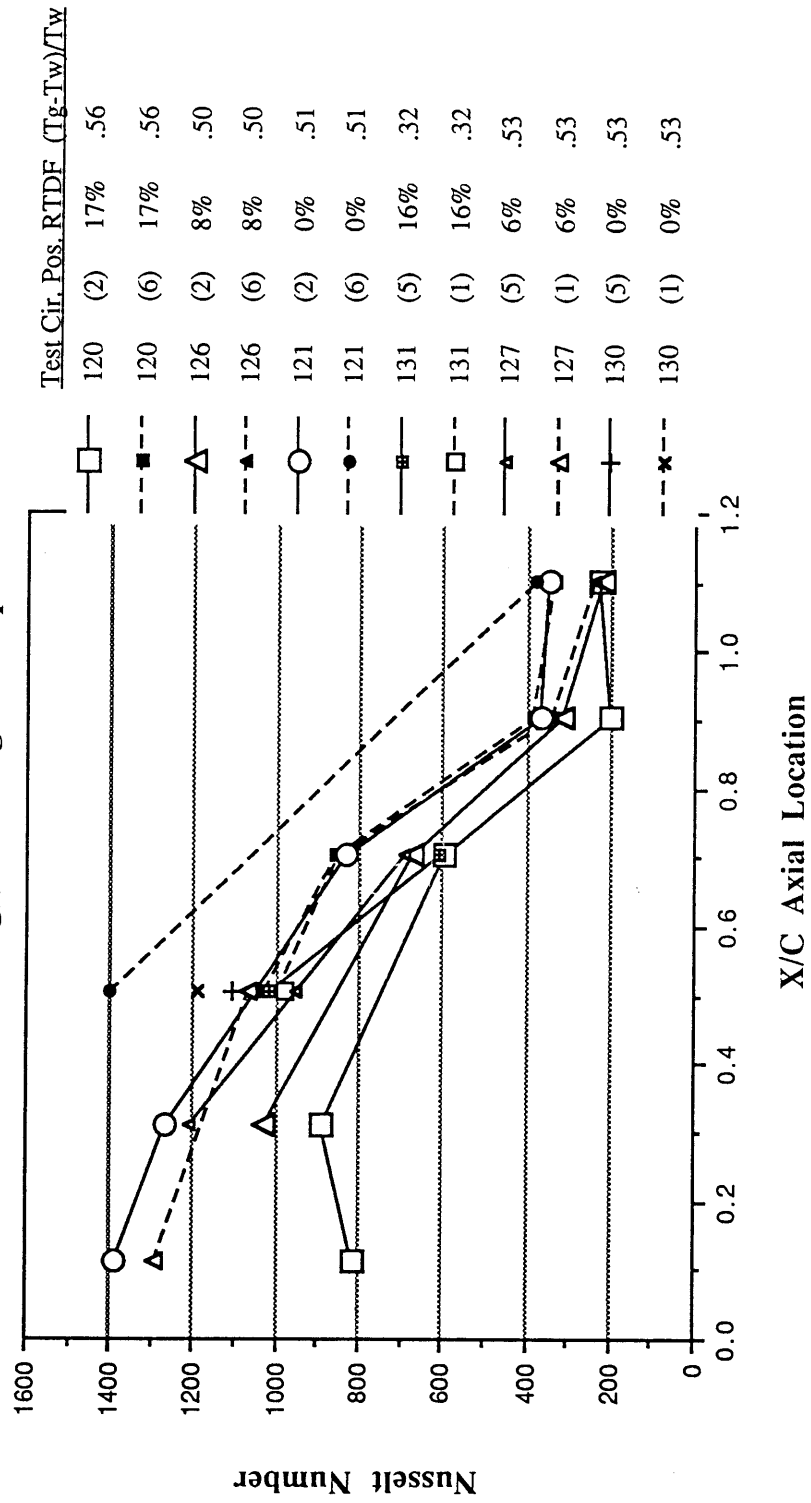
Figure 5-17

Nusselt Number Based on Bulk Average NGV Inlet Temperature (=Tg), Low Temperature Tests
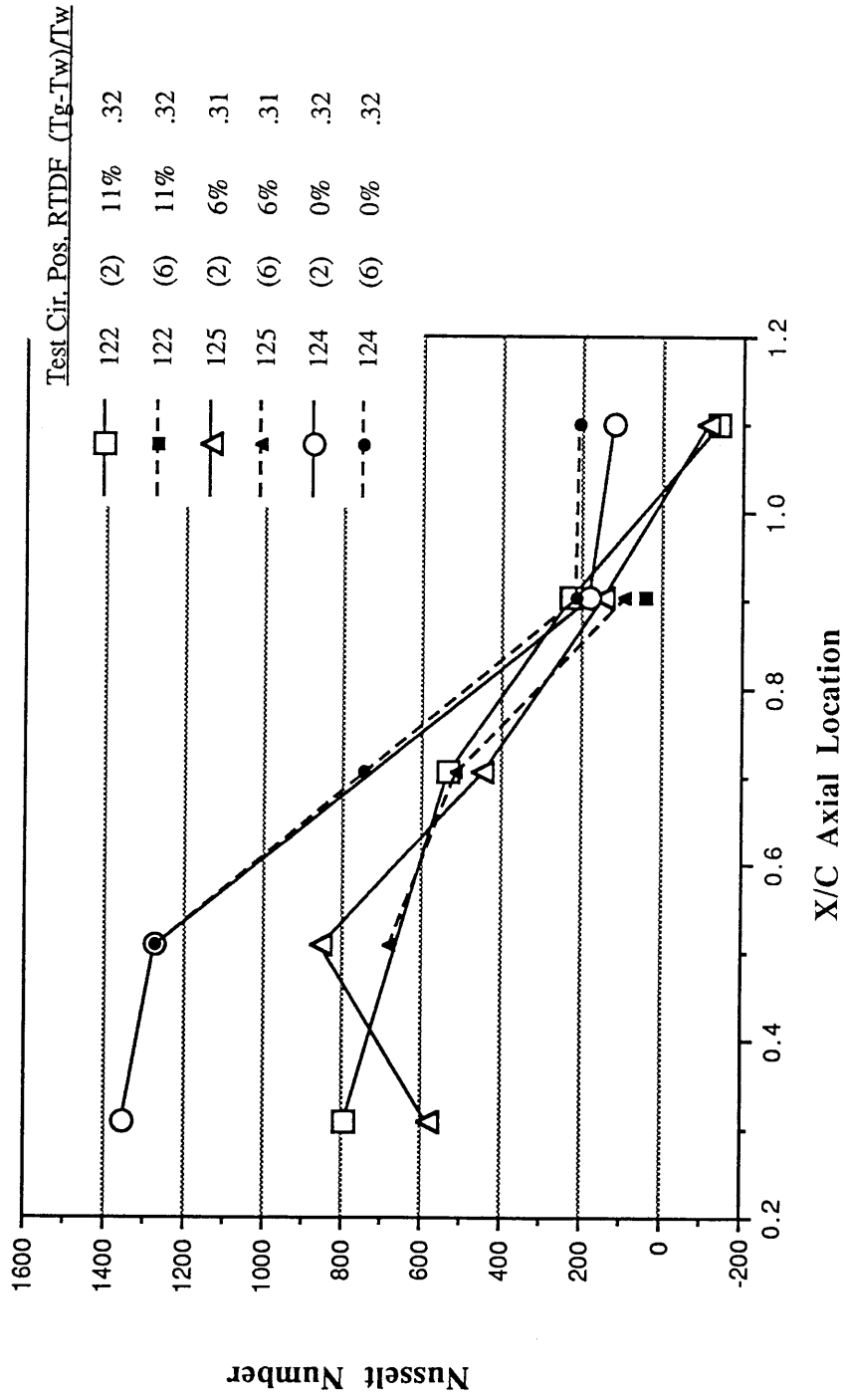
Figure 5-18

Nusselt Number Based on NGV Tip Streamline

Temperature (=Tg), High Temperature Tests
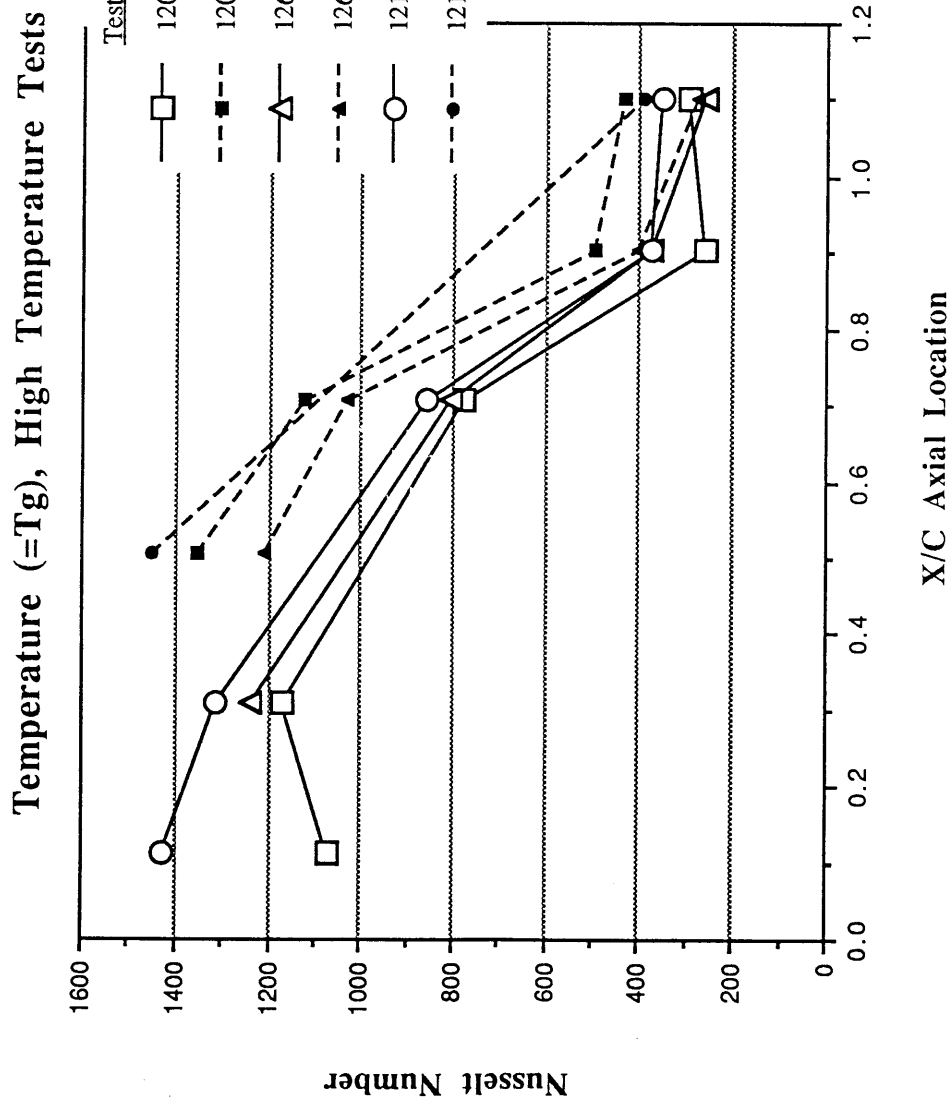
Figure 5-19 (a)

Nusselt Number Based on NGV Tip Streamline

Temperature, High Temperature (Casing Reversed) Tests
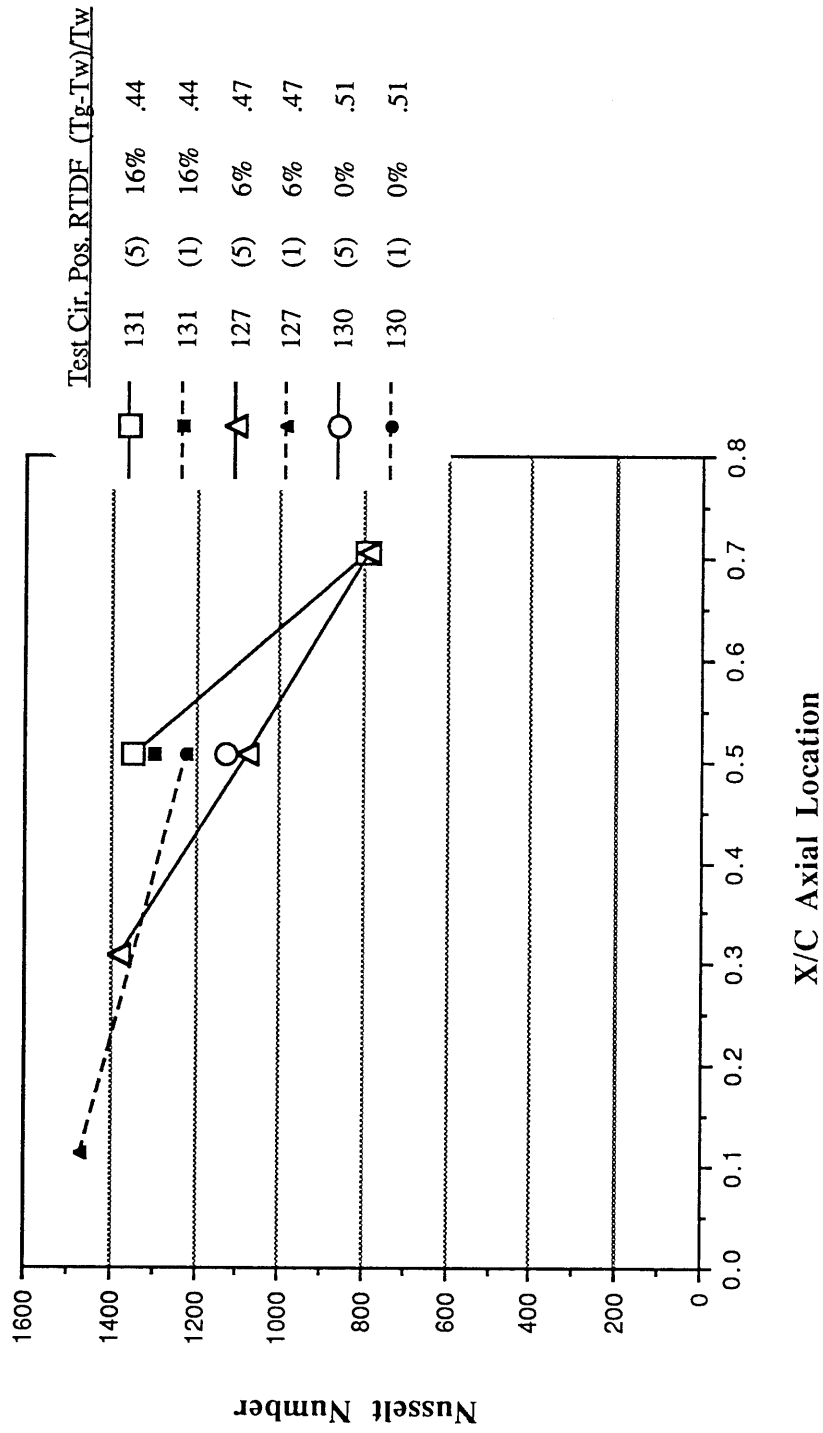
Figure 5-19 (b)

Nusselt Number Based on NGV Tip Streamline

Temperature (=Tg), All High Temperature Tests

	Test	Cir. Pos.	RTDF	(Tg-Tw)/Tw
□	120	(2)	17%	.44
■	120	(6)	17%	.44
△	126	(2)	8%	.42
◢	126	(6)	8%	.42
○	121	(2)	0%	.49
●	121	(6)	0%	.49
✗	131	(5)	16%	.44
◆	131	(1)	16%	.44
■	127	(5)	6%	.47
■	127	(1)	6%	.47
+	130	(5)	0%	.51
+	130	(1)	0%	.51

154
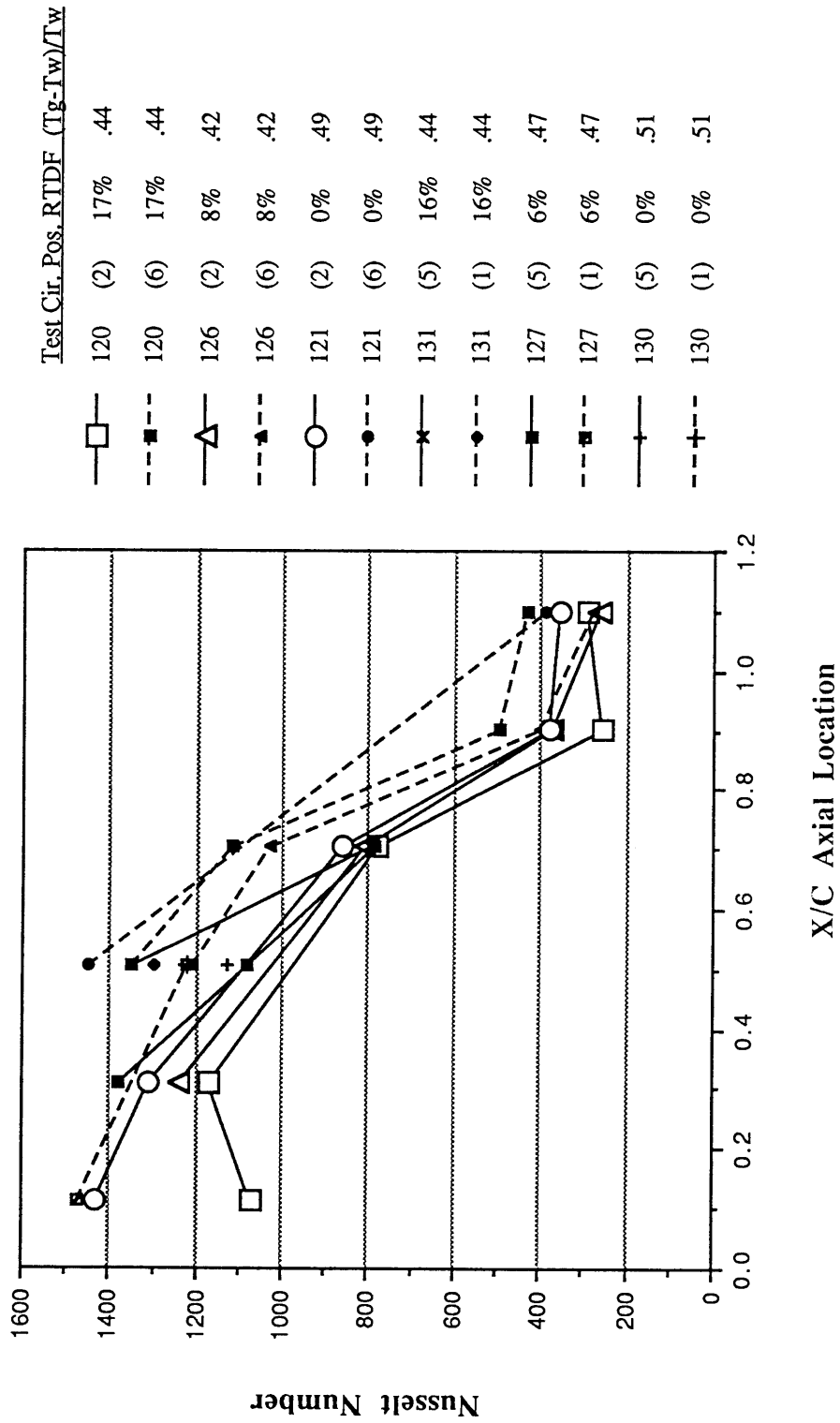
Figure 5-20

Nusselt Number Based on NGV Tip Streamline

Temperature, Low Temperature Tests

Test	Cir. Pos.	RTDF	(Tg-Tw)/Tw
122	(2)	11%	.23
122	(6)	11%	.23
125	(2)	6%	.25
125	(6)	6%	.25
124	(2)	0%	.32
124	(6)	0%	.32
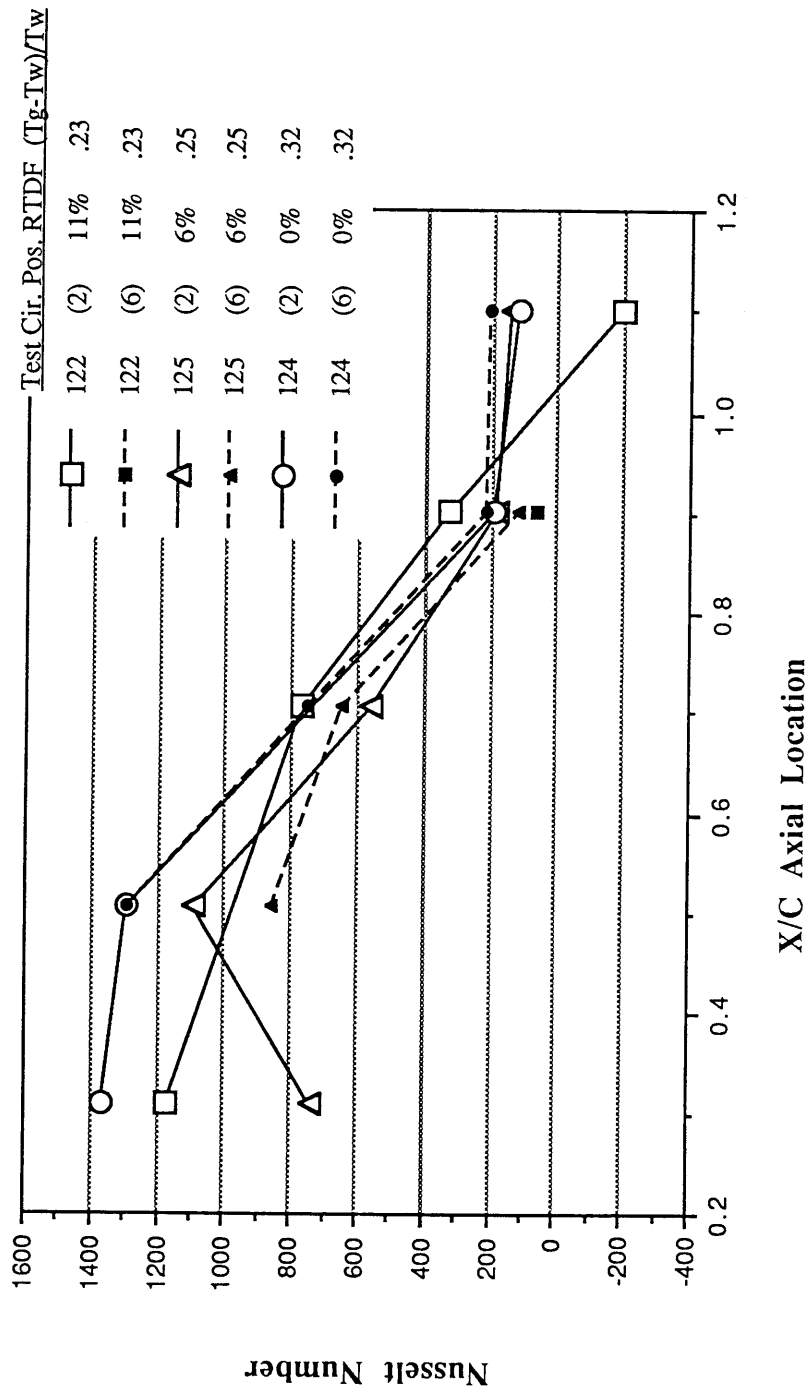
FIGURE 5-21(a): PRESSURE SIGNATURE FOR TRANSDUCER #1
TEST 120
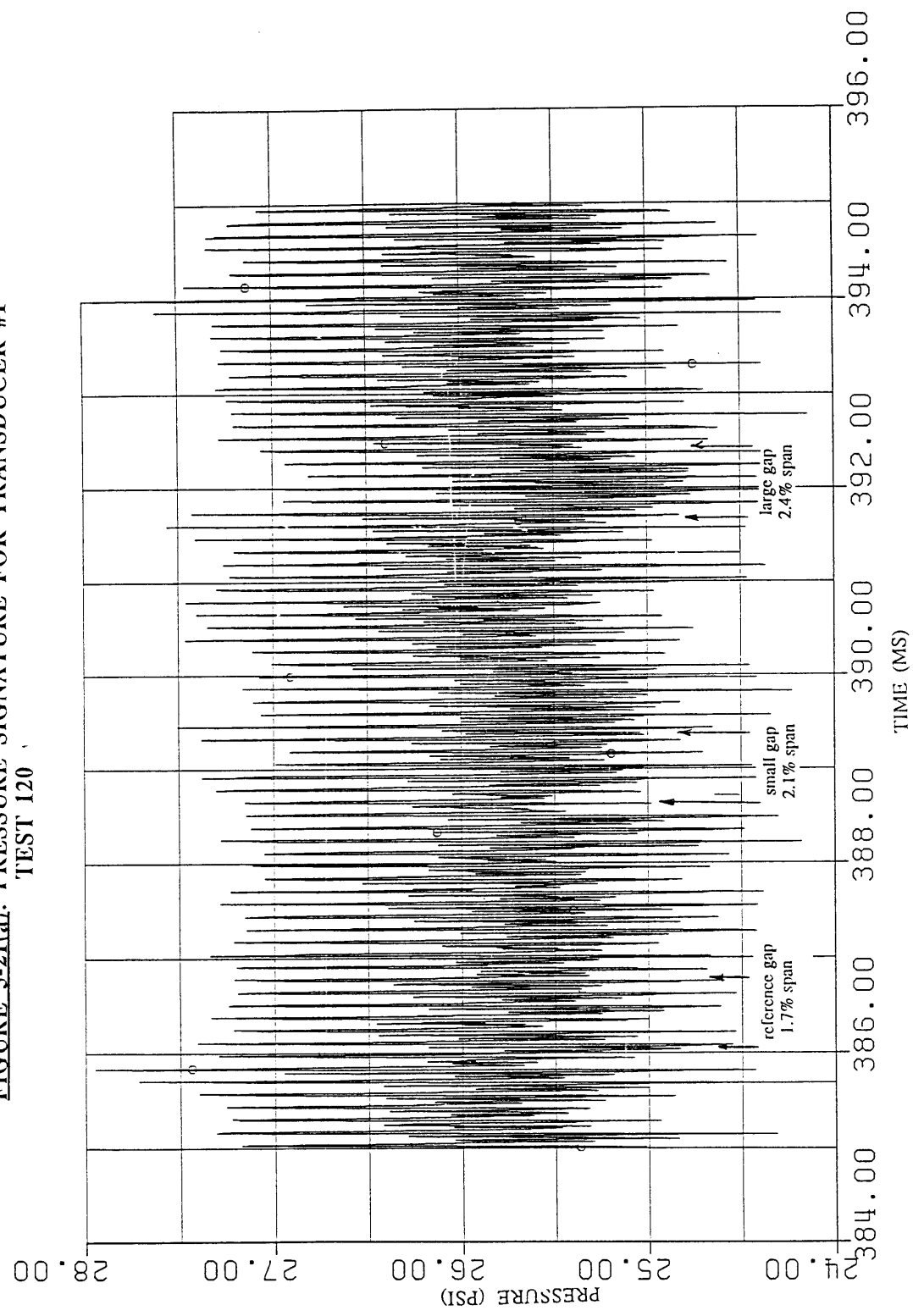
FIGURE 5-21(b): PRESSURE SIGNATURE FOR TRANSDUCER #2
TEST 120

157
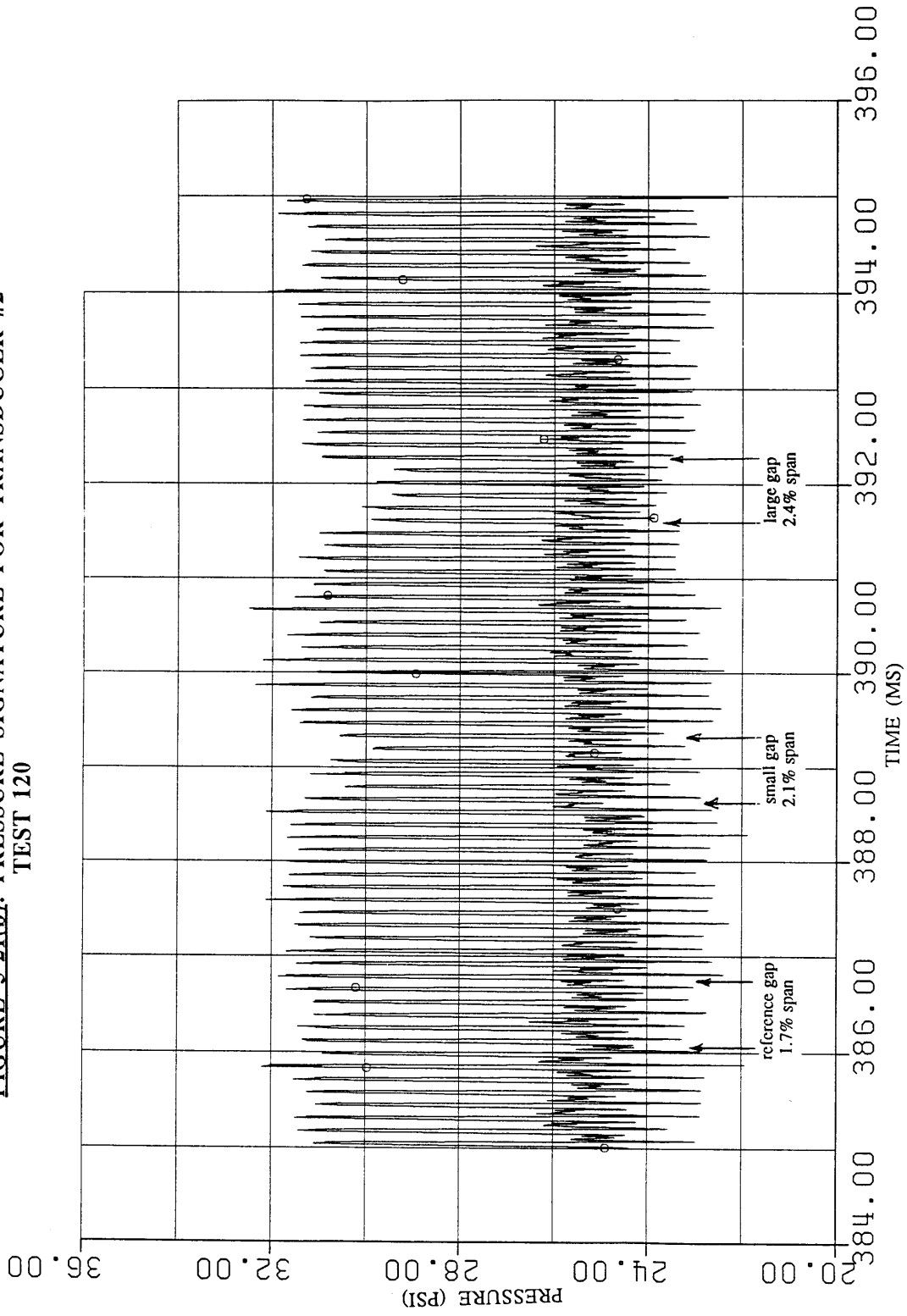
FIGURE 5-21(d): PRESSURE SIGNATURE FOR TRANSDUCER #4
TEST 120

158
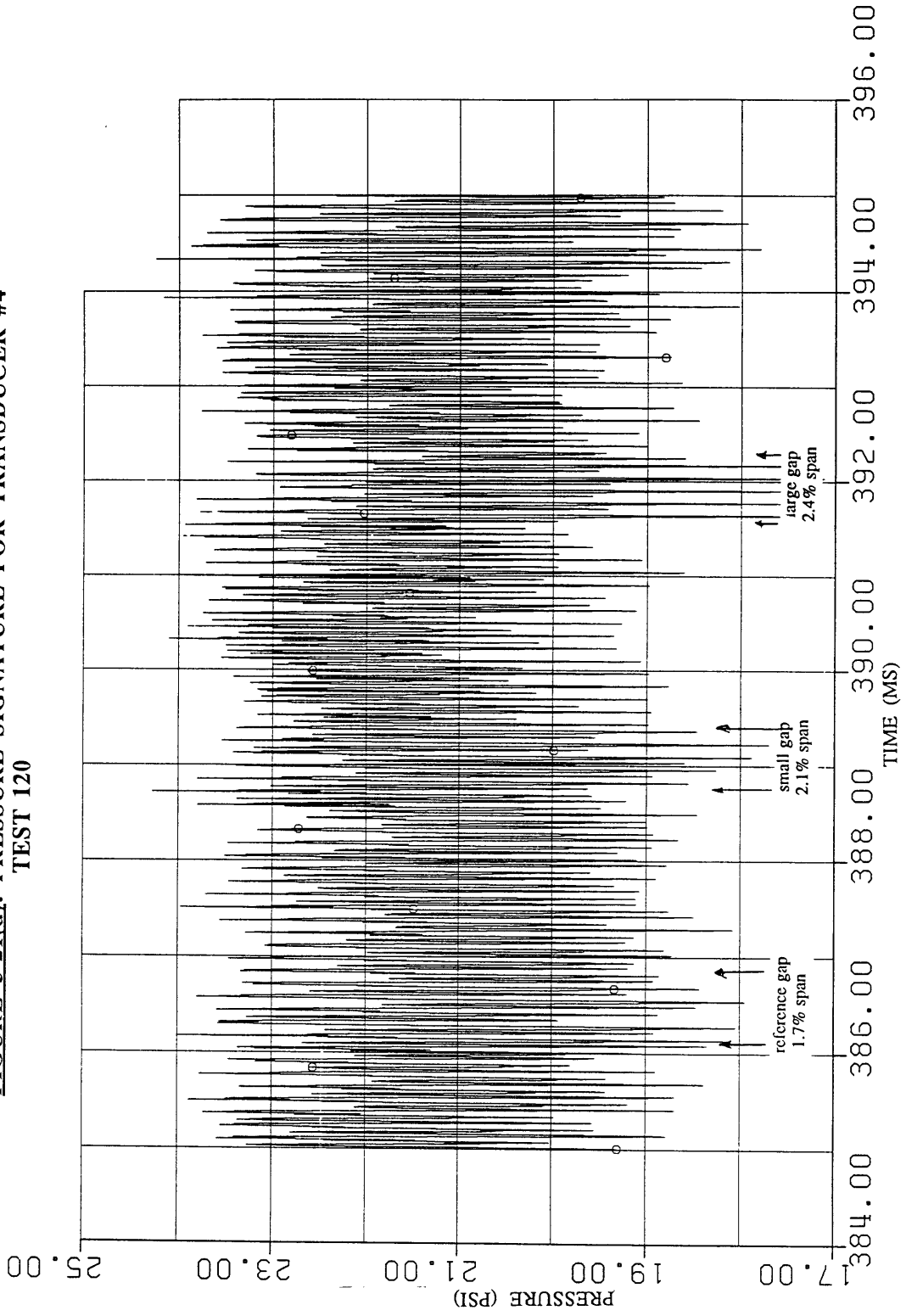
FIGURE 5-21(c): PRESSURE SIGNATURE FOR TRANSDUCER #3
TEST 120

large gap
2.4% span

small gap
2.1% span

reference gap
1.7% span

TIME (MS)

PRESSURE (PSI)

158

FIGURE 5-21(e): PRESSURE SIGNATURE FOR TRANSDUCER #5
TEST 120

160
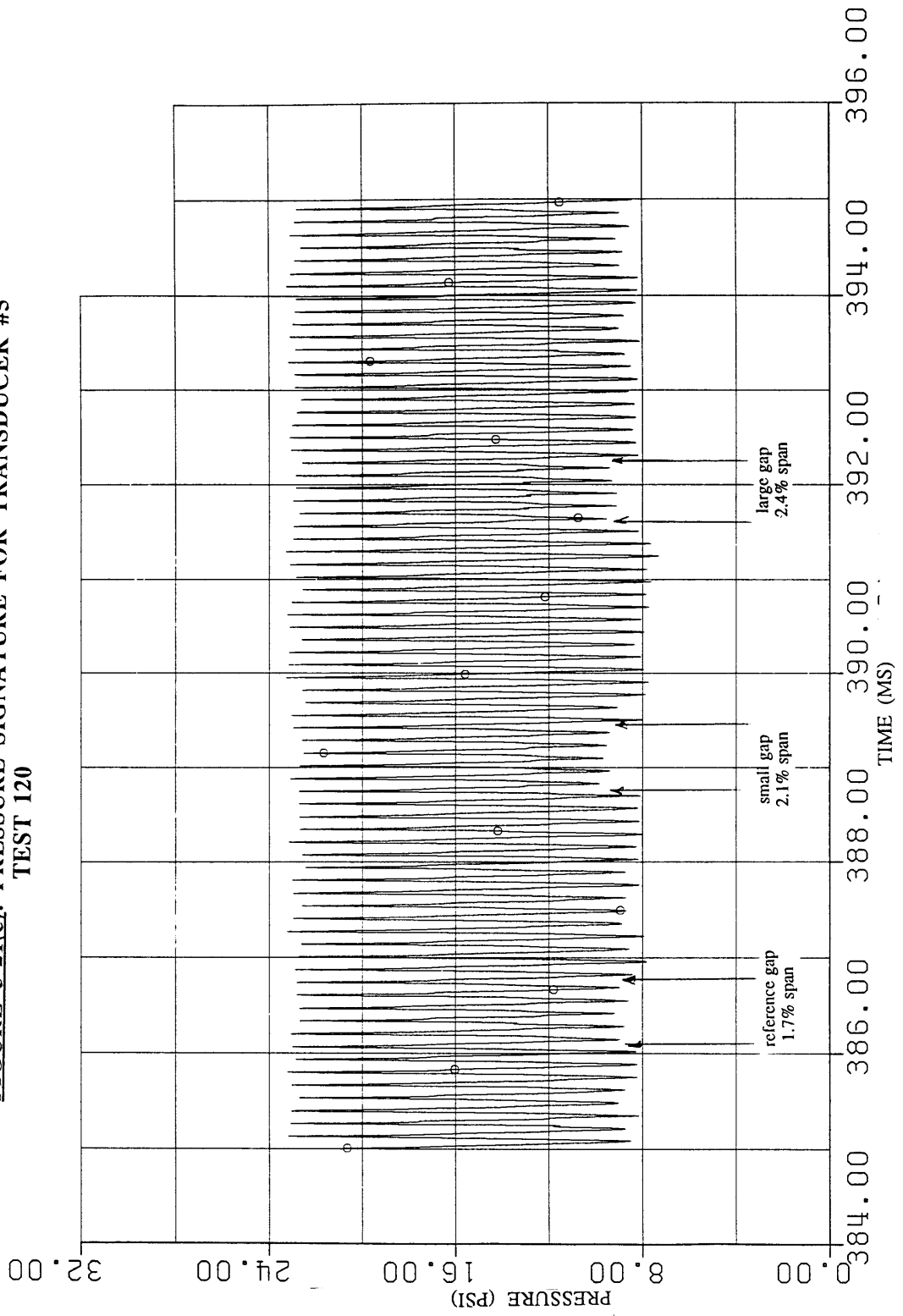
FIGURE 5-22
BLADE AVERAGED PRESSURE SIGNAL FOR 1.7% BLADE GAP
FOR HIGH TEMPERATURE RUNS, 16%, 8%, AND 0% RTDF
AXIAL LOCATION 1, CIRCUMFERENTIAL POSITION 5
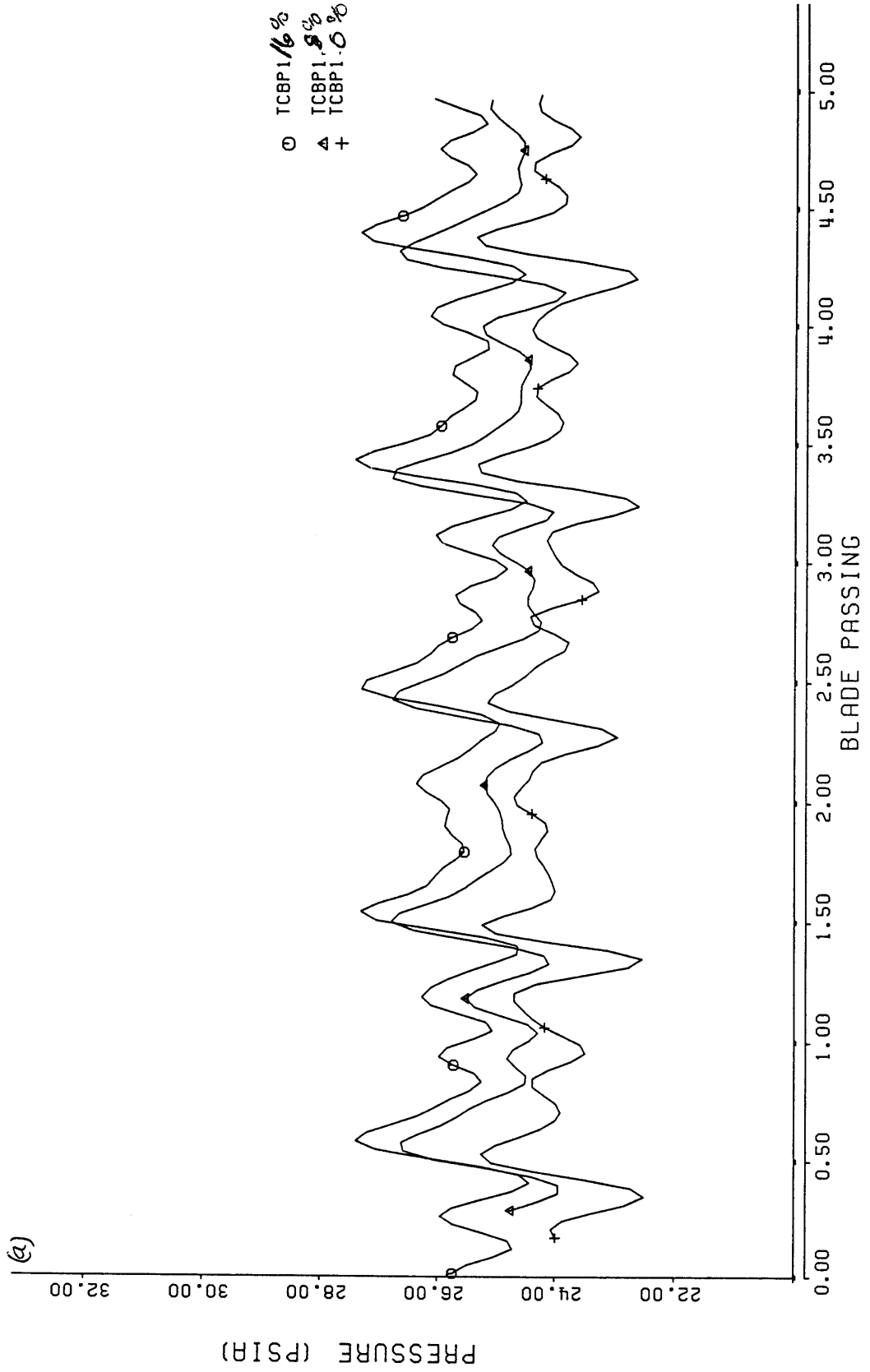
⊙ TCBP1.16%
△ TCBP1.8%
+ TCBP1.0%

(a)

PRESSURE (PSIA)

BLADE PASSING

161

FIGURE 5-22 (cont)
BLADE AVERAGED PRESSURE SIGNAL FOR 1.7% BLADE GAP
FOR HIGH TEMPERATURE RUNS, 16.8%, AND 0% RTDF
AXIAL LOCATION 2, CIRCUMFERENTIAL POSITION 4
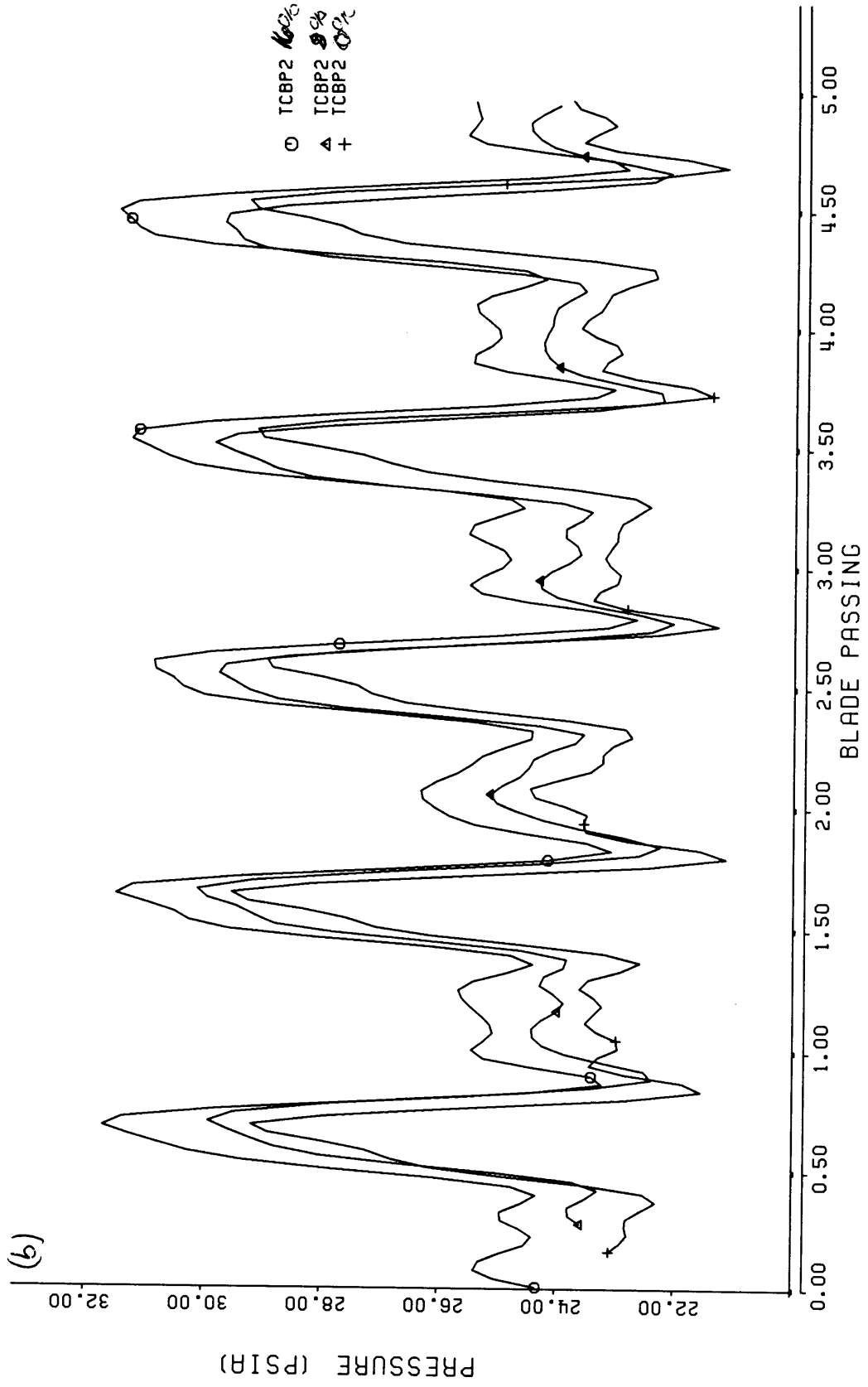
162

FIGURE 5-22 (cont)
BLADE AVERAGED PRESSURE SIGNAL FOR 1.7% BLADE GAP
FOR HIGH TEMPERATURE RUNS, 16.8%, AND 0% RTDF
AXIAL LOCATION 3, CIRCUMFERENTIAL POSITION 5
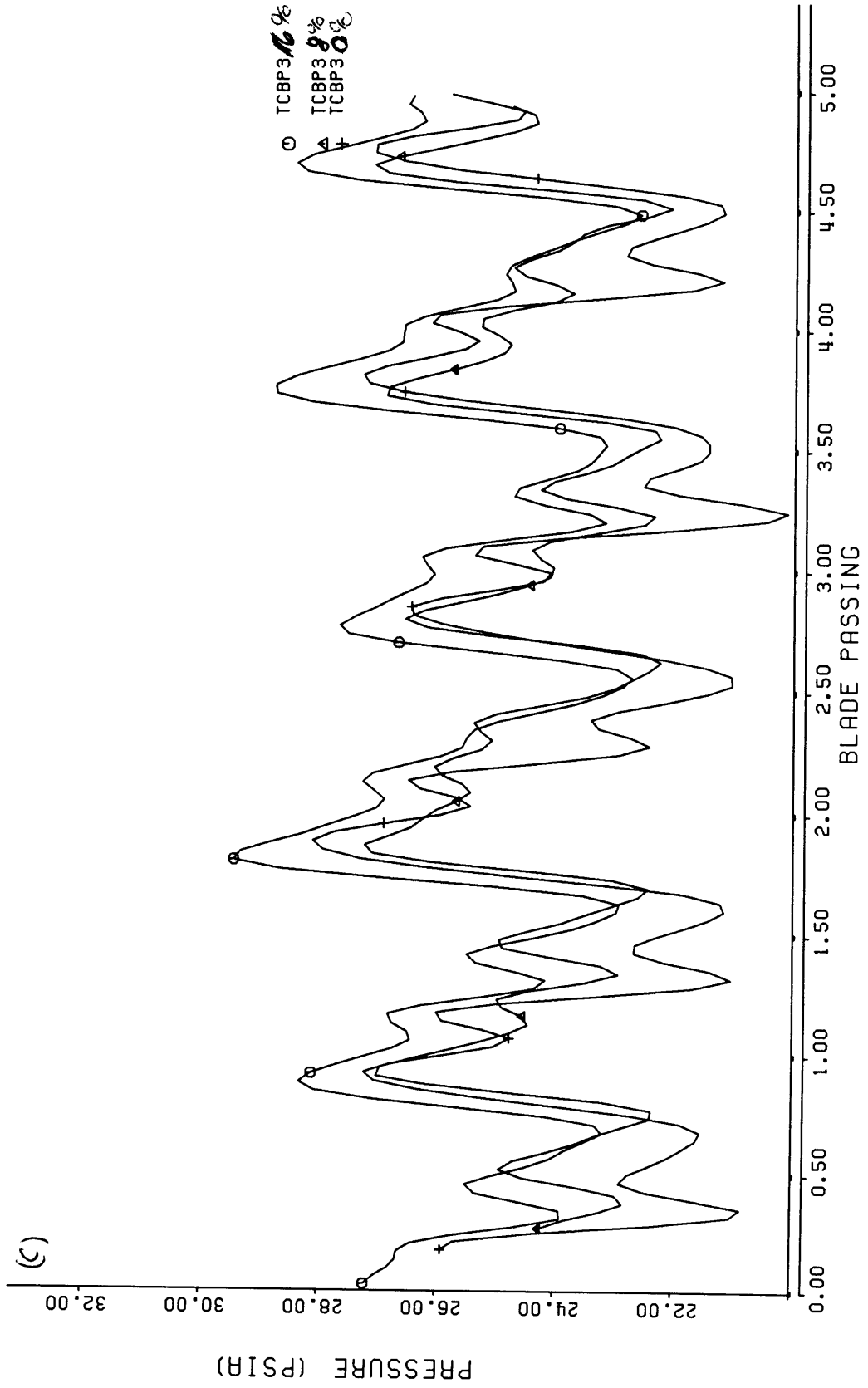
(c)

163

FIGURE 5-22 (c,l)
BLADE AVERAGED PRESSURE SIGNAL FOR 1.7% BLADE GAP
FOR HIGH TEMPERATURE RUNS 16%, 8%, AND 0% RTDF.
AXIAL LOCATION 4, CIRCUMFERENTIAL POSITION 4

Legend:
⊙ TCBP4 16%
△ TCBP4 8%
+ TCBP4 0%

FIGURE 5-23 (con't) BLADE AVERAGED PRESSURE SIGNAL FOR 1.7%, 8%, AND 0% RTDF FOR HIGH TEMPERATURE RUNS, 16% BLADE GAP AXIAL LOCATION 5 CIRCUMFERENTIAL POSITION 5

165
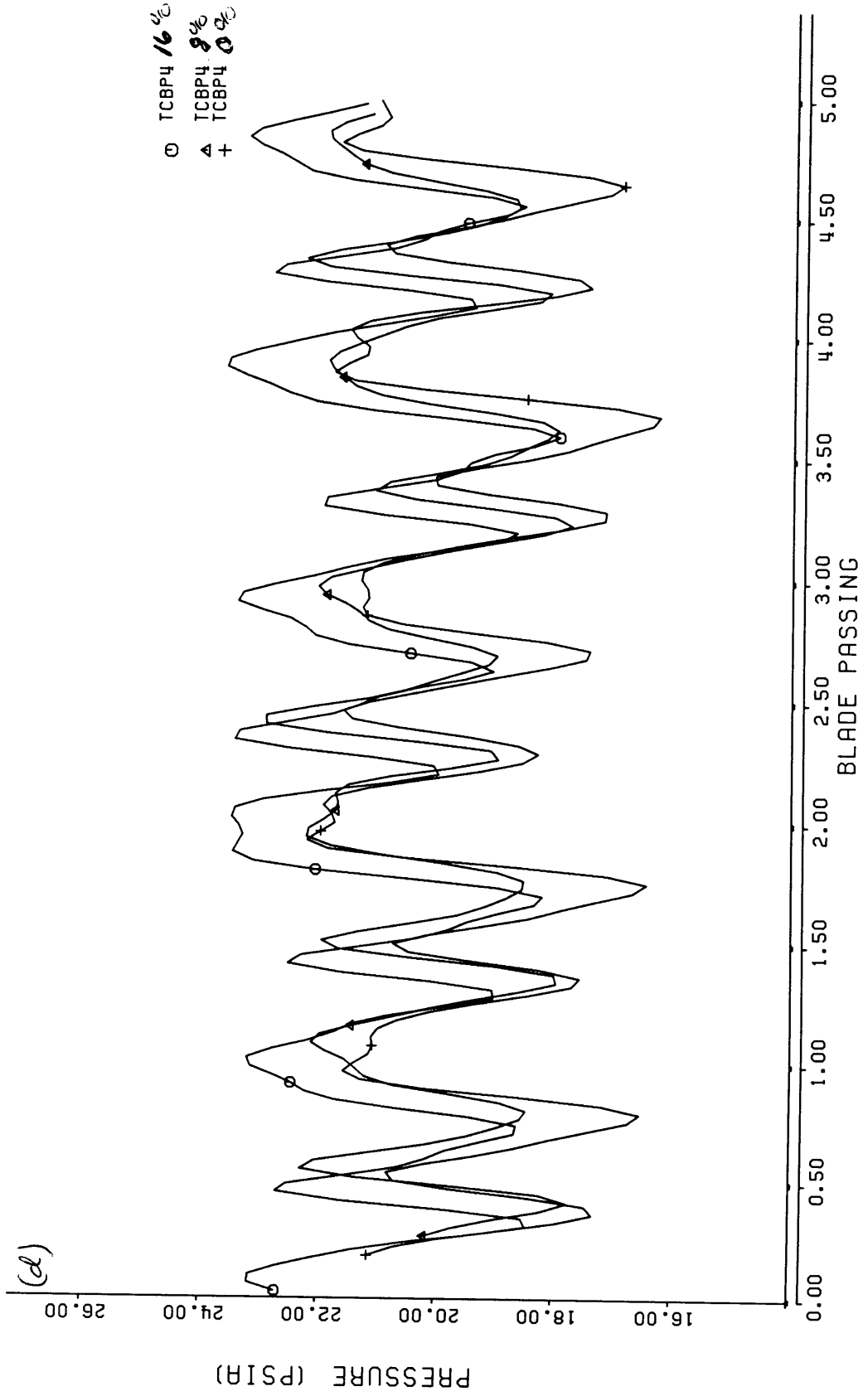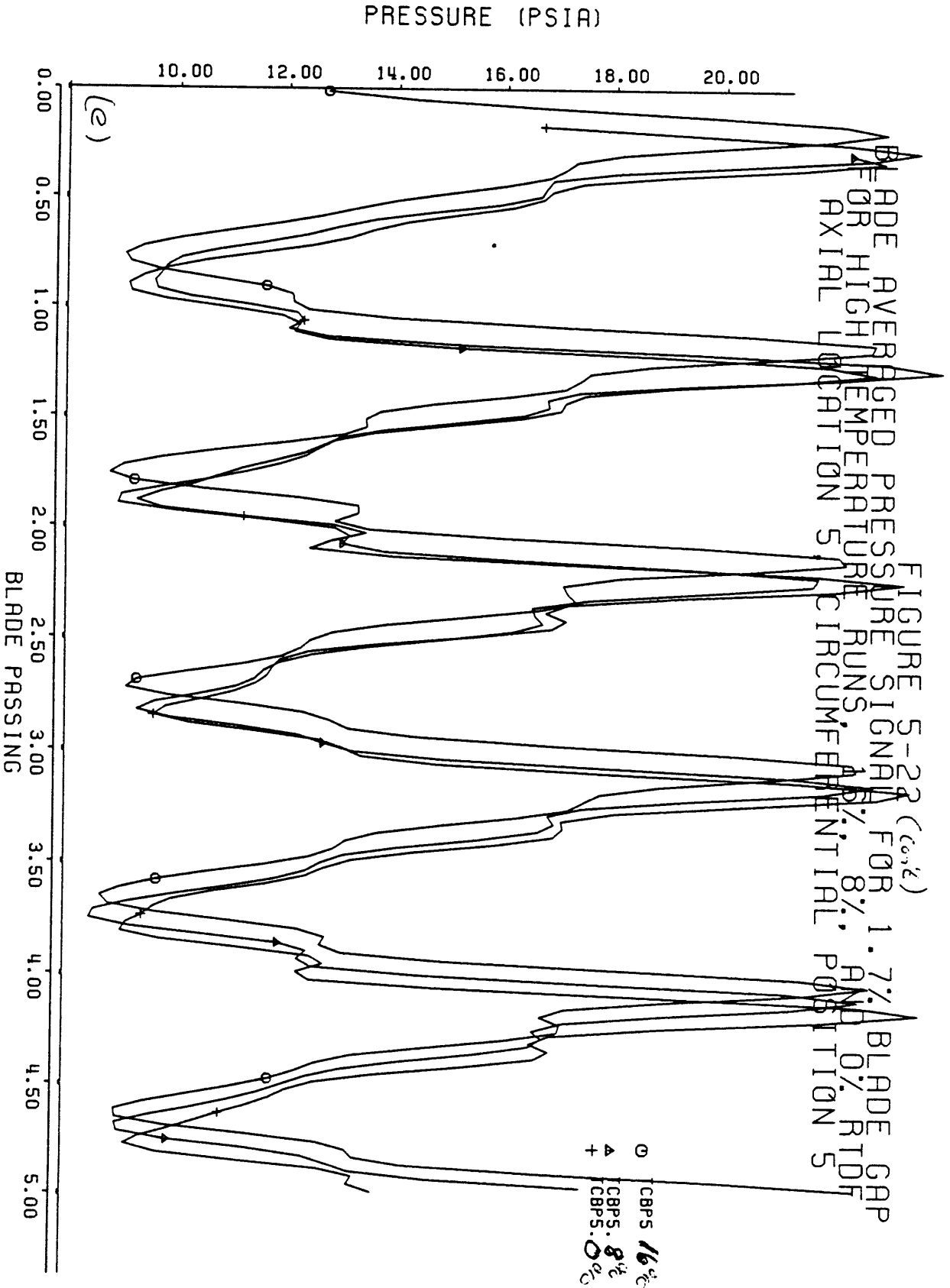
Figure 5-23

Time Averaged Pressure Data for High Temperature Tests 120, 121, and 126
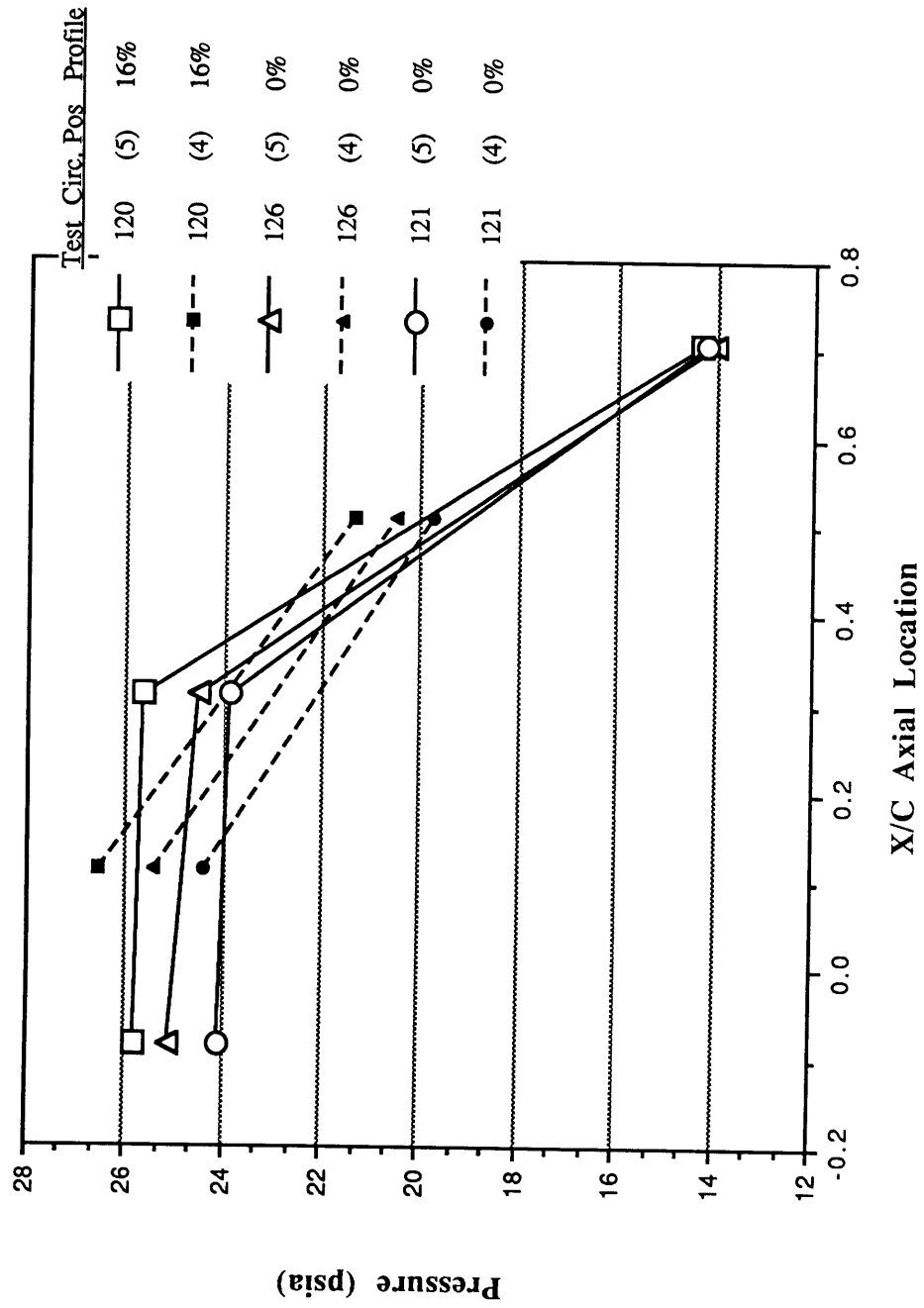
Chapter 6 Conclusions and Future Work

6.1 Conclusions

The data presented poise interesting questions which remain to be answered. In summary the data presented showed the following items:

* There was no variation in heat flux between the different blade gaps of 1.7% span and 2.5 % span for either the time averaged or the time resolved flows. This could be a function of the blade gap which was twice its design value of .8%.

* Circumferential variation exists and varies with both axial position and inlet conditions; existing as both a time-averaged and time-resolved phenomenon. This variation seems to be loosely coupled with the profile, which decreases as the profile decreases and increases towards the trailing edge of the tip casing. Variations of up to 50% have been observed, but the median variation is approximately 20%. This leads credence to the belief that the nozzle guide vane endwall flows may interact with the rotor endwall flow.

* In general the heat flux decayed with axial distance from the leading edge by approximately a factor of five to one (small difference existed for the different circumferential measuring locations), and the Nusselt number (based on NGV inlet tip temperature) decayed by a factor of approximately four to one for the high temperature tests and six to one for the low temperature tests.

* Not enough data points were available to draw concrete conclusions about the behavior of the uniform flow runs which only varied due to driving temperature ratio differences. However they seemed to move towards one one curve shape.

* Variations which existed in heat flux between runs at different average temperatures and different radial profiles seemed to collapse to one curve for each circumferential measuring station, when calculating the Nusselt number using the inlet temperature at the rake was used as the non-dimensionalizing reference temperature. While this number is not an exact representation of the tip temperature entering the rotor it represents a closer approximation than the average temperature which did not collapse the curves.

This is implies that any variation in tip shroud Nusselt number can be accounted for by normalizing out the driving temperature difference $(T_{ref}-T_{wall})$ used in calculating the heat transfer coefficient, h.

* The pressure data obtained shows influences of the blade gap differences in its measurements, but more work has to be done to verify the proper working condition of the different pressure transducers.

The end result is that the changes in flow patterns in the rotor endwall which were

anticipated due to the secondary flow generated by the radial temperature profiles were not measured. Leaving the reason for tip shroud degradation which occurs at the trailing edge of the tip shroud in some jet engines unresolved.

6.2 Future Work

Two separate items will be discussed in this section: future analysis which can be done with the present data and possible modifications to the experimental set-up which could be of benefit when running a similar experiment in the future.

6.2.1 Data Analysis

Basically, all the data reduction to this point has been at the level of the blade passage. How did one blade passage vary from another, how did they vary axially were all questions which were asked. The next level of analysis would be to break down where the AC heat flux occurs on the blade, what is the relationship between the heat flux and the pressure. This type of analysis would require more accurate timing information to accurately match the different signals and would require the data from the pressure transducer to be sorted out and verified. However it could yield interesting results. It may be that the Nusselt number (normalized by the appropriate driving temperature) over the blade is constant with axial position and that what really matters is the relative thickness of the blade. Another analytical technique would be to try to estimate the total temperature as a function of axial distance down the turbine stage. This could provide a better driving temperature difference. It would be useful to compare computer codes which estimate the pressure distribution across blade tips with the measured pressures if that data is ever recoverable.

Another option, requiring less work, is to concentrate on the uniform flow runs and to try to find the appropriate length scales which account for the different geometric variables. Since these runs do not have radial temperature profiles, the free stream temperature in the endwall region can be estimated from assuming a linear temperature drop across the turbine stage. This provides the opportunity to compare different axial locations. This could yield answers to interesting questions, such as "Does the heat transfer coefficient change axially?" and "Can one collapse the traditional curve developed by the tip temperature based Nusselt number to a line, given the right local length scale?" It would also be easy to obtain an estimate of the effect on blade width on the local heat transfer.

6.2.2 Experimental Apparatus

The following section will be of primary interest to people who plan to modify this experiment using the MIT blowdown facility. There are five areas in which specific actions can be recommended.

1)   Tip Casing Construction

The RTD's which were placed on the outside of the shroud might have been exposed to some gases. The time traces of the RTD's show definite position variations which seem to be independent of the RTD. Thus if RTD's are to be used it might be better to drill holes for them partially through the tip shroud from the back side (similar to the pressure transducer holes). This would insure that their measurements are true metal temperatures and not some combination of metal temperature and moving air. When positioning instrumentation, it would be worthwhile to have duplicate measuring locations offset by one nozzle guide vane to determine what the variation is between nozzle guide vane passages. If another tip casing experiment is performed it would be useful to increase the spatial resolution of the heat flux sensors which would serve the dual role of providing more detailed information and would provide back-up for individual gauge failure.

2) The Facility

The only real problem which was encountered during this experiment was the interconnection of the amplifier gains and biases with the instrumentation scales and zeros. It would be worthwhile to devise a system of calibrating each amplifier's gain and biases before each test, in this way if problems do occur and amplifiers have to be changed, the ability to back out the instrumentations physical calibration constants would be possible. It might also be useful to run a temperature bath calibration on the tip shroud before every test.

3) The Profile Generator

Besides "pickling" the insides of the generator with whatever method is deemed best (steam cleaning or a solvent bath), which is a requirement before the generator is used again, the best addition to the profile generator would be the addition of secondary heat exchangers which could help control the temperature and flow to each of the jackets independently. This could be accomplished by exchanging heat from either oil or water to a working secondary medium which actually flows through the RTDFG. An example of the layout is shown in Fig 6-1

Figure 6-1
Potential Reconfiguration of Cooling System for RTDFG

Inner Jacket
(T) outlet
(T)

Outer Jacket
outlet

RTDFG

Outer Jacket
inlet

Inner Jacket
(T) inlet
(T)

(T)

(T)

Secondary oil
reserves. Should
be mounted higher
than rest of system
to ensure gravity
feed.

⊕ Valve

(T) Themocouple

(T) out
(T) City water
(T) in

(T) Oil from
(T) supply tank
out

Secondary Heat Exchangers
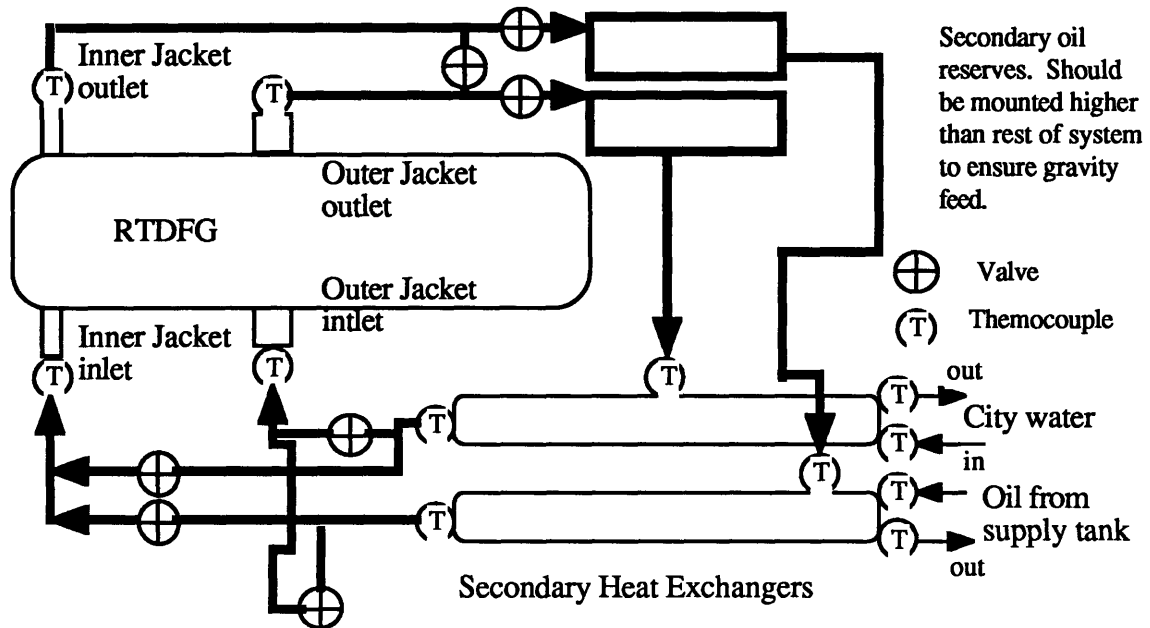
This type of design has many advantages. It provides a way to estimate the heat flux to the cooling jackets through the temperature change of the oil. In addition, this set-up allows both the inlet and outlet flows to be completely separated. In most cases, one would be trying to keep the jacket temperatures at the same temperature, thus the fluid temperatures in the jackets should only vary by the differences imposed by the different thermal conduction rates. This new configuration could allow the creation of a linear profile across the RTDFG to investigate secondary flow creation.

Bibliography

Booth, T.C. "Tip Clearance Effects in Axial Turbomachines: Importance of Tip Clearance Flows in Turbine Design" Presented at "The Von Karmin Institute for Fluid Dynamics Lecture Series: 1985-05" on April 15-19, 1985.

Butler, T.L. and O.P. Sharma "Redistribution of an Inlet Temperature Distortion in an Axial Flow Turbine Stage" AAIA-86-1468

Cattafesta, Lou "An Experimental Investigation of the Effects of Inlet Radial Temperature Profiles on the Aerodynamic Performance of a Transonic Turbine Stage"; Master's Thesis, Aeronautical and Astronautical Engineering Department, MIT, August 1988

Cook, R.O. and C. W. Hamm "Fiber Optic Lever Displacement Transducer"; Applied Optics, Vol. 18, No. 19, 1 October 1979

Cox, G.B; A.R. Tiller and J. LeTourneau "Pattern Factor Improvement in the F-100 Primary Combustion System" Journal of Engineering for Power, Transactions of the ASME 81-GT-25, March, 1980

Dils, R.R. "Use of Thermocouples for Gas Temperature Measurements in Gas Turbine Combustors" National Bureau of Standards no 561: Proceedings of the 10th Materials Research Symposium on Characterization High Temperature Vapors and Gases. October 1979

Epstein, Alan; Gerald Guenette and Rob Norton "The Design of the MIT Blowdown Turbine Facility"; Gas Turbine Lab Report no. 183, April 1985

Epstein, A; G. Guenette; R. Norton, and C. Yuzhang "High Frequency Response Heat Flux Gauge" in Review of Scientific Instruments: Vol. 57, No. 4, April 1986

Guenette, Gerald "A Fully Scaled Short Duration Turbine Experiment" MIT PhD. Thesis, Aeronautical and Astronautical Engineering Department, Aug 26, 1985

*Kaiser, J.F. and W.A. Red, Review of Scientific Instruments, 48, 1447 (1977) and 49, 1103 (1978)

Moffat, R.J. "Contributions to the Theory of Single Sample Uncertainty Analysis" in Journals of Fluids Engineering; Vol. 104, June 1982

*Oldfield, M.L.G.; H.J. Burd; and N.G. Doe "Design of Wide-Bandwidth Analogue Circuits for Heat Transfer Instrumentation in Transient Tunnels," Heat and Mass Transfer in Rotating Machinery, papers from the 16th Symposium at the International Center for Heat and Mass Transfer, Dubrovnik, Sept. 1982, Hemisphere Publ. Corp. N.Y.

Sabe, R.G.; W. Whitney, and T Mofitt, "Performance of a High-Work Low Aspect Ratio Turbine Test with Realistic Inlet Radial Temperature Profile" AAIA-84-1161

* These two references are from computer programs that have been used extensively and are considered quite valid. I am including them for anyone who wishes to trace them back to their source or analyze their algorithms in depth.

Appendix I

Temperature Profile Generator Drawings
Figures 1-4
(All Dimensions in Inches)

Figure 1: Main Cross-sectional View (facing downstream) of Generator

This diagram shows the locations of the other views given in figures 2, 3,and 4. It is also the easiest one to see the cooling water flow path. Cooling water for both jackets enters at the bottom (they could enter from the other side, but in our case they are connected to the bottom). for the outer jacket the water immediately enters a plenum at the bottom of a diagram and is forced to flow up both sides of the jacket to the top where it exits. The inner cooling water enters through a pipe in the strut (210 ° from TDC) on the downstream side of the RTDFG and flows into a cylindrical tank with a dividing wall in it. There is a one inch opening into a plenum at the bottom of the RTDFG where the water enters. It is forced through the jacket until it flows out of the upper plenunm,and into the other half of the cylindrical tank were it exits through the strut/pipe combination at 330 ° from TDC

Figure 2: Expanded View of Cooling Jackets (View A-A)

This view gives position of the bolt holes, struts as well as some of the dimensions for the cooling jackets.

Note A: These black dots are the mixing lobes. They are spaced around the cooling jacket to both provide support for the outer wall of the jacket and to stir up the flow inside.

Figure 3 and 4: View B-B is Lower Axial Cross-Section of RTDFG. View C-C is Sectional through Struts.

These drawings give more detailed measurements of the RTDFG.

Note A: These spacers were originally designed to line up the different matrices. However because of the one continuous piece of matrix used for the wire, these may either be shorter that tney are in the drawings or not there at all. No one was sure if they were put in or not and it was not an important issue at the time and presently there is no way to check.

Note B: The struts were originally made to fit with the alignment struts all ready present in the turbine facility . Upon arrival, the down stream struts had to be ground down by several tenths of an inch in order to get the struts to fit . Thus the cross-sections seen here may not be fully accurate.

Figure 5 Heater Matrix

This drawing shows the two different parts of the heater matrix. The smaller cross-sectional passageways are for heating the air, while the large one is for the heater wire. There are approximately 21 rows on either side of the center wire matrix.

Notes on Construction:

Looking at the main drawings, one probably notices three items which are not readily explainable. First, the RTDFG is broken into three sections. The metal supports which go from the outer wall to the center annulus are there to position the center annulus and support it. These posts also have matching faces to be used for alignment between the test section and the fast acting valve. Also by breaking the RTDFG into three sections the possibility of experimenting with circumferential temperature non-uniformities also exists. The second problem is the spacing in the matrix. One will note that the main heating matrix is broken into four sections with a gap between them while the section that the heater wire passes through is bigger and continuous. Kentucky Metals could not wrap the small matrix twenty inches long and if we put the matrices adjacent to each other then there may be an extraordinary pressure loss every time the flow enters a new section. The answer was to put a gap between the sections, but that would have exposed the heater wire to high power densities in that open area, possibly leading to burn out. Since the matrix for the heater wire had to be larger (to accommodate the wire) it had to be made a continuous piece and span the entire length of the RTDFG. The third point of interest is the pipe leading from the center section to atmosphere. This was designed as a relief pipe in case the water jacket leaked and water vapor built up inside the RTDFG. In actuality, the rubber seal between the inner section (normally at atmosphere) and the test annulus (at vaccum) could not support the pressure differential (probably due to the bad alignment of the parts) and had a tendency to pop open and cause a vaccum leak, necessitating the break down of the whole facility to get to it. As a result we hooked this pipe up to the vaccum system to keep both sides of the seal at the same relative pressure.
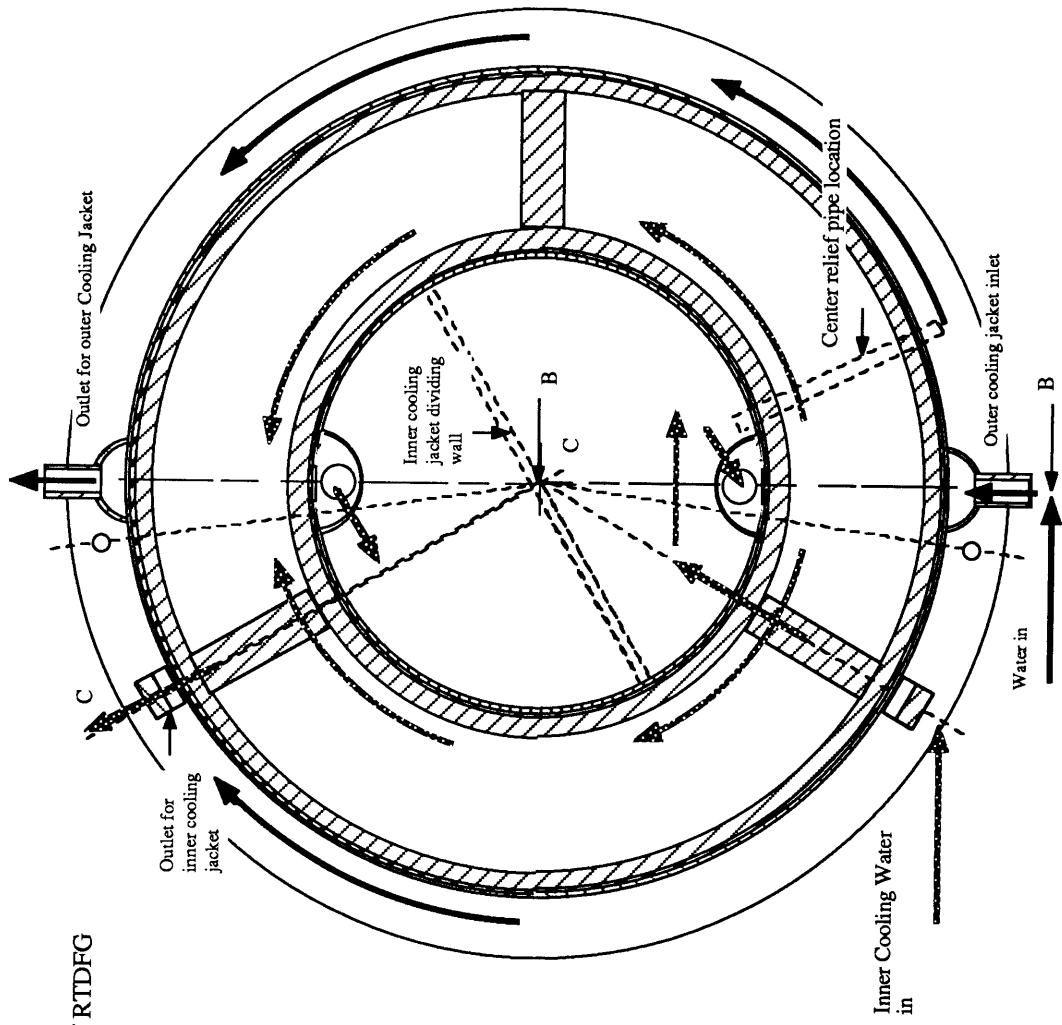
Figure 1
Main View of RTDFG

Labels within figure:

- Outlet for outer Cooling Jacket
- Center relief pipe location
- Outer cooling jacket inlet
- Inner cooling jacket dividing wall
- B
- C
- B
- Water in
- C
- Outlet for inner cooling jacket
- Inner Cooling Water in

Figure 2

**Expanded View
of Cooling Jackets**

Center

Seperating wall for inlet
and outlet of inner cooling jacket

A

3 Struts 120 deg apart

24 holes 5 deg apart

VIEW A-A
Blowup of Cooling Jackets 2 to 1 scale
.125 Typ .094 Typ See Note A

Inner Jacket Plenun

1"
D

Outer Jacket plenum

2" pipe

1.0

Figure 3

View B-B   Bottom Half of RTDFG (Cross-section)

Figure 4

Cross-section of struts

View C-C (Top Half of RTDFG, Cross-section)

View D-D
See Note B

Cross-Section of
Down-Stream Strut

Cross-section
Upstream Strut

Spacers .5"
See Note A

5.0"
Heater Matrix

Interior Cavity
Heater Wire Passage

Inner Cooling
Jacket outlet

Upstram
Strut

1.5

1.25

177
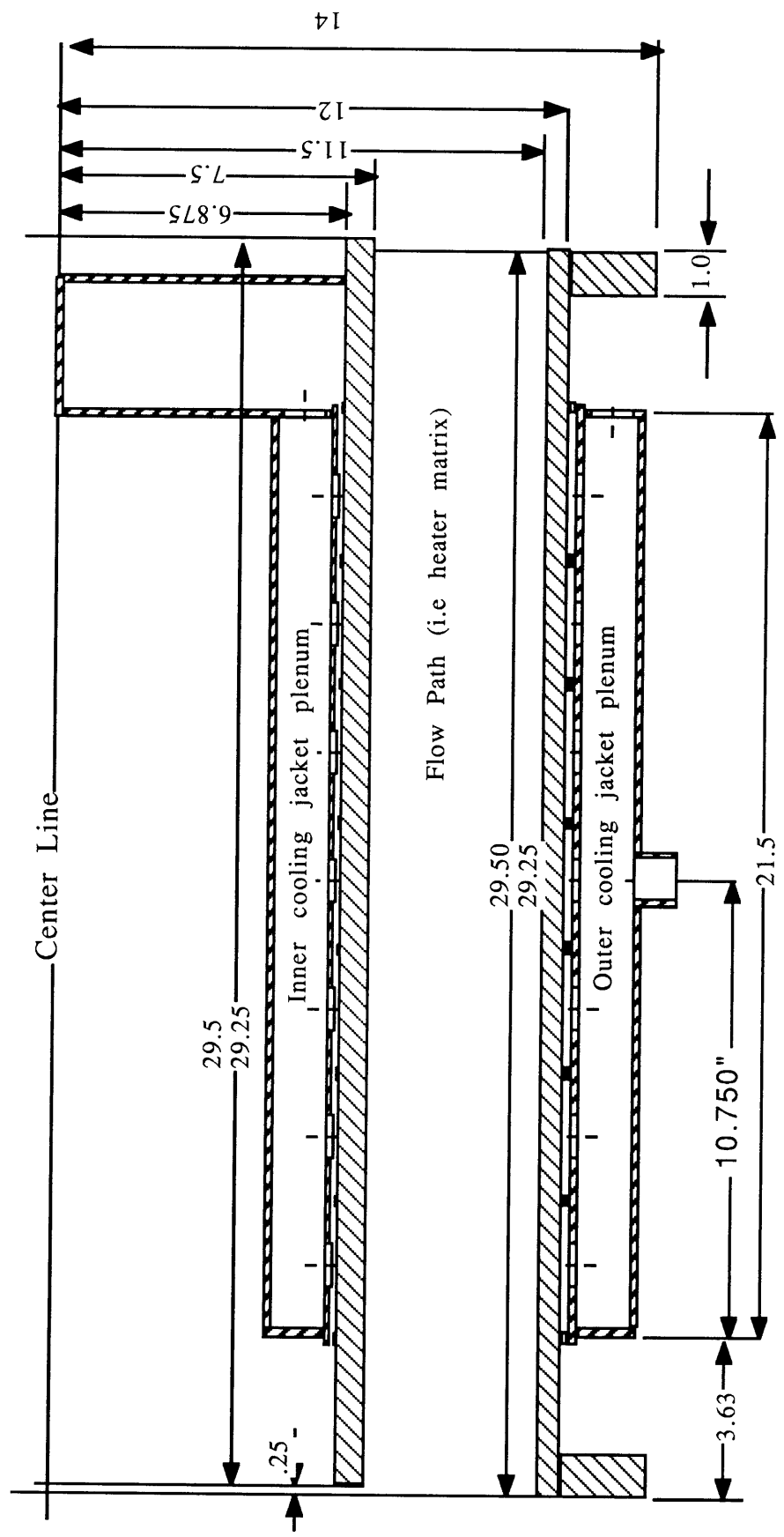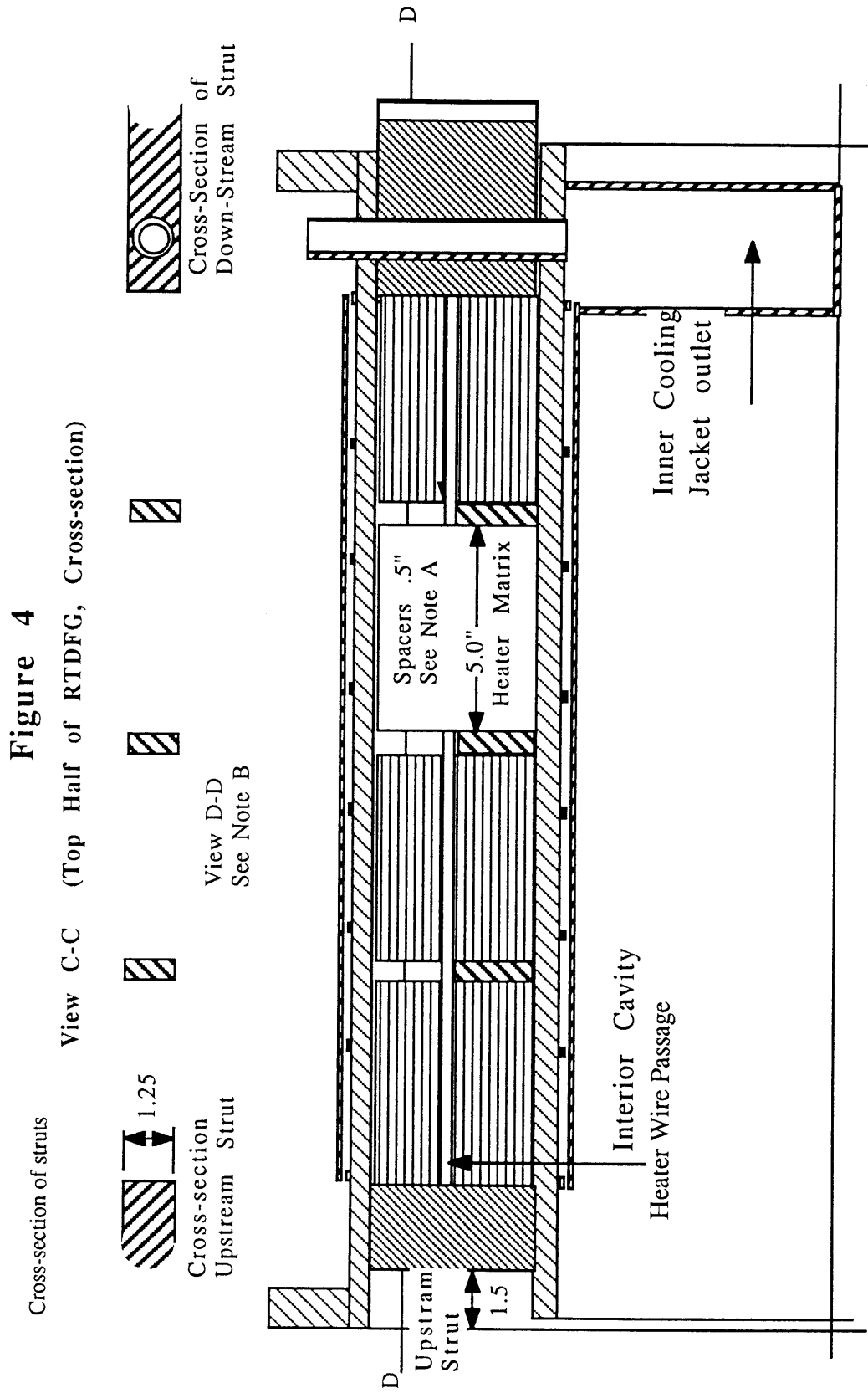
Figure 5 Heater Matrix (All dimensions in inches, Material: Stainless Steel)

scale .10 to 1

Approx. 43 layers total in matrix. Manufactured by wrapping alternate layers bent and straight pieces and brazing all at once

Center Matrix for Heater Wire (This one layer is continous along the length of the heat exchanger)

.01

.125

.01

.01

.250
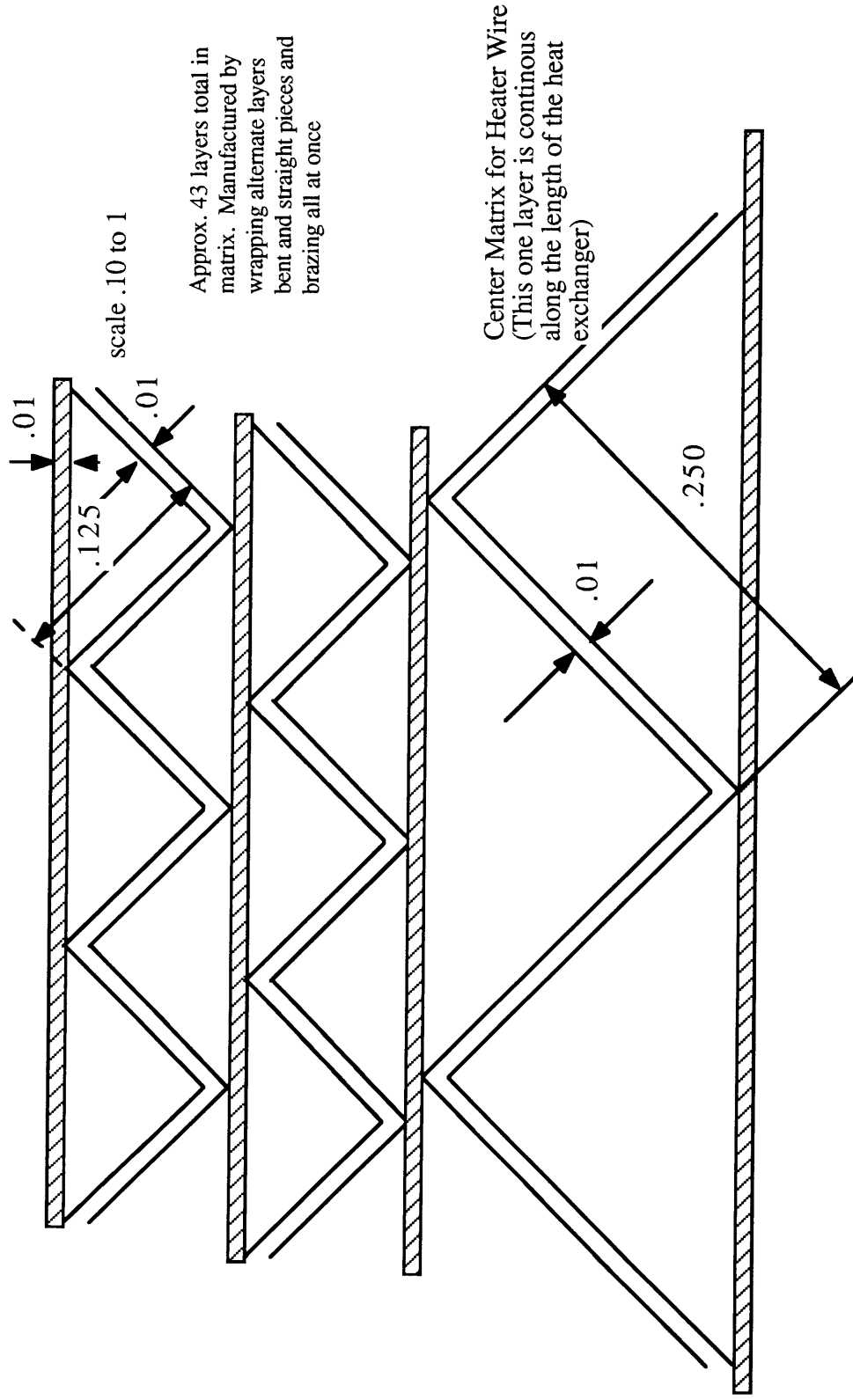
Appendix II

Instrumented Tip Shroud Drawings
Figures 1-4
(all Dimensions in Inches)

Figure 1: Instrument Location

This figure shows the location of every instrument on the shroud. The pressure transducer numbers correspond to the following Kulite numbers (for reference):

1~201   2~223   3~202   4~194   5~229   6~203   7~219

This drawing is not an actual machine drawing and leaves out some dimensions which have no importance to the actual instrumentation. The casing is designed to be rotated about the two center pins giving two different sets of measurements. In other words either gauges 41 and 51 will be facing upstream or gauges 57 and 47 will be.

Figure 2: Tip Casing components

For completeness this drawing which shows the various "accessories" which go with the tip casing are drawn here only because they show up in the assembly drawing. Other mounting hardware, such as the window and the window plate are not shown.

Figure 3: Tip Casing Assembly

This drawing shows how the various parts are put together. The wires go to the Bendix connectors which have an O-ring seal which mounts against the window. The force and congestion of the wires hold the connector plate up. The alignment pins can be machined down to accommodate any slack that might be needed when the casing is reversed.

Figure 4: Tip Casing Instrument Locations with Respect to NGV's

This figure shows the relationship between the gauge positions and the NGV's trailing edge.

Figure 1 Instrument Location

(Bottom View)

Placement of Instrumentation
and Key Dimensions (Scale 2:1)

Pressure Transducer holes

Feed-thru holes

Fifty Series Guage
Center Line

Pressure transducer
center lines

Two Center Pins
used for rotation
of Tip Casing

Rotation
Center
Line

Four holes
3/32 OD drilled
thru for RTD
leads

Instrument
Placement
Grid

Forty series Guage
Center Line

Mounting Platform
for covers

Note: Appearence of Mounting platform
for Covers changed during Machining

RTD 3

RTD 2

RTD 1

2.1625

.945

.4725

.4725

.2363

.4725

.1

.2

.2

.2

.2

.2

.2

.100

.100

.1006

.1

Figure 2: General Assembly of Tip Casing Components

View A Cover Assembly

R1 is Tip-casing radius=.25R

R2 is cover radius =.265 R

Eco Bond 104

Vector Board

Feed-thru pins

R1

R2

Tip Caseing Allignment pins

2 Bendix 20-41 male connectors with O-Ring

1.8

.687 R

.687 R

1.575

.15

.461

.2

21.7 D

View A
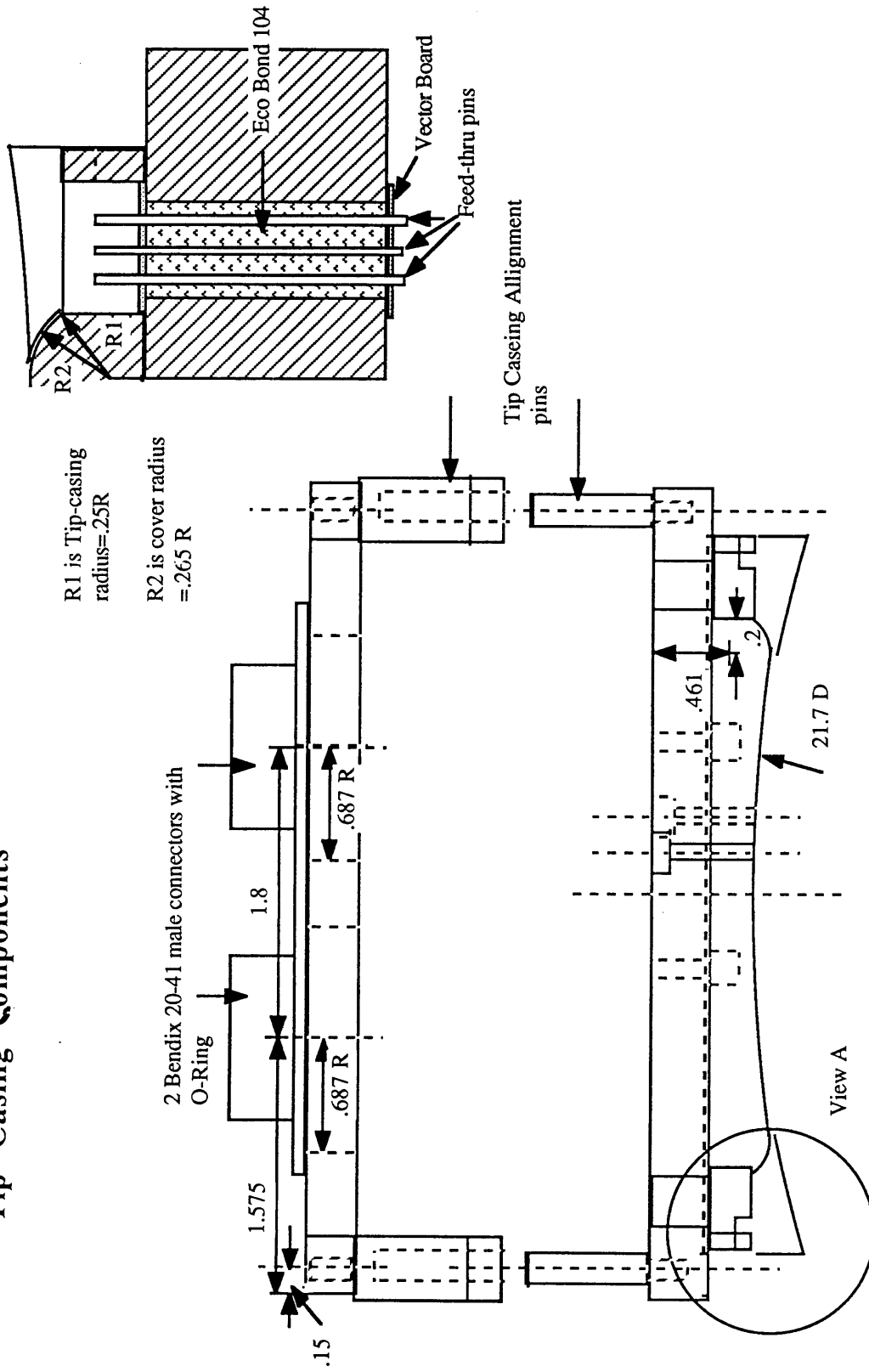
Figure 3 Tip Casing Componen

Tapped
for 8-32

Tapped for 8-32

Alignment Pins (Shown twice scale)
machined to provide clearence

2 Holes .25 deep
Drilled and Tapped
for 8-32

8 Holes drilled through plate and tapped
into bendix connectors for 2-64 screws.
Position: .937 R and .7 from center line

Bendix 20-41 male Connector with
O-Ring

O-Ring Groove

.95 R

.67 Nominal
R

.937 R

.687 R

.687 R
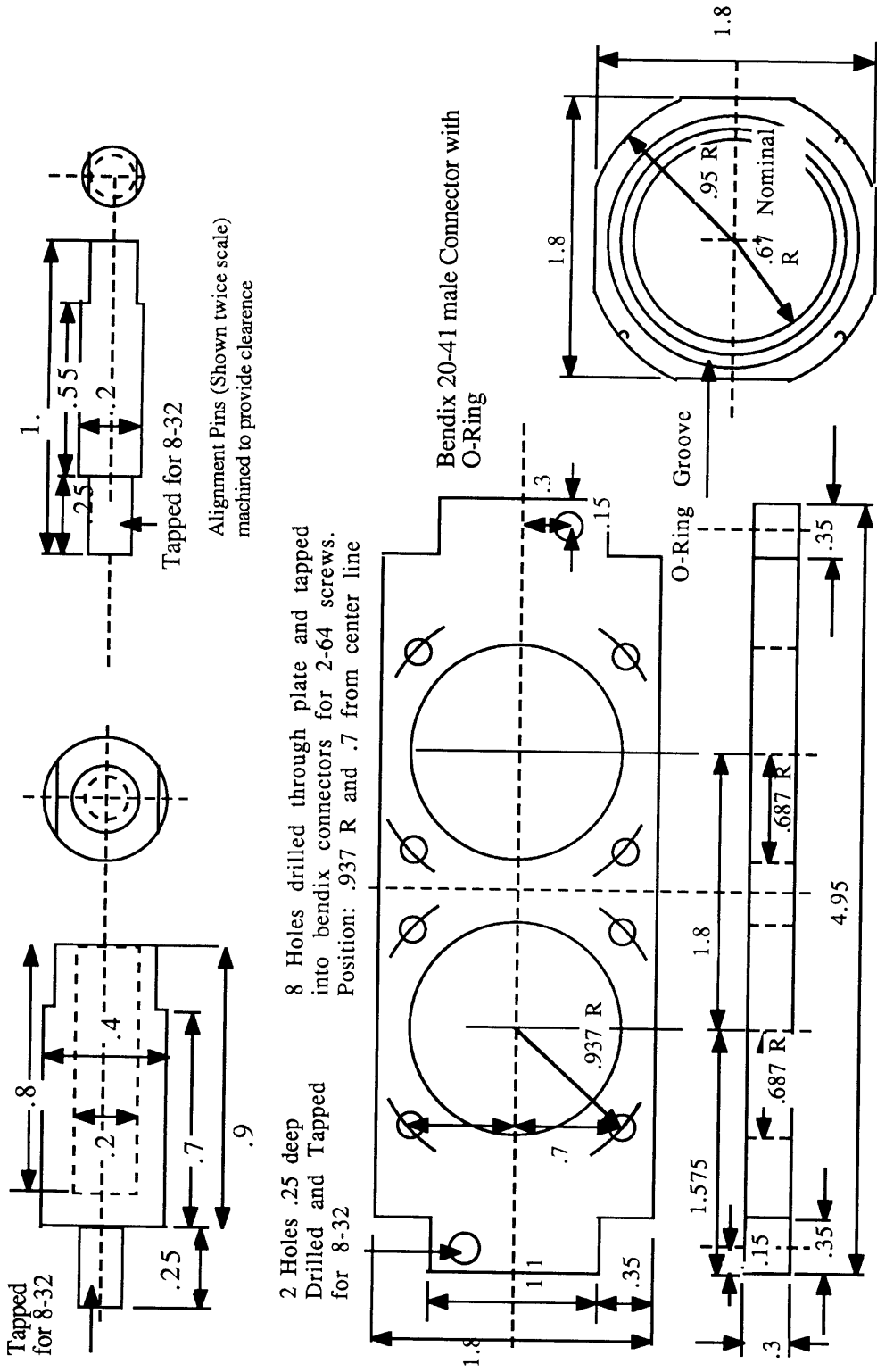
Figure 4
Instrumentation Location With Respect To Nozzle Guide Vanes
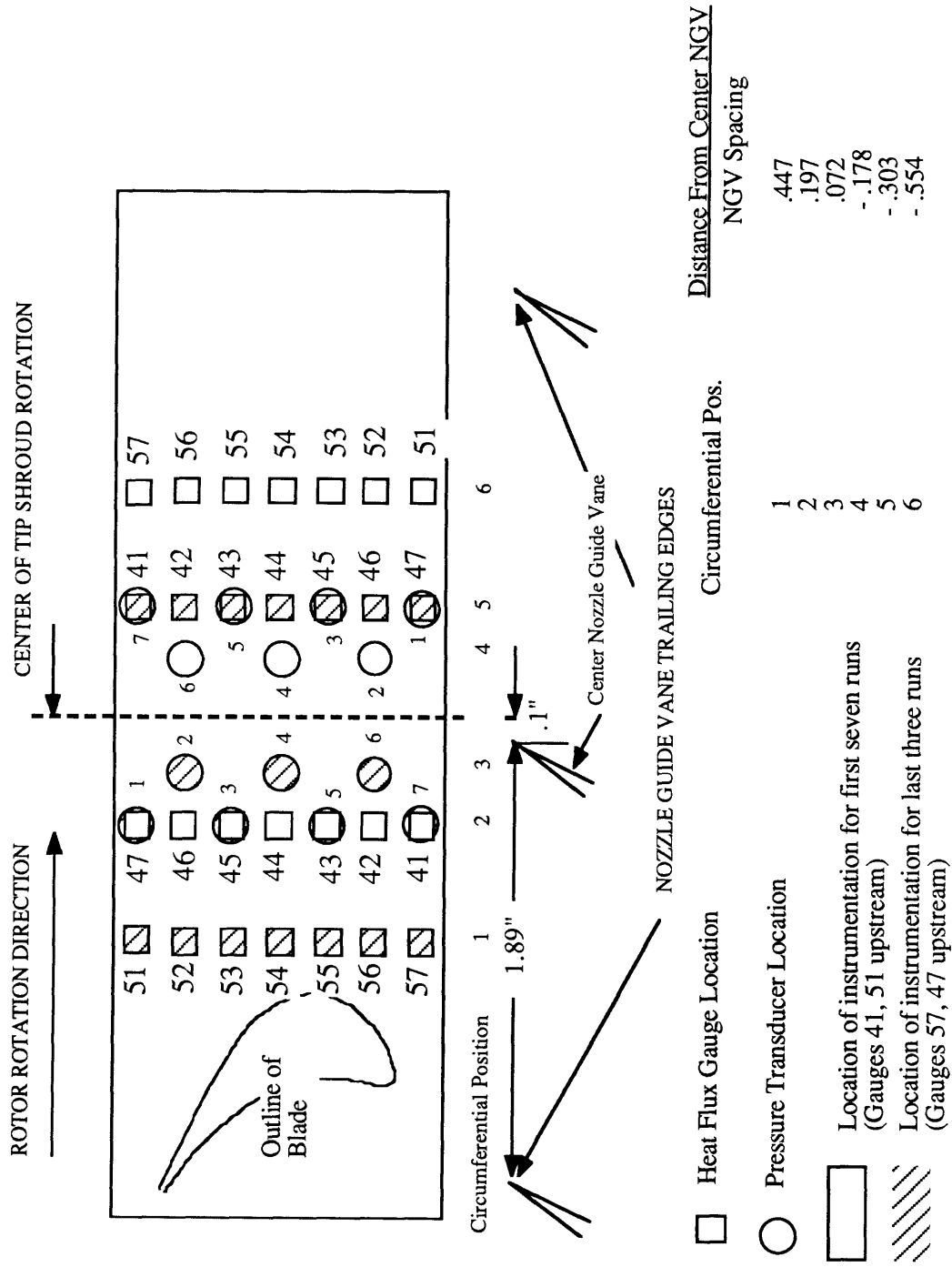
Appendix III

Characterization of Temperature Profile Generator Performance

Definitions used in figures 1-4

Figure 1: Run Conditions and Test Variances

TT2 Avg= Average Total Temperature of the gas leaving the matrix as measured by the upstream total temperature rake. The temperature rakes are designed so that each probe measures equal areas of the flow. Since there are five sensors on the upstream total temperature rake, each sensor measures 20% of the flow. Thus numerical averaging of the five sensors gives an area averaged measurement, which because of the relatively constant total pressure measurement (see table 2) is extremely similar to a mass- averaged measurement.

Figures 2-5 to 2-8 show the axial locations of the measuring ports as well as the radial locations of the sensors on the three probes used, upstream total temperature, upstream total pressure, and downstream total pressure.

RTDF= In this particular diagram, RTDF stands for an area averaged definition of T_{mean} based on the measured profile. Equation 1 on pg. 4 describes the parameter called the RTDF. But like many other non-dimensional fluid parameters, the actual number obtained depends on how one defines T_{mean}, T_{max}, T_{min}, and ultimately T_{ref}. Now in this case T_{ref} is not being debated, but the Rolls- Royce definition of T_{mean} might be improved upon for our situation. Since the inlet is an annulus, doing an area average of the temperature may yield a different mean temperature than the Rolls-Royce definition. There is also a problem in defining what the maximum and minimum temperatures are. Does one define the max and min to be what is actually measured, or does one fit a curve to the data and extrapolate. Since there is no clear answer to any of these questions, table 9 uses all three definitions. But in this case T_{mean} is based on an area average of the measured profile (not a fitted one)

Corr. Spd = Corrected speed which is the tip speed/square root of the ratio of the temperature to a reference temperature)

Speed = Tip Speed in Revolutions per Second

Fract. Spd = Fractional speed or Speed/Design Speed

PT2 = Area Averaged (i.e. average of the sensors) of the total pressure behind the RTDFG

PT5 = Area Averaged (i.e. average of the sensors) of the total pressure behind the rotor

Press. Ratio = PT2/PT5. This parameter along with the corrected speed should put us in one specific area of the turbine map, if one new the map. If these properties are held constant between the runs, then the turbine will always be operating with the same efficiency.

Avg = Average values for 375-400 ms

Test S = Values for start of test time 200-225 ms.

Test F = Values at end of test time 450-475 ms

Notice the average test times are not in the middle of total available test time. The averages are placed here for the simple reason that many other parameters which this data may also be compared to is typically evaluated in the range of 375-400 ms.

$\Delta\%$= (Test Final values-Test Start Values)*200/(Test Final values-Test Start values). this implies that the total variation from Start to Finish is twice what is recorded. This works fine since we are generally measuring around some average value which we take to be the actual run conditions. The only place where this measurement does not work well is with the low RTDF runs, where the values are small to begin with.

Table 2: Pressure Drop Across the Profile Generator (All Pressures in Atm.)

This table shows two things, the actual pressure drop and variation over time across the RTDFG, and the relative uniformity of the total pressure behind the RTDFG

PTOA= Total Pressure measurement in the supply tank

PT2ARx = name of sensor (radial locations are shown at the bottom of the table as well as in figure 2-7. The GTL system for naming its probes is shown here. PT-Total Pressure, 2 -axial location, A is Window or section that it is in. Thus this probe was positioned upstream of the optical lever window.

mean= Average of pressure measurements

S. Dev. = standard deviation of measurements from mean value

Press. Drop = pressure drop across the RTDFG

Dyn Hd= Dynamic head upstream of the RTDFG ($\rho_0 V^2$)
Delp/Hd= Pressure drop/ dynamic head
In Legend
        Avg Loss=Average Delp/Hd for all runs
        Max Variation= maximum variation of above number
        %= this variation represented as a percent of total loss.

Table 3: Variation in Rake Temperatures
(Temperatures given in degrees Kelvin)

This table basically shows how the individual rake sensors vary over the test time.

Rake location refers to the distance (in inches) the sensors are from the center of the annulus.

Goal Temp = test condition desired

ΔT= temperature at 475 ms - temp. at 225 ms

Mean = Average temperature

RTDF(1)= An RTDF based on a profile fitted to the data and using a Rolls-Royce definition of T_{mean}.

RTDF(2)= An RTDF based again on a profile fitted to the data, but using an area averaged definition for T_{mean}.

RTDF(3)= an RTDF based on the measured profile (thus smaller since there are no accurate measurements of the wall gas temperature) and an area based T_{mean}

The only place where RTDF(1) and (2) are not used is when working with a no RTDF run. In that case one would be trying to fit a parabola to something which does not really have that shape.

Table 4: Variation from Matrix Temperatures to Upstream Temperature Rake (Temperatures in Deg K)

This table basically shows how the individual rake sensors vary over the test time.

Rake location refers to the distance (in inches) the sensors are from the center of the annulus.

Goal Temp = test condition desired

Matrix Firing Temperatures = firing temperatures of the matrix thermocouples fitted to a parabola and extrapolated to the same radial locations at the temperature rake.

375-400 ms = temperatures of rakes at 375-400 ms (avg)

Eff.= Temperature of rake/Temperature (predicted) at matrix

Mean= Average of all temperature sensors (same as area averaging)

RDTF definitions as defined in previous table.

Table 1 Run Conditions and Test Variances

	Test120				Test 121				Test 122			
	Avg	Test S	Test F	Δ%	Avg	Test S	Test F	Δ%	Avg	Test S	Test F	Δ%
TT2 Avg	462.36	463.27	472.31	1.93	459.38	459.6	469.24	2.08	396.18	397.05	401.4	1.09
RTDF*	17.2	16.	17.1	6.65	.1	.3	.1	-100.00	12.6	11.5	12.5	8.33
Corr. Spd	1.4781	1.4909	1.475	-1.07	1.471	1.4985	1.4643	-2.31	1.4551	1.4575	1.4553	-0.15
Speed	122.466	122.54	122.331	-0.17	121.658	122.14	121.257	-0.73	111.826	111.489	111.871	0.34
Fract. Spd.	1.1983	1.2087	1.1959	-1.06	1.1926	1.2076	1.1872	-1.70	1.1797	1.1816	1.1799	-0.14
PT2	3.710	3.897	3.635	-6.968	3.529	3.791	3.422	-10.232	3.702	3.887	3.626	-6.94
PT5	0.885	0.902	0.888	-1.553	0.825	0.865	0.818	-5.600	0.881	0.902	0.881	-2.27
Press. Ratio	4.191	4.321	4.093	-5.416	4.279	4.385	4.186	-4.638	4.202	4.312	4.115	-4.68
	375-400	200-225	450-475	ms	375-400	200-225	450-475	ms	375-400	200-225	450-475	ms

	Test124				Test125				Test 126			
	Avg	Test S	Test F	Δ%	Avg	Test S	Test F	Δ%	Avg	Test S	Test F	Δ%
TT2 Avg	398.86	399.28	404.39	1.27	391.53	392.12	395.89	0.96	451.41	451.67	460.69	1.98
RTDF*	0.0	0.1	0.0	-200.0	6.7	6.2	6.7	7.8	8.5	8.2	9.1	10.40
Corr. Spd	1.47	1.47	1.47	0.38	1.49	1.48	1.49	0.61	1.52	1.52	1.52	-195.14
Speed	113.58	112.57	113.68	0.98	113.67	112.64	113.84	1.06	124.60	123.58	124.63	195.18
Fract. Spd.	1.19	1.18	1.19	0.99	1.21	1.20	1.21	0.61	1.23	1.23	1.23	-0.07
PT2	3.562	3.809	3.464	-9.481	3.639	3.850	3.551	-8.080	3.604	3.840	3.510	-8.99
PT5	0.854	0.883	0.838	-5.184	0.895	0.895	0.891	-0.370	0.879	0.889	0.876	-1.48
Press. Ratio	4.169	4.315	4.133	-4.303	4.068	4.304	3.985	-7.711	4.100	4.319	4.006	-7.51
	375-400	200-225	450-475	ms	375-400	200-225	450-475	ms	375-400	200-225	450-475	ms

	Test 127				Test 130				Test131			
	Avg	Test S	Test F	Δ%	Avg	Test S	Test F	Δ%	Avg	Test S	Test F	Δ%
TT2 Avg	459.09	459.80	468.26	1.82	462.50	462.77	472.68	2.12	459.87	461.04	469.21	1.76
RTDF*	7.4	6.7	7.3	8.6	0.5	0.7	0.4	-54.5	17.1	15.7	17.1	8.54
Corr. Spd	1.51	1.51	1.52	0.13	1.52	1.51	1.52	0.54	1.51	1.51	1.51	0.44
Speed	125.14	124.11	125.34	0.98	125.83	124.18	126.10	1.53	124.79	123.57	125.14	1.26
Fract. Spd.	1.23	1.23	1.23	0.13	1.23	1.22	1.23	0.53	1.22	1.22	1.23	0.45
PT2	3.599	3.831	3.506	-8.859	3.492	3.758	3.388	-10.364	3.734	3.910	3.661	-6.58
PT5	0.853	0.883	0.852	-3.631	0.825	0.859	0.817	-4.940	0.886	0.907	0.889	-2.07
Press. Ratio	4.218	4.338	4.116	-5.232	4.233	4.376	4.144	-5.431	4.213	4.309	4.119	-4.51
	375-400	200-225	450-475	ms	375-400	200-225	450-475	ms	375-400	200-225	450-475	ms

Table 2
Pressure Drop Across Profile Generator

Legend (boxed):

All Pressures in Atm Rake Location	" from Center
PT2AR	10.73
PT2AR	10.27
PT2AR	9.78
PT2AR	9.27
PT2AR	8.72
PT2AR	8.13
Avg Loss Delp/Hd	10.9
Max Var	.66
%	6.06

TURB120

	375-400 ms	200-225 ms	450-475 ms
PT0A	4.0406	4.2462	3.9546
PT2AR1	3.7426	3.9344	3.6652
PT2AR2	3.7279	3.9176	3.6513
PT2AR3	3.7288	3.9175	3.6523
PT2AR4	3.6793	3.8617	3.6051
PT2AR5	3.6796	3.8618	3.6056
PT2AR6	3.7034	3.889	3.6278
mean	3.7103	3.897	3.6346
S. Dev.	.027	.031	.0256
Press. Drp	.3303	.3492	.3201
Dyyn Hd		.0323	
DelP/Hd		10.8111	

TURB121

	375-400 ms	200-225 ms	450-475 ms
PT0A	3.8457	4.1411	3.7211
PT2AR1	3.5571	3.8245	3.4476
PT2AR2	3.5439	3.8083	3.4356
PT2AR3	3.5455	3.809	3.4372
PT2AR4	3.5029	3.7587	3.3978
PT2AR5	3.5038	3.7597	3.3987
PT2AR6	3.5221	3.7829	3.4152
mean	3.5292	3.7905	3.422
S. Dev.	.023	.0277	.0212
Press. Drp	.3165	.3506	.2991
Dyyn Hd		.0323	
DelP/Hd		10.854	

TURB122

	375-400 ms	200-225 ms	450-475 ms
PT0A	4.0255	4.2386	3.9374
PT2AR1	3.7358	3.9256	3.6578
PT2AR2	3.7186	3.9052	3.6416
PT2AR3	3.7201	3.906	3.6431
PT2AR4	3.6716	3.8531	3.5969
PT2AR5	3.6716	3.8523	3.5969
PT2AR6	3.6969	3.8817	3.6208
mean	3.7024	3.8873	3.6262
S. Dev.	.0269	.0302	.0256
Press. Drp	.3231	.3513	.3112
Dyyn Hd		.0322	
DelP/Hd		10.9094	

TURB124

	375-400 ms	200-225 ms	450-475 ms
PT0A	3.8877	4.1626	3.7771
PT2AR1	3.5906	3.8443	3.4909
PT2AR2	3.5781	3.8285	3.4795
PT2AR3	3.5793	3.8291	3.4806
PT2AR4	3.5349	3.7768	3.4392
PT2AR5	3.5349	3.7767	3.4391
PT2AR6	3.5532	3.7995	3.4557
mean	3.5618	3.8092	3.4642
S. Dev.	.0242	.029	.0226
Press. Drp	.3259	.3535	.3129
Dyyn Hd		.0327	
DelP/Hd		10.8089	

TURB125

	375-400 ms	200-225 ms	450-475 ms
PT0A	3.9559	4.1988	3.8568
PT2AR1	3.6741	3.8904	3.5846
PT2AR2	3.6493	3.8626	3.5606
PT2AR3	3.6512	3.8638	3.5626
PT2AR4	3.6138	3.8203	3.5278
PT2AR5	3.6134	3.8195	3.5274
PT2AR6	3.6311	3.8415	3.5432
mean	3.6388	3.8497	3.551
S. Dev.	.0238	.0278	.0224
Press. Drp	.3171	.3491	.3058
Dynam Hd		.0325	
Del P/Hd		10.7421	

TURB126

	375-400 ms	200-225 ms	450-475 ms
PT0A	3.9233	4.1871	3.8163
PT2AR1	3.634	3.8769	3.5378
PT2AR2	3.6137	3.8534	3.5187
PT2AR3	3.6152	3.854	3.5202
PT2AR4	3.579	3.8097	3.487
PT2AR5	3.5789	3.809	3.487
PT2AR6	3.6001	3.8353	3.5062
mean	3.6035	3.8397	3.5095
S. Dev.	.0219	.027	.0201
Press. Drp	.3198	.3474	.3068
Dynam Hd		.0327	
Del P/Hd		10.6233	

TURB127

	375-400 ms	200-225 ms	450-475 ms
PT0A	3.9221	4.182	3.8688
PT2AR1	3.6245	3.862	3.577
PT2AR2	3.6149	3.8502	3.568
PT2AR3	3.6158	3.85	3.5688
PT2AR4	3.5707	3.7978	3.525
PT2AR5	3.5717	3.7987	3.5261
PT2AR6	3.5934	3.8256	3.547
mean	3.5985	3.8307	3.552
S. Dev.	.0235	.0278	.0228
Press. Drp	.3236	.3513	.3168
Dynam Hd		.0322	
Del P/Hd		10.9094	

TURB130

	375-400 ms	200-225 ms	400-450 ms
PT0A	3.8365	4.1268	3.7196
PT2AR1	3.532	3.7926	3.4256
PT2AR2	3.5197	3.7778	3.4146
PT2AR3	3.4156	3.7359	3.3149
PT2AR4	3.4806	3.7311	3.3781
PT2AR5	3.5025	3.7571	3.3982
PT2AR6	3.4991	3.7537	3.3948
mean	3.4916	3.758	3.3877
S. Dev.	.0412	.0238	.0393
Press. Drp	.3449	.3688	.3319
Dynam Hd		.0319	
Del P/Hd		11.5601	

TURB131

	375-400 ms	200-225 ms	450-475 ms
PT0A	4.0554	4.2607	
PT2AR1	3.7598	3.9398	
PT2AR2	3.7507	3.9291	
PT2AR3	3.7516	3.9289	
PT2AR4	3.7402	3.876	
PT2AR5	3.7042	3.8758	
PT2AR6	3.7358	3.9114	
mean	3.7404	3.9102	
S. Dev.	.0197	.0281	
Press. Drp	.315	.3505	
Dynam Hd		.0322	
Del P/Hd		10.8861	

Table 3
Variation in Rake Temperatures
(as Measured by Upstream Temperature Rake)

Run	120			121			122			124			125		
	Goal Temp	375-400 ms	ΔT 225-475 ms	Goal Temp	375-400 ms	ΔT 225-475 ms	Goal Temp	375-400 ms	ΔT 225-475 ms	Goal Temp	375-400 ms	ΔT 225-475 ms	Goal Temp	375-400 ms	ΔT 225-475 ms
Rake Sensors															
TT2AR1	409.2	434.5	25.3	470	463.7	-6.3	339.2	372.3	33.1	400	402.2	2.2	371	377.1	6.1
TT2AR2	483.8	503.9	20.1	470	465.9	-4.1	413.8	426.2	12.4	400	402.2	2.2	408.3	407.5	-0.8
TT2AR3	514.5	518.9	4.4	470	468.4	-1.6	444.5	431.7	-12.8	400	403.7	3.7	423.7	412.2	-11.5
TT2AR4	492.6	484.3	-8.3	470	468.9	-1.1	422.6	415	-7.6	400	403.5	3.5	412.7	403.8	-8.9
TT2AR5	405.7	415.2	9.5	470	473	3	335.7	360.9	25.2	400	406.4	6.4	369.2	377.3	8.1
Mean	470	471.36	1.36	470	467.98	-2.02	400	401.22	1.22	400	403.6	3.6	401.4	395.58	-5.82
RTDF(1)	16	20.4		8	8.5	0.1	16	14.6		0	0	0	8	7.4	
RTDF(2)		17.2			7.4			12.6						6.7	
RTDF(3)		17			6.5			10.9						5.9	

Run	126			127			130			131		
	Goal Temp	375-400 ms	ΔT 225-475 ms	Goal Temp	375-400 ms	ΔT 225-475 ms	Goal Temp	375-400 ms	ΔT 225-475 ms	Goal Temp	375-400 ms	ΔT 225-475 ms
Rake Sensors												
TT2AR1	439.6	436.3	-3.3	439.6	449.9	10.3	470	467.6	-2.4	409.2	432.4	23.2
TT2AR2	476.9	476.9	0	476.9	481.6	4.7	470	470.5	0.5	483.8	502	18.2
TT2AR3	492.3	483.6	-8.7	492.3	485.7	-6.6	470	472.8	2.8	514.5	514.8	0.3
TT2AR4	481.3	468.4	-12.9	481.3	475.5	-5.8	470	472.3	2.3	492.6	485.1	-7.5
TT2AR5	437.8	433.4	-4.4	437.8	444.5	6.7	470	473.9	3.9	405.7	414	8.3
Mean	470	459.72	-10.28	470	467.44	-2.56	470	471.42	1.42	470	469.66	-0.34
RTDF(1)	8	10.3		8	8.5		0		0.5	16	20.1	
RTDF(2)		9.1			7.4						17.1	
RTDF(3)		8.5			6.5			0.5			16.1	

Temperatures in Degrees Kelvin

Rake locations (from centerline in inches)

TT2AR1 10.71
TT2AR2 10.14
TT2AR3 9.541
TT2AR4 8.896
TT2AR5 8.202

Table 4
Variation from Matrix Temperatures to Upstream Temperature Rake

Temperatures in Degrees Kelvin

Run	Rake Sensor	Goal Temp	375-400 ms Temp.	Matrix Firing ms Temp.	Matrix Eff. Tr/Tm
120	TT2AR1	409.2	434.5	451.7	.96
120	TT2AR2	483.8	503.9	496.5	1.01
120	TT2AR3	514.5	518.9	507.7	1.02
120	TT2AR4	492.6	484.3	478.5	1.01
120	TT2AR5	405.7	415.2	399.5	1.04
120	Mean	470	471.4	466.8	1.01
120	RTDF(1)	16	20.4		
120	RTDF(2)		17.2		
120	RTDF(3)		17		
121	TT2AR1	470	463.7	493.9	.94
121	TT2AR2	470	465.9	495.4	.94
121	TT2AR3	470	468.4	497	.94
121	TT2AR4	470	468.9	498.6	.94
121	TT2AR5	470	473	500.1	.95
121	Mean	470	468	497	.94
121	RTDF(1)	8			
121	RTDF(3)			0.1	
122	TT2AR1	339.2	372.3	390.4	.95
122	TT2AR2	413.8	426.2	419.6	1.02
122	TT2AR3	444.5	431.7	425.6	1.01
122	TT2AR4	422.6	415	403.7	1.03
122	TT2AR5	335.7	360.9	347.5	1.04
122	Mean	400	401.2	397.4	1.01
122	RTDF(1)	16	14.6		
122	RTDF(2)		12.6		
122	RTDF(3)		10.9	0	
124	TT2AR1	400	402.2	419.3	.96
124	TT2AR2	400	402.2	418.3	.96
124	TT2AR3	400	403.7	418.1	.97
124	TT2AR4	400	403.5	418.9	.96
124	TT2AR5	400	406.4	420.9	.97
124	Mean	400	403.6	419.1	.96
124	RTDF(1)	0			
124	RTDF(3)			0	
125	TT2AR1	371	377.1	393.4	.96
125	TT2AR2	408.3	407.5	408.9	1.
125	TT2AR3	423.7	412.2	413.3	1.
125	TT2AR4	412.7	403.8	404.3	1.
125	TT2AR5	369.2	377.3	378.8	1.
125	Mean	401.4	395.6	399.7	.99
125	RTDF(1)	8	7.4		
125	RTDF(2)		6.7		
125	RTDF(3)		5.9		
126	TT2AR1	439.6	436.3	460	.95
126	TT2AR2	476.9	476.9	480	.99
126	TT2AR3	492.3	483.6	485.1	1.
126	TT2AR4	481.3	468.4	472.5	.99
126	TT2AR5	437.8	433.4	437.9	.99
126	Mean	470	459.7	467.1	.98
126	RTDF(1)	8	10.3		
126	RTDF(2)		9.1		
126	RTDF(3)		8.5		
127	TT2AR1	439.6	449.9	469.9	.96
127	TT2AR2	476.9	481.6	488.5	.99
127	TT2AR3	492.3	485.7	493.3	.98
127	TT2AR4	481.3	475.5	481.3	.99
127	TT2AR5	437.8	444.5	448.8	.99
127	Mean	470	467.4	476.4	.98
127	RTDF(1)	8	8.5		
127	RTDF(2)		7.4		
127	RTDF(3)		6.5		
130	TT2AR1	470	467.6	495	.94
130	TT2AR2	470	470.5	496.3	.95
130	TT2AR3	470	472.8	497.3	.95
130	TT2AR4	470	472.3	498	.95
130	TT2AR5	470	473.9	498.2	.95
130	Mean	470	471.4	497	.95
130	RTDF(1)	0			
130	RTDF(3)			0.5	
131	TT2AR1	409.2	432.4	451.9	.96
131	TT2AR2	483.8	502	495.5	1.01
131	TT2AR3	514.5	514.8	506.6	1.02
131	TT2AR4	492.6	485.1	478.5	1.01
131	TT2AR5	405.7	414	402.1	1.03
131	Mean	470	469.7	466.9	1.01
131	RTDF(1)	16	20.1		
131	RTDF(2)		17.1		
131	RTDF(3)		16.1		

Rake locations (from centerline in inches)

TT2AR1	10.7
TT2AR2	10.1
TT2AR3	9.54
TT2AR4	8.9
TT2AR5	8.2